VOLUME 116 NUMBER 2

THE ASTROPHYSICAL JOURNAL

AN INTERNATIONAL REVIEW OF SPECTROSCOPY AND ASTRONOMICAL PHYSICS

SEPTEMBER 1952

PROBLEMS OF GALACTIC STRUCTURE — *J. H. Oort* — 233
A STUDY OF THE ORION AGGREGATE OF EARLY-TYPE STARS — *Stewart Sharpless* — 251
ON MAGNITUDE SYSTEMS — *Harold L. Johnson* — 272
THE SPECTRA AND LUMINOSITIES OF WHITE DWARFS — *Willem J. Luyten* — 283
ON THE DECAY OF A PRIMEVAL STELLAR MAGNETIC FIELD — *Marshal H. Wrubel* — 291
EQUATIONS OF MOTION FOR AN IDEAL PLASMA — *Lyman Spitzer, Jr.* — 299
INHOMOGENEOUS STELLAR MODELS. I. MODELS WITH A CONVECTIVE CORE AND A DISCONTINUITY IN THE CHEMICAL COMPOSITION — *J. B. Oke and M. Schwarzschild* — 317
THE SPECTRUM AND RADIAL VELOCITIES OF W VIRGINIS — *Roscoe F. Sanford* — 331
THE PREMINIMUM SPECTRUM OF R LEONIS — *Paul W. Merrill* — 337
MEASUREMENTS IN THE SPECTRA OF FOUR LONG-PERIOD VARIABLE STARS OF CLASS Mc — *Paul W. Merrill* — 344
THE CEPHEID VARIABLE S SAGITTAE. I. THE RADIAL-VELOCITY VARIATION — *G. H. Herbig and J. H. Moore* — 348
THE CEPHEID VARIABLE S SAGITTAE. II. THE EMISSION LINES — *George H. Herbig* — 369
A PHOTOELECTRIC LIGHT-CURVE OF DY PEG — *Braulio Iriarte* — 382
THE SPECTROSCOPIC ORBIT OF 26 AQUILAE — *K. L. Franklin* — 383
PHOTOELECTRIC OBSERVATIONS OF NU ERIDANI — *Marie F. Walker* — 391
THE RADIAL VELOCITY OF NU ERIDANI — *O. Struve, D. H. McNamara, S. M. Kung, R. P. Kraft, and A. D. Williams* — 398
THE CURVE OF LINE-WIDTH CORRELATION AND DOPPLER VELOCITIES IN STELLAR ATMOSPHERES. I. DELTA CANIS MAJORIS — *Su-shu Huang and Otto Struve* — 410
PRELIMINARY ANALYSIS OF THE TURBULENCE SPECTRUM OF THE SOLAR PHOTOSPHERE AT LONG WAVE LENGTHS — *F. W. Frenkiel and M. Schwarzschild* — 422
THE DEPRESSION OF THE CONTINUUM IN A K0 DWARF — *E. M. Lewis and William Liller* — 428
THE AURORAL SPECTRUM IN THE WAVE-LENGTH RANGE 3300–8900 A — *W. Petrie and R. Small* — 433

NOTES

IDENTIFICATION OF CARBON MONOXIDE IN THE ATMOSPHERE ABOVE FLAGSTAFF, ARIZONA — *Arthur Adel* — 442
NOTE ON THE THEORY OF THE STARK EFFECT IN STELLAR SPECTRA — *G. J. Odgers* — 444
NOTE ON THE STARK BROADENING OF $H\gamma$ — *Anne B. Underhill* — 446
ON THE ACCURACY OF JOHNSON'S COLORS AND MAGNITUDES OF THE PLEIADES — *W. A. Hiltner* — 449
THE RELATIVE POPULATIONS OF THE $He\,I\ 2^1S$ AND 2^3S STATES IN THE ORION NEBULA — *P. Wellmann* — 452
INTERNAL MOTIONS WITHIN INTERSTELLAR CLOUDS — *Lyman Spitzer, Jr., and Andrew Stanamich* — 452

REVIEWS — 455

THE UNIVERSITY OF CHICAGO PRESS
CHICAGO, ILLINOIS, U.S.A.

September 1952 Vol. 116, No. 2

THE ASTROPHYSICAL JOURNAL

AN INTERNATIONAL REVIEW OF SPECTROSCOPY AND ASTRONOMICAL PHYSICS

Published in Collaboration with the American Astronomical Society

S. CHANDRASEKHAR
Managing Editor

GERARD P. KUIPER
Associate Editor

Yerkes Observatory of the University of Chicago

EDITORIAL BOARD

O. HERZBERG (1952-56)
National Research Council, Ottawa

C. D. SHANE (1952-55)
Lick Observatory, University of California

FRED L. WHIPPLE (1952-54)
Harvard College Observatory

LYMAN SPITZER, JR. (1952-53)
Princeton University Observatory

PAUL W. MERRILL (1952)
Mount Wilson Observatory of the Carnegie Institution of Washington

---

The Astrophysical Journal is published bimonthly by the University of Chicago at the University of Chicago Press, 5750 Ellis Avenue, Chicago 37, Illinois, during January, March, May, July, September, and November. ¶Two volumes are published per year, one beginning with the January issue and the other beginning with the July issue. The subscription price is $6.00 per volume or $12.00 per year; the price of single copies is $3.00. (Orders for service of less than a volume will be charged at the single copy rate.) ¶Postage is prepaid by the publishers on all orders from the United States and its possessions. No extra charge is made for postage to countries in the Pan American Postal Union. ¶Postage is charged extra as follows: for Canada, 20 cents per volume, 40 cents per year (total $6.20 per volume, $12.40 per year); on single copies 5 cents (total $3.05); for all other countries in the Postal Union, 40 cents per volume, 75 cents per year (total $6.40 per volume, $12.75 per year), on single copies 10 cents (total $3.10). ¶Subscriptions are payable in advance. Please make all remittances payable to The University of Chicago Press, in United States currency or its equivalent by postal or express money orders or bank drafts.

The following is an authorized agent:

For the British Empire, except North America and Australasia: The Cambridge University Press, Bentley House, 200 Euston Road, London, N.W. 1, England. Prices of yearly subscriptions and of single copies may be had on application.

Claims for missing numbers should be made within the month following the regular month of publication. The publishers expect to supply missing numbers free only when losses have been sustained in transit, and when the reserve stock will permit.

Business correspondence should be addressed to The University of Chicago Press, Chicago 37, Illinois.

Communications for the editors and manuscripts should be addressed to: S. Chandrasekhar, Editor of THE ASTROPHYSICAL JOURNAL, Yerkes Observatory, Williams Bay, Wisconsin.

Line drawings and photographs should be made by the author, and all marginal notes such as co-ordinates, wave lengths, etc., should be included in the cuts. It will not be possible to set up such material in type.

One copy of the corrected galley proof should be returned as soon as possible to the editor, Yerkes Observatory, Williams Bay, Wisconsin. Authors should take notice that the manuscript will not be sent to them with the proof.

The cable address is "Observatory, Williamsbay, Wisconsin."

The articles in this journal are indexed in the *International Index to Periodicals*, New York, N.Y.

Applications for permission to quote from this journal should be addressed to The University of Chicago Press, and will be freely granted.

Microfilms of complete journal volumes are available to regular subscribers only and may be obtained at the end of the year. Orders and inquiries should be addressed to University Microfilms, 313 North First Street, Ann Arbor, Michigan.

Notice to subscribers: If you change your address, please notify us and your local postmaster immediately.

Entered as second-class matter, July 31, 1940, at the Post-Office at Chicago, Ill., under the Act of March 3, 1879.
Acceptance for mailing at special rate of postage provided for in United States Postal Act of October 3, 1917, Section 1103, amended February 28, 1925.

[PRINTED IN U.S.A.]

THE ASTROPHYSICAL JOURNAL

AN INTERNATIONAL REVIEW OF SPECTROSCOPY AND ASTRONOMICAL PHYSICS

VOLUME 116 SEPTEMBER 1952 NUMBER 2

PROBLEMS OF GALACTIC STRUCTURE*

J. H. OORT
Leiden Observatory
Received June 8, 1952

Since the first quantitative investigations of the Galactic System were started by William Herschel, two great developments have taken place in our knowledge of the structure of this system. The first of these may be tied up with the name of J. C. Kapteyn. Consistently pursuing the ideal of revealing the general structure of the entire stellar system, Kapteyn laid the foundations for much of the modern work in this line, thereby initiating essentially all the methods used today. Although Kapteyn succeeded in determining the structure in those parts of the system that are more than about 20° from the Milky Way, obtained important numerical results for the variation of star density with distance from the galactic plane, successfully investigated the peculiar distribution of the B stars, and in the course of this work discovered the first dynamically important phenomena in stellar motions, he did *not* reach the principal aim he had set out for, because of the unexpected strength of interstellar absorption near the galactic plane.

The second great development was initiated by Shapley's investigation of the distribution of the globular clusters. Here the absorption of light was comparatively unimportant, because the clusters have high velocities and a large fraction were well outside the thin galactic layer of absorbing matter. These high velocities insured also that the clusters were well shuffled and therefore distributed symmetrically around the gravitational center of the entire Galactic System. As a consequence, they indicated its true dimensions and the position of its center.

It seems that at present a third phase in the development of galactic research has begun by the successful reception of radiation at radio frequencies. This research is still in its early infancy, comparable perhaps to the stage that Sir William Herschel had reached some hundred and fifty years ago by his star gauges in the visible radiation. What has been reached in the few years since active radio-astronomical research was started can hardly be expected to give more than the faintest glimpse of the changes of insight that the next years are likely to bring about. This circumstance evidently renders risky the task I have set myself here, which is to take stock of what knowledge has been acquired from the visible wave lengths and to compare this with the tentative first observations of the new era.

Let us begin by considering the region for which we have extensive knowledge, namely, the cylindrical region with axis through the sun and perpendicular to the galactic

* Henry Norris Russell Lecture, delivered in Cleveland, Ohio, on December 27, 1951.

plane and with radius of the order of 1 kpc. In this cylinder we shall consider, in the first place, the density distribution in a direction perpendicular to the galactic plane. We are then very little hampered by absorption effects. For ordinary stars the density is found to vary rapidly, as well as smoothly; it falls to less than one-tenth the density near the galactic plane at distances for which fairly reliable data can still be obtained from proper motions and spectra. Let us follow the common practice and denote the distance from the galactic plane by z. For z larger than 300 parsecs the density falls off approximately as the inverse square of z.

The cause of this decrease in density must be the attractive force of the Galactic System, more particularly the z-component of this force. Indeed, when we add up the mass of all the stars we know, as well as the interstellar gas, in a unit volume near the sun, we find that, together with the extra central mass of the Galaxy needed to explain the observed galactic rotation, this yields just about enough attraction to explain the density decrease observed. And this not only near the galactic plane, but likewise up to the largest values of z for which we have any knowledge about the density. Put into other words we may say that the distribution in the z-direction seems approximately to fulfil the conditions of a steady state, and to satisfy Poisson's law. The mass density near the sun needed to satisfy Poisson's equation would be about 80 solar masses per 1000 cubic parsecs;[1] known stars provide for about 50,[2] interstellar gas for 12. These values, which are all rather uncertain, would leave about 20 per cent of the mass unaccounted for. This should be ascribed to the unknown stars fainter than about +15 absolute magnitude.

Different types of stars show great differences in their distribution perpendicular to the galactic plane. As I have just mentioned, there is some evidence that the distribution in this direction corresponds with at least some approximation to a well-mixed, or steady, state. If, as a working hypothesis, we suppose this to be so, the velocity and density distribution are directly related to each other, and knowledge of either suffices to decide about the other.

It appears that all those types of stars that are *common* in our neighborhood show approximately the same distribution in the z-direction, corresponding to an average distance of some 300 psc from the galactic plane. An entirely different picture is shown by the O- and B-type stars, with an average distance of only about 50 psc. A transition is formed by the A and F stars. On the other side the extreme is presented by those variables of the RR Lyrae type that have periods longer than 0.42 day. These have an average peculiar velocity of 64 km/sec in the direction perpendicular to the galactic plane. Average velocities of the same order are found for the globular clusters. Another type of stars that seem to belong in this category are the faint white stars in high galactic latitudes discovered by Humason and Zwicky. This is indicated by the few radial velocities that have recently been measured by Humason[3] and by proper motions measured at Minneapolis and at Leiden. Corresponding average distances from the galactic plane are about 3000 or 4000 psc. There are again various types of stars that are intermediate between this extreme and the ordinary stars. Such transitional stars are generally much more frequent than the objects of extremely high velocity. As examples, we may mention the long-period variables; their average velocity in the z-direction is about 30 km/sec, corresponding to roughly 1000 psc average distance from the plane.

Among the stars of common types, such as ordinary G, K, or M dwarfs, we also find a certain fraction (perhaps 10 per cent among the fainter dwarfs) that distinguish themselves by velocities higher than one would expect in a velocity distribution of exponential

[1] *B.A.N.*, **6**, 284, 1932 (slightly corrected with modern data).

[2] This value is given by Blaauw in *Ned. Tijdschrift v. Natuurkunde*, **17**, 34, 1951; see also Kuiper, *A.J.*, **53**, 194, 1948.

[3] I am indebted to Mr. Humason for permission to quote this unpublished result.

type; these velocities show a highly asymmetrical distribution. The Z-velocities of the common-type high-velocity stars are however *not* very high. In the z-direction these stars hardly distinguish themselves from the low-velocity dwarfs. In that respect there is a pronounced difference in character between the main-sequence stars of high velocity and the RR Lyrae variables, for instance, a difference that indicates a quite different origin.

Another thing that may be mentioned at this point is that, especially among the types of stars that contain many high velocities, like the long-period variables, there seems to be a *smooth* transition from subtypes with moderate velocities to those with highest velocities, so that it is impossible to draw a satisfactory dividing line between the two. In these cases, at least, it would be an unwarranted oversimplification to try to divide the stars into two groups, corresponding to the two populations introduced by Baade.

We must here digress for a moment to discuss the notion of these two populations.[4] This idea is a most important one, by which Baade not only has considerably clarified our insight into the differences between various types of stellar systems but has likewise inspired quite a number of most interesting new investigations.

When Baade first introduced the idea of populations of types I and II, the meaning of these terms was clearly meant to apply to the general population of a certain category of stellar systems or of a part of a stellar system. Recently a tendency has developed to designate various classes of stars as belonging to populations I or II according to whether they show strong or weak galactic concentration or have low or high velocities. This usage of the terms is liable to lead to confusion, because the objects in the Galactic System present all gradations of concentration to the galactic plane as well as of velocity dispersion. It appears an inadequate simplification to describe the population of the Galactic System as a mixture of two different kinds of populations. If we were to extend the notion of population to cover the complicated phenomena observed, we would have to introduce a considerable number of different populations, or "subsystems" as they were originally named by Lindblad, a term that Kukarkin has later adapted to modern data. It would seem preferable to reserve the terms "population I" and "population II" for characterizing the general type of population of a stellar *system*, and to specify the degree of galactic concentration of a given type of *stars* by other terms.

The differences in population noted so far relate necessarily to such rare stars of great intrinsic brightness as can be observed in other stellar systems. We do not know as yet whether the *common* stars in a globular cluster or elliptical nebula are also different from those in our surroundings. However, there are two kinds of observations that can tell us at least *something* about the more common ingredients that other systems are made of.

The first relates to the interstellar gas, which can be observed by its well-known emission lines or by the dark matter that usually accompanies it. In the near future, observations of the emission line of neutral hydrogen at 21-cm wave length may give additional information on the total amount of hydrogen contained in a galaxy. It is well known that systems of population II show little or no interstellar material, while the population I systems appear always to contain a considerable amount.

The second sort of observations that teach us something about the *common* population are the measures of rotation. In many cases these permit some estimate of the total mass contained in the inner part of a stellar system, and sometimes they even give information about the variation of mass density within the system. We can compare these data to the amounts of light and can form, for instance, the ratio of mass to light. We observe a great variety in the values of this ratio in different systems and in different parts of the same system. If both are expressed in the sun as a unit, the ratio is found to be about 2 in the neighborhood of the sun. In other galaxies much higher values have been found. In the Andromeda Nebula, for instance, it varies from 13 at 600 psc from the center to

[4] Cf. Baade, *Pub. Obs. U. Michigan*, **10**, 7, 1951.

about 70 at 5500 psc.[5] The high relative mass density per unit of light in this latter case must indicate either that the amount of interstellar gas must be some hundred times higher than in our surroundings or else that practically all the mass density is due to stars of extremely low intrinsic brightness, which contribute only little to the mass density near the sun.

A similar result is found for the outer parts of the elliptical system NGC 3115, where the ratio runs even up to about 250.[6] In this case the possibility of the high mass density being due to interstellar gas must probably be discarded, so that the mass must be made up practically entirely of very faint dwarfs having a ratio of mass to light of more than 1000:1. Contrary to the light-intensity, which is strongly concentrated toward the center of the nebula, the mass density is found to be practically constant over the larger part of the system. The stars responsible for this mass must therefore form an approximately homogeneous atmosphere, imbedded in which lies the luminous system. In the central part the ratio of mass to light is only about 20. The relative numbers of the giant stars that are probably responsible for most of the light and the very faint dwarfs that must make up the bulk of the mass, therefore, vary considerably over the nebula.

From the scant information that has been obtained on radial velocities of individual stars in globular clusters we infer that in *these* population II systems the ratio of mass to light is near unity; the relative frequency of the type of faint dwarfs that form the bulk of the population of NGC 3115 must therefore be insignificant in globular clusters.

The examples just given indicate that, at least in the relative numbers of different kinds of stars, there must be a great disparity between systems classed in the same population groups according to criteria used so far.

We must now return to the structure of the Galactic System. We have discussed the distribution in the direction perpendicular to the galactic plane. If we leave out for the moment the new radio data, our further *direct* knowledge of the general structure may be summarized in few words. It consists of an estimate of the direction and distance to the center by means of globular clusters and RR Lyrae variables, of the density distribution of globular clusters throughout the system, and, finally, of a determination of the inclination to the galactic plane of the surfaces of equal star density at a z of about 1000 and 1500 psc.

However, some additional knowledge can be derived from stellar *motions*. The information they provide is summarized in Tables 1 and 2. Table 1 gives a confrontation of various *direct* determinations of the galactic longitude of the center with the direction of the center derived from the *motions* on the supposition that the relative systematic motions are perpendicular to the radius vector. It is evident that this condition is fulfilled to a close approximation. Table 2 shows the interrelation of various determinations of the constants of differential galactic rotation. It is to be noted that the determinations listed are largely independent of one another, both in the character of the data used and in the method. They have been combined in a least-squares solution. The results for A and B, as well as for the rotational velocity itself and the distance R to the center, are given in the last lines. In deriving the velocity of rotation, no use has been made of the velocities of globular clusters, because it would seem an unwarranted hypothesis to suppose that the system of clusters has no rotation. On the contrary, the available data seem to indicate a rotation for this system of about 90 km/sec at a distance from the center equal to that of the sun.

Assuming that the rotational velocity of the Galactic System corresponds to the circular velocity, we can at once derive the value of the force K that is exerted by the system on a unit mass near the sun. The quantity that is most accurately determined is K/R; this is equal to $-(A - B)^2$ and is found with a mean error of about 12 per cent.

[5] Wyse and Mayall, *Ap. J.*, **95**, 24, 1942; *Lick Obs. Contr.*, Ser. II, No. 2.

[6] *Ap. J.*, **91**, 302, Table 4, 1940.

From this we can obtain an estimate about the measure in which the density must increase in the parts of the system nearer to the center. If we compute the attraction exerted by a homogeneous ellipsoid with a density equal to the local density in our neighborhood and such a flattening that near the sun its thickness corresponds to the mean thickness of the layer of common stars, we find that this attraction accounts for less than one-fourth of the value of $K:R$ found from the angular rotation. This means that there must be a considerable additional mass in the central part.

At present we cannot say very much about the way in which this mass is distributed, except that it cannot be much concentrated toward the center. This follows in the first place from a consideration of the dynamics of the system of globular clusters. Because we know velocities of globular clusters throughout the Galaxy and because, on account of their high random motions, it is probable that their arrangement in space corresponds to a steady state, they enable us to draw at least rough conclusions regarding the gravita-

TABLE 1

GALACTIC LONGITUDE OF CENTER OF GALACTIC SYSTEM

	l_c	m.e.
Direct determinations:		
Star counts in intermediate and high latitudes	324°	±5°
	335	±5
Globular clusters (Shapley)	325	±3
Planetary nebulae (Minkowski)	328	±3:
Infrared radiation (Stebbins and Whitford)	326	±2
Radiation at 100 Mc/sec (Bolton and Westfold)	329	±1
Radiation at 200 Mc/sec (Allen and Gum)	325	±1
Average	327	±1
From motions, on supposition that systematic motions are perpendicular to radius vector:		
From differential gal. rotation (various determinations)	325	±1
From the motions of high-velocity objects	323	±4

tional potential in the Galactic System. If we represent the central mass by a homogeneous ellipsoid, it can be made compatible with the distribution of the clusters only if it extends to at least three-fourths of the distance from the center to the sun. An uncertain indication in the same direction is given by the differential rotation. This gives not only K/R, but likewise dK/dR. Taking into account the value of the local density, we would require, in order to explain the observed value of dK/dR, a homogeneous central ellipsoid extending at least 0.85 of the distance from the center to the sun and having a sensible flattening.

A tentative working model of the distribution of mass in the Galactic System, fitting all data mentioned, is schematically shown in Figure 1. It consists of a set of superimposed concentric homogeneous ellipsoids. Those extending beyond the sun will be called "outer ellipsoids," while those which do not extend to the sun will be denoted as "central ellipsoids."[7] The model actually used in the calculations in this article contains some ten outer ellipsoids extending beyond the sun, which have been so chosen as to represent the observed distribution for dwarf stars in the z-direction, as well as the observed inclination of the equidensity surfaces between $z = 1000$ and $z = 1500$ psc. The most uncertain feature of the model is the axial ratio of the large central ellipsoid. In Figure 1 this ratio has been taken as 1:5, in rough analogy with the light-distribution in

[7] For details concerning a very similar model cf. *B.A.N.*, **9**, 185, 1941.

the central parts of spirals. As we shall see later on, this appears also to be in agreement with the distribution of "radio stars." The density in this ellipsoid must then be 2.2 times the mass density near the sun, this density being superimposed on that given by the outer ellipsoids. All dynamical observations might, however, be equally well represented by a different axial ratio, as long as the density is adjusted approximately in inverse proportion to the axial ratio assumed. For the purpose for which the model will

TABLE 2

(All errors indicated are estimated mean errors)

		Θ_c/R (km/sec psc)
$A = \frac{1}{2}\left(\frac{\Theta_c}{R} - \frac{d\Theta_c}{dR}\right)$ rad. vel. and p.m. $+0.0195 \pm 14$ $B = -\frac{1}{2}\left(\frac{\Theta_c}{R} + \frac{d\Theta_c}{dR}\right)$ proper m. -0.0069 ± 15	$\frac{-B}{A-B} = 0.26 \cdots \pm 6$	0.026 ± 2
From ellipsoidal velocity distribution b^2/a^2	$0.24 \ldots \pm 3$	
Vel. distr. and dens. gradient long-period variables		0.031 ± 5
Vel. and dens. distr. RR Lyrae vars. in z-direction		0.028 ± 6
Space distr. of glob. cl. and RR Lyrae vars. $R = 8500 \pm 1300$ psc Radial velocities local group of nebulae $\Theta_c = 308 \pm 60$ km/sec		0.036 ± 9
Vel. distr. and dens. gradient glob. clusters $\frac{\Theta_c^2}{R} = 2.5 \pm 0.4 \times 10^{-8}$		

Least-squares solution from all the above data:

$$R = 9400 \pm 1200 \text{ psc}^*; \quad \Theta_c = 259 \pm 32 \text{ km/sec}^*; \qquad 0.0275 \pm 17$$

$$A = +0.0206 \pm 14; \quad B = -0.0069 \pm 7; \quad \frac{d\Theta_c}{dR} = -0.0137 \pm 16;$$

$$\text{Period} = 223 \pm 13 \text{ million years}$$

* *Note added in proof.*—A provisional discussion of observations of the 21-cm hydrogen line obtained in recent months seems to point to somewhat lower values of R and Θ_c.

be used, the axial ratio of the inner ellipsoid is immaterial. I am indebted to Mr. Seeger for the calculation of this model and of the corresponding rotational velocities.

We can only vaguely speculate as to the composition of this central mass, in which two-thirds of the entire mass of the Galactic System is contained. The most positive thing we can say about it is that it must be composed of high-velocity stars. This is necessary in order to keep up its extension perpendicular to the galactic plane against the attraction corresponding to its high density. This conclusion holds for whatever axial ratio we assume. In the model drawn, the density of these high-velocity objects would have to be more than twice the total star density near the sun and therefore more than

twenty times the density of known high-velocity dwarfs in our surroundings. A density increase of such amount, which would have to take place in the distance interval of between 1 and 2 kpc that separates us from the edge of the inner ellipsoid, appears to be difficult to fit in with direct data about density gradients of high-velocity objects in our neighborhood. It does not seem possible at present to give a solution of this difficulty. Maybe the mass of the central ellipsoid is mainly made up of stars that are considerably fainter than the faintest dwarfs which we know. These would then have to possess a

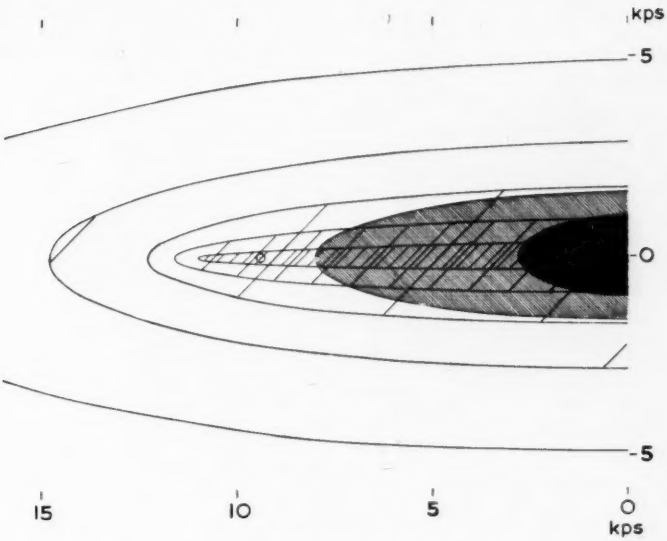

FIG. 1.—Schematic model of Galactic System. The diagram shows a section perpendicular to the galactic plane, through the center and the sun. The position of the sun is indicated by a small circle. The large central ellipsoid has axes of 8 and 1.6 kpc and a density 2.15 (using the density near the sun as a unit); the small central ellipsoid, with axes 2.8 and 1 kpc, has a density 3.13. The axes in kpc and densities of the five outer ellipsoids are as follows:

a	c	
11.0	0.3	0.446
11.6	0.9	104
12.3	1.7	026
14.8	2.8	007
20.3	4.9	0.003

The ellipsoids are superimposed upon one another.

velocity distribution such as to give a more or less homogeneous distribution over the whole extent of the central ellipsoid and a steep drop at the outer edge. We are reminded of the phenomena observed in the elliptical nebula NGC 3115, where we were forced to assume that the bulk of the mass was composed of stars that also were extremely faint intrinsically and had a homogeneous space distribution over the whole part of the nebula over which the rotation has been measured.

I should now like to refer briefly to considerations that have more relation to direct observations. In particular, through the observations of Australian scientists a fair picture has in recent years been obtained of the distribution of the surface intensity of radia-

tion at 100[8] and 200 Mc/sec.[9] It can be shown that, with any likely density of interstellar hydrogen, radiation at these wave lengths between 3 and $1\frac{1}{2}$ meters cannot have suffered appreciable absorption. The radio measures are therefore eminently suited to give information on the distribution of the sources of this radiation over the entire Galactic System, and in particular in its inner parts. Part of the radiation comes from the ionized clouds in interstellar space, but it seems probable that at 100 Mc/sec this is only a minor fraction of the total radiation, the bulk probably coming from so-called "point sources." It is now of interest to inquire after the distribution of these radio sources. We find that the distribution over the hemisphere surrounding the center does not resemble the distribution of globular clusters or RR Lyrae variables, lacking their concentration toward the center, and in particular also the nearly spherical symmetry of their distribution around the center, the equidensity lines of radio intensity showing a

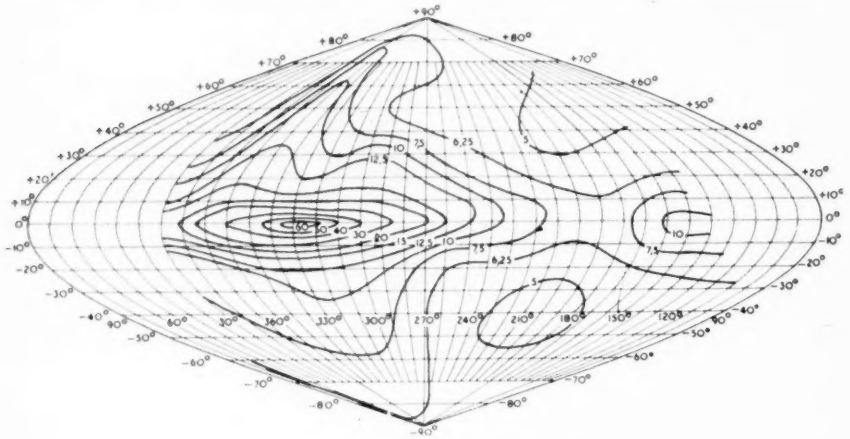

FIG. 2.—Equal-area charts of equivalent black-body temperature at 100 Mc/sec(λ 3 meters). From an article by Bolton and Westfold in *Australian J. Sci. Research*, **19**, 1950 (reproduced from H. C. van de Hulst, *Hemel en Dampkring*, **49**, 1951).

strong flattening. Neither does the distribution of the radio-frequency radiation show any resemblance to the distribution of objects like interstellar clouds or B-type stars that are strongly concentrated in the galactic plane. If, however, we compare its surface intensity distribution with that computed from the model of the mass distribution in the Galactic System, as outlined before, we find almost perfect agreement in all directions where the intensity given by the model is considerable (cf. Figs. 2 and 3). This shows that at least the major part of this radiation comes from sources having a spatial arrangement very similar to that of the mass, the main feature being a homogeneous ellipsoid of axial ratio about $\frac{1}{5}$ and extending almost to the sun. This does not, however, give the whole picture. There are indications that several different types of objects contribute to the radio intensity. This becomes particularly evident when we look at longitudes that are more than about 70° from the center or at regions above 20° latitude. Here the observed radio intensity is very much higher than that given by the model. Unless the difference is due to a large zero-point error that would have to be common to several independent series of observations, the residual intensity of about 600° points either to a large background

[8] Bolton and Westfold, *Australian J. Sci. Res.*, ser. A, **3**, 19, 1950.

[9] C. W. Allen and Gum, *Australian J. Sci. Res.*, ser. A, **3**, 224, 1950.

radiation from the universe or to radiation from a type of radio sources distributed as an extremely large envelope around the Galactic System. The fact that various observers have found a pronounced unevenness of the intensity over the galactic polar cap, with generally greater intensity in longitudes near that of the center, may make the latter interpretation more probable than the first. But more accurate observations, especially in high latitudes, are required before this question can be even tentatively settled.

It is interesting to remark in passing that convincing evidence has recently been found by B. Y. Mills that, besides the ordinary radio-point sources, which, partly, at least,

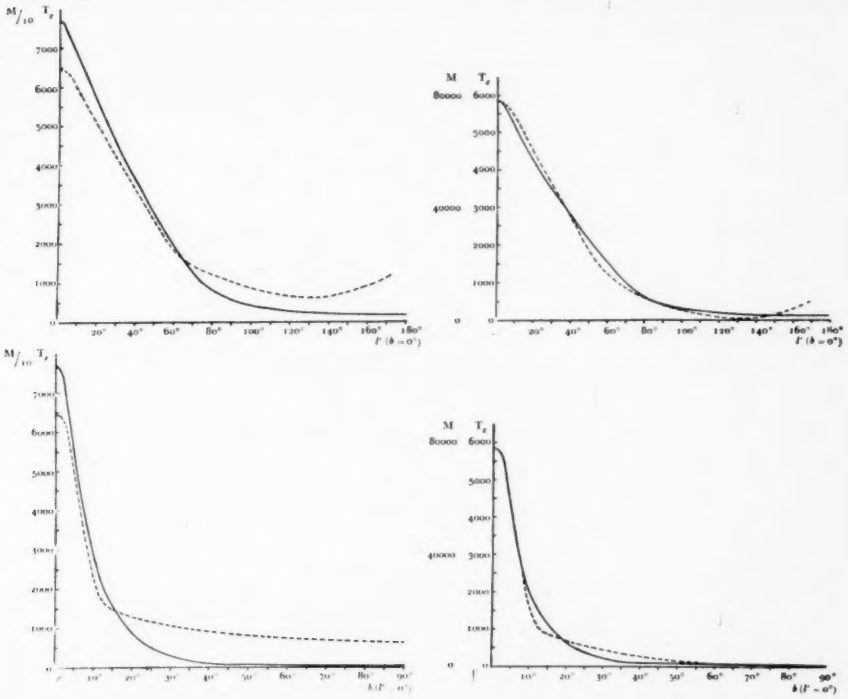

FIG. 3.—Comparison of Bolton and Westfold's measured temperatures (*dotted curves*) with the values computed from the hypothetical model of the Galactic System (*left*). In the comparisons at the right a background temperature of 600° has been subtracted from the observed temperatures. l' denotes the difference in longitude from the center of the galaxy at $l = 327°$.

seem to be near-by objects showing a uniform distribution over the sky, there exists another class of sources, strongly concentrated in the Milky Way and presumably far more distant than the ordinary sources.

We must now return to our model of the Galactic System and discuss the information about such a model that can be obtained from another type of observation in the region of the short radio waves. These are the observations of the emission line of neutral interstellar hydrogen, suggested by van de Hulst in 1944. The first successful observations of this line were made by Ewen and Purcell of Harvard in March of this year, and a little later by C. A. Muller in the Netherlands, as well as by Christiansen and Hindman in

Australia.[10] When observed in the direction of the center or anticenter, the line has a half-width of about 25 km/sec, corresponding to an average random radial velocity of the interstellar clouds of 5 km/sec. From the average galactic latitude at which the intensity falls to half its maximum value in the Milky Way, we deduce that, in the central part of the line, unit optical thickness is reached in a layer of about 1000 parsecs when we observe in the direction of the center or anticenter. It is probably not possible, therefore, to obtain information about the density of the interstellar gas in the central parts of the Galaxy from observations right in the direction of the center. However, if one observes

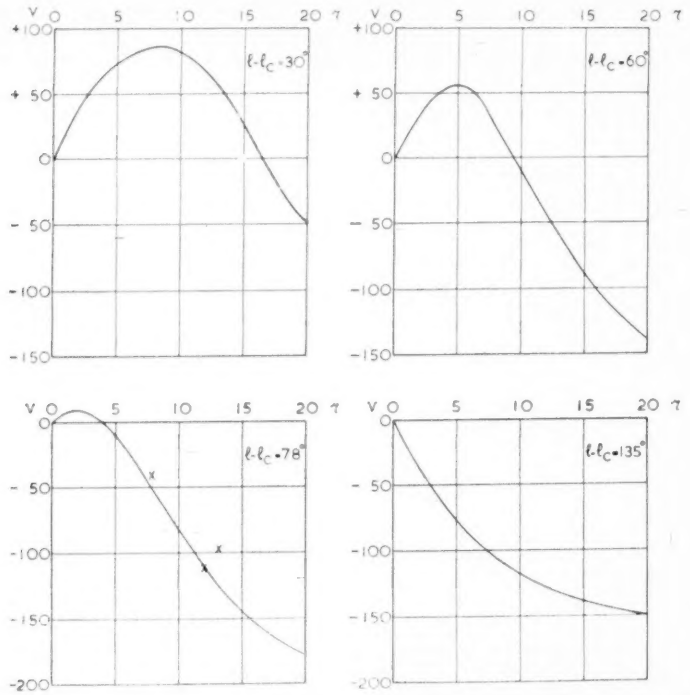

FIG. 4.—Variation of radial velocity with distance from the sun for gas clouds in different galactic longitudes. The curves were computed on the basis of the model of the Galactic System described above.

in longitudes differing more than a few degrees from that of the center, the Doppler effect due to the differential rotation of the Galactic System may change the frequency of the line to such an extent that the radiation from the central region is no longer absorbed by the clouds nearer to the sun. Observations of the intensity of the hydrogen 21-cm line may thus be expected to provide information on the distribution of the interstellar gas in different parts of our Galaxy. And, equally important, they give a means of determining the rotational velocity of the system at various distances from the center. As the velocity of rotation of the interstellar gas will probably practically coincide with the circular velocity, they will therefore provide us with a fairly complete picture of the gravitational force in the galactic plane at various distances from the center up to the

[10] *Nature*, **168**, 356, 1951.

distance of the sun. Such measures are now being made by Mr. Muller at the Kootwijk Transmitting Station in the Netherlands. The accompanying diagrams indicate the way in which the observations are arranged. Figure 4, calculated on the basis of the model sketched previously, shows how, in four different longitudes, the radial velocity relative to the average of the bright stars in the vicinity of the sun varies with distance. The crosses in the graph for $l - l_c = 78°$ indicate the radial velocities of the very distant δ Cephei variables in this direction that were measured by Joy. In the model the circular velocity varies with distance R from the center, as shown in Figure 5. You will note that it increases fairly linearly with R up to a distance of about 8 kpc, and then begins gradu-

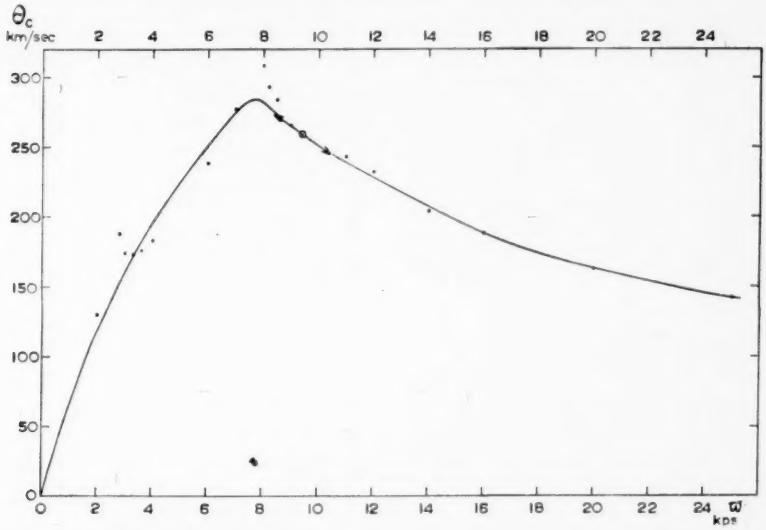

FIG. 5.—Variation of the circular velocity of rotation in the Galactic System with distance from the center. The small circle indicates the position of the sun and the estimated circular velocity in our neighborhood. The arrows indicate the slope of the curve as derived from the observed differential galactic rotation. The dots were computed from the model used; the curve has been drawn so as to smooth out the artificiality of the sharp boundaries of the discrete ellipsoids.

ally to decrease. The inclined arrows on the downward branch indicate the part around the sun's distance where the slope of the curve can be found from the constants of galactic rotation. The derivative there is equal to $-A - B$. It may be noted that the general shape of this curve bears great resemblance to what is observed in spiral nebulae, in which generally over the whole of their brighter parts the velocity of rotation increases in rough proportion to the distance from the center. Only in two cases, viz., the Andromeda Nebula and M33, where rotations have been measured from emission nebulae, the observations extend to regions comparable to the situation of the sun in the Galactic System. It is only in these cases that the declining part of the rotation curve has also been observed.[11] Figure 6 gives a schematic picture of the contours of the 21-cm line that would correspond with the radial-velocity curves of Figure 4 if the hydrogen forms a

[11] A comparison of the rotation of M31, M33, and the Galaxy has recently been made by N. U. Mayall, *Pub. Michigan U. Obs.*, **10**, 19, 1951.

homogeneous disk of 120 psc thickness* and extending to $R = 15$ kpc, and if it is observed with a 7.5-meter paraboloid like that actually used, having a beam width to half-power of 2°.8. The unit of intensity is that corresponding to black-body radiation at the temperature of the neutral interstellar hydrogen. Abscissae are radial velocities in km/sec.

Let us consider the curves for $l - l_c = 30°$ as an example. The radial velocity has a rather flat maximum of +86 km/sec, at a distance of 8.2 kpc. It is symmetrical about this point, becoming zero again at 16.5 kpc, where the line of sight intersects the circle with radius equal to the sun's distance from the center. At still larger distances it becomes negative. This run is depicted in the theoretical line contour of Figure 6. At distances beyond 2.5 kpc the acceptance cone of the 7.5-meter paraboloid will no longer be completely filled by the radiation from the thin layer of interstellar gas; this is why the curve already begins to fall off at $V = +60$ km/sec. It is planned to construct an instrument

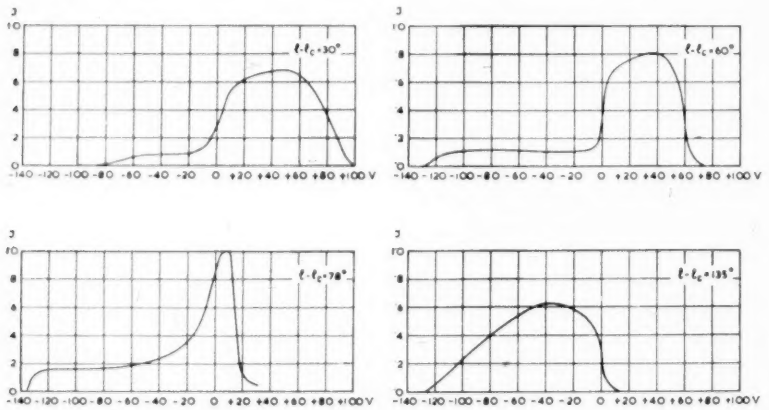

FIG. 6.—Line contours for observations of the 21-cm line, computed on the basis of uniform distribution of hydrogen.

with a 3.2 times larger aperture. With that instrument the measured intensity would become unity from about +65 to +86 km/sec and show a steep drop beginning at the maximum radial velocity of +86 km/sec. This would evidently allow an accurate determination of the rotational velocity at half the sun's distance from the center.

The toe shown by the line contour for negative velocities corresponds to matter situated at the other side of the system at distances from the center larger than that of the sun.

A rather provisional measure of the downward slope of the line contour just considered has been made at Kootwijk in June, 1951. This indicated an effective width of the emission line of about 70 km/sec, in good enough agreement with the predicted width of about 80 km/sec. That the matter observed at frequencies corresponding to the right-hand edge of the line contour is indeed at a large distance is shown by Figure 7. The three upper graphs illustrate the distribution of the line intensity in galactic latitude when the meas-

* *Note added to proof.*—This is the approximate equivalent thickness of the layer of B stars. There is evidence, however, indicating that the equivalent thickness of the *gas* layer is considerably higher. Van Rhijn (*Gron. Pub.*, No. 50, pp. 10 and 11) estimates it to be 240 psc. A similar thickness has been found for the layer of solid particles. It is probable, therefore, that the abscissae in Fig. 6 should be considerably increased for the larger distances.

urements are made at frequencies corresponding to the frequency of the undisplaced hydrogen line. They show the interstellar gas within roughly 1000 psc. of the sun. The tracings were made in right ascension, the vertical lines are 20 minutes of time apart. The spots at which the tracings intersected the galactic circle, and the corresponding galactic longitudes, are indicated by arrows. The galactic co-ordinates of the beginning and end of each tracing are also shown. The observations were made differentially, the receiver being switched 30 times per second between two frequencies, one of which is in the line and one outside, 110 kc/sec away. The bottom curve gives a similar tracing made at frequency 250 kc/sec below the normal frequency of the line, thus correspond-

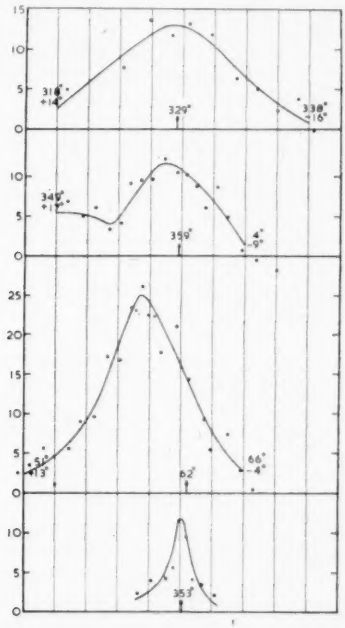

FIG. 7.—Distribution of intensity of hydrogen emission at 21 cm. The three upper curves were obtained at the normal frequency of the emission line, and refer presumably to interstellar matter within 1 kpc. The lower curve supposedly refers to matter at distances of the order of 9 kpc.

ing to a radial velocity of +55 km/sec. It is evident that this tracing is much narrower than the first three, indicating that the radiation comes from matter at a much greater distance. Its width is indeed no larger than would correspond to the beam width of the instrument.

The predicted line contours are, of course, meant only to give a schematic picture. It is likely that the actual curves will show important differences from those in Figure 6. If the gas in the Galactic System is concentrated in spiral arms, the observations of the line contours will probably indicate this.[12]

So far we have considered only the smoothed-out, over-all structure of the Galactic System. It is of evident interest also to investigate another aspect of its structure,

[12] NOTE ADDED MAY, 1952.—The first measures made by Mr. C. A. Muller with a greatly improved receiver indeed show big humps in the line contours, probably due to important concentrations of hydrogen at distances up to 8 kpc.

namely, the spiral-like formations that, judging from the analogy in other respects between the Galactic System and the later-type spiral nebulae, our stellar system presumably contains.

As has been pointed out particularly by Hubble and Baade, interstellar matter as well as the closely related early-type stars are of particular significance for the spiral structure. It even seems probable that, directly or indirectly, the interstellar gas is the determining factor for the origin of this structure. At one time I thought that the dynamics of spirals might perhaps be explained as the consequence of instability caused by the rapid contraction of interstellar gas in the equatorial plane. It may be, however, that the spiral forms are due to turbulence-like effects on interstellar matter, a hypothesis especially advocated by von Weizsäcker.

The most precise evidence concerning the relation of interstellar matter to spiral arms has been produced by Baade, who showed how closely emission nebulae as well as dark matter in the Andromeda Nebula are confined to spiral arms, which, in this case, appear to have a width of not more than 200 psc.

But also in the Galactic System the study of the distribution and motions of interstellar matter has made rapid progress. I need only refer to the subject of a former Russell lecture, in which Adams outlined the results of his observations of the multiple interstellar lines. These observations furnish the most systematic information on interstellar clouds. In a recent discussion Blaauw has considered the effects of the blending that must have been quite general for clouds with velocities less than about 10 km/sec. He concludes that the average peculiar velocity of the clouds in one co-ordinate is around 5 km/sec, and that a line of sight of 1 kpc length cuts, on the average, between 8 and 12 independent clouds.

A great deal of information may be expected from observations of the 21-cm line. From the few preliminary observations already made it has been possible to obtain a first rough estimate of the temperature as well as of the average density of neutral hydrogen in a region of about 1 kpc radius around the sun. As I have already indicated, observations in the direction of the center or anticenter of the system can inform us about the mean velocity of the clouds, as well as about the average absorption coefficient in the central part of the emission line. The mean random velocity in the line of sight is found to be about 5 km/sec, in good agreement with the value from the interstellar absorption lines. The absorption coefficient is observed to be roughly 1/kpc. The third observation we can make concerns the intensity in the central part of the line. It is clear that in combination with the known transition probability and with the fact that the two hyperfine-structure levels between which the transition takes place are almost equally populated, the measured intensity determines the number of neutral hydrogen atoms in the column of 1 kpc that is observed. We thus find that there is, on the average, about one *H* atom/cm^3. The same measurement of surface intensity also defines the black-body temperature corresponding to this transition. Ewen and Purcell found a value of 35°, but more recent measures in Australia and the Netherlands indicate that the temperature is rather higher, near 100°. This is an interesting datum, because it must be equal to the ordinary gas-kinetic temperature of the neutral hydrogen clouds. The value found gives a beautiful confirmation of the temperature that has been deduced by Spitzer and Savedoff in a theoretical way, from a consideration of the ionization and excitation processes in *H*I regions. They find about 50°, with an uncertainty that is considerably larger than the difference from 100° found from the 21-cm line.

This much about what the first rather tentative observations have indicated. Further observations may be expected to give considerably more. I have already mentioned the data on galactic rotation and on the general distribution of the interstellar gas. It is probable that with better equipment the complex structure of the 21-cm line can also be unraveled and that a great amount of information on motions and distribution of individual clouds will be obtained.

So far we have mainly discussed the *H*I regions. For *H*II regions important data have been obtained by the observation of the Balmer emission, started by Struve and widely extended by Strömgren and W. W. Morgan. From the systematic study of the emission regions, together with the comprehensive survey of O and B supergiants undertaken by Morgan and Nassau and by Luis Münch, Morgan has very recently been able to show that these objects are arranged in two long stretches that should most probably be identified with parts of spiral arms. It seems that thus for the first time success has been attained in revealing some of the spiral structure of our own stellar system.[13] This is evidently a step of the very greatest importance, and one that is likely to lead to a clarification of several unsolved problems, not only about galactic structure but likewise about the origin of spiral structure in general. The arms indicated by Morgan's investigation show striking resemblance with the arms defined by emission objects in the Andromeda Nebula. From the first evidence produced it seems that the galactic spiral rotates like a winding spring, with the convex side of the arms preceding.

The ionized regions also emit continuous radiation at radio frequencies, which should have a well-measurable intensity if observations are made near the Milky Way and with instruments of sufficient resolving power. In the surveys made so far, all with low resolving power, it is not possible to discern how much of the measured intensity is due to continuous radiation from ionized interstellar clouds and how much comes from the distant point-sources. The interstellar radiation is likely to be relatively more important at lower wave lengths.

For wave lengths less than a few meters the absorption coefficient of the gas is so small that we can probably neglect the absorption, even for paths of the order of the diameter of the Galactic System. This circumstance should render it possible to get a survey of the density distribution of ionized hydrogen through the entire system as soon as sufficiently large antennas have been built, if a way can be found to separate the interstellar radiation from that of other sources.

At the meter wave lengths the radiation between 50° and 120° longitude appears to be between two and three times larger than that in the corresponding region, between 170° and 240° longitude, on the other side of the center. Bolton and Westfold have attributed this, and particularly some more detailed features in Cygnus, to a spiral arm. It is noteworthy that Morgan's outline of the run of the spiral arms in our vicinity shows that the region between 170° and 240° longitude falls entirely in the open region between two arms. It is not yet clear whether the excess radiation comes from interstellar gas or from point-sources. This very interesting feature certainly deserves accurate further investigation.

The irregularity in the distribution of early-type stars and δ Cephei variables is well known. It is found in its extreme form in the Wolf-Rayet stars, as shown in Figure 8, taken from Miss Payne's book on *Stars of High Luminosity*. They are nearly all contained in two clusterings, in Cygnus and Carina, and in a more scattered group in the direction of the center. The Carina region is also exceptionally rich in faint O and B stars and in faint δ Cephei variables.

These features may partly be considered as local aggregates, though of very large size, and partly as revealing some of the large-scale structure of the Galactic System.

Ambarzumian puts the concentrations of Wolf-Rayet stars in the same general class as the groupings of early-type stars in general. These loose groups, stellar associations, aggregates, or relationships, as they have alternatively been called, are of particular interest. They have been known for a long time, ever since spectral classes have been determined, and several have been extensively investigated. It had also been realized that, because of their looseness, these clouds of early-type stars must be torn up by the effects

[13] A brief account of Dr. Morgan's investigation is given in *Sky and Telescope*, **11**, 134, 1952; see also *A.J.*, **57**, 3, 1952 (abstr.).

of differential galactic rotation in a period of the order of one revolution of the Galaxy and that therefore they must be comparatively young. During the last few years considerable work on the problems presented by the B-star clouds has been done by Ambarzumian and his co-workers at the Erevan Observatory, who have made a systematic search for and study of these "associations."[14] In particular, Ambarzumian has stressed their significance for the cosmogony of the massive stars. The most important new concept that, I believe, has first been suggested by Ambarzumian is that the associations are expanding. And this not only because of galactic rotation but also as an essential property of their own. This has proved to be a fertile idea, which seems, in a somewhat unexpected manner, to give an insight into the origin and the meaning of these groups.

In a still unpublished investigation on a group of B stars surrounding ζ Persei,[15] Blaauw has succeeded in proving such an expansion by direct observation. This loose clustering, measuring about 40×20 psc, is situated between 12° and 20° southern galactic latitude, at a distance of roughtly 300 psc. The reality of the relationship between the stars can hardly be doubted. However, in 1944, when he first discovered the group, Blaauw was already struck by the fact that the proper motions of the members showed rather unexpected divergences. Recently he has determined independent new

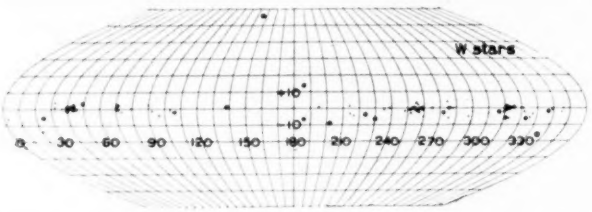

FIG. 8.—Distribution of Wolf-Rayet stars (from a tabulation in *The Stars of High Luminosity* by Cecilia H. Payne).

proper motions, in the same way as H. R. Morgan has determined the proper motions of his N30 system. These new proper motions confirm the divergences found previously and prove that the group is expanding at a rate of $0''.0028 \pm 0''.0004$ m.e. per year and per degree distance from its center. This surprisingly rapid expansion, which averages about 12 km/sec, corresponds to an age of only 1.3 million years (with a mean error of about 14 per cent). The actual motions are illustrated in the accompanying diagram (Fig. 9). Low though this age may seem, it is entirely compatible with the age that may be ascribed on theoretical grounds to the most luminous members of the group, like the O star ξ Persie.

The most straightforward interpretation of these observations is that the members of this group were formed about thirteen hundred thousand years ago as a consequence of a dense conglomeration of interstellar clouds with "turbulent" motions of the order of 5 km/sec. These velocities now show up roughly as an expansion of the group, which has already grown very considerably since its birth. Even today the whole region is full of dark as well as luminous interstellar matter, as is well shown on a picture of this region in Barnard's *Atlas of the Milky Way*. An especially interesting feature is the small and rather compact cluster of faint stars south of o Persei. The Russian investigators have drawn attention to the frequent occurrence of such open clusters as a sort of nuclei in the large associations. Another well-known example is the Trapezium cluster in Orion. I believe this is the first direct evidence of the birth of stars from interstellar clouds. A re-

[14] *Abh. Berlin Akad., Kl. f. Math. u. allg. Naturw.*, No. 2, 1950; and *A.J.U.S.S.R.*, **26**, 3 and 329, 1949.

[15] Now appearing in print in *B.A.N.*, Vol. **11**, No. 433, 1952.

markable thing is the extremely short time in which these stars must have contracted from interstellar clouds into actual stars. The available time is only barely long enough for a cloud with a radius of the order of 1 psc to contract under its own gravitation.

It is likely that the ζ Persei aggregate is rather exceptional in the rapidity of its expansion. At least it is certain that in the other B-star clouds for which data are available the expansions are considerably less rapid. By far the longest-and best-known association of B stars is the large Scorpio-Centaurus cloud. The most complete investigation has again been made by Blaauw.[16] It is the only B-star group for which the space distribution can be determined. It is considerably larger than the ζ Persei group and has a strikingly oblong shape, with a long axis of about 290 psc, the other axes being about 100 and 70 psc, respectively. It is tempting to suppose that this aggregate has also formed from a

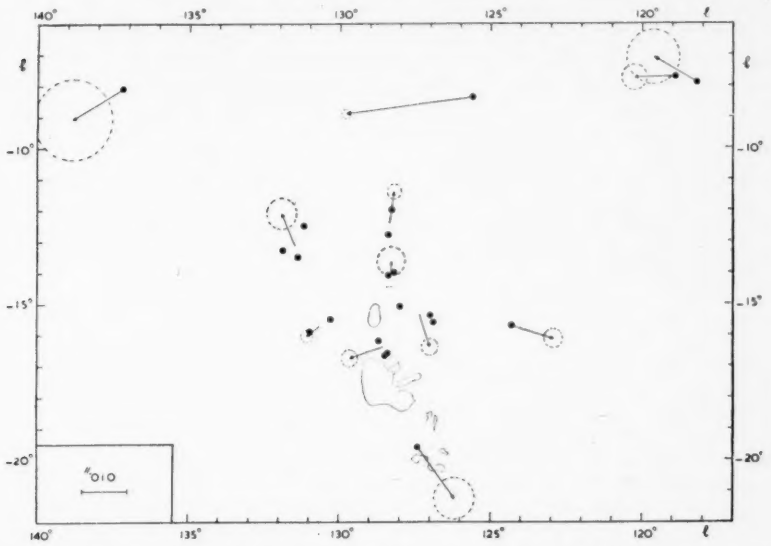

FIG. 9.—Proper motions of stars in Blaauw's ζ Persei group. The stars are plotted in galactic co-ordinates. The arrows show the relative proper motions; some of them refer to the mean of two or three stars that are close together. The radii of the dotted circles indicate the probable errors of the motions. The four stars in the upper part of the diagram have no relation to the group (cf. Blaauw, *B.A.N.*, No. 433).

much smaller conglomeration of interstellar clouds, the stars having dispersed as a consequence of motions in this conglomeration. The motions of the stars are not yet known with sufficient accuracy to determine the amount of expansion, but they suffice to show that it is much smaller than in the case of the ζ Persei group, probably not much larger than 1 km/sec. The Scorpio-Centaurus cloud does not contain very bright supergiants; the ages of the brightest stars might be estimated to be of the order of 50 or 100 million years. Blaauw has noted that both the strong elongation of the group and its orientation in space can be understood as the natural consequence of expansion combined with the differential rotation of the Galactic System. In fact, if an expansional velocity of 1 km/sec is assumed, the cloud would in 60 million years have got the dimensions, the amount of elongation, as well as the orientation in space, that are observed today.[17]

[16] *Pub. Kapteyn Lab. Groningen*, No. 52, 1946.

[17] A. Blaauw, *op. cit.*, p. 414.

As Blaauw has remarked, clouds like this are frequently observed in later-type spirals, where parts of broken-up arms are sometimes considerably inclined to the tangential direction. It is clear that, if this is the correct interpretation of these features, the spirals must rotate again like winding springs.

It is, of course, impossible in the compass of this lecture to give a survey of all the problems concerning galactic structure, not even when limiting the discussion to the more general features. My choice of topics has naturally been influenced by the things with which I have recently been in contact. But also I have primarily selected problems that have reached the stage where at least *some* general insight and understanding appear to have been attained.

I regret particularly that, because of this choice, there is no opportunity to discuss the entire domain of research dealing with the distribution in the galactic plane of the more common stars. Especially by such investigations as have been carried out at Harvard and at the Warner and Swasey Observatory here in Cleveland, evidence of the fairly large-scale unevenness in the distribution of these stars has been rapidly accumulating. But it has not yet been possible to draw a coherent picture of the observed variations in star density and in mixture of spectral types, or to discover the relation that should exist between the density variations and that other striking deviation from a smooth state that has long been known, namely, the difference of about 20° between the vertex of the star-streaming of the brighter stars and the longitude of the galactic center.

It appears probable, however, that, with the accumulation of more, and especially more accurate, data, the near future will bring a solution of these problems, as well as of the intriguing problem of the relation between the distribution of the common stars and the galactic spiral arms.

A STUDY OF THE ORION AGGREGATE OF EARLY-TYPE STARS

STEWART SHARPLESS
Yerkes Observatory
Received June 10, 1952

ABSTRACT

A catalogue of spectroscopic and photoelectric observations of 190 members of the Orion aggregate is given. The photoelectric observations were made with the 82-inch and 13-inch reflectors of the McDonald Observatory; the spectrograms were taken with the 40-inch refractor of the Yerkes Observatory. A spectroscopic distance modulus of 8.5 mag. was obtained for the aggregate. This material has also made possible an investigation of the anomalous reddening in Orion, the absolute magnitudes of the O-type stars associated with the aggregate, and the radial distribution of color excess within the Orion Nebula. The high ratio of total to selective absorption found by Baade and Minkowski for the Trapezium stars is found to apply also to other reddened stars in the aggregate; however, their hypothesis of a transparent region in the center of the nebula is not confirmed. The correlation between reddening and the diffuse interstellar features in the spectra of the Orion stars is discussed.

I. INTRODUCTION

Investigations of the great aggregates of early-type stars such as h–χ Persei, the Cygnus region, and Orion have proved to be of considerable importance in the field of galactic structure. The work of Hubble[1] and Baade[2] on extragalactic nebulae has shown that spiral arms consist primarily of just such concentrations of bright blue stars as well as regions of ionized hydrogen and obscuring matter. In these three respects, the Orion aggregate is a typical population I object. Recent results have indicated that a knowledge of the detailed structure of our own galaxy[3] in the vicinity of the sun can be obtained through investigations of the B-star aggregates and the *H* II regions.

Various methods have been employed in the past to obtain the parallax of the Orion Nebula or of the aggregate of early-type stars with which it is associated. Some of them, however, have led to widely differing results. The present investigation is based on a series of spectroscopic and photoelectric observations of the brighter B stars in Orion obtained recently at the Yerkes and McDonald Observatories. These are described in Sections III and IV below. In Sections V and VI the problem of the spectroscopic parallax of the Orion aggregate and of the stars in the immediate vicinity of the nebula is reexamined in the light of these new data.

Photoelectric observations of the colors and magnitudes of B stars in an aggregate which suffer various amounts of interstellar absorption can be used to investigate the relation between reddening and total absorption for the region considered. This problem is discussed in Sections V and VII, and the results are used in evaluating the total absorption for the Orion stars. The color excesses of the stars immersed in the Orion Nebula are also considered in Section VI.

The determination of the absolute magnitudes of the O-type stars has presented a difficult problem because of their scarcity and the fact that they are often associated with dense nebulosity, which makes it difficult to evaluate their interstellar absorption accurately. Since a number of O stars are associated with the Orion aggregate, their absolute magnitudes can be obtained from their colors and magnitudes and the distance modulus of the aggregate. These results are listed in Section V.

A possible explanation of the anomalous reddening in Orion is discussed in Section VIII, and an attempt is made to correlate it with existing observations of the diffuse interstellar features in the spectra of the Orion stars.

[1] *Ap. J.*, **63**, 236, 1926; **69**, 103, 1929.

[2] *Problems of Cosmical Aerodynamics* (Dayton, Ohio: Central Air Documents Office, 1951), p. 185.

[3] Morgan, Sharpless, and Osterbrock, *A.J.*, **57**, 3, 1952.

II. HISTORICAL

The first attempt to obtain the distance of the Orion Nebula was made by Pickering[4] in 1917 and was based on a statistical investigation[5] of the brightness of the stars within about 1° of the nebula. Color indices were found by comparing photographic magnitudes with visual magnitudes determined earlier by Bond. Counts of the blue stars in this region indicated a frequency maximum at 13.0 mag. and a mean magnitude of 10.5. An average spectral type of B3 and a mean absolute magnitude of −1 was assumed for these stars, and a distance of 2000 parsecs was obtained.

Kapteyn,[6] in the same year, investigated the somewhat larger group of B stars, which he designated the "Nebula-group," extending from R.A. 5^h20^m to 5^h40^m and Dec. −7° to +2°. A mean parallax for the B stars in several regions outside the Nebula-group was obtained from an analysis of proper motions in the Boss catalogue. The frequency-curves of apparent magnitudes for the Nebula-group and the surrounding regions were then compared, to find the ratio of the parallaxes for the stars within and outside the Nebula-group. From this, a parallax of $0''.0054 \pm 0''.0009$ was adopted for the Orion stars, corresponding to a distance of 185 parsecs.

These two determinations of the distance of the Orion Nebula were discussed by Pickering[7] in 1919. The discrepancy between the two values was attributed primarily to the differences in the selection of the stars considered, since Kapteyn included in his investigation only the brighter B stars surrounding the nebula. The faintness of the stars investigated by Pickering, hence the overestimation of their distance, is probably due to the greatly increased absorption in the region of the nebula and to the fact that he may have included more distant field stars. Adopting more recent values for the absolute magnitudes of the B stars, Pickering revised his value of the parallax of the nebula to $0''.0020$, which corresponds to 500 parsecs. An important result of this investigation was the recognition of the great range of intrinsic luminosity among the B-type stars. The dwarf nature of the variable stars in the nebula was also established in this discussion.

Pannekoek,[8] in 1929, in his investigation of the B stars in the *Henry Draper Catalogue* found a concentration in Orion elongated parallel to the galactic plane from 5^h18^m, +5°, to 5^h32^m, −7°.5. He distinguished three subgroups centered on ψ Orionis, the "belt," and the "sword" of Orion but assumed that they formed a physically connected system. He ascribed the great differences in apparent brightness of the Orion stars both to differences in intrinsic brightness and to interstellar absorption. From mean absolute magnitudes for the Draper classes he derived an apparent distance modulus of 7.6 mag., corresponding to a distance of 330 parsecs. Plots made by Pannekoek of the distribution of A stars in the Orion region indicate no concentration for those stars brighter than 8.75 mag. but indicate a decided concentration for those between 8.75 and 9.25 mag. For the K stars brighter than 9.25 mag. in this region there appears to be no concentration.

In 1931 the Trapezium cluster[9] was discovered by Trumpler. A photograph, taken in the spectral region from 7000 to 7600 A in order to suppress the nebulosity, showed a small cluster centered on θ^1 Orionis and containing sixty-two stars within a radius of two minutes of arc. Apparent distance moduli were found for sixteen stars in the cluster from their spectral types and apparent magnitudes. A mean absorption of 0.6 mag. was estimated from the observed color excesses. The distance of the Trapezium cluster thus obtained was 500 parsecs. Another determination based on the classification and angular diameter of the cluster yielded a distance of 690 parsecs. The same two methods were then applied to NGC 1981, which lies 1° south of the Trapezium cluster and which was assumed to be at the same distance. A final mean of 540 parsecs was adopted by Trumpler as the distance to the Orion Nebula.

[4] *Harvard Circ.*, No. 205, 1917.
[5] *Harvard Ann.*, Vol. **32**, 1895.
[6] *Ap. J.*, **47**, 146, 1918.
[7] *Pub. A.S.P.*, **31**, 86, 1919.
[8] *Pubs. Astr. Inst. Amsterdam*, No. 2, 1929.
[9] *Pub. A.S.P.*, **43**, 255, 1931.

The Trapezium cluster was later independently discovered by Baade and Minkowski.[10] As compared with other clusters of similar stellar content, it was found to be smaller than average by a factor of about ten. Baade and Minkowski concluded that it is a normal cluster which is blotted out by the obscuring matter of the nebula except for a small region about the Trapezium, i.e., that in the immediate vicinity of the exciting stars the nebula is less opaque than elsewhere. To obtain more data on the optical properties of the nebula, three of the Trapezium stars, θ^1 (A), (C), and (D) Orionis, were investigated spectrophotometrically and the resulting extinction-curves were found to deviate appreciably from those of reddened B stars in other parts of the sky. This peculiarity in the reddening of θ^1 Orionis has been confirmed by the six-color observations of Stebbins and Whitford.[11] Baade and Minkowski analyzed their extinction-curves on the basis of the known optical constants of iron and carbon and found that the effective size of the absorbing particles in the Orion Nebula was larger by a factor of 2 than in other regions. They attributed this to the effect of radiation pressure from the exciting stars which has removed the smallest particles, shifting the frequency maximum to a larger size. A new determination of the distance of the Orion Nebula was later made by Minkowski[12] in the light of this investigation. After making certain assumptions regarding the properties of the interstellar dust in the center of the nebula, the total absorption was estimated, and the resulting corrected distance modulus was found to be 7.38 mag., corresponding to a distance of 300 parsecs.

A study of the Orion region was made by Markowitz[13] in 1948, based on spectroscopic, photometric, and radial-velocity data available at that time. Stars in the central region of Orion, i.e., the region of the "sword" and "belt," were found to have a mean radial velocity of about 9 km/sec greater than the value expected from the solar motion and galactic rotation. Having thus confirmed the existence of an extended cluster of B stars in Orion, he obtained a spectroscopic distance modulus of 8.57 mag. from observations of normally colored stars of spectral types B1–B3 in Orion. This value agrees well with the one found in the present investigation.

It is apparent that the aggregate of B stars in Orion and the stars in the immediate vicinity of the Orion Nebula have often in the past been treated separately, even though there is little doubt as to their physical connection and common distance. In the present investigation an attempt has been made to obtain observations which are as homogeneous as possible of stars throughout the entire region. Special emphasis, however, has been placed on the region within several degrees of the Orion Nebula with regard to both the spectroscopic and the photoelectric observations. The limits of the Orion aggregate have been taken to be from R.A. 5^h00^m to 5^h48^m, and from Dec. $+6°$ to $-8°$.

III. SPECTROSCOPIC OBSERVATIONS

Spectral classifications for many of the B stars in Orion were determined from slit spectrograms taken with the one-prism spectrograph attached to the 40-inch telescope. The dispersion is about 125 A/mm at $H\gamma$. Many of the plates[14] were taken for the Yerkes program of spectroscopic parallaxes. In addition, a special program was undertaken with the same equipment to obtain spectrograms of most of the remaining B stars in Orion brighter than 8.0 mag. and various fainter stars of special interest, particularly in the nebulous regions. Spectral types and luminosity classes were assigned to these stars according to the criteria of the Yerkes *Atlas of Stellar Spectra*.[15] Many of the brighter Orion stars are fundamental O- and B-type standards in the MKK system.

Special attention was given to the region 5° in diameter centered on the Orion Nebula.

[10] *Ap. J.*, **86**, 119 and 123, 1937.
[11] *Ap. J.*, **102**, 318, 1945.
[12] *Pub. A.S.P.*, **58**, 356, 1946.
[13] *A.J.*, **54**, 111, 1948.
[14] Dr. W. W. Morgan kindly put these plates at the author's disposal.
[15] By Morgan, Keenan, and Kellman (Chicago: University of Chicago Press, 1943).

Spectral types from slit spectrograms of about thirty-five B stars in this region were determined, and spectral types for the remaining stars to about the tenth magnitude were estimated from two objective-prism plates taken with the 24–36-inch Schmidt camera of the Warner and Swasey Observatory.[16] Stars whose spectral types were known from slit spectrograms were used to set up a sequence of standards on the objective-prism plates, and the remaining stars were classified according to these. The intensities of the *He* I lines and the visibility of the K line were used as criteria.[17] The accuracy of the classification of the objective-prism spectra is necessarily somewhat lower than that of the slit spectrograms. It is sufficient, however, for the assignment of normal colors, which will be used in investigating the color excesses in this region.

IV. PHOTOELECTRIC OBSERVATIONS

The photoelectric observations of the colors and magnitudes of the B stars in Orion were made in November and December, 1951, at the McDonald Observatory. Observations were made on eleven nights with the 13-inch and three nights with the 82-inch telescopes. The time with the 13-inch was devoted primarily to the B stars in the Orion aggregate brighter than 8.0 mag. in relatively unobscured areas. This limiting magnitude corresponds approximately to spectral type B8. Several multiple stars in this category could not be observed because of the limited resolving power of the 13-inch. The 82-inch observations were restricted to the following B stars in Orion: (1) stars involved in bright nebulosity where a high resolving power is necessary to evaluate the brightness of the nebula in the immediate vicinity of the star, (2) close multiple stars, and (3) highly obscured stars in the region of the nebula and elsewhere. While almost all the brighter stars in the aggregate were observed, it was not possible to obtain completeness in the case of the fainter stars. For the latter, priority was given to those for which slit or objective-prism spectra were available.

The same photometer and amplifier were used for both the 13-inch and the 82-inch observations. The amplifier was designed and constructed by H. L. Johnson, and both the amplifier and the photometer have been described elsewhere.[18] An independent calibration of the gain of the amplifier in terms of magnitude steps was made during the interval over which the observations extended. This calibration was used in the computation of the magnitudes. Observations were made through three filters, a Corning 3384 (yellow), a Corning 5030 + Schott GG 13 (blue), and a Corning 9863 (ultraviolet). The effective wave lengths of the filter-photomultiplier combination are approximately 5540, 4420, and 3550 A. A Brown recording potentiometer was used to record the observations.

The deflections were made symmetrically in the three colors. Only the results of the blue and yellow deflections will be discussed in this paper. In practically every case the star deflections were followed immediately by a sky reading with the same diaphragm and a deflection from a standard light-source. All star deflections were corrected for sky in the usual manner and were referred to the standard source in order to eliminate the effects of cell fatigue. The observed colors, C_{y0}, and the observed magnitudes, m_{y0}, both uncorrected for extinction, were computed as follows:

$$C_{y0} = 2.5 \log \frac{y}{b},$$

$$m_{y0} = -2.5 \log \frac{y}{100},$$

where y and b represent the yellow and blue deflections.

[16] The author is indebted to Dr. J. J. Nassau for the use of these plates.

[17] W. W. Morgan, *Pub. Obs. U. Michigan*, Vol. **10**, 1951.

[18] H. L. Johnson and W. W. Morgan, *Ap. J.*, **114**, 522, 1951.

The extinction determinations were made following the method of Johnson and Morgan.[19] Ten stars of differing color and in different parts of the sky were selected as extinction standards: 10 Lac, HR 875, α Ari, HR 8832, β Cnc, η Hya, π^3 Ori, π^4 Ori, υ Ori, and Cin 705. When possible, two observations were made of each extinction star on each night: one observation at culmination and one at two or more air masses. On the nights when the 82-inch was used, fewer observations were made on these stars, and four additional standards—HD 37526, 36559, 35640, and 37481—within 3° of the Orion Nebula were each observed twice in the same manner. It was assumed for each extinction observation that C_y, the color of an extinction star outside the atmosphere, is given by the relation

$$C_y = C_{y_{mi}} - K_m \sec z_{mi} ,$$

where $C_{y_{mi}}$ and Z_{mi} are the observed color and the zenith distance for the ith observation on the mth night, and K_m is the color extinction coefficient for that particular star on the mth night. For each extinction star a simultaneous least-squares solution was made over all nights for a single value of C_y and the various K_m's. This method assumes

TABLE 1

EXTINCTION COEFFICIENTS

Date 1951	K_1	K_2	Date 1951	K_1	K_2
Nov. 6	0.075±0.003	−0.033±0.004	Nov. 19	0.081±0.003	−0.027±0.004
Nov. 7	.095	− .024	Nov. 20	.084	− .031
Nov. 8	.087	− .030	Nov. 26	.082	− .028
Nov. 12*	.086	− .027	Nov. 27	.098	− .018
Nov. 13	.084	− .029	Nov. 28	.094	− .025
Nov. 14	.092	− .025	Dec. 2	.085	− .026
Nov. 18	0.089	−0.026	Dec. 6	0.069	−0.035

* Mean coefficients were used on this night because of the insufficiency of extinction observations.

that the color of the extinction star outside the atmosphere is the same on all nights, and greater leverage in the least-squares solution for nightly extinction coefficients is thus obtained. The computed values of C_y and K_m were then regrouped according to nights, and for each night it was assumed that the relation

$$K_m = K_1 + K_2 C_y$$

was valid for all the extinction stars. For each night the coefficients K_1 and K_2 were computed by least squares. The individual values of K_1 and K_2 are listed in Table 1. Natural colors were then computed for all the observed stars by means of the relation

$$C_y = \frac{C_{y_0} - K_1 \sec z}{1 + K_2 \sec z} .$$

The values of C_y for the extinction stars resulting from the above-mentioned least-squares solution are not of the highest accuracy, since the weight of the observations is divided in the solution among C_y and about ten extinction coefficients. Consequently, values of C_y for the extinction stars were recomputed by means of the above formula. Separate averages of these values were then made for the observations with the 82-inch

[19] *Loc. cit.*

and 13-inch telescopes. A comparison of these values indicated a small zero-point difference between the two telescopes amounting to 0.015 mag. This probably arises from slightly different reflective properties of the two mirrors. All observations made with the 82-inch were corrected by this amount to put them on the color system of the 13-inch.

It was not possible to compute nightly magnitude extinction coefficients in the same manner as the color extinction coefficients because of night-to-night variations in the absolute sensitivity of the equipment and in the intensity of the standard light-source. Thus a mean magnitude extinction coefficient, $\bar{Q}_y$, was computed by least squares for each extinction star, using as the equation of condition:

$$m_y = m_{y0} - \bar{Q}_y \sec z ,$$

where m_y is the magnitude outside the atmosphere referred to a full-scale deflection. It was then assumed that, for each extinction star,

$$\bar{Q}_y = \bar{Q}_{y_1} + \bar{Q}_{y_2} C_y .$$

The quantities $\bar{Q}_{y_1}$ and $\bar{Q}_{y_2}$ were computed by least squares, with the result that

$$\bar{Q}_{y_1} = 0.129 ,$$

$$\bar{Q}_{y_2} = -0.004 .$$

The ratio of Q_{y_1} and the mean of K_1 was found, and similarly the ratio of Q_{y_2} and the mean of K_2. This ratio was assumed to be the same on all nights, and the nightly magnitude extinction coefficients, Q_{y_1} and Q_{y_2}, were then given by the relation

$$Q_{y_1} = 1.506 K_1 ,$$

$$Q_{y_2} = 0.157 K_2 .$$

Natural magnitudes could then be computed from the relation

$$m_y = m_{y0} - (Q_{y_1} + Q_{y_2} C_y) \sec z .$$

Zero-point corrections to the magnitudes were found from the nightly means of m_y for the ten standard stars. This correction arises from the night-to-night variability of the standard source. A mean of all the 13-inch observations of m_y for each standard star and the deviation from the mean of each value of m_y were found. For a given night the deviations were averaged to obtain the zero-point corrections, Z, for all observations made on that night. These corrections ranged from 0.001 to 0.161 mag., with an average probable error of $\pm .003$ mag. The 82-inch observations were then referred to the means of the 13-inch observations, and the zero-point corrections for these nights were found in the same way. The quantity mag_y was then computed for all observations where

$$\mathrm{mag}_y = m_y + Z + S ,$$

where S is a correction to refer all observations to the same amplifier gain.

The following equations of condition were used to relate the natural system of colors and magnitudes described above to the $B - V$ system:[20]

$$B - V = A + BC_y ,$$

$$V = \text{mag}_y + C + D\,(B - V) .$$

In addition to the observations of the ten extinction stars, from one to five observations each were made of twenty-six stars in various parts of the sky for which V and $B - V$ had been observed by Johnson. The means of these observations were then used to solve for the four transformation coefficients by least squares. In the least-squares solution the means of the values of C_y and mag_y of the ten extinction stars were given weights

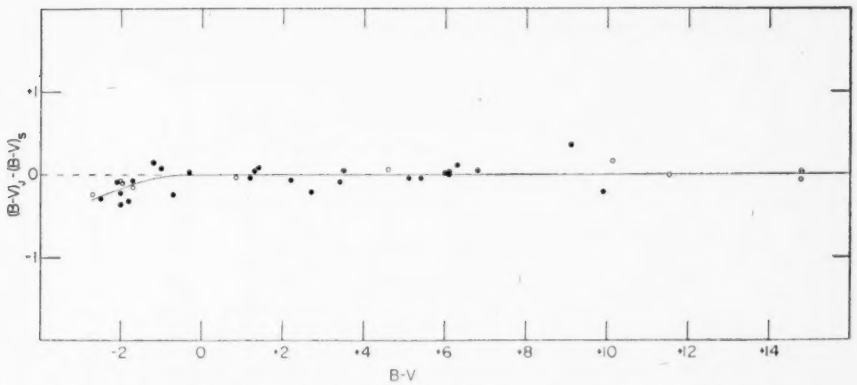

FIG. 1.—A comparison between the colors obtained by Johnson and those by Sharpless. The solid line represents the adopted transformation. The open circles represent the ten extinction standards.

corresponding to five observations, although the actual number of observations of each was considerably greater. The coefficients of the transformation were found to be:

$$\begin{aligned} A &= 0.916 \pm 0.003 , \\ B &= 1.131 \pm 0.004 , \\ C &= -0.614 \pm 0.004 , \\ D &= -0.086 \pm 0.006 . \end{aligned}$$

Values of V and $B - V$ were then computed for the thirty-six standard stars by the use of the transformation derived above. Figure 1 gives a comparison between these values and those obtained by Johnson. The open circles represent the ten extinction stars and consequently have greater weight. This comparison indicates a slight non-linearity at the extreme blue end of the color system derived here as compared with that of Johnson. This is interpreted as due to a slightly different ultraviolet cutoff of the blue filters used in the two investigations. Although the filters are of the same type, their characteristics are evidently not identical. The observed colors of the bluest stars are thus quite sensitive to the slightly different amount of ultraviolet light transmitted.

All observations of blue stars were corrected by the necessary amount, as read from Figure 1, to put them on the $B - V$ system as defined by Johnson. Table 2 lists the natural and transformed magnitudes and colors of the thirty-six standard stars. The

[20] H. L. Johnson and W. W. Morgan, unpublished.

values of V and $B - V$ listed in Table 2 have been corrected for the nonlinearity described above. For comparison, the observations of Johnson have been included. All observations of the Orion stars were similarly transformed.

The internal probable errors for the natural colors and magnitudes were computed on the basis of those Orion stars which were observed two or more times, and were found to be:

$$\left.\begin{aligned} C_y\text{: p.e.} &= \pm 0^{m}.008 \\ m_y\text{: p.e.} &= \pm 0^{m}.012 \end{aligned}\right\} \text{for one observation .}$$

The observations on which these probable errors are based were made at an average air mass of about 1.5.

The results of the observations of the Orion stars are given in Table 3. The first column

TABLE 2

COLORS AND MAGNITUDES OF STANDARD STARS

Star	Sp.	$\bar{C}_y$	$\overline{\text{mag}_y}$	$B-V$*	$B-V$†	V*	V†	No.
β Cas	F2 IV	−0.505	2.920	+0.35	+0.345	2.25	2.28	2
50 And	F8 IV–V	−0.329	4.765	+0.54	+0.544	4.08	4.10	5
HR 483	G2 V	−0.263	5.621	+0.63	+0.618	4.94	4.95	5
β Ari	A5 V	−0.694	3.289	+0.14	+0.131	2.62	2.56	5
α Ari	K2 III	+0.210	2.717	+1.153	+1.154	1.99	2.00	18
δ Tri	G0 V	−0.271	5.519	+0.61	+0.609	4.86	4.85	3
16 Per	F2 III	−0.502	4.871	+0.34	+0.348	4.22	4.23	2
HR 875	A1 V	−0.732	5.775	+0.085	+0.088	5.17	5.15	18
ι Per	G0 V	−0.281	4.713	+0.60	+0.598	4.04	4.05	5
κ Cet	G5 V	−0.213	5.500	+0.68	+0.675	4.82	4.83	4
ϵ Eri	K2 V	−0.038	4.401	+0.91	+0.873	3.75	3.71	4
ζ Per	B1 Ib	−0.699	3.465	+0.13	+0.125	2.83	2.84	4
ϵ Per	B0.5 V	−0.954	3.479	−0.17	−0.17	2.88	2.88	4
π^3 Ori	F6 V	−0.408	3.838	+0.46	+0.454	3.16	3.19	22
π^4 Ori	B2 III	−0.947	4.272	−0.17	−0.17	3.70	3.67	20
β Eri	A3 III	−0.701	3.403	+0.12	+0.123	2.77	2.78	2
β Ori	B8 Ia	−0.839	0.770	−0.03	−0.033	0.15	0.16	1
τ Ori	B5 III	−0.905	4.173	−0.10	−0.108	3.60	3.57	2
HD 35299	B1 V	−0.988	6.264	−0.21	−0.22	5.71	5.67	2
HD 35899	B5 V	−0.929	8.123	−0.12	−0.14	7.56	7.52	2
HD 36591	B1 V	−0.967	5.911	−0.20	−0.19	5.36	5.31	2
Cin 705	M1 V	+0.495	8.704	+1.48	+1.476	7.96	7.96	18
υ Ori	B0 V	−1.027	5.200	−0.27	−0.27	4.59	4.61	18
α Lep	F0 Ib	−0.610	3.205	+0.22	+0.226	2.61	2.57	1
ι Ori	O9 III	−1.006	3.348	−0.25	−0.25	2.74	2.75	2
ϵ Ori	B0 Ia	−0.955	2.264	−0.20	−0.18	1.71	1.66	1
κ Ori	B0.5 Ia	−0.940	2.682	−0.18	−0.16	2.04	2.08	1
δ Aur	K0 III	+0.084	4.405	+0.99	+1.011	3.69	3.70	2
χ^2 Ori	B2 Ia	−0.552	5.243	+0.27	+0.291	4.63	4.60	1
ι CMa	B3 II	−0.850	5.024	−0.07	−0.046	4.36	4.41	2
β Cnc	K4 III	+0.502	4.260	+1.478	+1.484	3.53	3.52	15
η Hya	B3 V	−0.974	4.879	−0.196	−0.20	4.31	4.28	13
10 Lac	O9 V	−0.980	5.472	−0.200	−0.21	4.87	4.88	20
HR 8832	K3 V	+0.071	6.255	+1.013	+0.996	5.56	5.56	20
υ Peg	F8 IV	−0.274	5.092	+0.61	+0.606	4.38	4.43	1
ι Psc	F8 V	−0.355	4.788	+0.51	+0.514	4.13	4.13	2

* From H. L. Johnson and W. W. Morgan, unpublished.

† Computed values.

TABLE 3

OBSERVATIONS OF STARS IN THE ORION AGGREGATE

Star	V	$B-V$	ϵ	Sp.	E_y	Remarks
30836	3.67	−0.17	2	B2 III	+0.06	π^4 Ori
31237	3.70	− .20	5	B2 III	+ .03	π^5 Ori (var.)
−3°1013	10.12	+ .24	6	B9 V	+ .31	
33647	6.68	− .05	6	B8 V	+ .05	
34179	8.02	− .03	6	B8 V	+ .07	
34317	6.41	− .02	6	A0 V	− .02	
34511	7.39	− .10	6	B5 V	+ .06	
34748	6.30	− .10	6	B1.5 V	+ .15	
34959	6.50	− .11	6	B5p	+ .05	
34989	5.78	− .13	6	B1 V	+ .14	
35007	5.65	− .12	6	B3 V	+ .08	
35008	7.09	− .11	8			
35039	4.72	− .16	6	B2	+ .07	22 Ori
35079	7.06	− .03	6	B3 V	+ .17	
35149				B2		23 Ori
35203	7.97	− .09	8	B6 V	+ .06	
35298	7.88	− .14	6	B9 V	− .07	
35299	5.67	− .22	6	B1 V	+ .05	
35407	6.31	− .16	6	B5 V	.00	
35411	3.33	− .19	6	B1 V	+ .08	η Ori
35439	4.92	− .21	6	B2e	+ .02	25 Ori
35501	7.42	− .06	6	B8 V	+ .04	
35502	7.35	− .03	6	B5 V	+ .13	
35575	6.41	− .17	6	B3 V	+ .03	
35588	6.15	− .18	6	B3 V	+ .02	
35640	6.24	− .05	3	B9 V:	+ .02	
35673	6.50	.00	6	B9 V	+ .07	
35715	4.56	− .23	6	B2	.00	ψ Ori
35718	8.72	+ .03	6	B8–9	+ .11	OP
35730	7.20	− .15	6	B5p	+ .01	
35762	6.74	− .18	6	B2 V	+ .05	
35777	6.60	− .18	6	B2 V	+ .05	
35792	7.20	− .14	6	B3 V	+ .06	
35834	7.67	− .05	6	B8 V	+ .05	
35881	7.77	− .09	6	B8 V	+ .01	
35882	7.74	− .06	8			
35899	7.52	− .14	6	B5 V	+ .02	
35901	9.04	− .02	8	B8–9	+ .06	OP
35910	7.58	− .10	6	B6 V	+ .05	
35912	6.35	− .18	6	B2	+ .05	
36012	7.24	− .10	6			
36013	6.88	− .13	6	B1.5 V	+ .12	
36120	7.96	− .03	6	B8–9	+ .05	OP
36133	6.94	− .09	8	B2 V	+ .14	
36151	6.71	− .13	8	B5 V	+ .03	
36166	5.76	− .20	6	B1.5 V	+ .05	
36219	7.59	− .06	6			
36234	8.64	− .07	6	B8–9	+ .01	OP
36267				B5 V		32 Ori
36285	6.33	− .17	8	B1.5 V	+ .08	
36324	9.00	+ .08	8	A0	+ .08	OP
36351	5.42	− .18	6	B1.5 V	+ .07	33 Ori
−3°1119	10.33	+ .21	8	B8–9	+ .29	OP
36366	8.09	+ .12	8	A0	+ .12	OP
36392	7.56	− .14	6	B3 V	+ .06	
36411	9.71	+ .10	8	B8–9	+ .18	OP
36429	7.56	− .13	6	B5 V	+ .03	
36430	6.23	− .15	8	B2 V	+ .08	
36486	2.19	− .21	6	O9.5 II	+ .10	δ Ori (var.)
36487	7.81	− .11	8	B8–9	− .03	OP
36512	4.61	− .27	2	B0 V	+ .03	υ Ori
36513	9.50	+0.03	8	B8–9	+0.11	OP

TABLE 3—*Continued*

Star	V	$B-V$	n	Sp.	E_{B-V}	Remarks
36527	9.48	+0.14	8	A		OP
36540	8.11	+ .05	8	B8–9	+0.13	OP
36541	7.69	− .08	8	B8–9	.00	OP
36550				B8–9		OP
36559	8.81	− .05	4	B8–9	+ .03	OP
36560	8.28	− .09	8	B8–9	− .01	OP
36591	5.31	− .19	6	B1 V	+ .08	
36607	9.23	− .04	8	B8–9	+ .04	OP
36627	7.56	− .11	6	B6 V	+ .04	
36629	7.64	+ .02	8	B2 V	+ .25	
36646				B3 V		
36655	8.60	− .04	3	B8–9	+ .04	OP
36670	8.94	− .01	8	B8–9	+ .07	OP
36695	5.31	− .17	6	B1 V	+ .10	VV Ori (var.)
36697	8.67	+ .06	8	B8–9	+ .14	OP
36741	6.58	− .20	6	B2 V	+ .03	
36779	6.24	− .19	6	B3 V	+ .01	
36783	9.50	+ .01	8	B8–9	+ .09	OP
−3°1140	10.22	+ .26	8	B8–9	+ .34	OP
36824	6.69	− .15	6	B3 V	+ .05	
36842	8.09	− .11	8	B3	+ .09	OP
36865	7.40	− .07	8	B8–9	+ .01	OP
36867	9.30	− .02	8	B8–9	+ .06	OP
36883	7.22	− .08	8	B8–9	.00	OP
36898	7.04	− .07	6			
36899	9.63	+ .05	8	B8–9	+ .13	OP
36916	6.73	− .10	8	B8–9	− .02	OP
36917	7.96	+ .16	6	A0	+ .16	OP
36918				B		OP R
36936	7.52	− .11	8	B5	+ .05	OP
36938	8.88	+ .07	8	B8–9	+ .15	OP
36939	9.01	+ .01	8	B8–9	+ .09	OP
36954	6.92	− .09	6	B3 V	+ .11	
36957	8.83	+ .05	8	B8–9	+ .13	OP
36958	7.36	− .07	8	B3	+ .13	OP
36959	5.67	− .22	8	B1 V	+ .05	
36960	4.77	− .25	6	B0 V	+ .05	
36981	7.83	− .10	6	B3	+ .10	OP
−3°1143	9.88	+ .17	8	B8–9	+ .25	OP
36982	8.45	+ .12	8	B1.5 Vp	+ .37	R
36983	9.19	.00	8	B8–9	+ .08	OP
36998	8.98	.00	8	B8–9	+ .08	OP
36999	8.48	− .09	6	B8–9	− .01	OP
37000	7.49	− .13	6	B5	+ .03	OP
37001	8.89	− .06	8	B8–9	+ .02	OP
37016	6.22	− .17	8	B3 V	+ .03	
37017	6.54	− .14	8	B1.5 V	+ .11	
37018	4.59	− .20	6	B2	+ .03	42 Ori
−4°1181	9.54	+ .32	8	B3	+ .52	OP
37019	9.37	+ .04	8	B8–9	+ .12	OP
37020	6.75	+ .06	8	B1:	+ .33	θ^1(C) Ori = Bond 619
37021	7.96	+ .24	8	B3:	+ .44	θ^1(D) Ori = Bond 624
37022	5.14	+ .06	5	O6	+ .44	θ^1(A) Ori = Bond 628
37023	6.70	+ .11	5	B1:	+ .38	θ^1(B) Ori = Bond 640
37025	7.17	− .12	6	B3	+ .08	OP
37040	6.29	− .14	8	B2–3	+ .08	
Bond 669	9.73	+ .25	8	B2:	+ .48	
37041	5.07	− .05	8	O9 V	+ .27	θ^2 Ori
37042	6.38	− .05	8	B1 V	+ .22	
37043	2.75	− .25	6	O9 III	+ .07	ϵ Ori
37055	6.40	− .12	8	B3 V	+ .08	
37056	8.36	− .06	6	B8–9	+ .02	OP
37057	9.29	+ .02	8	B8–9	+ .10	OP
37058	7.34	− .16	6	B2 Vp	+ .07	R
37059	9.10	−0.02	8	B8–9	+0.06	OP

TABLE 3—*Continued*

Star	V	$B-V$	ϵ	Sp.	E_{y}	Remarks
37060	9.38	+0.02	8	B8–9	+0.10	OP
37061	6.86	+0.29	8	B1 V	+0.56	
37062	8.24	+0.05	8	B5 V	+0.21	
−5°1328	9.89	+0.09	8	A0:	+0.09	OP
37114	8.99	−0.04	8	B8 V	+0.06	
37115	7.08	−0.06	6	B6 V	+0.09	
37128	1.66	−0.18	8	B0 I*a*	+0.12	ϵ Ori
37129	7.13	−0.14	8	B2 Vp	+0.09	R
37130	9.99	+0.16	8	B8–9	+0.24	OP
37150	6.57	−0.19	6	B3 V	+0.01	
37151	7.40	−0.08	8	B8 V	+0.02	
37174	9.17	−0.03	8	B8:	+0.07	
37187	8.12	−0.01	6	B9 V	+0.06	
−3°1154	9.68	+0.02	8	B8–9	+0.10	OP
37209	5.71	−0.23	8	B2	0.00	
37210	8.10	−0.07	8	B8–9	+0.01	OP
37232	6.09	−0.18	6	B1.5 V	+0.07	
37273	9.94	+0.16	8	B8–9	+0.24	OP
37303	6.02	−0.20	8	B1 V	+0.07	
37321	7.08	−0.08	6	B3 V	+0.12	
37322	9.80	+0.07	8	B8–9	+0.15	OP
37330	7.32	−0.05	6	B6 V	+0.10	
37334	7.19	−0.17	8	B3	+0.03	
37342	8.00	−0.12	5	B5 V	+0.04	
37356	.....	.....	.....	B1.5 V	.....	
37357	8.85	+0.12	8	B8–9	+0.20	OP
37373	8.30	−0.09	8	B8–9	−0.01	OP
37390	9.48	+0.17	8	B8–9	+0.25	OP
37397	6.83	−0.15	6	B3 V	+0.05	
37411	9.88	+0.16	8	B8–9	+0.24	OP
37428	8.82	+0.15	8	B8–9	+0.23	OP
37468	3.73	−0.24	8	O9.5 V	+0.07	σ Ori
−6°1273	10.40	+0.31	8	B8–9	+0.38	OP
37469	9.62	+0.22	8	B8–9	+0.30	OP
37470	8.22	+0.06	8	B8–9	+0.14	OP
37480	9.21	+0.01	8	B8–9	+0.09	OP
37481	5.96	−0.23	3	B1 V	+0.04	
37490	4.41	−0.06	6	B2e	+0.17	R
37526	7.61	−0.12	4	B3 V	+0.08	
37547	9.33	0.00	8	B8–9	+0.08	OP
37606	6.90	−0.07	6	B8 V	+0.03	
37641	7.53	−0.05	8	.....	.....	
37663	9.19	−0.02	8	B8–9	+0.06	OP
37700	7.96	−0.09	6	B8–9	−0.01	OP
37742	1.72	−0.21	6	O9.5 I*b*	+0.10	ζ Ori
37744	6.20	−0.23	6	B1 V	+0.04	
37745	9.20	+0.02	8	B8–9	+0.10	
37756	4.91	−0.22	6	B2	+0.01	
37776	6.97	−0.14	6	B2	+0.09	
37807	7.89	−0.09	8	B2	+0.14	OP
37887	7.70	−0.01	6	A0 V	−0.01	
37888	9.21	+0.05	8	B8–9	+0.13	OP
37889	.....	.....	.....	B2 V	.....	
37903	7.80	+0.09	8	B1.5 V	+0.34	
38051	8.53	+0.38	8	B3	+0.57	OP
38087	.....	.....	.....	B3:	.....	
38088	9.69	+0.16	8	B8–9	+0.24	OP
38120	9.10	+0.04	8	B8–9	+0.12	OP
38239	9.22	+0.06	8	A0	+0.06	OP
38563(Cl)	10.49	+0.62	5	.....	+0.78	M78 (A)
" "	10.73	+1.23	6	B1	+1.50	M78 (B) R
38755	7.68	−0.11	6	B6 V	+0.04	
38771	2.08	−0.16	8	B0.5 I*a*	+0.13	κ Ori
39291	5.33	−0.19	6	B2	+0.04	55 Ori
39777	6.54	−0.19	6	B2 V	+0.04	

NOTES TO TABLE 3

36918	The spectrum overlaps with that of BD−6°1232.
36982	The hydrogen lines in the spectrum are stronger than normal.
37058 37129	The helium lines in the spectrum are weaker than normal. This effect appears to be characteristic of certain stars situated near the bottom edge of the main sequence. Such stars should be discussed separately from normal main-sequence members.
37490	A small nebulosity is associated with this star.
38563	The magnitudes of the components are estimated to be 11.0 and 12.5.

contains the number of the stars in the *Henry Draper Catalogue*. For stars not listed in the latter, the BD or Bond number is given. The second and third columns contain the observed magnitude, V, and color, $B - V$. The fourth column lists a quantity ϵ such that the probable error of $B - V$ is $\pm 0.0010\ \epsilon$ and the probable error of V is $\pm 0.0015\ \epsilon$. The spectral type appears in the fifth column. The color excess, as described below, is listed in the sixth column. In those cases where the spectral classification was made from objective-prism spectra, "OP" is indicated in the last column.

V. THE ORION AGGREGATE

This section will be devoted to an investigation of the brighter stars and the obscuring matter within the limits from R.A. 5^h00^m to 5^h48^m, and from Dec. $+6°$ to $-8°$. The pronounced clustering of B stars within these limits is shown in Figure 2, where the stars brighter than 7.0 mag. and of types B3 and earlier have been plotted from the *Henry Draper Catalogue*.

The nebulous background in Orion consists of a complex network of bright and dark markings.[21] The emission nebulosities include the Orion Nebula itself, which is one of the brightest and most dense of the nearer *H* II regions. It is surrounded by an extended region of feeble hydrogen emission. Also appearing in emission is Barnard's Great Curved Nebula, which extends about 12° on the eastern side of the aggregate. In view of Strömgren's analysis[22] of *H* II regions, there seems to be little doubt that the star responsible for the ionization of hydrogen in these nebulae is the O-type star, θ^1(A) Orionis, the brightest star of the Trapezium. The central position of the latter with respect to these nebulae helps confirm this identification. The object IC 434, which contains the Horsehead Nebula, and NGC 2024 are both apparently excited by the O9.5 star ζ Orionis.

Numerous nebulae which shine by reflection are also to be found in Orion. Typical of these is the group of nebulae—NGC 2064, 2067, 2068, and 2071, several degrees northeast of ζ Orionis. This group will be considered in more detail later.

Extended dark markings are also a noticeable feature of the Orion aggregate, especially since many of these can be seen superposed on the bright nebulosities. The Horsehead Nebula is evidently a superposition of dark matter on IC 434, and the Orion Nebula seems to be separated from NGC 1981 only as a result of a somewhat nearer obscuring cloud.[23] Other dark markings are apparent from the variations in the surface density of the stars, in particular on the eastern side of the aggregate.

The foregoing remarks suggest that the Orion aggregate may have an appreciable extension in depth. The coexistence of both emission and reflection nebulae at approximately the same angular distance from the Trapezium can most probably be explained as being due to an appreciable difference in linear distance, i.e., an extension along the line of sight. The overlapping of dark and bright nebulae indicate the same thing. If the extension of the aggregate along the line of sight is equal to the maximum transverse dimension, then the true distance modulus of a member can differ from the mean by as much as 0.2 mag. This will have the effect of increasing the dispersion of the observed main sequence and introducing additional uncertainties in the absolute magnitudes of the higher-luminosity stars.

[21] See Ross, *Atlas of the Milky Way* (Chicago: University of Chicago Press, 1934), Pl. 34.

[22] *Ap. J.*, **108**, 242, 1948.

[23] This was pointed out by Dr. Morgan.

The data in Table 3 can be used to compute the color excesses of the Orion stars. The normal colors on the $B - V$ system for the stars of spectral types O6–A0 were derived by H. L. Johnson[24] from observations of near-by B stars and various galactic clusters. These are listed in Table 4. The relation between color excesses on the $B - V$ and C_1 systems is established by transformations derived by Johnson[24] and is given by

$$E_1 = 0.425\, E_y ,$$

where E_y is the color excess on the $B - V$ system.

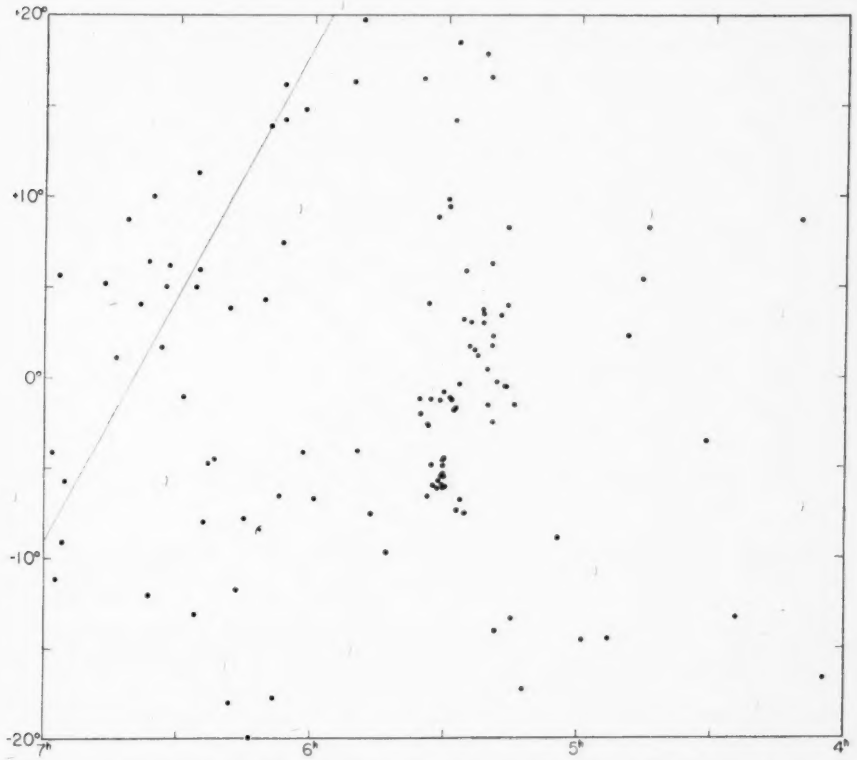

FIG. 2.—The apparent distribution of stars in the *Henry Draper Catalogue* brighter than 7.0 mag. of types B3 and earlier. The diagonal line represents the galactic equator.

TABLE 4

NORMAL COLORS OF THE O AND B STARS ($B - V$ SYSTEM)

O6	−0.38	O9.5	−0.31	B1.5	−0.25	B6	−0.15
O7	− .36	B0	− .30	B2	− .23	B8	− .10
O8	− .34	B0.5	− .29	B3	− .20	B9	− .07
O9	−0.32	B1	−0.27	B5	−0.16	A0	0.00

[24] Unpublished.

Since the ratio of total to selective absorption is known to be peculiar in the case of θ^1 Orionis,[25] it is of interest to investigate it for the Orion aggregate as a whole. The relation between the apparent magnitude of a star, m, and the apparent magnitude corrected for interstellar absorption, m_0, is given by

$$m_0 = m - AE ,$$

where E is the color excess and A is the appropriate ratio of total to selective absorption. If one selects from the Orion stars a group of stars having as nearly as possible the same spectral characteristics, e.g., those classified as B2 V, then for such a group the dispersion in absolute magnitude will be relatively small. If these stars are assumed to be at about the same distance, then the corrected apparent magnitude, m_0, will be approxi-

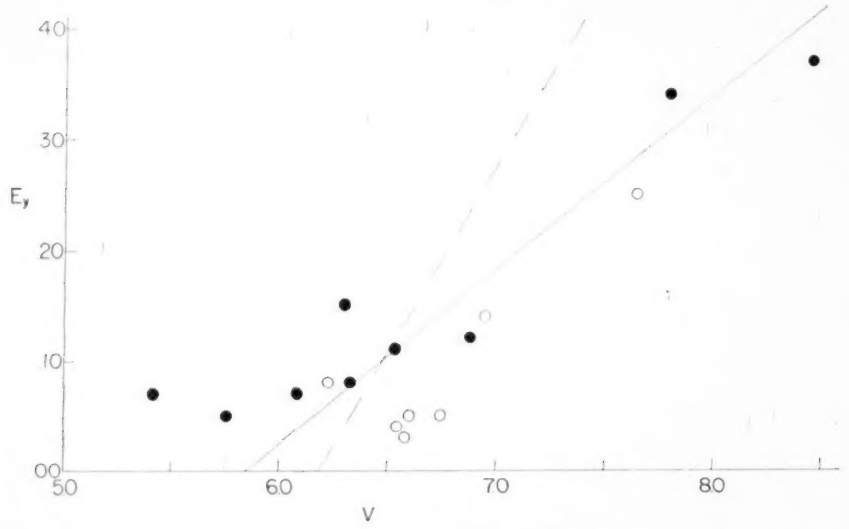

FIG. 3.—The relation between color excess and apparent visual magnitude for the B1.5 V stars (*solid circles*) and the B2 V stars (*open circles*) in the Orion aggregate. The dotted and solid lines correspond to ratios of total to selective absorption of 3 and 6, respectively, on the $B - V$ system.

mately the same for all. As a consequence, a linear relation will exist between m and E, the slope of which will give the ratio of total to selective absorption for the stars considered. This relation is plotted in Figure 3 for the B1.5 V and B2 V stars in Orion. The solid line has been drawn to fit the points, whereas the dotted line has a slope corresponding to the normal ratio of total to selective absorption. Apparently, the ratio is abnormally high for stars in the aggregate other than the Trapezium stars. The ratio for these stars was estimated from Figure 3 to be 6 on the $B - V$ system, or 14 on the C_1 system. The latter value agrees fairly well with the value of 16 ± 1 predicted by van de Hulst[26] for θ^1 Orionis on the basis of the six-color observations of Stebbins and Whitford. Figure 4 contains a similar plot for the B8–9 stars within $2\frac{1}{2}°$ of the Orion Nebula. A similarly high ratio of total to selective absorption is indicated by these stars.

The relation between m and E illustrated in Figures 3 and 4 is complicated by the

[25] van de Hulst, *Utrecht Pub.*, Vol. 11, No. 2, 1949. [26] *Ibid.*

fact that the Orion aggregate may have an appreciable extension in depth as compared with its distance. This will have the effect of introducing a dispersion in m of the points about the line in Figure 3 of an amount corresponding to the dispersion in distance, i.e., about 0.2 mag. This will be added to the dispersion of the points resulting from a true spread in the absolute magnitudes of the stars considered. The latter quantity, however, is considerably larger, amounting to about 0.5 mag. Neither of these effects will alter the observed ratio of total to selective absorption but will decrease the accuracy with which it can be determined. If the obscuring material in Orion were distributed more or less uniformly throughout the aggregate, however, the effect would exist that the more distant stars in the aggregate are also, on the average, redder as a result of their being seen through a thicker layer of interstellar material. They will also be, on the average, slightly

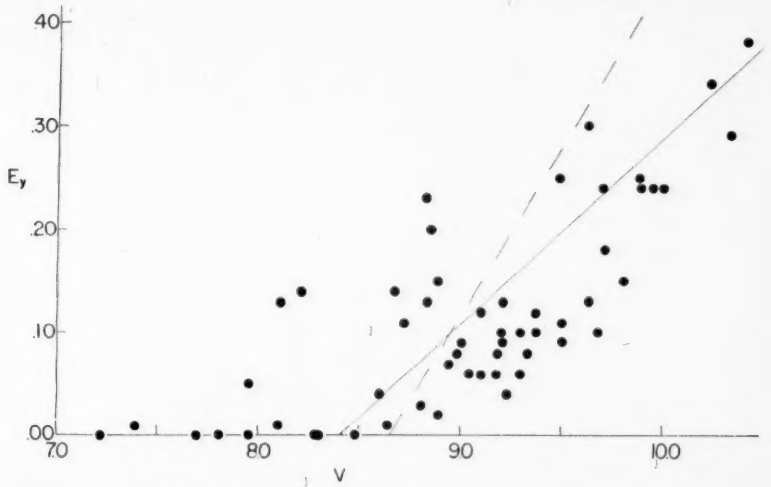

FIG. 4.—The relation between color excess and apparent visual magnitude for the B8–B9 stars within 2½° of the Orion Nebula. The dotted and solid lines correspond to ratios of total to selective absorption of 3 and 6, respectively, on the $B - V$ system.

fainter by virtue of their greater distance. This will have the effect of causing a spurious increase of the ratio of total to selective absorption as derived from Figure 3. If it is assumed that C_1 increases systematically by 0.025 mag. per 10 parsecs along the line of sight within the aggregate, then the true ratio of total to selective absorption will be smaller than the ratio determined above by about 1 on the C_1 system. Since this represents an extreme case, it will be assumed that the ratio determined from Figure 3 is correct within the observational errors. Reddened stars of other spectral types also confirm a high ratio of total to selective absorption, although the scatter is again fairly large. The stars in the northern part of the aggregate are practically unreddened; hence the present discussion does not apply to them. Owing to the uncertainties mentioned above, a probable error of ± 1 is estimated for the ratio of 6 on the $B - V$ system determined above, and in the following it will be assumed that this ratio applies to the Orion stars in general. An exception to this will be discussed below. The precise ratio for particular parts of the aggregate or for particular stars can be found only from multicolor observations of the type made and described by Whitford.[27]

[27] *Ap. J.*, **107**, 102, 1948.

In Figure 5 the H-R diagram has been plotted for the stars in Orion for which both slit spectrograms and photoelectric observations are available from Table 3. All the brighter B stars in Orion are included, with only two exceptions: γ Ori and 32 Ori. These, on the basis of their individual spectroscopic parallaxes, were judged to be nonmembers. Other stars which, on the basis of the H-R diagram, are probably not members of the aggregate are indicated in Figure 5 by open circles. The mean corrected apparent magnitude, m_0, was estimated from Figure 5 for the main-sequence stars of types B1, B2, B3, and B5. These were then subtracted from the corresponding absolute magnitudes[28]

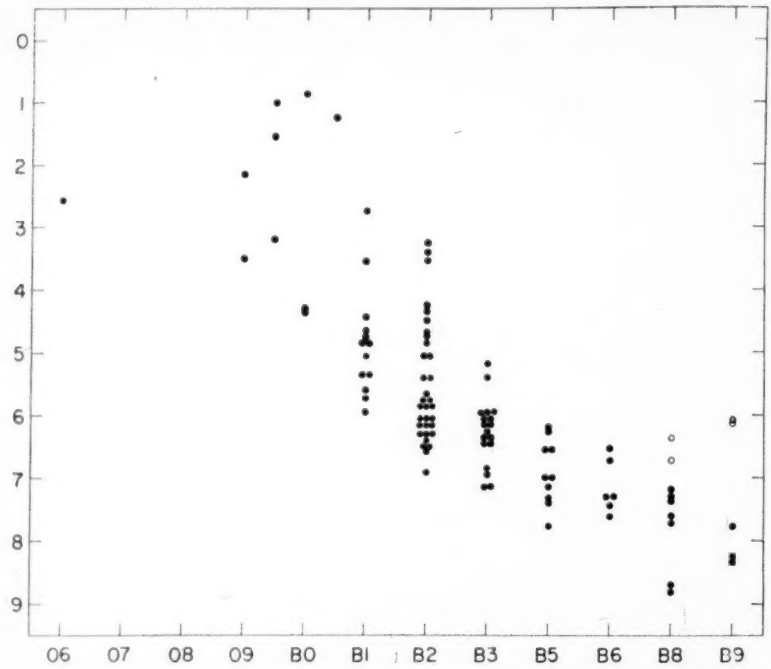

FIG. 5.—The H–R diagram for the brighter stars in the Orion aggregate. Apparent visual magnitude corrected for interstellar absorption is plotted against spectral type. Open circles represent stars which are probably not members of the aggregate. Stars of type B1.5 have been grouped with those of type B2.

to obtain a distance modulus. These values are shown in Table 5. Stars of spectral type later than B5 were not used in obtaining the distance modulus, since the corresponding portion of the H-R diagram is not complete and is complicated by an admixture of field stars which causes a spurious turning-up of the main sequence with later types. The mean distance modulus resulting from the data in Table 5 is 8.5 mag., corresponding to a distance of 500 parsecs. An uncertainty of about ± 0.3 mag. is estimated.

A comparison of the H-R diagrams of the Orion aggregate and the h–χ Persei cluster[29] indicates several significant differences between the two groups of stars. The B-type supergiants in h–χ Persei have spectral types in the range B0.5–B3, whereas the super-

[28] Hynek, *Astrophysics* (New York: McGraw-Hill Book Co., Inc., 1951), p. 23. A zero-point correction of -0.10 mag. has been applied to these values to put them on the $B - V$ system.

[29] W. P. Bidelman, *Ap. J.*, **98**, 61, 1943.

giants in Orion—ζ, ϵ, and κ Orionis—have spectral types which are, on the average, somewhat earlier, i.e., O9.5–B0.5. In addition, the number of O stars in Orion seems to be significantly larger, since in h–χ Persei there is only one star earlier than O9.5. The most striking difference between the two diagrams, however, lies in the presence of A- and M-type[30] supergiants in the double cluster. There is no evidence for the association of supergiants of spectral types later than B with the Orion aggregate.

Once the distance of the aggregate has been determined from the main-sequence stars, the absolute magnitudes of the high-luminosity stars in Orion can be derived from their distance modulus and their apparent magnitudes corrected for interstellar absorption. Table 6 contains these results for the stars of spectral types B0.5 and earlier. A maximum error of 0.3 mag. is estimated for these values on the basis of the possible extension of the aggregate along the line of sight and the uncertainty of the color excesses.

TABLE 5

DETERMINATION OF DISTANCE MODULUS FOR BRIGHTER STARS OF ORION AGGREGATE

Sp.	$\overline{m_0}$	M_v	$\overline{m_0} - M_v$
B1 V	5.1	−3.3	8.4
B2 V	6.1	−2.7	8.8
B3 V	6.4	−2.1	8.5
B5 V	6.9	−1.4	8.3
Mean	.....	.....	8.5

TABLE 6

ABSOLUTE MAGNITUDES OF EARLY-TYPE STARS IN ORION

	V	III	II	Ib	Ia
O6	−6.0	.....	.....	.....	.....
O9	−5.0	−6.2	.....	.....	.....
O9.5	−5.2	.....	−6.9	−7.4	.....
B0	−4.0	.....	.....	.....	−7.6
B0.5	.....	.....	.....	.....	−7.2

The absolute magnitudes of the stars of luminosity class I*a* average slightly higher than the value of −7.2[31] obtained for stars of types A5–M2 from the equation of galactic rotation. For class B0 V the agreement with the presently adopted absolute-magnitude calibration is within the uncertainties mentioned above. In the case of the O-type dwarf stars, the absolute magnitudes average several tenths of a magnitude brighter than those determined in a similar way by Roman[32] for the O stars in the Cygnus concentration of early-type stars. In both cases the absolute magnitudes are similar to what would be expected from an extrapolation of the main sequence to earlier types. The late O stars belonging to the giant and intermediate supergiant classes, however, have considerably higher luminosities than the B stars of similar luminosity classes. They apparently are similar in absolute magnitude to the supergiant stars of types F and later. A complete

[30] W. P. Bidelman, *Ap. J.*, **105**, 492, 1947.

[31] Hynek, *op. cit.*, pp. 22, 23.

[32] *Ap. J.*, **114**, 492, 1951.

absolute-magnitude calibration of the luminosity classes for the O stars, however, will require studies of additional concentrations of early-type stars.

VI. THE REGION OF THE ORION NEBULA

The region of the "sword" of Orion is of particular interest, in that it contains the three earliest O stars of the aggregate and one of the brightest hydrogen-emission regions in the sky. It contains a rather compact group of bright stars which seems to form a subsystem in the Orion aggregate.

The H-R diagram for the stars within $2\frac{1}{2}°$ of the Orion Nebula is plotted in Figure 6. The observations in this region are complete to about tenth magnitude; consequently

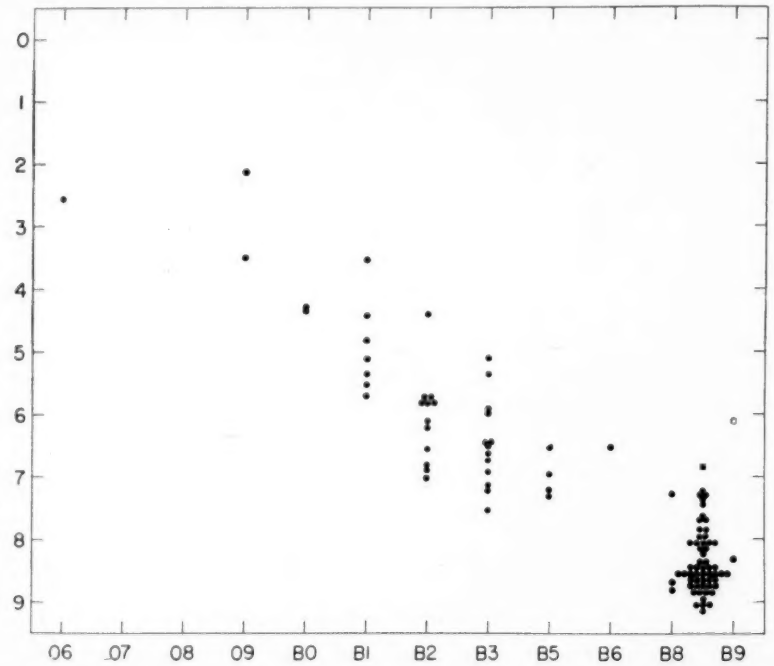

FIG. 6.—The H-R diagram for the stars within $2\frac{1}{2}°$ of the Orion Nebula. Apparent visual magnitude corrected for interstellar absorption is plotted against spectral type. The star represented by the open circle is probably not a member of the aggregate.

the H-R diagram can be expected to be reasonably complete to B9. The distance modulus was obtained for these stars in the same way as for the stars brighter than 8.0 mag. in the aggregate, the result being that $m_0 - M = 8^m6$. This does not differ greatly from the value of 8.5 mag. determined for the aggregate as a whole. The latter value will be adopted as the mean distance modulus of the entire aggregate, since it is based on a greater number of stars. If the aggregate is assumed to be elongated as a result of the shearing effects of galactic rotation, then the part of the aggregate at higher galactic longitude, i.e., that containing the nebula, would be expected to be at a somewhat greater distance. The internal accuracy of the distance moduli determined here, however, is not quite high enough to attribute their difference to this effect.

Figure 6 illustrates the great numbers of B8–9 stars relative to those of earlier spectral types. The theory of the dynamics of star clusters[33] predicts that the square of the ratio of the velocity dispersion to the radius of the cluster is proportional to the density. Since the stars within several degrees of the nebula are known to have a lower velocity dispersion than the other B stars in Orion,[34] it follows that the density of the aggregate as a whole should be at least as great as in the region of the nebula. This suggests that the B8–9 stars should be at least as frequent throughout the entire aggregate. Although

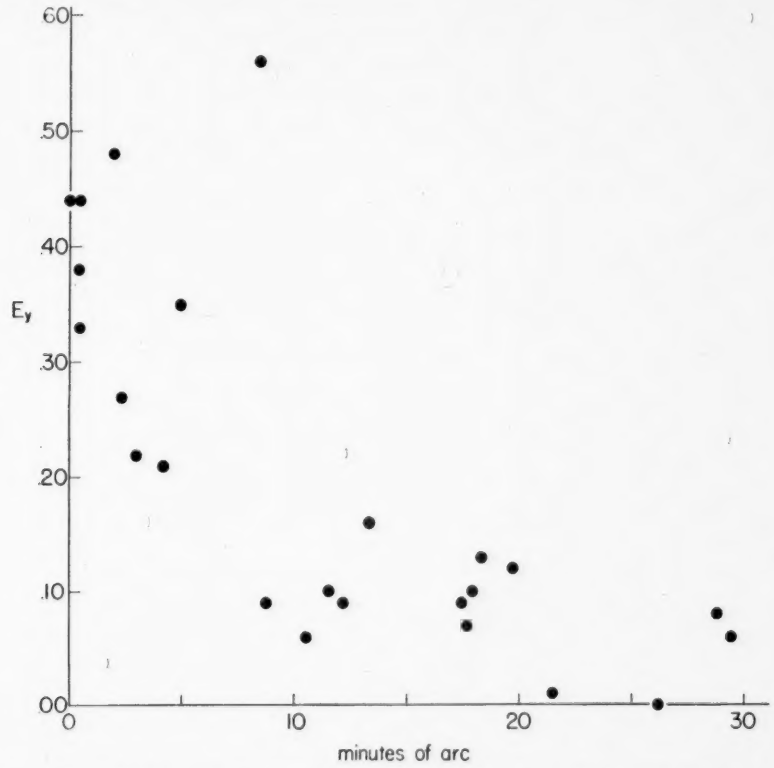

FIG. 7.—The relation between color excess and angular distance from θ^1(A) Orionis for the B stars in the Orion Nebula. The star having a color excess of +0.56 is located in a dense, detached part of the nebula.

the present investigation does not go sufficiently faint to prove this, counts of stars in the *Henry Draper Extension*[35] seem to confirm it.

It is of interest to examine the distribution of color excesses within the Orion Nebula. In Figure 7 the color excesses of all the B stars within 30 minutes of arc of the center of the Trapezium are plotted against angular distance from the latter. It is apparent that,

[33] S. Chandrasekhar, *Principles of Stellar Dynamics* (Chicago: University of Chicago Press, 1942).

[34] Bendler, unpublished thesis, University of Michigan Libraries.

[35] *Harvard Ann.*, Vol. 112, 1949.

on the average, the color excesses increase smoothly with decreasing distance from the Trapezium and that the Trapezium stars themselves, at the extreme left of the diagram, have color excesses which are not out of line with those of the surrounding stars. The hypothesis that the central part of the Orion Nebula is more transparent than elsewhere is evidently not confirmed by observations of color excesses. In order for the total absorption in the Trapezium region to be low, the ratio of total to selective absorption there would have to be correspondingly low, but this is doubtful in view of the abnormally high ratio elsewhere in the aggregate and would require that the four Trapezium stars have lower than average luminosities for their spectral types.

VII. REFLECTION NEBULAE IN ORION

Several highly obscured stars in reflection nebulae in Orion have been observed and are included in Table 3. Since there seems to be no doubt that these are illuminated portions of the general obscuring material in Orion, the illuminating stars can be considered members of the aggregate.

NGC 2068 = M78 and its companions NGC 2067 and NGC 2064 have been studied by Collins[36] and by Struve and Story[37] and are illustrated in Figure 8. The photograph suggests that they are portions of the same nebula partially obscured by nearer dark matter. That they are situated in a region of extremely high obscuration is indicated by the very low surface density of stars there. NGC 2068 contains two tenth-magnitude stars, designated M78 (A) and M78 (B), of which photoelectric observations were obtained, and a third star several magnitudes fainter. Together they form the cluster HD 38563. M78 (A) occupies a central position with respect to NGC 2068. The nebula, however, shades off evenly in all directions except to the north, where a sharp, ragged boundary again suggests nearer obscuring material. It thus seems possible that M78 (B), the northernmost star of the three, may occupy the true central position in the nebula and be primarily responsible for its illumination. This star is a visual binary with $\Delta m = 1^m.5$. Several slit spectrograms were obtained, and the spectral type is B1 V. If the absolute magnitude were assumed to be -3.3 and the distance modulus the same as for the other Orion stars, the apparent magnitude corrected for interstellar absorption would be 5.2. Since, from Table 3, the apparent magnitude is approximately 11.0, the amount of absorption would be 5.8. This, combined with the color excess, results in a ratio of total to selective absorption between 8 and 9 on the C_1 system. The spectral type of the brighter star in NGC 2068 was not obtained in the present investigation but is listed by Hubble[38] as B5. This spectral type, combined with the photoelectric data in Table 3 and an assumed distance modulus of 8.5 mag., leads to a ratio of total to selective absorption of about 10. The values of the ratio for the stars in NGC 2068 are nearer to the normal ratio than to that estimated earlier for the other Orion stars.

The reflection nebula NGC 1788, which has been illustrated by Collins,[39] is situated on the opposite side of the Orion aggregate from NGC 2068. It contains two illuminating stars, the brighter being BD $-3°3013$, for which a slit spectrogram was obtained. The spectral type is B9 V. The photoelectric observations are included in Table 3. Assuming an absolute magnitude of -0.1 and a distance modulus, again, of 8.5 mag., the total absorption is 1.7 mag. This results in a ratio of total to selective absorption of 12 on the C_1 system.

The differences in the values of the ratio of total to selective absorption found, on the one hand, for BD $-3°3013$ and the Orion aggregate as a whole and, on the other hand, for the stars in NGC 2068 cannot be explained entirely on the basis of the uncertainties of the observed quantities. The explanation may lie in the extreme density of the interstellar dust of which NGC 2068 forms an illuminated part. If the

[36] *Ap. J.*, **86**, 529, 1937.

[37] *Ap. J.*, **84**, 219, 1936.

[38] *Ap. J.*, **56**, 400, 1922.

[39] *Loc. cit.*

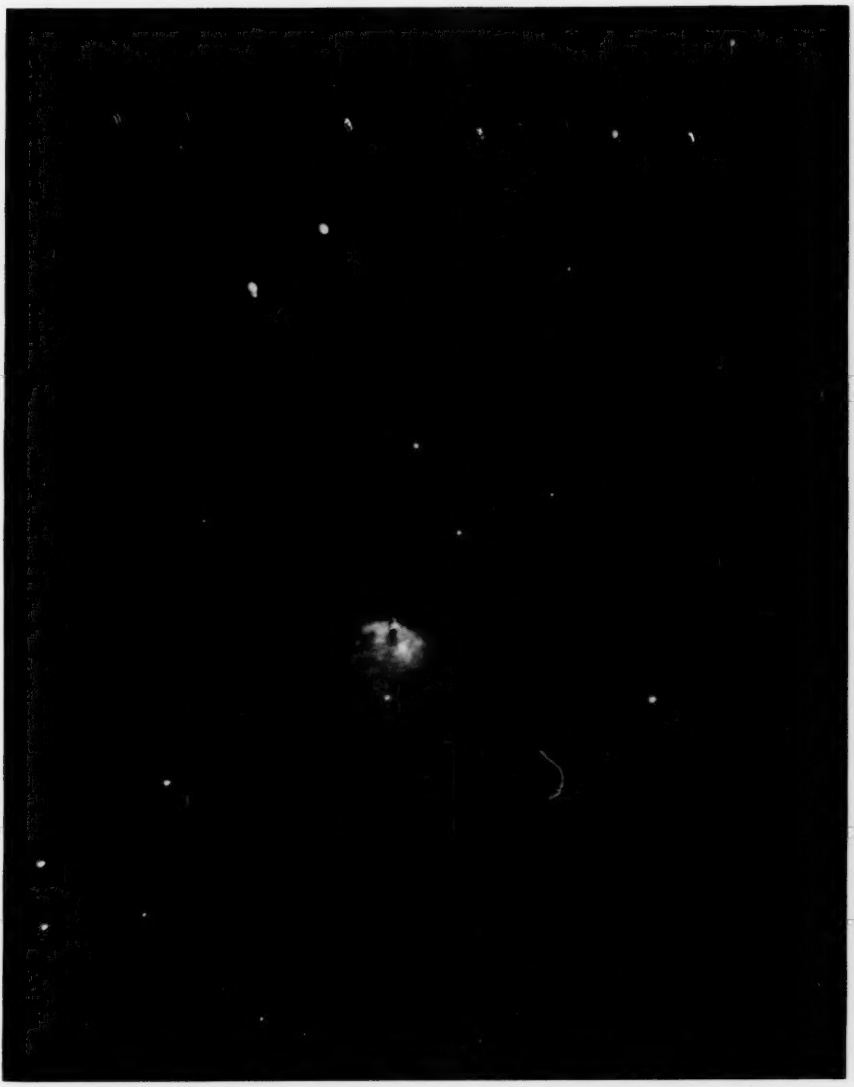

FIG. 8.—A photograph of NGC 2068 taken with the Yerkes 24-inch reflector. The scale is approximately $2\frac{1}{2}'$ per inch. NGC 2071 is at the upper left, while NGC 2067 and NGC 2064 are to the right of NGC 2068.

optical thickness of the matter along the path between θ^1 Orionis and NGC 2068 is high enough, the pressure of radiation, to which the high ratio of total to selective absorption is attributed, may be inoperative near the latter. Observations in more than two colors would be necessary for a complete description of the reddening in NGC 2068.

VIII. INTERSTELLAR FEATURES

An additional peculiarity of the absorbing material in Orion, as was first pointed out by Morgan,[40] is that the interstellar band at λ 4430 is abnormally weak in the spectra of the Orion stars as compared with other stars of comparable reddening. It was suggested that the radiation from the hottest stars modifies the surrounding interstellar material so that it cannot absorb λ 4430 as strongly as in other regions. Recent measurements made by Duke[41] of the central intensities of λ 4430 indicate that the band is at least 25 per cent weaker in the Orion stars than in other stars of similar reddening. The star M78 (B), which has a color excess of 0.70 mag. on the C_1 system, has a barely visible λ 4430 band, whereas a central absorption of over 20 per cent would be expected on the basis of its reddening. In view of the abnormally low color excesses of the Orion stars for a given amount of total absorption, one might expect the opposite effect.

The equivalent width of the diffuse interstellar feature at λ 6284 has been measured[42] in the spectrum of θ^1 (A) Orionis. The relationship between the equivalent width of λ 6284 and color excess found by Merrill and Wilson[43] predicts a value of about 0.5 A for a star having a color excess similar to that of θ^1 (A) Ori. The measured equivalent width, however, is 0.26 A, which suggests that λ 6284 may also be abnormally weak in the spectra of the Orion stars. Observations of more stars, however, would be needed to establish this.

It was first suggested by Baade and Minkowski[44] that the peculiar reddening in Orion might be due to the removal of the smaller interstellar particles by the radiation pressure of the hotter stars. The theoretical extinction-curves computed by van de Hulst indicate that an increase of the mean particle size by about 20 per cent will increase the ratio of total to selective absorption from the normal value to one similar to that observed in Orion. This relative decrease in the number of smaller particles in Orion may also explain the weakening of the diffuse interstellar features there, assuming that the latter are produced by, or are connected in some way with, small interstellar particles.

Observations of the equivalent widths of the sodium D lines in eight of the Orion stars indicate that the empirical relation between color excess and $0.5 \times (D_1 + D_2)$ is, within the observational errors, the same for them as for stars in general.

In addition to their valuable advice and discussions, the author is indebted to Dr. W. W. Morgan for suggesting this investigation and for making available to him much of the observational material on which it is based; to Dr. Bengt Strömgren for the use of the observational facilities at the Yerkes and McDonald Observatories; and to Dr. Harold Johnson for the use of his photoelectric equipment. He is also indebted to Dr. J. J. Nassau for the use of objective-prism plates taken at the Warner and Swasey Observatory.

[40] *A.J.*, **51**, 21, 1944.

[41] *Ap. J.*, **113**, 100, 1951.

[42] Merrill, Sanford, Wilson, and Burwell, *Ap. J.*, **86**, 274, 1937.

[43] *Ap. J.*, **87**, 9, 1938.

[44] *Op. cit.*

ON MAGNITUDE SYSTEMS*

HAROLD L. JOHNSON
Yerkes and McDonald Observatories
Received December 10, 1951

ABSTRACT

The relations between several accurate systems of magnitudes and colors are discussed. It is shown that the inclusion of radiation to the violet of 3800 A in the measurements makes the relations between different color systems nonlinear and, in most cases, multivalued. The North Polar Sequence is shown to be inadequate as a standard region, because of the absence of blue, supergiant, heavily reddened, and red dwarf stars.

During the course of work, the first portion of which is reported in an earlier paper,[1] it became apparent that comparisons with, and transformations to, other accurate photometric series are much more difficult to make with sufficient accuracy than has been supposed. The first indication of these difficulties came at the time the NPS transformations given in Paper I were derived. The difference in color index between the stars NPS 6 and NPS 10 is $C_6 - C_{10} = -0.06$, according to Stebbins, Whitford, and Johnson,[2] and $C_6 - C_{10} = -0.12$, according to my recent measures.[1] It is impossible that either series of measures could be in error by the necessary amount; Stebbins, Whitford, and Johnson have a total of 19 observations on each of the two stars, while my McDonald values are the results of 13 observations on each star. The difference between the two series is certainly real and must be explained. Further discordances of this type will be noted among the other NPS stars, particularly for NPS 19.

The only significant difference between the filters used in the two investigations is the ultraviolet cutoff of the blue filter, which occurs at about 3550 A for the observations of Stebbins, Whitford, and Johnson and at about 3800 A for my McDonald work. It seems unbelievable, at first glance, that this small change could produce significant differences, but, as will be shown below, it does.

A comparison between Eggen's[3] colors for the near-by stars and the McDonald values is shown in Figure 1. The value on the International System is $P_0 - V$, according to the linear transformation equations given in Paper I; the significance of the subscript 0 on P is discussed later.

The straight line is the transformation equation given by Eggen:[4] $P - V = -0.10 + 1.10C_p^g$. It is evident that a straight line is not an adequate transformation between the two color systems.

Comparisons between Eggen's[3] photographic magnitudes, Pg_p^g, and the McDonald values[1] are shown in Figure 2. The magnitude from the linear transformation to the NPS given in Paper I is P_0; the color index, $B - V = C_y + 1.040$.[5] Figure 1, *a*, can be interpreted as indicating that a large scale difference, amounting to nearly 0.3 mag. in 10 mag., exists between the two photoelectric magnitude systems. That such a scale error cannot exist in my work will be shown in a later paper of this series; it is *not* proposed that

* *Contributions from the McDonald Observatory, University of Texas*, No. 208.

[1] H. L. Johnson and W. W. Morgan, *Ap. J.*, **114**, 522, 1951. Hereafter, this paper is referred to as "Paper I."

[2] *Ap. J.*, **112**, 469, 1950.

[3] *Ap. J.*, **111**, 65, 81, 414, 1950; **112**, 141, 1950; **113**, 657, 663, 1951.

[4] *Ap. J.*, **114**, 141, 1951.

[5] B is a magnitude obtained directly from the blue filter. The zero point of $B-V$ has been set at spectral type A0; this point will be discussed in detail in a later paper of this series.

such a scale error exists in Eggen's work. Since all the bright stars in the comparison are blue and all the faint ones are red, the scale error can be interpreted as a color equation between the two systems, as in Figure 2, *b*. It will be shown that the latter is the correct interpretation.

The ultraviolet measures, made with the filter described in Paper I, make possible a series of tests of the effect of the inclusion of the region beyond 3800 A in the blue filter. Four blue filters, containing different amounts of ultraviolet, were formed by taking the observed blue deflection and adding to it a constant, a, times the ultraviolet deflection.

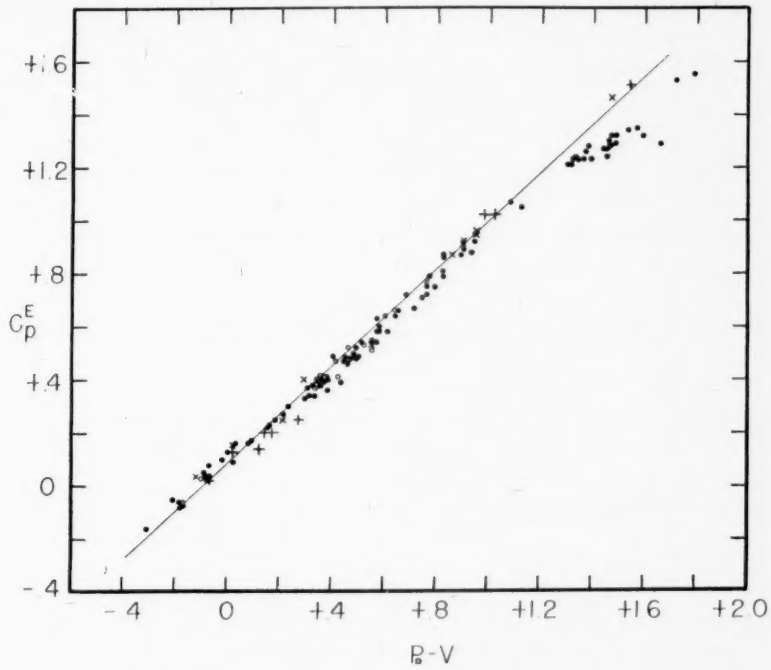

FIG. 1.—Eggen's colors, C_p^E, versus $P_o - V$. The symbols are defined as follows. *filled circles:* luminosity class V; *open circles:* luminosity class IV; *crosses:* luminosity class III; *plus signs:* NPS stars.

The filters thus obtained are illustrated in Figure 3. The procedure is legitimate, since the response of the photocell is linear and its output is strictly proportional to the area under the response-curve.

The magnitudes and colors obtained in each case have been transformed by linear relations to the NPS. The photographic magnitudes so obtained are designated P_0, $P_{0.5}$, $P_{1.0}$, and $P_{2.7}$, according to the value of a. The relations are:

$$P_0 - V = +0.96 + 1.09C_0\,, \tag{1}$$

$$P_{0.5} - V = +1.06 + 1.00C_{0.5}\,, \tag{2}$$

$$P_{1.0} - V = +1.12 + 0.93C_{1.0}\,, \tag{3}$$

$$P_{2.7} - V = +1.29 + 0.79C_{2.7}\,. \tag{4}$$

The quality of the fit to the NPS may be estimated from the values given in Table 1 (upper half); in no case is the fit unsatisfactory, although it is better in some cases than in others. The color indices on the International System are given for a number of other stars in Table 1 (lower half); it is evident that the values obtained for intrinsically blue, or high-luminosity, stars depend very strongly upon the amount of ultraviolet included in the blue filter.

V has no color equation to the International photovisual magnitudes in the NPS. Table 2 shows that the effective wave lengths for $P_{0.5}$ agree very well with those given by

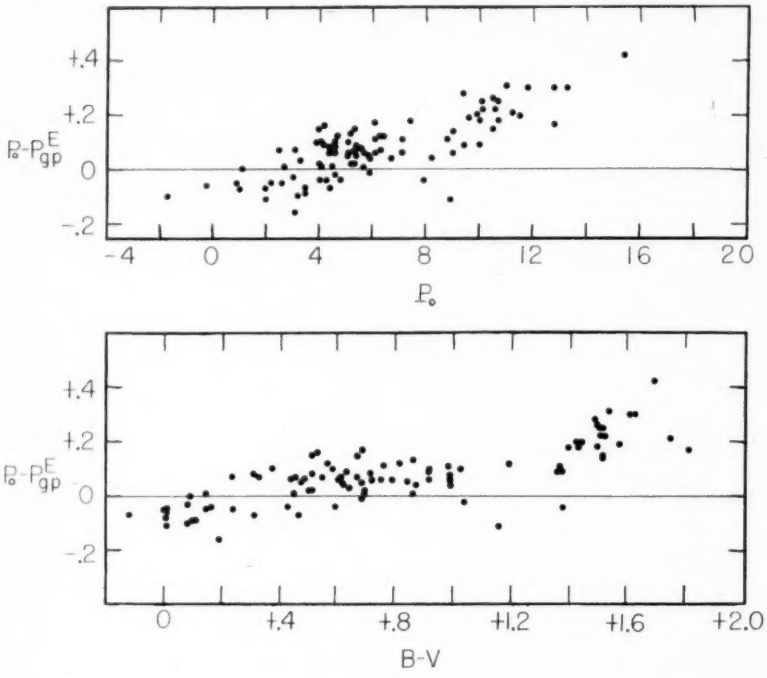

FIG. 2.—Comparisons of P_o with Pg_p^E, as a function of P_o and of $B - V$

Seares[6] for $IIPg$, for 3000° K and 11,000° K. Table 3 shows that the intrinsic colors for $a = 0.5$ agree very well with Seares's[6] values on the International System. It appears, therefore, that $P_{0.5}$ corresponds closely to the photographic magnitudes on the International System.

Figure 4, *a* and *b*, shows comparisons of $P_{0.5}$ and $P_{1.0}$, respectively, with Eggen's[3] photographic magnitudes, Pg_p^E. It is evident that increasing the ultraviolet content of the blue filter to $a = 1.0$ results in much better agreement between Eggen's photographic magnitudes and mine. Figure 4, *b*, shows little color equation between the two systems. The addition of somewhat more ultraviolet might make the agreement even better for the red dwarfs, and calculations show that the color equation disappears completely for $a \simeq 1.5$. It is evident that the entire amount of the scale divergence appearing

[6] *Ap. J.*, **98**, 261, 1943.

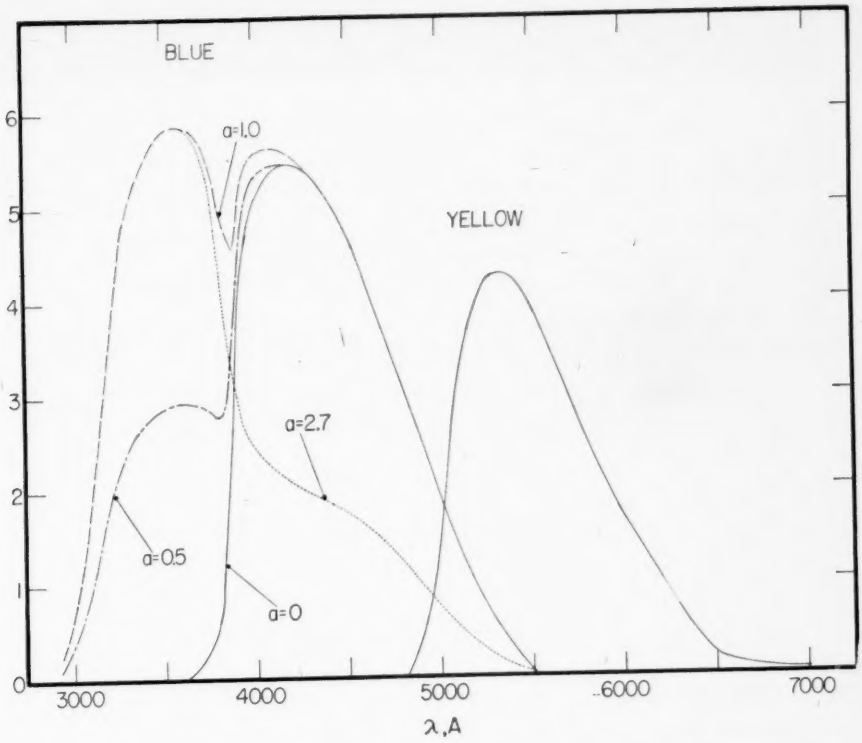

FIG. 3.—The response of the photometer to equal intensity of radiation at all wave lengths. The four blue filters are described in detail in the text.

TABLE 1

COLORS OF STARS ON THE INTERNATIONAL SYSTEM

Star	P_0-V	$P_{1.0}-V$	$P_{1.5}-V$	$P_{2.7}-V$	Sp.	C_p(SWJ)
NPS 6	+0.02	+0.03	+0.04	+0.06	.....	+0.06
NPS 10	+0.14	+0.13	+0.13	+0.13	.....	+0.12
NPS 16	+0.35	+0.33	+0.33	+0.31	.....	+0.32
NPS 19	+0.45	+0.43	+0.42	+0.40	.....	+0.41
NPS 2r	+1.54	+1.55	+1.55	+1.56	.....	+1.56
NPS 4r	+0.98	+1.01	+1.01	+1.02	.....	+1.02
NPS 8r	+1.02	+1.03	+1.03	+1.03	.....	+1.02
α Lyr	−0.17	−0.16	−0.14	−0.11	A0 V	.....
α Aql	+ .08	+ .08	+ .09	+0.10	A7 IV, V	.....
α Cyg	− .07	− .11	− .13	−0.13	A2 I*a*	.....
9 Cep	+ .15	+ .04	− .02	−0.10	B2 I*b*	.....
λ Cep	+ .10	− .06	− .14	−0.24	O6f	.....
β Ori	− .20	− .33	− .38	−0.44	B8 I*a*	.....
τ CMa	− .34	− .54	− .62	−0.70	O9 III	.....
HD 14633	− .41	− .64	− .72	−0.80	O8	.....
ι Ori	− .45	− .68	− .77	−0.84	O9 III	.....
υ Ori	− .47	− .70	− .78	−0.86	B0 V	.....
BD+28°4211	−0.56	−0.83	−0.93	−1.01	Op	.....

in Figure 2, *a*, is due to ultraviolet beyond 3800 A included in Eggen's blue filter but excluded from mine. Furthermore, the systematic discordances apparent in Figure 1 can be explained in this same manner.

Figure 4, *c*, shows a comparison of V with Eggen's[3] photovisual magnitudes, Pv_p^E. The zero-point correction at $C_{int} = 0$, +0.07 mag., is just the value one would expect from Figure 4, *b*, and Eggen's linear transformation to the NPS. The slightly nonlinear relation between V and Pv_p^E probably is caused by his linear NPS color transformation reflecting a small amount of the ultraviolet difficulties into his visual magnitudes. Such a reflection can occur only if the effective wave length for the yellow magnitudes differs significantly from that for IPv; this is the case for Eggen's[3] yellow magnitudes, but not for mine.[1]

Figure 5 illustrates the relation between $P_{1.0} - V$ and $P_0 - V$. The straight line represents the linear transformation, based upon the NPS, between the two color systems.

TABLE 2

EFFECTIVE WAVE LENGTHS FOR $P_{0.5}$

Temp. ° K	$P_{0.5}$ (A)	IPg (Seares) (A)
3,000	4590	4560
11,000	4210	4240

TABLE 3

COMPARISON OF $P_{0.5}-V$ WITH C_{int}

Sp.	$P_{0.5}-V$	C_{int} (Seares)	Sp.	$P_{0.5}-V$	C_{int} (Seares)
B3	−0.51	(−0.50)	A5	0.00	−0.01
B5	− .42	− .42	F0	+ .15	+ .12
A0	− .17	− .17	F5	+ .27	+ .27
A2	−0.10	−0.06	G0 V	+0.44	+0.45

Figure 5 should be compared with Figure 1, since, as has been shown above, $P_{1.0}$ is fairly close to Eggen's Pg_p. If we restrict our attention to $P_0 - V < +1.2$, the same nonlinear relationship appears in both figures, for the giants (*crosses*), subgiants (*open circles*), and dwarfs (*filled circles*).[7] The relation between the two systems is not only nonlinear but *multivalued*, since the supergiants (*triangles*) and reddened stars deviate greatly from the relation defined by the lower-luminosity, unreddened stars. The use of a linear transformation between the data making up either Figure 1 or Figure 5 will result in systematic errors much larger than the accidental observational errors.

Figures 1 and 5 differ significantly for $P_0 - V > +1.2$. Figure 1 shows a large systematic deviation for the M dwarfs; Figure 5 exhibits a smaller deviation, but in the same direction. The explanation may be that the contribution of the ultraviolet beyond

[7] The smaller scatter in Fig. 5 is due principally to the fact that the ordinate and abscissa are independent only to the extent of the ultraviolet present in $P_{1.0}$, but not present in P_0. The figure therefore exhibits the effect of the ultraviolet much more clearly than if entirely independent observations were used.

3800 A to Eggen's blue magnitudes is an even greater fraction of the total than in the case of $P_{1.0}$.

Figure 6 gives a comparison between P_0 and $P_{0.5}$. Since it has been shown above that $P_{0.5}$ is fairly close to IPg, it is evident that the linear transformation from the blue magnitudes, m_p (or B), to the NPS (see Paper I) is inadequate. Such a linear transformation is only a crude approximation for $B - V > 0$ and is useless for blue stars, supergiants,

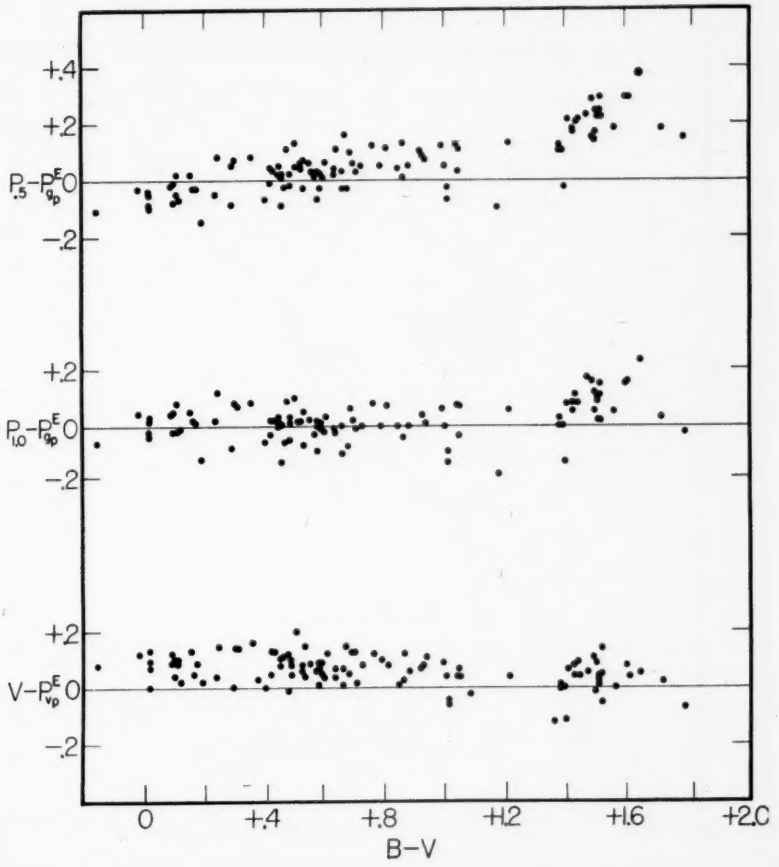

FIG. 4.—Comparisons of $P_{0.5}$ and $P_{1.0}$ with Eggen's Pg_p^E and a comparison of V with Eggen's Pv_p^E

and reddened stars. A comparison of Eggen's Pg_p^E with $P_{0.5}$ is very similar—practically the only difference is a change of sign of the ordinate. It is very clear that *neither* series of photoelectric observations can be transformed to the NPS system, *using the stars available there*, with sufficient accuracy to warrant the transformation. The same statement can be made with regard to most other series of photoelectric observations.

The quality of the transformation possible between two systems both of which discard the ultraviolet beyond 3800 A is shown by a comparison between $B - V$ and Stebbins

and Whitford's[8] six-color $V - G$, illustrated in Figure 7. The relation is not exactly linear, although it is nearly so. It should be noted, especially, that the supergiants (*triangles*) and reddened stars fall upon the same sequence as do the other stars. This is in marked contrast with Figures 5 and 6.

The relation between $B - V$ and the six-color $V - I^8$ is shown in Figure 8. Even a *large* change in the yellow filter has only a minor effect on the quality of transformation.

An even more stringent test of the transformability of $B - V$ to other systems not

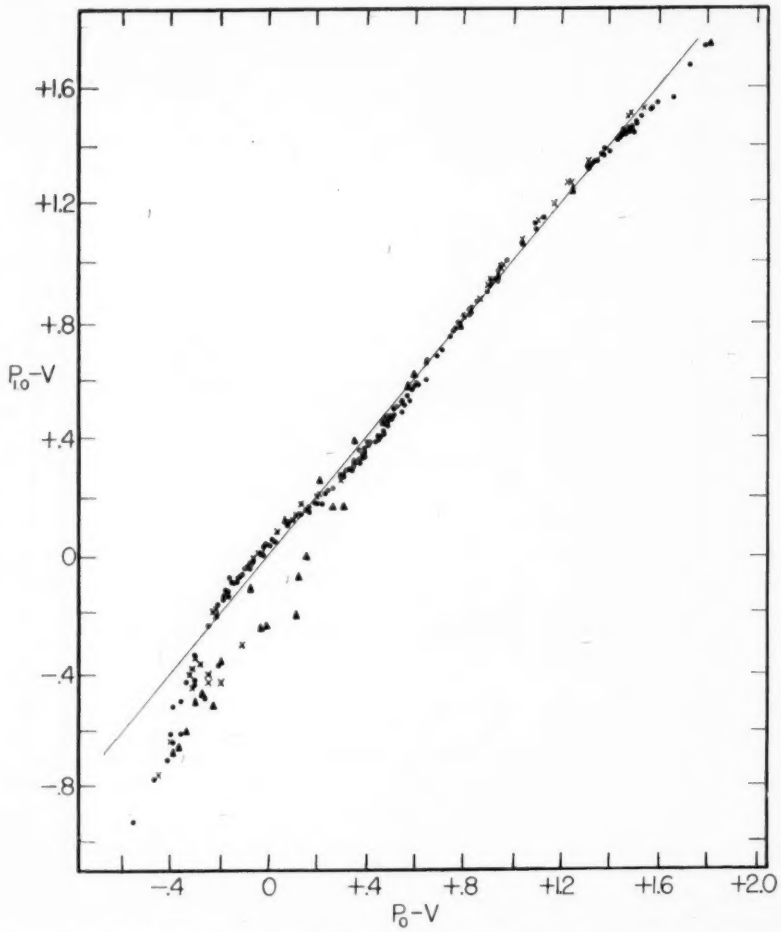

FIG. 5.—Comparison between two color systems, $P_{1.0} - V$ and $P_0 - V$, both on the International System according to the NPS stars. The symbols are defined as follows: *filled circles:* luminosity class V; *open circles:* luminosity class IV; *crosses:* luminosity class III; *triangles:* luminosity classes Ia, Ib, and II.

[8] *Ap. J.*, **102**, 318, 1945.

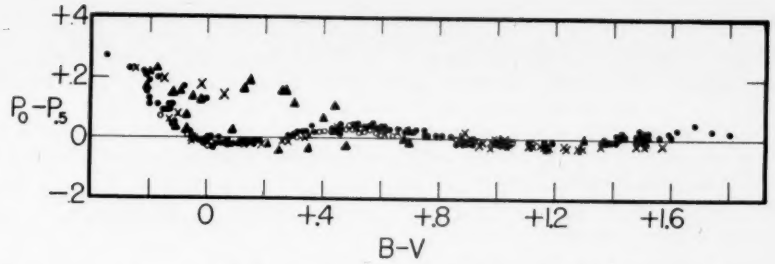

FIG. 6.—Comparison of P_0 with $P_{0.5}$ as a function of $B - V$. The symbols are the same as for Fig. 5

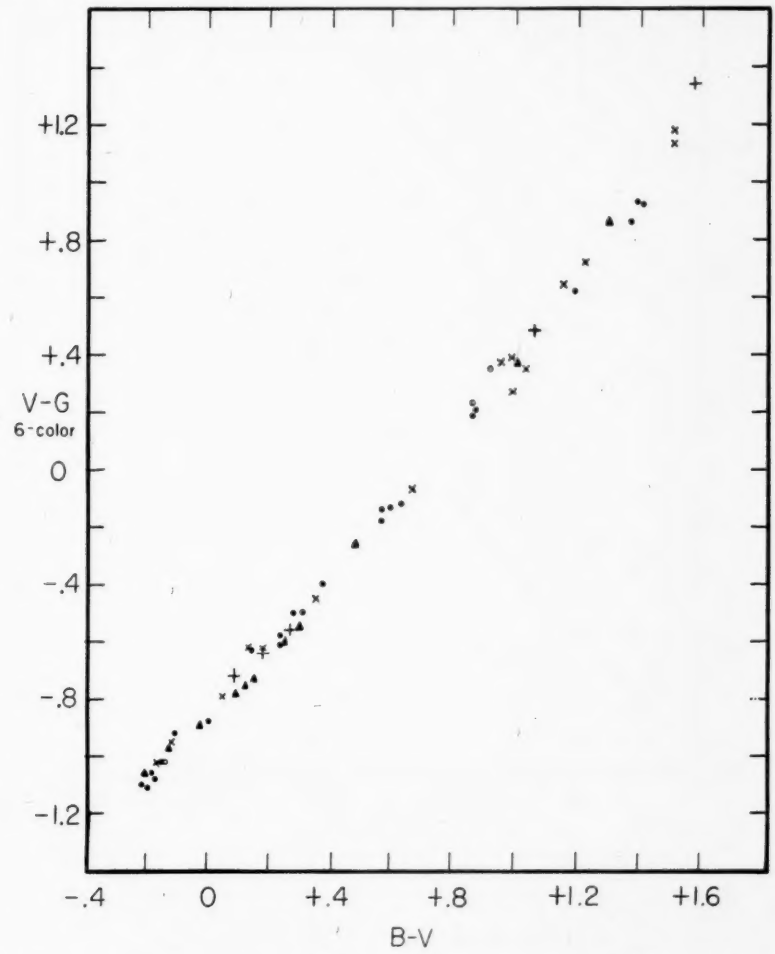

FIG. 7.—Six-color $V - G$ versus $B - V$. The symbols are the same as for Fig. 5, except *plus signs:* NPS stars.

containing ultraviolet is shown in Figure 9, *a*, where the gradients from Greenwich,[9] Mount Stromlo,[10] and Hall,[11] all transformed to the Greenwich system, are compared with $B - V$. The relationship is not linear but is smooth in the region of $B - V = 0$, indicating that the effect of hydrogen absorption on B is small. Figure 9, *b*, shows the relations between the same gradients and $P - V$, as determined from three different filters and linear transformations to the NPS. Curve *a* is the mean relation, $\overline{(P_0 - V)}$ vs. G; curve *b*, $\overline{(P_{0.5} - V)}$ vs. G; and curve *c* is the mean relation given by Eggen,[12] transformed by his equation[4] to $P - V$.

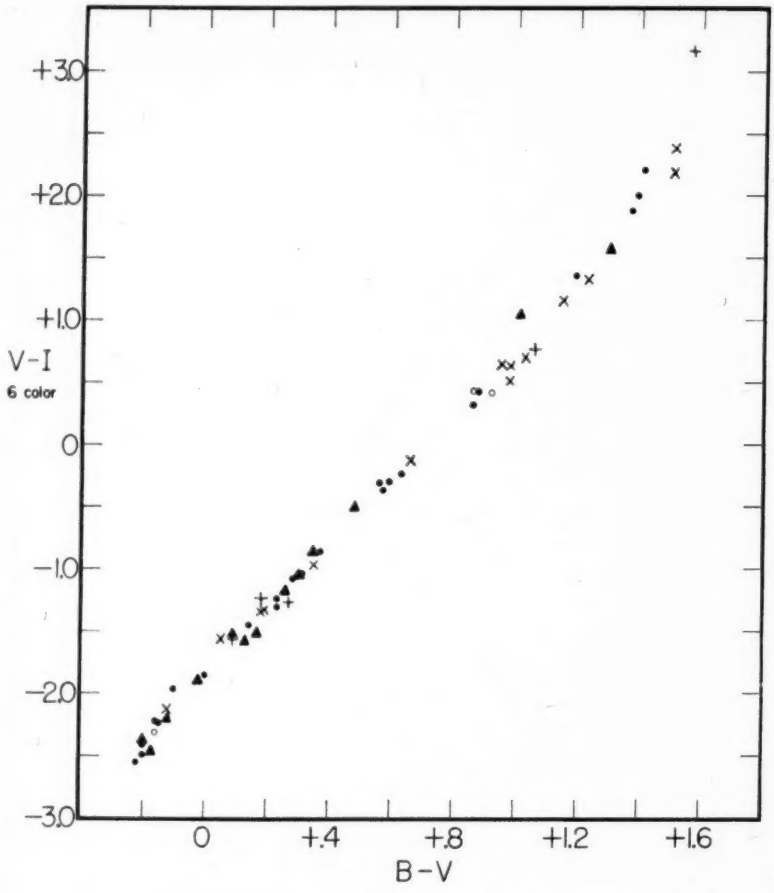

FIG. 8.—Six-color $V - I$ versus $B - V$. The symbols are the same as for Fig. 7

[9] *M.N.*, **100**, 189, 1939.
[10] S. C. B. Gascoigne, *M.N.*, **110**, 15, 1950.
[11] *Ap. J.*, **95**, 231, 1942.
[12] *Ap. J.*, **113**, 663, 1951.

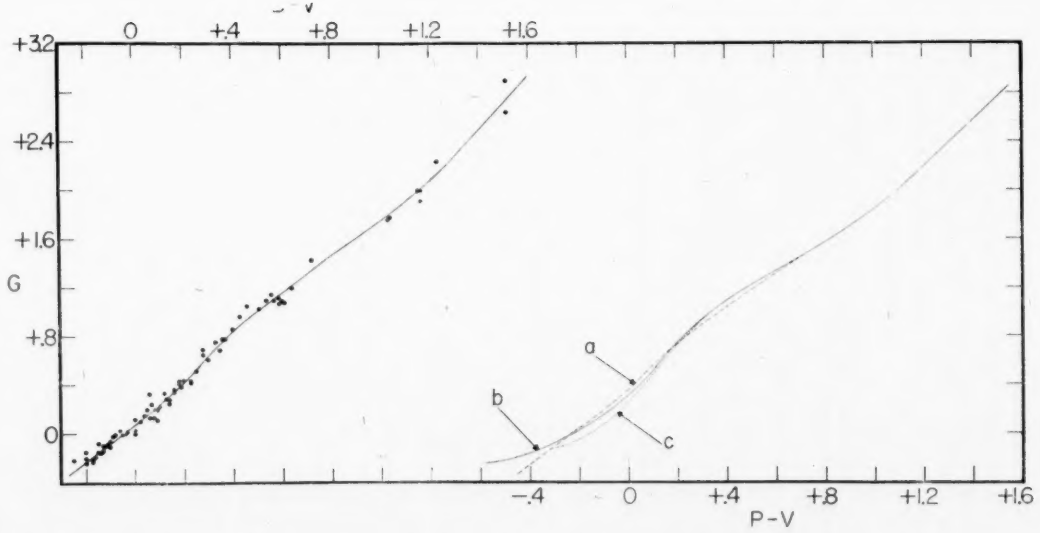

FIG. 9.—*a:* The Greenwich gradients, G, versus $B - V$. *b:* The mean relations between the gradients and three color systems, all based on the NPS. The curves are as follows: *a:* $P_0 - V$ versus G; *b:* $P_{0.5} - V$ versus G; *c:* C_p^E versus G, transformed to $P - V$ by Eggen's transformation.

The data presented above make it possible to draw a number of conclusions about magnitude systems.[13] These are:

1. Transformations between different color or magnitude systems are, in general, nonlinear.

2. Transformations between different color or magnitude systems, one or both of which include appreciable radiation to the violet of 3800 A, are, in general, multivalued as well as nonlinear. The type of transformation depends upon the spectral types and luminosity classes of the stars, as well as the observed magnitudes and colors. Minor changes in the ultraviolet response of the photometer can produce large changes in the observed results.

3. The North Polar Sequence is clearly inadequate as a standard region. The numbers of stars of the necessary kinds are entirely too small to permit accurate transformations to be made. This is especially true if ultraviolet beyond 3800 A is included in the measurements, as in *IPg*, since very blue stars, supergiants, reddened B stars, and red dwarfs are necessary but are not available in the NPS.

4. If only radiation to the red of approximately 3800 A is included in the measurements, fairly simple (but usually nonlinear) transformations between quite dissimilar color systems are possible.

[13] W. Becker (*Veröff. Göttingen*, Nos. 79–82, 1946) has independently arrived at some of these same conclusions.

THE SPECTRA AND LUMINOSITIES OF WHITE DWARFS

WILLEM J. LUYTEN
University of Minnesota
Received April 4, 1952

ABSTRACT

From observations made with several spectrographs attached to the 82-inch McDonald and the 100-inch Hooker telescopes preliminary spectral classifications are given for forty-four white dwarfs. Using all available parallaxes and color indices for these stars, it is shown that the white dwarfs appear to occupy a single sequence with considerable scattering in the H-R diagram, roughly parallel to the main sequence. Furthermore, it appears to be indicated that the diameters of most white dwarfs lie between four times and one-half that of the earth.

In January, 1945, through the kindness of Dr. Otto Struve, director of the Yerkes and McDonald Observatories, the writer was given the opportunity to use the 82-inch telescope for the spectroscopic observation of some faint white dwarfs. Subsequently, a cooperative observing arrangement was entered into with the McDonald Observatory whereby the staff of that observatory would continue to take spectrograms of these stars and forward them to Minnesota for analysis. In 1948 a contract was entered into with the Office of Naval Research which made it possible to continue this same arrangement with the McDonald Observatory for another year. The last of the observations under this contract were made by the writer personally during a brief stay at the McDonald Observatory in 1949. Finally, the writer was given guest investigator privileges at the Mount Wilson Observatory during the summer of 1950 and permitted to use the 100-inch telescope for four nights for this same work. All together, some 150 observing hours with the 82-inch telescope and 20 hours with the 100-inch telescope were devoted to the taking of spectra of white dwarfs.

Since most of the stars concerned are faint and require exposures of two hours and upward, only forty-four different stars could be observed, and most of these only once. This represents only the beginning of a really systematic program of observation of white-dwarf spectra: each of the seventy-five-odd known white dwarfs north of declination $-40°$ should be observed at least three times and, preferably, with different dispersions.

However, there now appears little likelihood that further observing time can be obtained; it would seem best, therefore, to publish at least some preliminary results and conclusions obtained from the material at hand.

With the 82-inch telescope the following spectroscopic equipment and designations were used: "Q": quartz spectrograph with $f/1$ Schmidt camera and a dispersion of 340 A/mm; "A": one-prism (glass) spectrograph with a dispersion of 340 A/mm—both of these were used in the Cassegrain focus; "B": a grating spectrograph designed by Dr. Thornton Page for nebular work and used in the prime focus—dispersion 390 A/mm at $H\gamma$; "W": at Mount Wilson the one-prism spectrograph with a dispersion of 165 A/mm used in the Cassegrain focus of the 100-inch telescope.

The spectra of white dwarfs are often, if not usually, unlike those of any other stars; in classifying them, the following arbitrary and empirical rules were followed.

If mainly the Balmer series of hydrogen was visible, the designation "DA" was used, followed by numbers ranging from 0 to 7, the lower numbers indicating broad and shallow lines and an intensity maximum farthest in the violet, the higher numbers indicating sharper lines with an intensity maximum shifting toward the red. Sometimes still further qualifying letters, "s" and "n" for very sharp and nebulous lines, have been added.

For two spectra which show only helium lines and no others, the letters "DB" have

been used, "DB-0" where the lines are stronger, "DB-1" where they are weaker. In the case of spectra which appear wholly continuous, the designation "DC" has been used. For van Maanen's star, whose spectrum shows strong *Ca* II lines and very little else, the designation "DF" has been used.

Provisionally, the designation "SDF" is suggested for those "intermediates" whose spectra show a resemblance to that of ordinary class F. While the writer objects to the nomenclature "subdwarfs" or "underluminous" for these stars, which are much more luminous than the real white dwarfs, at least the letters "SD" preceding the usual letter of classification fit with the writer's proposed classification indicating semidegenerate stars and entail a minimum of change from the previous "sd" prefix.

A summary of the spectral classification of forty-four white dwarfs and five intermediates is given in Table 1, the first four columns of which require no further explanation. The fifth column gives the color index as previously determined by the writer; the sixth column, the equipment used for obtaining the spectra, the letters "Q," "A," "B," and "W" having been explained above. The seventh column gives the spectral classification, while the eighth contains some further descriptive material on most spectra.

Before commenting on the above data, the extremely provisional character of these classifications should again be emphasized. The variety of equipment used, the small dispersion, the faintness of the stars often resulting in weak exposures, combined with the inherent peculiarity of most of these spectra, may well tend to produce differences in appearance which are not real. If the spectra of these stars could be obtained in a standardized manner, the need for as many as eight subdivisions in the DA class might well be materially reduced, while, in addition, a larger dispersion might well reveal lines in some spectra now classified as DC. As an illustration of this it may be pointed out that Kuiper,[1] using a spectrogram obtained with the 82-inch telescope, classified the spectrum of L 898-25 as "continuous," whereas on my own McDonald spectrogram the hydrogen lines are clearly seen.

Two conclusions, however, appear fairly clearly indicated: (*a*) For stars whose spectra show pronounced hydrogen lines there is a rough correlation between spectral class and color index, which is to be expected, of course, the DA-0–2 stars being bluer than the DA-3–7 stars. The relationship is not very close, suggesting that factors other than temperature—possibly the extent of hydrogen exhaustion—play an important role in producing the detailed features of the spectrum. For this reason no plot is given of the data, as this would have little meaning at present. (*b*) The stars classified as DC appear to be distributed over the entire temperature scale, ranging from H-Z 43, with a color index of −0.96, to W 489, with a color index of +0.77, the yellowest white dwarf for which a spectral classification—"continuous," made by Kuiper[2]—is available.

The two stars showing only helium and no hydrogen lines are not as blue and, therefore, presumably not as hot as a number of other white dwarfs which do show hydrogen but no helium lines. In view of current suggestions as to the origin of white dwarfs, it might be tempting to infer that these two helium stars represent that stage at which virtually all the hydrogen has been exhausted, and processes other than the usual ones may have to be called upon to explain the energy production in these stars.

In addition to these general conclusions, a number of anomalies may be noted:

A spectrogram of W 1516 taken with the quartz *f*/1 spectrograph of the 82-inch telescope, as well as one taken by Dr. Minkowski with the 100-inch telescope and kindly lent to the writer, shows a completely continuous spectrum. A spectrogram obtained by the writer with the 100-inch telescope shows, however, strong hydrogen lines down to $H\nu$ as well as the K line, a spectrum rather similar to that of an intermediate.

The anomalies with some of the spectra obtained for L 1126-68 and L 1140-73 have been commented upon in Table 1.

[1] *Pub. A.S.P.*, **53**, 248, 1941. [2] *Op. cit.*

TABLE 1

Star	1950 R.A.	1950 Dec.	m_{pg}	I.C.	Instr.	Sp.	Remarks
LDS 1 A	0h08m7	−21°00′	12.1	+0.30	Q, A, W	SDF	Hydrogen lines visible up to $H\mu$; K equals H–$H\epsilon$
LDS 1 B	08 7	−21 00	14.2	+ .69	Q, A, W	SDG	Clearly later than brighter component
L 1011-71	33 1	+ 1 37	15.3	+ .24	Q	DA-6	H lines sharper than those of W 1346 but not so sharp as in L 532-81; no K line
v Ma 1	46.5	+ 5 11	12.9	+ .69	Q	DF	H and K strong; almost no other lines visible with this dispersion
L 796-10	53 3	−11 45	15.1	+ .03	Q	DA-7	Very similar to L 1011-71 but seems a little less blue from the spectrum
W 1516	1 15 4	+15 56	13.6	− .23	Q, W	DC	No lines visible at all
R 548	33 7	−11 36	13.9	− .30	Q, W	DA-3	Slightly broader lines than VR 7
L 870-2	35 5	− 5 16	13.0	+ .13	Q, W	DA-4s	Lines much sharper than in VR 7 or in o_2 Eri B
Oxf +25°6725	2 05 9	+25 00	12.9	− .38	Q	DA-4	Spectrum very similar to that of VR 7
L 587-77 A	3 26 8	−27 34	13.9	+ .36	Q	DA-4s	Hydrogen lines fairly strong and sharp and similar to those in L 870-2
Z 10	4 07 3	+17 54	14.0	+ .01	Q	DA-4	Similar to VR 7
o_2 Eri B	13 0	− 7 44	9.4	.....	Q	DA-4	Prototype of white dwarfs showing hydrogen lines
VR 7	21 0	+16 14	14.1	+ .09	Q	DA-4	Spectrum very similar to that of o_2 Eri B
Z 9 = L 1239-16	29 4	+17 38	14.0	+ .24	Q	DA-4	Similar to VR 7
L 1244-26	6 12 4	+17 45	12.7	− .72	Q	DA-1	Hydrogen lines very broad; no helium lines visible
He 3	6 44 3	+37 36	11.2	− .80	Q	DA-0	This spectrum appears to be the bluest of all those showing hydrogen lines
L 384-24	7 32 0	−42 47	13.8	.....	Q	DA-3	Star too far south for accurate classification
L 745-46 A	38 0	−17 17	12.8	− .17	A	DA-3	Rather weak hydrogen lines
L 817-13	52 8	−14 38	13.3	− .21	Q	DA-4	Similar to VR 7
L 532-81	8 39 7	−32 47	11.7	+ .05	Q	DA-4s	Very sharp hydrogen lines; no K line visible
LDS 235 B	8 45 3	−18 48	14.6	− .45	Q	DA:	Underexposed spectrogram; difficult to classify
LDS 275 AB	9 35 0	−37 07	14.3	+ .15	Q, A, B	DC	Star too far south for useful estimate of intensity distribution but looks very blue
L 898-25	10 55 1	− 7 15	14.3	+ .04	Q	DA-5n	Hydrogen lines very broad and shallow
L 971-14	11 15 8	− 2 58	14.9	− .13	Q	DC:	Very faint star; suspicion of $H\beta$, similar to LDS 678 A
L 1405-40	47 7	+25 35	15.4	− .27	A	DAs:	Extremely difficult star; hydrogen lines appear rather sharp
L 1261-24	11 54 2	+18 39	15.4	− .22	B	DC:	Very faint star; spectrum looks continuous and rather similar to that of LDS 275
Z 43	13 14 0	+29 22	11.9	− .96	Q, B	DC	Several spectrograms were obtained; none show any lines at all
−7°3632	27 7	− 8 18	12.1	− .40	Q	DA-2	Very similar to W 1346
LDS 455 A	34 3	−16 04	14.9	− .35	Q	DA-4	Very faint and somewhat uncertain
L 619-50	48 1	−27 18	15.0	− .35	Q, B	DA-2	Very faint but very blue
L 1126-68	14 48 4	+ 7 47	15.0	− .38	B	DF:	See notes to table
LDS 539 B	15 41 9	−38 10	15.0	+ 4:	Q	SDF-5	Very broad hydrogen lines; strong K line
L 1491-27	16 37 4	+33 32	14.2	− .12	W	DF:	Hydrogen lines weak; K line strong and rather sharp
W 672 A	17 16 2	+ 2 00	14.2	− .03	B	DA-4	Similar to VR 7
L 1065-7	18 37 1	+ 3 42	13.0	+ .3:	W	SDF-5	Sharp and strong K line
L 1281-37	18 41 6	+15 59	12.8	+ .2:	W	SDF-2	Sharp and strong K line
LDS 678 A	19 17 7	− 7 46	11.9	− .14	Q	DC	Well-exposed spectrogram shows no lines, but clearly star is less blue than Z 43
LDS 683 B	32 9	−13 36	15.0	− .20	Q, W	DA-4	Very broad and weak hydrogen lines
L 1573-31	40 4	+37 24	14.1	− .19	Q	DB-1	No hydrogen lines visible; helium lines fairly strong but not so strong as in L 930-80
L 1140-73	41 9	+ 8 47	14.2	+ .44	B, W	DA-3	See notes to table
W 1346	20 32 3	+24 55	11.2	− .30	Q	DA-2	Wide, shallow hydrogen lines
LDS 749 B	21 29 6	0 00	14.2	− .39	Q	DA-3	Rather fuzzy hydrogen lines
L 930-80	45 0	− 7 58	14.2	− .40	Q, W	DB-0	See notes to table
LDS 766 A	54 9	−43 42	14.0	+ 1:	A	DA:	These stars are so far south that the spectra obtained are difficult to classify; both show faint hydrogen lines
LDS 785 B	22 24 6	−34 27	14.5	+ .2:	A	DA:	
L 1512-34	23 41 4	+32 15	13.0	+ .06	W	DA-4	Very similar to VR 7
LDS 826 A	51 5	−33 33	14.6	+ .25	Q	DA-4s	Star too far south for accurate observation; spectrum similar to that of L 587-77 A
L 505-42	51 7	−36 50	14.8	+0.02	Q	DA-5	Spectrum possibly similar to that of L 796-10, but star too far south

NOTES TO TABLE 1

L 1126-68 The spectrogram taken with the B spectrograph at the McDonald Observatory and sent to the writer shows a strong K line. Kuiper classified it as wA. Since the color index suggests that the star is blue, there is a possibility that the wrong star was observed at McDonald.

L 1140-73 The McDonald spectrogram shows a strong K line and suggests a spectral class of SDF. The writer's spectrogram taken with the 100-inch telescope at Mount Wilson shows broad and weak hydrogen lines and no *Ca* II. Because of the large positive color index it seems probable that the writer misidentified the star.

L 930-80 Dr. W. W. Morgan, at the Yerkes Observatory, has kindly examined the spectrograms and permits me to quote his description of them: "The hydrogen lines are probably absent. The *He* I lines at λ 3889 and λ 4471 are outstanding in intensity; they are of the same order of strength as the $H\gamma$ line in main-sequence B3 stars and are probably stronger than in any known stellar absorption spectrum. The lines of *He* I at λ 4922 and λ 4026 are also present."

For L 1491-27 the spectrogram obtained by the writer with the 100-inch telescope shows weak hydrogen lines but a strong K line, rather similar to that of an SDF spectrum. The color index, however, suggests that the star is much bluer and hotter than this.

To these may be added the case of star No. 41, found blue by Humason and Zwicky near the North Galactic Pole. Their spectrogram of it was classified as F, and they suggested that the apparent blue color might have been due to a flaw on one of the plates used in their color survey. The writer has redetermined the color of this star with the 36-inch telescope at Tucson, and there can be no doubt that the star is very blue.

For R 640, likewise, the writer finds a color index of −0.33, but Kuiper classifies the spectrum as wF5.[3]

The simplest solution of these difficulties—and perhaps the most probable one—is that of misidentification of the star when a slit-spectrogram was taken. Against this it can be argued that the fields of all the above stars, with the exception of L 1140-73, contain few stars and that identification of the white dwarfs should have been easy. Perhaps the matter of such misidentification could be conclusively settled by slitless spectra; but,

TABLE 2

Star	1950 R.A.	1950 Dec.	m_{pg}	I.C.	Sp.	μ	p
L 587-77 B	3^h26^m8	−27° 34′	15.6	2.07	M5:	0″.81	0″.045
LDS 235 A	8 45.3	−18 48	12.6	1.22	K2	.13	.013
L 1405-41	11 47.7	+25 35	16.4	0.93	K:	.30	.015
LDS 455 B	13 34.3	−16 04	15.2	1.18	K–M:	.09	.008
L 619-49	13 48.1	−27 18	13.9	1.60	.....	.24	.023
W 672 B	17 16.2	+ 2 00	15.5	1.46	M3*	.56	.025
LDS 678 B	19 17.7	− 7 46	13.7	1.81	M3	.20	.030
LDS 683 A	19 32.9	−13 36	14.9	1.52	K–M:	.14	.011
LDS 749 A	21 29.6	0 00	11.0	0.90	K2	.41	.031
L 1512-35	23 41.4	+32 15	13.2	1.65	M2	.22	.048
LDS 826 B	23 51.5	−33 33	15.0	1.60	M1:	0.50	0.025

* Spectral class by Kuiper, *Ap. J.*, **91**, 269, 1940.

until it is settled, the possibility, however remote and however much it smacks of spectroscopic heresy, may well be kept in mind that the spectra of some white dwarfs undergo radical changes over short periods of time. The apparent disagreement between spectra showing *Ca* II lines and negative color indices could perhaps be explained in terms of the very high densities of some of these white dwarfs, which would keep at least some calcium in the singly ionized state at rather high temperatures.

For a number of wide binaries containing one white- and one red-dwarf component, spectra and color indices were obtained for the red components also. Data for eleven of these are given in Table 2. The first seven columns are self-explanatory; the estimated values for the parallax shown in the last column were derived (*a*) from assuming that the red star in question is an ordinary main-sequence star and (*b*) by also giving some consideration to a value for the parallax as indicated by the size of the proper motion alone.

Trigonometric parallaxes are now available for twenty-six white dwarfs; for four further stars which appear to belong to the Hyades the cluster parallax may be used, while for three other stars with large parallaxes the question of whether they are wholly degenerate stars is somewhat in doubt. Finally, parallaxes and luminosities may at least be estimated for the eleven white-dwarf components of binaries for whose red components data and estimated parallaxes were given in Table 2.

[3] *Op. cit.*

TABLE 3

Star	1950 R.A.	1950 Dec.	m_{pg}	Sp.	$\bar{p}$	M_{pg}	I.C.
v Ma 1	0^h46^m5	+ 5° 11′	12.9	DF	0".245	14.8	+0.69
L 870-2	1 35.5	− 5 16	13.0	DA	.065	12.1	+0.13
h Per 1166	2 14.0	+56 53	13.2	DA	.011	8.4	−0.59
W 219	3 41.6	+18 18	15.1	DF	.066	14.2	+0.73
o_2 Eri B	4 13.0	− 7 44	9.5	DA	.200	11.0	−0.1:
L 82-61	6 15.5	−59 11	13.7	a–f	.041	11.8	+0.2:
α CMa B	6 43.0	−16 39	8.8	DA	.376	11.7	+0.3:
He 3	6 44.3	+37 36	11.2	DA	.066	10.3	−0.80
α CMi B	7 36.7	+ 5 21	11.3	f:	.294	13.6	+0.4:
L 745-46 A	7 38.0	−17 17	12.8	DA	.158	13.8	−0.17
L 97-12	7 52.8	−67 38	15.0	g	.170	16.2	+0.5:
L 532-81	8 39.7	−32 47	11.7	DA	.102	11.8	+0.05
SA 29-130	9 43.5	+44 08	12.9	DA	.035	10.6	−0.57
R 627	11 21.7	+21 39	13.8	DA	.079	13.3	−0.54
L 145-141	11 42.9	−64 34	11.9	DA	.204	13.2	−0.1:
W 457	12 57.7	+ 3 46	16.0	DC	.076	15.4	+0.15
BD−7°3632	13 27.7	− 8 18	12.1	DA	.062	11.1	−0.40
W 489	13 34.3	+ 3 58	15.5	DC	.129	16.1	+0.77
Grw+70°5824	13 37.8	+70 33	12.3	DA	.028	9.5	−0.62
CPD−37°6571 B	15 44.2	−37 45	13.5	DA	.074	12.8	0.0:
Grw+70°8247	19 00.6	+70 34	12.7	DC:	.074	12.0	−0.31
L 997-21	19 54.0	− 1 09	13.7	DA	.074	13.0	0.00
W 1346	20 32.3	+24 55	11.2	DA	.074	10.5	−0.30
LDS 749 B	21 29.6	0 00	14.2	DA	.025	11.2	−0.39
Grw+82°3818	21 36.7	+82 49	12.5	DA	.050	11.0	−0.55
L 362-81	23 59.6	−43 25	12.8	DA	.127	13.3	0.0:
VR 7	4 21.0	+16 14	14.1	DA	.026	11.2	+0.09
VR 16	4 25.7	+16 52	13.5	DA	.026	10.6	−0.47
Z 9	4 29.4	+17 38	14.0	DA	.026	11.1	+0.24
Z 7	4 31.0	+12 35	13.6	DA	.026	10.7	−0.54
L 68-28	12 25.6	−71 13	15.7	k–m	.15:	16.6	+1.1:
L 68-27	12 25.6	−71 13	17.7	k–m	.15:	18.6	+1.0:
BD+4°4048 B	19 14.6	+ 5 05	19.5	m	.170	20.7	+1.4
L 587-77 A	3 26.8	−27 34	13.9	DA	.045	11.2	+0.3:
LDS 235 B	8 45.3	−18 48	14.6	DA	.013	10.2	−0.45
L 1405-40	11 47.7	+23 35	15.4	DA	.015	11.3	−0.27
LDS 455 A	13 34.3	−16 04	14.9	DA	.008	9.4	−0.35
L 619-50	13 48.1	−27 18	15.0	DA	.023	11.8	−0.35
W 672 A	17 16.2	+ 2 00	14.2	DA	.025	11.2	−0.03
LDS 678 A	19 17.7	− 7 46	11.9	DC	.030	9.3	−0.14
LDS 683 B	19 32.9	−13 36	15.3	DA	.011	10.5	−0.11
L 1512-34	23 41.4	+32 15	12.9	DA	.048	11.3	+0.06
LDS 826 A	23 51.5	−33 33	14.6	DA	0.025	11.6	+0.25:

Data for the forty-three stars in these four groups are given in Table 3, the first three columns of which need no further comment. The fourth column gives the photographic magnitudes, mainly those determined by the writer at Tucson, the fifth column the spectral or color class, without, however, the details mentioned above. The sixth and seventh columns give the adopted parallax and the corresponding (photographic) absolute magnitude, while the eighth column again gives the writer's color index, either that determined at Tucson or the best guess that can now be made.

The color-luminosity diagram from these data is plotted in Figure 1, where the scales have been so chosen as to equalize the linear values of the estimated uncertainties in both

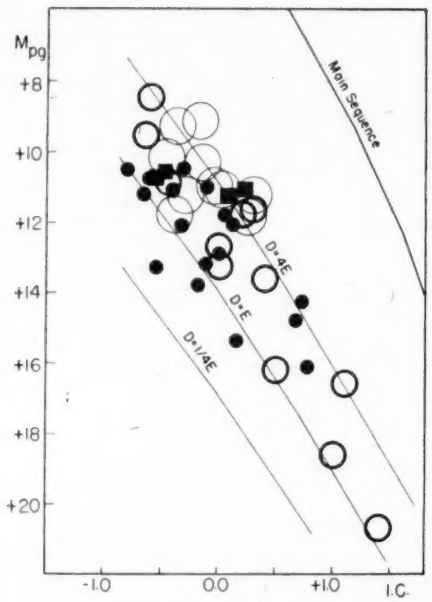

FIG. 1.—Relationship between absolute magnitude and color index for white dwarfs of known parallax. Black squares indicate the four white dwarfs in the Hyades; black circles, those seventeen stars for which the data are most certain, the radius of the circles indicating the probable errors in these data. Heavy open circles indicate more uncertain data; thin, open circles, the most uncertain data.

co-ordinates for the seventeen stars with the best parallax and color-index determinations. Each of these well-determined objects is represented by a full circle whose radius equals the probable error in each co-ordinate. The four white dwarfs in the Hyades are represented by similar black squares. Those stars for which either the color index or the parallax is uncertain are represented by heavy open circles, those for which both are uncertain by larger, and thinner, open circles.

The horizontal scale represents the writer's Tucson color indices, expressed on a rather arbitrary and uncalibrated scale. Reducing these very roughly to the International System and thence to temperature, and allowing for the bolometric correction to the luminosities, we may find the approximate loci for stars of constant diameter, assuming that the white dwarfs radiate as black bodies. Three curves are drawn, viz., for stars whose diameters are four times that of the earth, equal to that of the earth, and one-fourth that of the earth, respectively. It is seen, if both the data and the assumptions can

be trusted, that the diameters of most white dwarfs lie between those of the earth and of Uranus, and none are so small as that of the moon. The smallest of them appears to be R 627, found white by van Maanen and Humason.[4] It is about as large as Mercury, or around 0.004 ⊙; if it has a mass roughly equal to that of the sun, the red shift should amount to more than 100 km/sec.

The main conclusion to be drawn from the diagram is that, while there seems to be an unmistakable relationship between absolute magnitude and color index—which, of course, is nothing new and has been known or suspected for a long time—there exists also a considerable cosmic dispersion, and the range in luminosity for a given color appears to be at least 3 mag. The width of the band seems to be more than ten times the now estimated uncertainty in the data, and, on the basis of the present data, there seems to be no justification for identifying more than one separate sequence.

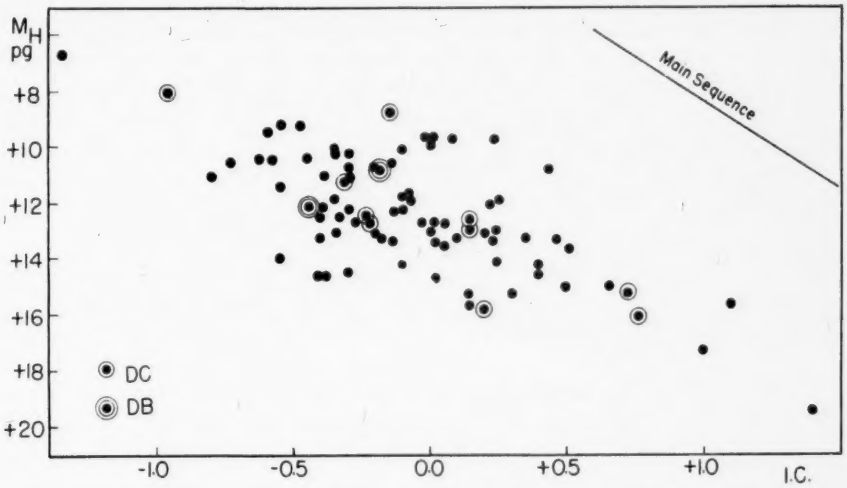

FIG. 2.—Relationship between estimated absolute magnitude and color index for white dwarfs of known proper motion. The absolute magnitudes have been derived statistically from the formula $M = m + 5 + 5 \log \mu$. Stars with continuous spectra are indicated by a single circle around the dot; stars with helium lines in their spectra, by two circles.

Attention may be called to the three open circles in the lower-right-hand corner; for all three of these the color has been estimated differentially by the writer, and it is always possible that these three stars will eventually turn out to be ordinary M dwarfs. The faintest of them is Van Biesbroeck's companion to BD+4°4048.

Still another diagram, Figure 2, shows the same relationship for all white dwarfs for which reasonably accurate colors are known. Here the absolute magnitudes have been obtained statistically from the proper motions alone, using the formula $M = 0.90\ H - 3.3$, derived from the data shown in Table 3, where $H = m + 5 + 5 \log \mu$. In this diagram the stars whose spectra appear virtually continuous are indicated by a circle around the dot; it is evident that their distribution is essentially the same as for those stars whose spectra show strong hydrogen lines, and they do not seem to form a separate sequence. Among them we find H-Z 43 (I.C. = −0.96, $\mu = 0''.14$) and BD+28°4211 (I.C. = −1.35, $\mu = 0''.12$); these two are shown at the extreme upper left. The only two white

[4] *Pub. A.S.P.*, **48**, 179, 1936.

dwarfs known to show helium lines in their spectra are indicated by a double ring; these likewise do not seem to occupy a position in the diagram noticeably different from that of the others, and it would thus seem that color index is a better indicator of luminosity for a white dwarf than spectral characteristics.

A few remarks about "intermediates" may be added, even though these stars may not be too closely related to the white dwarfs which form the main subject of the present discussion. While the terminology "intermediate" did not appear in the literature until 1923, the discovery of these stars appears to antedate that of the regular white dwarfs. As soon as the Hertzsprung-Russell diagram was being used, it became known that Kapteyn's star was much less luminous than other stars of its spectral class. In 1923, I pointed out that this star—on the basis of the then existing data—lay as far below the main sequence as Arcturus was above it. As late as 1935, Kuiper disagreed with this and stated flatly that "if anything, the data point to a normal red dwarf."[5] In 1940 he finally became convinced; but then, characteristically, he claimed that he himself now had "the first M-type subdwarf definitely established."[6] Since that time Kuiper has published several lists of such intermediates, while, from the general color survey conducted by the writer, well over one thousand possible stars of this kind have been identified.

In spite of the several kinds of data which have now been gathered on white dwarfs, it is evident that the only definite statement that can now be made is that no really definite conclusions are possible until a great many more detailed observations on white dwarfs have been obtained. The paradox of these stars is that they are at once the easiest stars to identify and the hardest to observe, because nearly all of them are so extremely faint and so blue that one cannot see them on the slit of the spectrograph. With the recent improvement in photoelectric techniques, there is every hope that before long we shall have really accurate and homogeneous color indices for most of these stars. But in the matter of parallaxes the prospect is most gloomy of all: almost no telescopes now being used for parallax work can go fainter than the twelfth magnitude, and the bulk of white dwarfs are fainter than the fourteenth.

A large number of the spectroscopic observations at the McDonald Observatory were obtained under a contract with the Office of Naval Research, for which the writer wishes to express his deep appreciation, as these observations have been of vital importance in this discussion. The writer is further indebted to Dr. Otto Struve, Dr. Paul D. Jose, and Mr. William C. Miller for their very effective aid in the actual making of the spectroscopic observations at the McDonald and Mount Wilson Observatories.

[5] *Pub. A.S.P.*, **47**, 96, 1935.

[6] *Ap. J.*, **91**, 269, 1940.

ON THE DECAY OF A PRIMEVAL STELLAR MAGNETIC FIELD*

MARSHAL H. WRUBEL
Indiana University
Received March 28, 1952

ABSTRACT

The shapes and decay times of three possible stellar magnetic fields were calculated by using a radial distribution of conductivity derived from Schwarzschild's temperature distribution. These particular fields would be expected to have the greatest longevity. Their decay times were found to be in the ratio 1.00:0.40:0.24; in the case of the sun, the fundamental field would decay to $1/e$ of its initial value in 4.08×10^9 years. More massive stars would be expected to have fields with lifetimes longer by a factor proportional to $R^2 T_c^{3/2}$. The effect of a different temperature distribution on these results is also discussed.

I. INTRODUCTION

In 1945, T. G. Cowling[1] showed that the magnetic field in a star, once created, would decay so slowly that any contemporary field could be interpreted as "a relic from a different primeval state." That such a field would decay if the conductivity were finite is obvious, since energy must be dissipated by the electric currents in the form of Joule heat. Horace Lamb[2] solved the problem of a field left to itself in a sphere of uniform conductivity. Cowling extended this work to the case of a star by deriving a conductivity distribution from the temperature distribution and integrating the equations of the problem numerically. Actually, Cowling considered only that field which decays slowest, namely, the fundamental field. However, an arbitrary initial field may contain other modes which may not decay so rapidly that every trace of them is gone in the contemporary field. The calculations which follow were made to determine the nature of some of the higher modes.

II. THE EQUATIONS OF THE PROBLEM

As is well known, Maxwell's equations appropriate to the problem on hand can be reduced to (cf. Cowling, *op. cit.*, eq. [4])

$$\nabla^2 \boldsymbol{E} = 4\pi\sigma \frac{\partial \boldsymbol{E}}{\partial t}, \tag{1}$$

where $\boldsymbol{E}$ denotes the electric field strength and σ the electrical conductivity. We seek solutions of this equation having axial symmetry, in particular those in which the currents travel in circles about the axis. If we refer to a system of spherical co-ordinates, this implies that the only component of the electric field which is not zero is the azimuthal component, E_φ, which is not itself a function of the azimuthal angle φ. In terms of the appropriate form of the operator ∇^2, equation (1) reduces to

$$\left\{ \frac{\partial^2}{\partial r^2} + \frac{2}{r}\frac{\partial}{\partial r} + \frac{1-\mu^2}{r^2}\frac{\partial^2}{\partial \mu^2} - \frac{2\mu}{r^2}\frac{\partial}{\partial \mu} - \frac{1}{r^2(1-\mu^2)} \right\} E_\varphi = 4\pi\sigma \frac{\partial E_\varphi}{\partial t}, \tag{2}$$

where $\mu = \cos\vartheta$. The form of this equation suggests that we seek a solution of the form

$$E_\varphi = g(r) P_n^1(\mu)\, e^{-t/\tau}, \tag{3}$$

* *Publications of the Goethe Link Observatory, Indiana University*, No. 7. This research was supported in part by funds of the Eugene Higgins Trust allocated to Princeton University and in part by a grant from the Graduate School of Indiana University.

[1] *M.N.*, **105**, 166, 1945.

[2] *Phil. Trans.*, **174**, 519, 1883.

where P_n^1 is the associated Legendre function of the first kind and τ is the "decay time." With this substitution, we readily verify that equation (2) becomes

$$\frac{d^2g}{dr^2}+\frac{2}{r}\frac{dg}{dr}-\frac{n(n+1)}{r^2}\,g+\frac{4\pi\sigma}{\tau}\,g=0\,. \tag{4}$$

If the conductivity, σ, is known as a function of r, this equation can be integrated numerically, subject to the boundary conditions that the field be finite at the center of the star ($r = 0$) and join the field for zero conductivity at $r = R$, where R is the radius of the star. Since these conditions cannot be met for arbitrary values of τ, this is an eigen-value problem. Solutions may be classified in two ways: according to the value of n in the Legendre polynomial and according to the number of times the radial eigenfunction passes through zero. Since the electric vector vanishes when $g(r)$ vanishes, the zeros of $g(r)$ represent spheres of zero current within the star.

In practice it is more convenient to deal with dimensionless variables. Thus with the substitutions

$$r = xR \qquad \text{and} \qquad p = x\,g\,, \tag{5}$$

we have

$$\frac{d^2p}{dx^2}+\left[\frac{4\pi\sigma R^2}{\tau}-\frac{n(n+1)}{x^2}\right]p=0\,. \tag{6}$$

The approximate distribution of conductivity through the star can be found from the temperature distribution by the formula (cf. Cowling[1])

$$\sigma = 5.87\times 10^{-15}T_c^{3/2}\theta^{3/2}\,, \tag{7}$$

where θ is the temperature in units of the central temperature, T_c. In the calculations which follow, we have used a temperature distribution derived by M. Schwarzschild.[3]

TABLE 1

VARIATION OF CONDUCTIVITY THROUGH THE MODEL STAR

x	$\theta^{3/2}$	x	$\theta^{3/2}$	x	$\theta^{3/2}$
0.00	1.0000	0.40	0.1464	0.80	0.01030
.10	0.8079	.50	.08160	0.90	.003052
.20	0.4735	.60	.04474	1.00	0.000000
0.30	0.2637	0.70	0.02311		

Although this has been superseded by more recent calculations, the order of magnitude of the final results cannot be changed appreciably. Table 1 provides a condensation of the conductivity distribution used in the numerical integration.

Using equation (7), we may now write equation (6) in the form

$$\frac{d^2p}{dx^2}+\left[\Gamma\theta^{3/2}-\frac{n(n+1)}{x^2}\right]p=0\,, \tag{8}$$

where

$$\Gamma = 5.87\times 10^{-15}\,\frac{4\pi}{\tau}\,R^2T_c^{3/2} \tag{9}$$

is the eigen-value to be determined. The boundary condition at the center requires that p behaves as x^{n+1} for small x. At $x = 1$, that is, at the surface of the star, p must behave

[3] *Ap. J.*, **104**, 203, 1946.

as x^{-n}, so that equation (6) is fulfilled outside the star ($x > 1$, $\sigma = 0$) by a solution that vanishes at infinity. This condition may be expressed as a condition on the derivative; thus

$$\left(\frac{dp}{dx}\right)_{x=1} = -n\,(p)_{x=1}\,. \tag{10}$$

The solutions may be found by assuming a value for Γ and deriving a power-series expansion valid for small x. This may be continued numerically by standard methods.[4] The

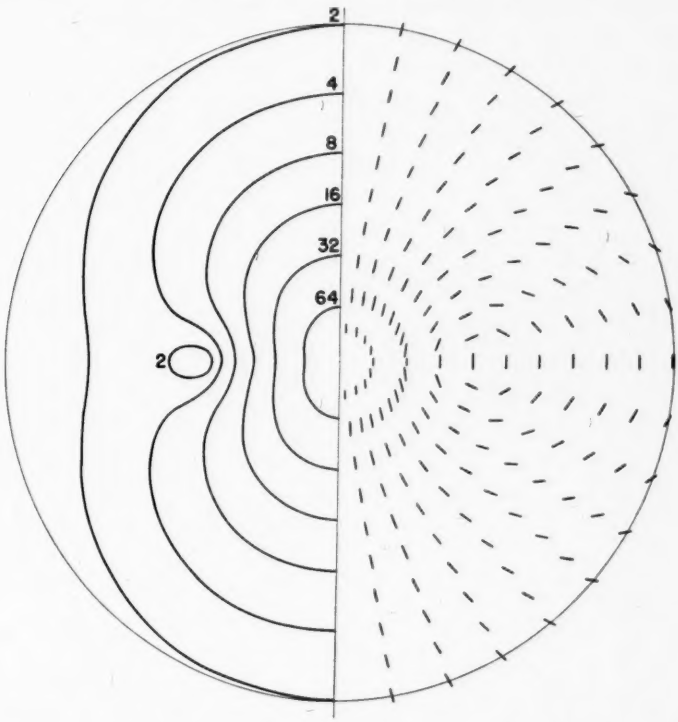

FIG. 1.—Contours and direction of the magnetic field for the case $n = 1$, no node, in the radial eigenfunction.

first derivative is calculated at $x = 1$, and the boundary condition equation (10) is tested. In successive trials the eigen-value is adjusted until equation (10) is satisfied.

If $p(x)$ is a solution of equation (8), then a constant times $p(x)$ is also a solution. This arbitrary constant may be determined if the initial field is specified. Once $p(x)$ is known, $g(x)$ follows from equation (5), and the electric field is given by

$$E_\varphi = A\,g\,(x)\,P_n^1\,(\mu)\;e^{-t/\tau}\,, \tag{11}$$

where A is an arbitrary constant.

[4] H. Levy and E. A. Baggott, *Numerical Solutions of Differential Equations* (Dover, 1950), chap. v.

The magnetic field can also be expressed in terms of $g(x)$. Thus, writing

$$\boldsymbol{H} = \boldsymbol{h}\, e^{-t/\tau}\,, \tag{12}$$

we have from Maxwell's equations,

$$\text{curl}\ \boldsymbol{E} = -\frac{\partial \boldsymbol{H}}{\partial t} = \frac{\boldsymbol{h}}{\tau} e^{-t/\tau}. \tag{13}$$

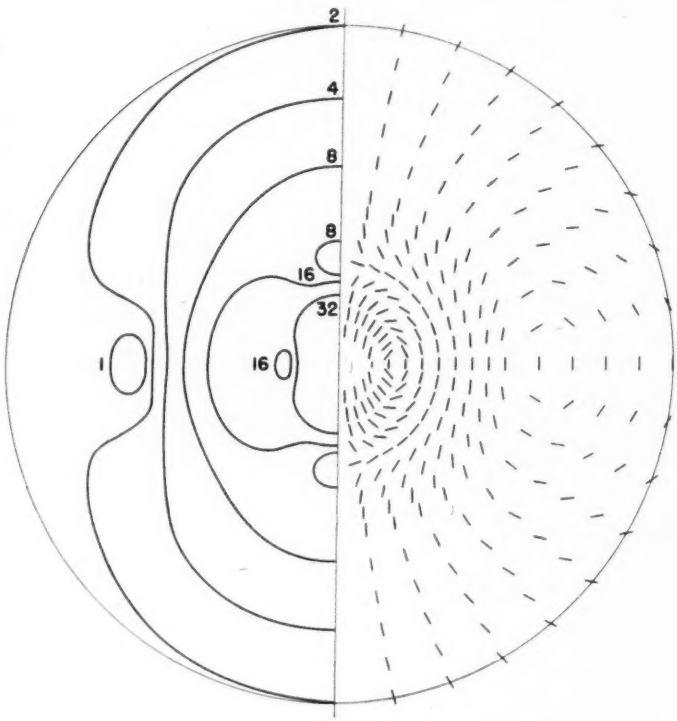

FIG. 2.—Contours and direction of the magnetic field for the case $n = 1$, one node, in the radial eigenfunction.

Expressing the curl in spherical co-ordinates, we find the components of $\boldsymbol{h}$ are:

$$h_r = \frac{A}{R}\,\frac{g(x)}{x}\left[\frac{\mu}{(1-\mu^2)^{1/2}}\,P_n^1(\mu) - (1-\mu^2)^{1/2}\,\frac{dP_n^1(\mu)}{d\mu}\right]\tau\,,$$
$$h_\vartheta = -\frac{A}{R}\left(\frac{dg}{dx}+\frac{g}{x}\right)P_n^1(\mu)\,\tau \qquad \text{and} \qquad h_\varphi = 0\,. \tag{14}$$

If we consider only those magnetic fields with opposite polarity at $\mu = 1$ and $\mu = -1$, we are restricted to odd values of n.

III. NUMERICAL RESULTS

Solutions were found for the following cases: $n = 1$, no node in the radial eigenfunction; $n = 1$, one node; $n = 3$, no node. The appropriate Legendre polynomials are

$$P_1^1(\cos\vartheta) = \sin\vartheta\ ,$$
$$P_3^1(\cos\vartheta) = \tfrac{3}{8}(\sin\vartheta + 5\sin 3\vartheta)\ . \tag{15}$$

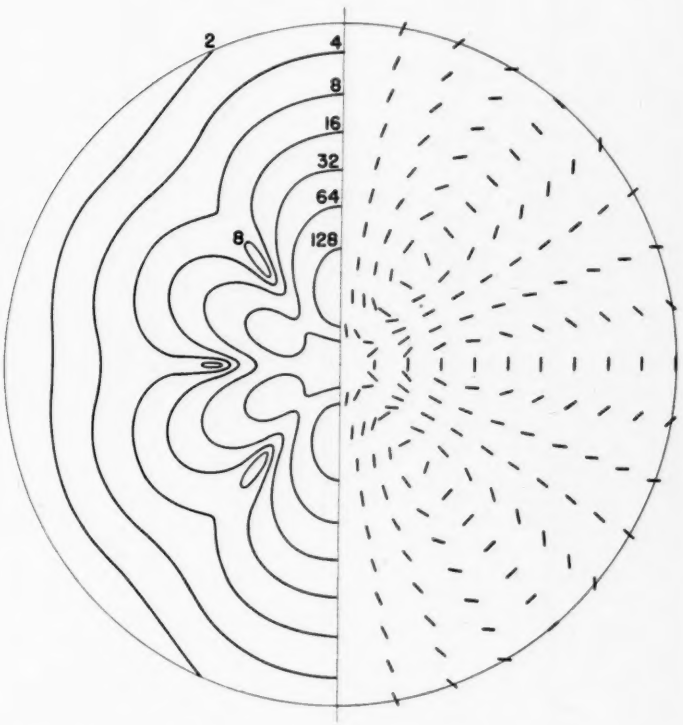

FIG. 3.—Contours and direction of the magnetic field for the case $n = 3$, no node, in the radial eigenfunction.

The radial eigenfunctions, normalized to unity at the surface, are given, together with their derivatives, in Table 2. The magnetic fields are illustrated in Figures 1, 2, and 3; contours are plotted on the left in units of the equatorial field at the surface; the direction of the field is indicated on the right. Table 3 gives the eigen-values, Γ; the decay times for the sun, $\tau_\odot$, according to equation (9) and assuming a central temperature of $15 \times 10^{6\circ}$ K; and the magnetic fields at the center in units of the equatorial field at the surface.

TABLE 2

THE RADIAL EIGENFUNCTION AND ITS DERIVATIVE

x	$n=1$ No Node		$n=1$ One Node		$n=3$ No Node	
	$g(x)$	dg/dx	$g(x)$	dg/dx	$g(x)$	dg/dx
0.00	0.000	+45.9	−0.000	−82.0	0.00000	+ 0.00
.01	0.458	+45.7	−0.817	−81.0	0.00587	+ 1.76
.02	0.912	+45.0	−1.614	−78.1	0.0464	+ 6.90
.03	1.357	+44.0	−2.37	−73.4	0.1540	+ 15.1
.04	1.790	+42.5	−3.08	−67.2	0.356	+ 25.6
.05	2.20	+40.7	−3.71	−59.6	0.673	+ 38.0
.06	2.60	+38.5	−4.26	−50.9	1.118	+ 51.2
.07	2.98	+36.1	−4.73	−41.7	1.697	+ 64.4
.08	3.32	+33.6	−5.10	−31.8	2.40	+ 77.0
.09	3.65	+30.8	−5.36	−22.2	3.23	+ 88.2
.10	3.94	+28.0	−5.54	−12.6	4.16	+ 97.6
.11	4.21	+25.2	−5.62	− 3.6	5.18	+104.6
.12	4.44	+22.3	−5.61	+ 4.6	6.25	+109.4
.13	4.65	+19.6	−5.53	+12.2	7.36	+111.8
.14	4.84	+16.9	−5.37	+18.6	8.48	+111.9
.15	4.99	+14.4	−5.16	+24.1	9.59	+109.7
.16	5.12	+11.9	−4.90	+28.8	10.66	+105.6
.17	5.23	+ 9.63	−4.59	+32.4	11.70	+100.0
.18	5.32	+ 7.46	−4.25	+35.3	12.66	+ 93.0
.19	5.38	+ 5.46	−3.88	+37.3	13.55	+ 84.7
.20	5.43	+ 3.60	−3.50	+38.7	14.35	+ 75.7
.21	5.45	+ 1.90	−3.11	+39.4	15.06	+ 66.0
.22	5.46	+ 0.35	−2.72	+39.3	15.67	+ 56.2
.23	5.46	− 1.06	−2.32	+39.1	16.18	+ 46.4
.24	5.44	− 2.34	−1.937	+38.4	16.60	+ 36.7
.25	5.41	− 3.47	−1.559	+37.4	16.92	+ 27.1
.26	5.37	− 4.48	−1.193	+35.8	17.14	+ 18.1
.27	5.32	− 5.38	−0.843	+34.2	17.28	+ 9.7
.28	5.27	− 6.16	−0.510	+32.4	17.34	+ 1.9
.29	5.20	− 6.85	−0.1952	+30.5	17.32	− 5.3
.30	5.13	− 7.42	+0.1003	+28.6	17.24	− 11.9
.31	5.05	− 7.91	+0.376	+26.6	17.09	− 17.8
.32	4.97	− 8.33	+0.632	+24.5	16.88	− 23.0
.33	4.89	− 8.69	+0.867	+22.6	16.63	− 27.6
.34	4.80	− 8.97	+1.083	+20.6	16.33	− 31.5
.35	4.71	− 9.19	+1.280	+18.8	16.00	− 34.9
.36	4.62	− 9.35	+1.458	+16.9	15.64	− 37.7
.37	4.52	− 9.46	+1.618	+15.2	15.25	− 39.9
.38	4.43	− 9.55	+1.761	+13.5	14.84	− 41.7
.39	4.33	− 9.59	+1.888	+11.9	14.42	− 43.0
.40	4.23	− 9.58	+2.00	+10.5	13.98	− 44.1
.41	4.14	− 9.56	+2.10	+ 9.0	13.54	− 44.8
.42	4.04	− 9.50	+2.18	+ 7.8	13.08	− 45.0
.43	3.95	− 9.43	+2.25	+ 6.6	12.63	− 45.1
.44	3.86	− 9.34	+2.31	+ 5.4	12.18	− 45.0
.45	3.76	− 9.22	+2.36	+ 4.4	11.74	− 44.6
.46	3.67	− 9.10	+2.40	+ 3.4	11.29	− 44.0
.47	3.58	− 8.96	+2.43	+ 2.6	10.85	− 43.3
.48	3.49	− 8.81	+2.45	+ 1.8	10.43	− 42.4
.49	3.40	− 8.64	+2.46	+ 1.0	10.01	− 41.6
.50	3.32	− 8.48	+2.47	+ 0.4	9.60	− 40.6
.51	3.23	− 8.31	+2.47	− 0.2	9.20	− 39.4
.52	3.15	− 8.14	+2.47	− 0.8	8.81	− 38.3
.53	3.07	− 7.96	+2.46	− 1.2	8.43	− 37.1
.54	2.99	− 7.77	+2.44	− 1.6	8.06	− 35.9
.55	2.92	− 7.59	+2.42	− 2.0	7.71	− 34.6
.56	2.84	− 7.40	+2.40	− 2.4	7.37	− 33.4
0.57	2.77	− 7.22	+2.38	− 2.6	7.04	− 32.2

TABLE 2—*Continued*

x	$n=1$ No Node		$n=1$ One Node		$n=3$ No Node	
	$g(x)$	dg/dx	$g(x)$	dg/dx	$g(x)$	dg/dx
0.58	2.70	− 7.04	+2.35	− 2.9	6.73	− 31.0
0.59	2.63	− 6.84	+2.32	− 3.1	6.42	− 29.8
0.60	2.56	− 6.67	+2.29	− 3.3	6.13	− 28.6
0.61	2.49	− 6.49	+2.25	− 3.4	5.85	− 27.4
0.62	2.43	− 6.32	+2.22	− 3.6	5.58	− 26.2
0.63	2.37	− 6.14	+2.18	− 3.6	5.33	− 25.2
0.64	2.31	− 5.96	+2.15	− 3.8	5.08	− 24.0
0.65	2.25	− 5.80	+2.11	− 3.8	4.85	− 23.0
0.66	2.19	− 5.64	+2.07	− 3.8	4.62	− 22.0
0.67	2.14	− 5.48	+2.03	− 3.9	4.41	− 21.0
0.68	2.08	− 5.31	+1.990	− 3.92	4.20	− 20.0
0.69	2.03	− 5.16	+1.951	− 3.94	4.01	− 19.0
0.70	1.979	− 5.02	+1.912	− 3.93	3.82	− 18.2
0.71	1.929	− 4.86	+1.873	− 3.90	3.64	− 17.3
0.72	1.882	− 4.70	+1.834	− 3.88	3.48	− 16.5
0.73	1.835	− 4.87	+1.795	− 3.84	3.31	− 15.8
0.74	1.790	− 4.44	+1.757	− 3.80	3.16	− 15.0
0.75	1.746	− 4.30	+1.719	− 3.75	3.01	− 14.2
0.76	1.704	− 4.16	+1.682	− 3.70	2.88	− 13.5
0.77	1.663	− 4.04	+1.645	− 3.64	2.74	− 12.9
0.78	1.624	− 3.92	+1.609	− 3.58	2.62	− 12.2
0.79	1.585	− 3.80	+1.574	− 3.50	2.50	− 11.6
0.80	1.548	− 3.68	+1.539	− 3.44	2.38	− 11.1
0.81	1.511	− 3.57	+1.505	− 3.36	2.28	− 10.6
0.82	1.476	− 3.46	+1.472	− 3.29	2.17	− 10.0
0.83	1.442	− 3.35	+1.439	− 3.22	2.08	− 9.5
0.84	1.409	− 3.24	+1.407	− 3.14	1.984	− 9.05
0.85	1.377	− 3.15	+1.376	− 3.06	1.896	− 8.58
0.86	1.346	− 3.06	+1.346	− 2.99	1.813	− 8.16
0.87	1.316	− 2.96	+1.317	− 2.91	1.733	− 7.75
0.88	1.287	− 2.86	+1.288	− 2.84	1.658	− 7.36
0.89	1.259	− 2.78	+1.260	− 2.76	1.586	− 6.98
0.90	1.231	− 2.69	+1.233	− 2.68	1.518	− 6.63
0.91	1.205	− 2.60	+1.206	− 2.60	1.453	− 6.30
0.92	1.179	− 2.53	+1.181	− 2.54	1.392	− 5.98
0.93	1.154	− 2.46	+1.156	− 2.46	1.334	− 5.68
0.94	1.130	− 2.38	+1.131	− 2.39	1.278	− 5.39
0.95	1.107	− 2.30	+1.108	− 2.32	1.226	− 5.12
0.96	1.084	− 2.23	+1.085	− 2.26	1.176	− 4.86
0.97	1.063	− 2.17	+1.063	− 2.18	1.129	− 4.62
0.98	1.041	− 2.10	+1.041	− 2.12	1.084	− 4.40
0.99	1.020	− 2.04	+1.020	− 2.06	1.041	− 4.18
1.00	1.000	− 1.98	+1.000	− 2.00	1.000	− 3.99

TABLE 3

Solution	Γ	$\tau_{\odot}\times10^{-9}$ Years	Central Field
$n=1$, no node	160.8	4.08	92
$n=1$, one node	398.9	1.645	164
$n=3$, no node	659.87	0.995	0

The case $n = 1$, no node, corresponds to the case considered by Cowling. Small deviations from his results are to be expected because of differences in the temperature distributions adopted.

The ratio of the decay times is 1.00:0.40:0.24. This would be 1.00:0.25:0.30 if the conductivity were uniform, according to Lamb.[5] The relative increase for the case $n = 1$, one node, and decrease for $n = 3$, no node, can be explained in terms of the position of the maxima of the appropriate radial eigenfunctions. The maximum of $g(x)$ for $n = 1$, one node, occurs at smaller x and, therefore, at a point of higher temperature and greater conductivity than $g(x)$ for $n = 1$, no node. This increases its relative decay time. The reverse is true for the case $n = 3$, no node. A steeper temperature distribution would tend to accentuate this effect.

Equation (9) gives, for the decay times,

$$\tau = \frac{4\pi}{\Gamma} \times 5.87 \times 10^{-15} R^2 T_c^{3/2}. \tag{16}$$

Larger stars may therefore have decay times of the order of one hundred times those tabulated for the sun in Table 3. Since, under these circumstances, the decay time for the case $n = 3$, no node, would be of the order of 10^{11} years, it would appear that the higher modes should be present today if they were present when the star was formed.

It is a pleasure to thank Dr. Martin Schwarzschild for his stimulating interest in this problem and Mr. Thomas L. Swihart for his assistance with the numerical calculations.

[5] *Loc. cit.*

EQUATIONS OF MOTION FOR AN IDEAL PLASMA

LYMAN SPITZER, JR.
Princeton University Observatory
Received March 28, 1952

ABSTRACT

Equations are presented for the motion of a completely ionized gas, or plasma, in a magnetic field sufficiently strong so that during a single gyration around a Larmor circle the relative changes in all macroscopic quantities, such as the electrical and magnetic fields, $\boldsymbol{E}$ and $\boldsymbol{B}$, the particle density, n, and the kinetic temperature, T, are very small. The ratio of the radius of curvature, a, of a Larmor circle to the mean free path, λ, is also assumed small. Successive approximations are developed in increasing powers of these small quantities.

Since, in the plane perpendicular to $\boldsymbol{B}$, an electrical current arises primarily from a pressure gradient, while an electrical field produces a uniform velocity of the plasma, the current density and the electrical field have no direct relationship. Hence the electrical resistivity is most conveniently defined in terms of the energy dissipated into heat by an electrical current. So defined, the transverse resistivity is 1.96 times the normal resistivity for currents parallel to the magnetic field. While no steady current parallel to $\boldsymbol{E}$ is directly produced by a transverse electrical field, a change in $\boldsymbol{E}$ produces a polarization of the plasma; in interstellar space the transverse dielectric constant is about 10^{9}. The Hall current, perpendicular to both $\boldsymbol{E}$ and $\boldsymbol{B}$, appears only in the third approximation and is generally negligible.

Approximate equations for the transverse viscosity and heat conductivity are given. Both of these effects are very small.

The motion of a plasma, or ionized gas, in crossed electric and magnetic fields, has been studied by a number of workers, most recently by A. Schlüter[1] and T. G. Cowling [2] This problem is obviously one of great astrophysical interest, since accumulating evidence indicates that electromagnetic effects may be important in the interstellar plasma, as well as in stellar atmospheres. It does not seem to have been generally realized that under certain idealized conditions, which are fulfilled in many astrophysical situations, the motion of a plasma and the electrical currents present may be found from relatively simple equations, which are presented in this paper.

The basic conditions that we shall assume here are threefold: (*a*) the plasma is completely ionized; (*b*) the macroscopic density and velocity change only very slightly during the time of one gyration or over the distance of one radius of gyration; (*c*) the mean free path between collisions is very great, compared to the radius of gyration. A plasma which satisfies these three conditions will be called an "ideal plasma." Condition *a* is in some ways the most restrictive of the three; this assumption is obviously fulfilled in interstellar *H* II regions and in the solar corona, although not in *H* I interstellar clouds or in the solar photosphere.

Condition *b* is likely to be satisfied in most situations, unless strong plasma oscillations of short wave length are present. In a field of magnetic intensity B, a proton will complete a gyration in about $6.6 \times 10^{-4}/B$ seconds. In interstellar space, where a magnetic field of 10^{-5} gauss seems a reasonable[3, 4] value, about a minute is required for a single gyration. Electrons gyrate several thousand times as rapidly. In the sun, where a magnetic field of much more than 10^{-5} gauss seems likely, even more rapid gyration may be assumed. Apart from rapid oscillations, which require separate treatment, no appreciable change in density, velocity, or electric current will occur in so short a time. Similarly,

[1] *Zs. f. Naturforsch.*, **5a**, 72, 1950; **6a**, 73, 1951.

[2] Lectures at Princeton University during the spring of 1951. I am much indebted to Dr. Cowling for a number of stimulating discussions on these problems.

[3] G. K. Batchelor, *Proc. R. Soc. London, A*, **201**, 405, 1950.

[4] L. Biermann and A. Schlüter, *Phys. Rev.*, **82**, 863, 1951.

changes over a distance equal to the radius of gyration—about 10^7 cm for protons at 10,000° in a field of 10^{-5} gauss—should also be small.

Condition *c* is also likely to be satisfied in most situations. In an interstellar *H* II region, for example, the mean free path of an electron or proton[5] is about 10^{12} cm, some 10^5 times the radius of gyration assumed for these regions. In the solar corona the mean free path is less by a factor of about 10^5, but the radius of gyration will also be decreased, and the ratio of mean free path to radius of gyration should still be large. We may conclude, then, that the ideal plasma considered here does correspond in many cases to actual plasmas in astrophysics.

The system of approximation used for an ideal plasma is described in Section I. Successive approximations are then developed in succeeding sections. Collisions between particles, which are neglected in Sections II, III, and IV, are considered in Sections V and VI. Attention is given chiefly to the equations describing the material motion of the plasma. The actual motion of a plasma in a particular case will also depend on the variation of the electromagnetic field, which depends, in turn, on the currents in the plasma. Variations of density, resulting from divergence of the velocity, must also be taken into account. It is planned to consider such effects in a subsequent paper.

I. SYSTEM OF APPROXIMATION

The motions of particles in an ideal plasma are simplest when the magnetic field, $\boldsymbol{B}$, is constant in space and time, and no external force $\boldsymbol{F}$ is present. Let $w_\perp$ and $w_\parallel$ denote the components of the particle velocity perpendicular and parallel, respectively, to $\boldsymbol{B}$. Then, as is well known, in a plane perpendicular to $\boldsymbol{B}$ the particle gyrates with angular frequency ω in a Larmor circle of radius a, where

$$\omega = \frac{w_\perp}{a} = \frac{|Z|\, eB}{m\, c}. \tag{1}$$

In this equation B and $w_\perp$ denote the scalar magnitudes of the vectors $\boldsymbol{B}$ and $\boldsymbol{w}_\perp$; c is the velocity of light, since e is measured in electrostatic units. In the direction of $\boldsymbol{B}$ the particle moves with the constant velocity $w_\parallel$. Thus the "guiding center" about which the particle gyrates moves with constant velocity along a line of force. In general, we shall denote the velocity of this guiding center by $\boldsymbol{V}$.

In any actual plasma the conditions experienced by a charged particle will change during the course of a single gyration. However, in accordance with condition *b*, such changes will be small in an ideal plasma, and hence such quantities as $dX/X\omega dt$ will be small, where X stands for such physical quantities as the magnetic field $\boldsymbol{B}$, the potential energy, the particle density, etc. We may therefore expand the motion of the particles in an infinite series of such quantities, with the expectation that such a series will converge rapidly. Similarly, the ratio of the radius of gyration, a, to the mean free path, λ, may be assumed small, and we may expand the actual motion in an infinite series in a/λ.

We thus arrive at a twofold system of approximation. In general, we shall let the (n, m) approximation denote the approximation in which terms of the order $(dX/X\omega dt)^n$ and $(a/\lambda)^m$ are considered. Actually, these two expansion parameters do not appear explicitly in the subsequent analysis, but it is readily verified that the ratio of terms in successive approximations is of the order of these expansion parameters.

The properties of the two lowest approximations are relatively obvious. On the basic (0, 0) approximation, already discussed above, the particles simply spiral about the

[5] L. Spitzer, Jr., *Ap. J.*, **93**, 369, 1941.

rectilinear lines of force. In this approximation we must also assume that the particle density is uniform; the distribution of particle velocities is entirely arbitrary but must be the same in all regions. Uniform motion parallel to $\boldsymbol{B}$ may be included in this approximation.

In the (0, 1) approximation, collisions are introduced in a uniform medium. The only effect is to produce a Maxwellian distribution of velocities. If $f^{(0)}(\boldsymbol{w})$ is the density of particles in phase space in this approximation, we have

$$f^{(0)}(\boldsymbol{w}) = \frac{nl^3}{\pi^{3/2}} e^{-l^2w^2}, \tag{2}$$

where

$$l^2 = \frac{m}{2kT}, \tag{3}$$

n is the particle density, w the total velocity, and T the so-called "kinetic temperature." Equation (2) is given for the frame of reference in which the particles have no systematic velocity.

In the remainder of the paper, approximations as high as (3, 0) and (3, 1) will be considered.

II. MOTIONS IN THE (1, 0) APPROXIMATION

We consider the (1, 0) approximation for particles all of the same mass m and charge Ze, subject to an external force $\boldsymbol{F}$. As before, we denote by $\boldsymbol{w}$ the velocity of a single particle. The mean velocity of all particles in a cubic centimeter will be denoted by $\boldsymbol{v}$. While we shall be concerned primarily with $\boldsymbol{v}$, the macroscopic velocity, the results for the (1, 0) approximation will be derived from consideration of the microscopic velocity, $\boldsymbol{w}$.

If we now neglect collisions, consider only the first derivatives of B, and assume other forces constant, the motion of a charged particle is given by the usual "first-order theory," whose results may be taken from H. Alfvén.[6] Here we shall use electrostatic units for charge and field strength, but electromagnetic units for current and resistivity. In the present notation we have

$$\boldsymbol{V}_\perp = -\frac{c\boldsymbol{B}\times\boldsymbol{F}}{ZeB^2} + \frac{mc}{ZeB^3}\left\{\tfrac{1}{2}w_\perp^2\boldsymbol{B}\times\nabla B + w_\parallel^2\boldsymbol{B}\times\left(\boldsymbol{B}\cdot\nabla\frac{\boldsymbol{B}}{B}\right)\right\}, \tag{4}$$

where $\boldsymbol{V}_\perp$ represents the two components of $\boldsymbol{V}$ perpendicular to $\boldsymbol{B}$. The first term in braces represents the drift due to the change of B in a direction perpendicular to the lines of force. The second term represents the drift due to the centrifugal force of a particle moving along a line of force whose radius of curvature is R; $\boldsymbol{B}/B$ is the unit vector, $\boldsymbol{q}$, along the line of force, and $\boldsymbol{q}\cdot\nabla\boldsymbol{q}$ equals $\boldsymbol{R}/R^2$. It may be noted that, if no currents are present, so that $\nabla\times\boldsymbol{B}$ vanishes, and if also $\boldsymbol{B}\cdot\nabla B$ vanishes (B constant along a line of force), then

$$\boldsymbol{B}\cdot\nabla\frac{\boldsymbol{B}}{B} = \nabla B. \tag{5}$$

If equation (5) holds, equation (4) can be considerably simplified, and for an isotropic velocity distribution the drift velocities given by the two terms in braces in equation (4) are exactly equal, on the average.

For $V_\parallel$ we have the equation

$$\frac{dV_\parallel}{dt} = \frac{dw_\parallel}{dt} = \frac{\boldsymbol{F}\cdot\boldsymbol{B}}{mB} - \frac{w_\perp^2\boldsymbol{B}\cdot\nabla B}{2B^2}. \tag{6}$$

[6] *Cosmical Electrodynamics* (Oxford: Clarendon Press, 1950), chap. ii.

Equation (6), together with the energy integral, yields the result

$$\frac{d}{dt}\left(\frac{w_\perp^2}{B}\right) = 0\,, \tag{7}$$

an equation which is also valid in the first-order theory when B changes with time at each point.

We now consider the macroscopic velocity $\boldsymbol{v}$. One might expect that $\boldsymbol{v}$, the average velocity of all the particles in a small volume, would equal $\bar{\boldsymbol{V}}$, the average velocity of all the guiding centers in the same volume. Actually, this is not the case. There are three effects which must be considered: (1) electrical fields, (2) inhomogeneity of the magnetic field, (3) inhomogeneity of the density distribution. Only the first of these produces the same effect on both $\bar{\boldsymbol{V}}$ and $\boldsymbol{v}$. The second affects $\bar{\boldsymbol{V}}$ but has no direct effect on $\boldsymbol{v}$, while the third affects $\boldsymbol{v}$ but not $\bar{\boldsymbol{V}}$. We consider each of these effects in turn.

The electrical field $\boldsymbol{E}$ produces, as we have seen, a drift velocity $\boldsymbol{V}_\mathrm{T}$ and an acceleration $dV_\parallel/dt$. In a homogeneous magnetic field, with a uniform density distribution, all particles will experience the same drift velocity and the same acceleration, and it is obvious that the mean velocity $\boldsymbol{v}$ will in this case equal the average velocity of the guiding centers. Since we are here concerned with the first-order theory, the presence of magnetic inhomogeneities and density gradients will not affect the conclusion that an electrical field produces the same effect on $\boldsymbol{v}$ as it does on $\bar{\boldsymbol{V}}$.

Next we consider the velocity produced by inhomogeneities of the magnetic field. Taking the first term in braces in equation (4), we let $\boldsymbol{B}$ be parallel to the z-axis and let $\boldsymbol{\nabla} B$ be directed along the x-axis. Let $\boldsymbol{v}$ be the mean velocity of all the particles in a cube L cm on a side, and let L be large compared to a. We shall compute the difference between $\boldsymbol{v}$ and $\bar{\boldsymbol{V}}$, defined as the mean velocity of all the guiding centers which lie within this volume. If these two averages referred to the same group of particles, $\boldsymbol{v}$ and $\bar{\boldsymbol{V}}$ would be equal. However, some of the particles included in the average for $\boldsymbol{v}$ are not included in the average for $\bar{\boldsymbol{V}}$ and vice versa, and we shall show that the difference exactly cancels any dependence of $\boldsymbol{v}$ on dB/dx.

We denote by the symbol I all particles which lie within the cube we are considering; let there be N such particles. Of these particles, some will have guiding centers outside the cube; we denote this group, a subgroup of I, by the symbol II. There will also be particles which lie outside the cube but whose guiding centers lie inside the cube; we denote these particles by III. Since the mean velocity of each group of particles is the mean velocity of the guiding centers for the group, we have

$$N\bar{\boldsymbol{V}} = \sum_I \boldsymbol{w} - \sum_{II} \boldsymbol{w} + \sum_{III} \boldsymbol{w}\,, \tag{8}$$

since the number of particles in II equals that in III, to the first order. Hence we have

$$\boldsymbol{v} = \bar{\boldsymbol{V}} + \frac{1}{N}\left(\sum_{II} \boldsymbol{w} - \sum_{III} \boldsymbol{w}\right). \tag{9}$$

In the computation of $\Sigma \boldsymbol{w}$ for groups II and III we need not consider whether particles lie inside or outside of the cube in the y- or z-direction, since conditions in these directions are assumed uniform. As shown in Figure 1, we consider guiding centers at a point P, a distance x from the left-hand side of the cube, such that a fraction θ_1/π of the particles concerned lie outside the cube and are hence members of group III. We shall consider, first, all particles which have particular velocity components $w_\perp$ and

$w_\parallel$. Of the guiding centers at P, the mean velocity in the y-direction of those in group III is evidently given by

$$\bar{w}_y = \frac{1}{\theta_1}\int_0^{\theta_1} w_\perp \cos\theta\, d\theta = \frac{w_\perp \sin\theta_1}{\theta_1}. \tag{10}$$

Since nL^2dx is the number of guiding centers whose distance from the left-hand side of the cube lies between x and $x + dx$, we immediately have

$$\sum_{III} w_y = \int_0^a nL^2 dx\, \frac{\theta_1}{\pi}\frac{w_\perp \sin\theta_1}{\theta_1}. \tag{11}$$

The quantity θ_1 is evidently $\cos^{-1} x/a$, and a simple integration yields

$$\sum_{III} w_y = \tfrac{1}{4} nL^2 a w_\perp. \tag{12}$$

The component Σw_z for group III vanishes by symmetry.

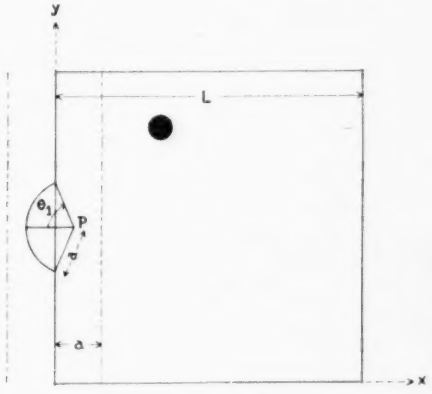

FIG. 1

Consideration of Σw_y for group II indicates that this is equal in magnitude to the corresponding sum for group III, but opposite in sign. The corresponding sums at the right-hand side of the cube in Figure 1 are also given by equation (12), except that now the signs are reversed and a differs by the amount Lda/dx. Since N also equals nL^3, we find that, for particles with a particular $w_\perp$,

$$\frac{1}{N}\left(\sum_{II} w_y - \sum_{III} w_y\right) = \tfrac{1}{2} w_\perp \frac{da}{dx}. \tag{13}$$

On substituting equation (1) in this expression, we obtain the same expression as is found from equation (4) for $\bar{V}_y$ in the present case, but with the opposite sign. Hence, from equation (9), we see that these particles give no contribution to the mean velocity v_y. Since this result is independent of any particular value of w_y, we conclude that in this case

$$v_\perp = 0. \tag{14}$$

Similarly, when the second term in braces in equation (4) is considered and a curving magnetic field is assumed, equation (14) is again valid, provided that the particle density and temperature are again uniform. In this case our basic volume is not a cube but a cylinder, whose cross-section is bounded by two circular arcs parallel to the magnetic field, as shown in Figure 2. In this case the difference between the correction terms on the left- and right-hand sides of the figure arises from the different lengths of these two sides, and again cancels the mean value of $\boldsymbol{V}$.

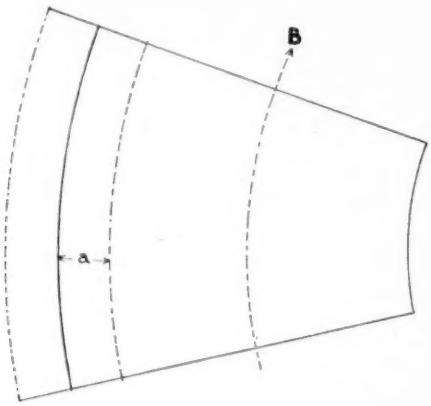

FIG. 2

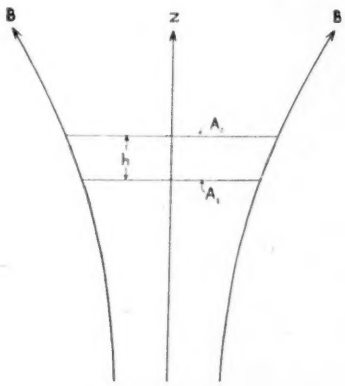

FIG. 3

In addition, the acceleration given in equation (7) cancels out when $dv_\parallel/dt$ is computed. We consider a slab perpendicular to the mean direction of $\boldsymbol{B}$, which is taken to be the direction of the z-axis. The slab is bounded top and bottom by parallel planes and on the side by the lines of magnetic force, as shown in Figure 3. Let the areas of the two faces of the slab be A_1 and A_2, respectively, and let h be the thickness of the slab. We

define $\boldsymbol{P}$ to be the change per second of the momentum in the slab. Evidently, if the particle density is uniform,

$$P_z = nAhm\frac{dw_z}{dt} + nA_1mw_{1z}^2 - nA_2mw_{2z}^2, \tag{15}$$

averaged over all particles in the slab or crossing the surfaces; A is the average of A_1 and A_2. If the mean square velocities are assumed the same at faces A_1 and A_2 (constant pressure), if $dw_\parallel/dt$ is obtained from equation (6) (with $\boldsymbol{F}$ set equal to zero), and if $A_2 - A_1$ is determined from the fact that AB is constant, we obtain

$$P_z = \frac{nAhm}{B}\frac{dB}{dz}\left(-\tfrac{1}{2}\overline{w_\perp^2} + \overline{w^2}\right), \tag{16}$$

since w_z is $w_\parallel$ in the present case. If the velocity distribution is isotropic, P_z vanishes, and hence, in this case,

$$\frac{dv_\parallel}{dt} = 0. \tag{17}$$

Thus we see that in this first-order theory the particle velocities and accelerations induced by the inhomogeneity of the magnetic field have no counterpart in the macroscopic velocity $\boldsymbol{v}$, provided that the density and velocity distribution are constant in space and the velocity distribution is isotropic. From general considerations it may be seen that this result must be true to all orders, since in an inclosure at thermodynamic equilibrium no macroscopic velocities relative to the inclosure can appear. This result has been emphasized by Cowling.[2,7]

Next we turn to a consideration of the pressure gradient, which, unlike the inhomogeneity in the magnetic field, may have a large effect on $\boldsymbol{v}$. Let us consider, first, a gradient of $n\overline{w_\perp^2}$ in the x-direction, with B assumed uniform and in the z-direction. In this (1, 0) approximation we consider a linear gradient of $n\overline{w_\perp^2}$. We consider the same cube of length L on a side considered in Figure 1, and determine $\boldsymbol{v}$ from equation (9) as before, although in the present case $\overline{\boldsymbol{V}}$ vanishes. Equation (12) still gives Σw_y for group *III* and, with a change in sign, for group *II* also. When the contributions from the left- and right-hand sides of the cube are combined, taking into account the pressure gradient, we have, averaging over all particles present,

$$v_y = \frac{1}{2n}\frac{d}{dx}(n\bar{a}\overline{w_\perp}). \tag{18}$$

More generally, we have

$$\boldsymbol{v}_\perp = \frac{mc}{2ZeB^2n}\boldsymbol{B}\times\boldsymbol{\nabla}(n\overline{w_\perp^2}). \tag{19}$$

In the presence of a pressure gradient with a component parallel to $\boldsymbol{B}$, we have the familiar result,

$$\frac{dv_\parallel}{dt} = -\frac{\boldsymbol{B}\cdot\boldsymbol{\nabla}(n\overline{w_\parallel^2})}{Bn}. \tag{20}$$

The above results may be combined to give final equations determining $v_\perp$ and $v_\parallel$. From equations (4) and (19) we have

$$\boldsymbol{v}_\perp = \frac{c}{ZeB^2}\boldsymbol{B}\times\left[-\boldsymbol{F} + \frac{1}{n}\boldsymbol{\nabla}p\right], \tag{21}$$

[7] *M.N.*, **90**, 140, 1929; **92**, 407, 1932.

where we have assumed that the pressure distribution is isotropic and that therefore

$$p = \tfrac{1}{2} n m \overline{w_\perp^2} . \tag{22}$$

It may be noted that, if isothermal conditions are assumed and if $\boldsymbol{F}$ is purely electrostatic, then

$$\boldsymbol{F} = -Ze\nabla\phi , \tag{23}$$

and

$$\boldsymbol{v}_\perp = \frac{c}{ZeB^2} \boldsymbol{B} \times \nabla [Ze\phi + kT \log n] . \tag{24}$$

For the velocity parallel to $\boldsymbol{B}$ we have, combining equations (6) and (20),

$$\frac{d v_\parallel}{dt} = -\frac{1}{Bm} \boldsymbol{B} \cdot \left[-\boldsymbol{F} + \frac{1}{n} \nabla p \right] , \tag{25}$$

and, if $\boldsymbol{F}$ is purely electrostatic and T is constant,

$$\frac{d v_\parallel}{dt} = -\frac{1}{Bm} \boldsymbol{B} \cdot \nabla [Ze\phi + kT \log n] . \tag{26}$$

Equations (24) and (26) are implicit in the work of previous investigators, notably L. Tonks and W. P. Allis.[8]

These results may now be compared with the general equation of motion,

$$\frac{d\boldsymbol{v}}{dt} = \frac{\partial \boldsymbol{v}}{\partial t} + \boldsymbol{v} \cdot \nabla \boldsymbol{v} = \frac{1}{m} \boldsymbol{F} + \frac{Ze}{mc} \boldsymbol{v} \times \boldsymbol{B} - \frac{1}{n} \nabla \cdot \boldsymbol{\Psi} , \tag{27}$$

where $\boldsymbol{\Psi}$ is the material energy-stress tensor, defined by

$$\boldsymbol{\Psi} = \sum_k \boldsymbol{w}_k \boldsymbol{w}_k , \tag{28}$$

summed over all particles, k; $\boldsymbol{w}_k$ is here the random velocity of particle k, measured in a frame of reference in which the local value of $\boldsymbol{v}$, the mean velocity, vanishes. If in this frame of reference the distribution of velocities is isotropic, then

$$\nabla \cdot \boldsymbol{\Psi} = \frac{1}{m} \nabla p = \frac{1}{m} \nabla (nkT) , \tag{29}$$

where p is the pressure.

If equation (27) is applied to one type of particle, an additional force term must be added to take into account the momentum transferred from one type to another in collisions. When equation (27) is summed over all types of particles, the net transfer of momentum in collisions vanishes, and the equation in its present form is generally valid. Collisions then produce an effect through alteration of the form of $\boldsymbol{\Psi}$.

It is readily seen that, if we substitute equation (29) in equation (27) and neglect $d\boldsymbol{v}_\perp/dt$, we obtain directly equations (21) and (24). It is believed that the derivation of these equations from consideration of individual particle velocities makes the physical situation somewhat more clear. However, for obtaining certain higher approximations, it is most convenient to employ the macroscopic equation of motion. In accordance with the earlier discussion we set

$$\boldsymbol{v} = \boldsymbol{v}(0, 0) + \boldsymbol{v}(1, 0) + \boldsymbol{v}(2, 0) + \boldsymbol{v}(3, 0) \ldots + \boldsymbol{v}(1, 1) + \boldsymbol{v}(2, 1) + \boldsymbol{v}(3, 1) \ldots . \tag{30}$$

[8] *Phys. Rev.*, **52**, 710, 1937.

It is evident from the discussion in Section I that $\boldsymbol{v}(0, 0)$ represents simply the velocity of the frame of reference parallel to $\boldsymbol{B}$ and that $\boldsymbol{v}(0, 1)$ vanishes. The term $\boldsymbol{v}(1, 0)$ is a solution of equation (27) when $d\boldsymbol{v}/dt$ is ignored and equation (29) is assumed. The term $\boldsymbol{v}(2, 0)$ is the additional velocity found from equation (27) when the value of $d\boldsymbol{v}(1, 0)/dt$ obtained from the first approximation is substituted in this equation and when the first-order corrections to equation (29) are considered. This process can, in principle, be extended to any accuracy desired. For the computation of $\boldsymbol{v}(n, 1)$ a consideration of individual particles is again essential. The $(n, 2)$ and higher approximations are not considered in this paper.

As a summary of the results obtained in this section, we now give final equations for the over-all macroscopic velocity $\boldsymbol{v}$ and for the electric current. If $\boldsymbol{v}_i$ is the macroscopic velocity for particles of type i, then we have

$$\boldsymbol{v} = \frac{1}{\rho} \sum_i n_i m_i \boldsymbol{v}_i , \tag{31}$$

where ρ is the density of the plasma, equal to $\sum_i n_i m_i$. Employing equation (21), we find, if we assume that the external force is electrical,

$$\boldsymbol{v}_\perp (1, 0) = c \frac{\boldsymbol{E} \times \boldsymbol{B}}{B^2} + \frac{c}{eB^2 \rho} \boldsymbol{B} \times \sum_i \frac{m_i \nabla p_i}{Z_i} , \tag{32}$$

where Z_i is -1 for electrons. Evidently, the electrons contribute very little to the motion of the plasma, which is essentially given by the motion of the heavy positive ions.

The current density $\boldsymbol{j}$, in electromagnetic units, may be written

$$\boldsymbol{j} = \frac{e}{c} \sum_i n_i Z_i \boldsymbol{v}_i . \tag{33}$$

As before, we obtain from equation (21),

$$\boldsymbol{j}_\perp (1, 0) = \frac{1}{B^2} \boldsymbol{B} \times \Big[- \sum_i n_i \boldsymbol{F}_i + \nabla \sum_i p_i \Big] . \tag{34}$$

If the external force is entirely electrical, $\boldsymbol{F}_i$ becomes $Z_i e \boldsymbol{E}$. The first term in brackets then becomes the electrical force on the net charge density in the plasma; since even a small net charge density gives rise to relatively large electrostatic fields, this net force is usually small and may be neglected. Hence in this approximation the component of $\boldsymbol{j}$ perpendicular to the magnetic field is determined entirely by the gradient of the total pressure.

III. THE (2, 0) APPROXIMATION; POLARIZATION

We have seen that the equations for $\boldsymbol{v}$ in the (1, 0) approximation satisfy the general equation of motion—equation (27)—provided that $d\boldsymbol{v}_\perp/dt$ is neglected and an isotropic pressure is assumed. We consider, first, the effect of the acceleration term. To obtain the (2, 0) approximation, we compute $d\boldsymbol{v}_\perp/dt$ from the (1, 0) approximation, substitute in equation (27), and solve for $\boldsymbol{v}$. In this way we obtain

$$\boldsymbol{v}_\perp (2, 0) = \frac{mc}{Ze B^2} \boldsymbol{B} \times \frac{d\boldsymbol{v}(1, 0)}{dt} ; \tag{35}$$

the time derivative is the change of $\boldsymbol{v}$ along a dynamical path in the (1, 0) approximation. The velocity $\boldsymbol{v}_\parallel$, parallel to $\boldsymbol{B}$, is obtained in the conventional way from equation (25), and the only contribution of the (2, 0) approximation to $\boldsymbol{v}_\parallel$ is through the $\boldsymbol{v} \cdot \nabla \boldsymbol{v}$ term,

which depends on $v_\perp(1, 0)$. Since the emphasis in the present paper is primarily on the determination of $\boldsymbol{v}_\perp$, we shall not consider these additional effects.

The value of $\boldsymbol{v}_\perp(2, 0)$ found from equation (35) will depend on many complicated variations of $\boldsymbol{F}$, $\boldsymbol{B}$, n, and p in time and space. We shall not consider all these dependences in detail, since a number of them lead simply to small changes in the velocity. The most important result of the second approximation is the appearance of space charges produced by secondary currents. When conditions change with time, such space charges may produce a large effect on the velocity found in the first approximation and will therefore be considered in detail here.

We consider, first, acceleration corresponding to the $\partial \boldsymbol{v}/\partial t$ term in equation (27). Of particular importance is the acceleration in the direction of $\boldsymbol{v}_\perp(1, 0)$, since this necessarily produces a component of $\boldsymbol{v}_\perp(2, 0)$ at right angles to $\boldsymbol{v}_\perp(1, 0)$. Let us consider, for example, a situation in which the electrostatic field $\boldsymbol{E}_\perp$ varies with time. Then, from equations (21) and (35), we have

$$\boldsymbol{v}_\perp(2, 0) = \frac{m c^2}{Z e B^2} \frac{d\boldsymbol{E}_\perp}{dt}. \tag{36}$$

Summing over all components, in accordance with equation (33), the current density becomes

$$\boldsymbol{j}_\perp(2, 0) = \frac{\rho c}{B^2} \frac{d\boldsymbol{E}_\perp}{dt}. \tag{37}$$

A current proportional to dE/dt is usually described as a change of the polarization P. Hence, with P in e.s.u., we have

$$\boldsymbol{P}_\perp = \frac{\rho c^2}{B^2} \boldsymbol{E}_\perp. \tag{38}$$

If the dielectric constant κ is defined in the usual way as

$$\kappa = 1 + 4\pi \frac{P_\perp}{E_\perp}, \tag{39}$$

we find

$$\kappa = 1 + \frac{4\pi \rho c^2}{B^2}. \tag{40}$$

Except in very strong fields, κ is half the ratio of the material energy density, including rest mass, to the density of magnetic energy. In interstellar space we may set ρ equal to 10^{-24} gm/cm^3, and B to 10^{-5} gauss, and obtain a value of 10^8 for κ. The velocity of an electromagnetic disturbance, whose period is long compared with the gyration frequency, ω—about 0.1 per second for protons in interstellar space—and in which $\boldsymbol{E}$ is perpendicular to $\boldsymbol{B}$, will therefore be $c/10^4$, or 30 km/sec. The velocity $c/(\kappa)^{1/2}$ is simply the familiar velocity for a magneto-hydrodynamic wave. Such waves in an ideal plasma have been analyzed in some detail by E. Aström,[9] who obtained equation (40) for κ in the special case of a sinusoidal magneto-hydrodynamic wave.

When $\boldsymbol{B}$ varies, a current perpendicular to $\boldsymbol{v}_\perp(1, 0)$ again arises. This current density can still be regarded as a change of polarization, but amounts in this case to only half the value of $d\boldsymbol{P}/dt$ found on differentiating equation (38) with respect to B.

A change of kinetic temperature with time will also produce currents in the (2, 0) approximation. If n is constant in time, then, from equations (21), (33), and (35), we find for the over-all current,

$$i_\perp(2, 0) = \frac{c}{B^2} \sum_i \left\{ n_i m_i \frac{d\boldsymbol{E}_\perp}{dt} - \frac{m_i}{e Z_i} \nabla_\perp \left(n_i k \frac{dT}{dt} \right) \right\}. \tag{41}$$

[9] *Ark. f. Fys.*, **2**, No. 42, 443, 1950.

The electrical field must be included, since the current produced by an increase of T produces, in turn, an electrostatic field. The value of $\boldsymbol{E}$ may be determined from Poisson's equation, which becomes, on partial differentiation with respect to time,

$$\nabla \cdot \frac{\partial \boldsymbol{E}}{\partial t} = -4\pi c \nabla \cdot \boldsymbol{j}. \tag{42}$$

Since the quantity $\boldsymbol{j}$ in equation (42) includes the internal currents in the plasma, no dielectric constant (in these units) is needed in Poisson's equation. The value of κ given in equation (40) is applicable when the internal currents are not considered directly and the response of the plasma to extraneous fields or currents is considered. Equation (42) may be integrated at once to find $\partial \boldsymbol{E}/\partial t$. In general, an additional vector function, with vanishing divergence, must also be added to satisfy the boundary conditions and the condition that $\nabla \times \boldsymbol{E}$ vanishes. In the present case, if the gradients of n_i, T, and B^2 are parallel and if no external electrostatic fields are present, this additional function vanishes. Now $\boldsymbol{j}_\perp$ can be eliminated from equations (41) and (42), and we find

$$\frac{\partial \boldsymbol{E}}{\partial t}\left(\rho + \frac{B^2}{4\pi c^2}\right) = \sum_i \frac{m_i}{eZ_i} \nabla_\perp \left(n_i k \frac{\partial T}{\partial t}\right), \tag{43}$$

provided that we replace $d\boldsymbol{E}/d\tau$ and $dt/d\tau$ by $\partial \boldsymbol{E}/\partial \tau$ and $\partial t/\partial \tau$. If we assume that B^2 and n_i are both constant with time, equation (43) may be integrated at once over time. If the resultant relation between $\boldsymbol{E}$ and T is used to eliminate $\boldsymbol{E}$ from equation (32), we obtain for $\Delta \boldsymbol{v}_\perp(1, 0)$ the increase in the total velocity resulting from the increase of temperature,

$$\Delta \boldsymbol{v}_\perp(1, 0) = \frac{c}{\kappa \rho e B^2} \boldsymbol{B} \times \sum_i \frac{m_i}{Z_i} \nabla_\perp (\Delta p_i), \tag{44}$$

where κ is defined in equation (40). A comparison of equations (32) and (44) shows that an increase of pressure in this way produces in this case a relatively small increase of the velocity, if κ is large. The electrical currents produced in the (2, 0) approximation give rise to an electrostatic field that nearly cancels the velocity corresponding to the increased pressure gradient. If κ is extremely large, the mean velocities of different types of charged particles will not be reduced by exactly κ; but, when the velocities of all types of atoms are combined, the total macroscopic velocity obeys equation (44). The increase in $\boldsymbol{j}_\perp(1, 0)$ found from equation (34) for an increase in p_i is apparently not counterbalanced by any such secondary effect. In the general case this increase of $\boldsymbol{j}_\perp(1, 0)$ will modify $\boldsymbol{B}$, an effect ignored in equation (44).

We now turn to a consideration of the currents perpendicular to $\boldsymbol{B}$ produced by the $\boldsymbol{v} \cdot \nabla \boldsymbol{v}$ term. If the stream lines are curved, this term will yield a centrifugal acceleration, perpendicular to $\boldsymbol{v}$. From equation (35) we see that curvature of $\boldsymbol{v}_\perp(1, 0)$ will produce a secondary velocity parallel to $\boldsymbol{v}_\perp(1, 0)$, and will also change the magnitude of $\boldsymbol{j}_\perp(1, 0)$. These effects do not seem very important. If the magnetic lines of force are curved, with a vector radius of curvature $\boldsymbol{R}$, the motion $v_\parallel$ will produce secondary velocities and currents perpendicular to $\boldsymbol{B}$. For the current we find

$$\boldsymbol{j}_\perp(2, 0) = \frac{\sum_i n_i m_i v_{i\parallel}}{B^2 R^2} \boldsymbol{B} \times \boldsymbol{R}, \tag{45}$$

where the sum extends over all types of charged particles. If $n_i m_i v_i^2/R$ is small compared with the pressure gradient ∇p_i, $\boldsymbol{j}_\perp(2, 0)$ given by equation (45) will be small compared

to $\boldsymbol{j}_\perp(1, 0)$. Whether this secondary current produces space charges and electrostatic fields depends on the detailed configuration of $\boldsymbol{B}$ and v^2 in the plasma.

Finally, the second derivative of p must be included in the (2, 0) approximation. In a plane perpendicular to $\boldsymbol{B}$ the distribution of velocities at any point depends on the density of guiding centers at neighboring points. If second derivatives of this density are considered, the mean square random velocities in different directions become unequal, and the pressure gradient must be replaced by the divergence of the material stress-energy tensor. The effective pressure will now be different in different directions. The magnitude of $\boldsymbol{v}_\perp$ and $\boldsymbol{j}_\perp$ will be altered in this higher approximation, but it would appear that no appreciable velocities or currents in other directions will be produced.

IV. THE (3, 0) APPROXIMATION; HALL CURRENT

Many effects occur in the (3, 0) approximation. We shall here consider only one of these, the currents produced by the acceleration in $\boldsymbol{v}_\perp(2, 0)$. As in equation (35), we have

$$\boldsymbol{v}_\perp(3, 0) = \frac{m c}{Z e B^2} \boldsymbol{B} \times \frac{d\boldsymbol{v}(2, 0)}{dt}. \tag{46}$$

Considering only those velocities due to an electrical field, we now take $\boldsymbol{v}_\perp(2, 0)$ from equation (36). From the definition of $\boldsymbol{j}$ in equation (33) we obtain

$$\boldsymbol{j}_\perp(3, 0) = \frac{c^2}{eB^3} \left(\sum_i \frac{n_i m_i^2}{Z_i} \right) \boldsymbol{B} \times \frac{d^2 \boldsymbol{E}}{dt^2}. \tag{47}$$

The current obtained from equation (47) is perpendicular to $\boldsymbol{B}$ and $\boldsymbol{E}$ and corresponds to the usual Hall current. The occurrence of m_i^2 in equation (47) indicates that the Hall current is carried primarily by the positive ions, whereas usually the Hall current is attributed to the electrons. This apparent contradiction is simply a difference of point of view. When E increases, the electrons rapidly reach the velocity cE/B; the positive ions take longer to reach this same velocity. In the frame of reference in which E is measured, the electrons actually carry the Hall current. In the present instance, however, the velocities obtained from equation (46) measure the deviation from the velocity cE/B. Since this deviation is greatest for the heavy positive ions, the Hall current is therefore attributed to these ions. In any case, it is the difference in mass between the positive ions and electrons that is reponsible for the Hall current.

It may be noted that the ratio of the velocities involved in the Hall current to the velocity cE/B is simply $d^2E/\omega^2 E dt^2$. In an ideal plasma this quantity is, by definition, very small, and the Hall current is virtually negligible.

V. THE (1, 1) APPROXIMATION; ELECTRON-ION COLLISIONS

The previous results describe the motion of a plasma when collisions are entirely absent. The perturbations produced by collisions may be classified into two different types, depending on whether the collisions are between like or unlike particles. Collisions between unlike particles, with different mean motions, may produce an effective force on each group of particles, and this produces effects in the (1, 1) approximation, which may be treated by simply adding this force term to the basic equation of motion. However, if a group of identical particles is considered, mutual collisions obviously produce no net force on the group; in this case, considered in more detail in the following section, the anisotropy of the velocity distribution must be considered, and the resultant effects occur in higher orders of approximation.

We now treat the collisions between positive ions, all assumed to have the same charge Z, and electrons. Let $\boldsymbol{F}_{e,i}$ be the mean force on an electron resulting from collisions with

positive ions. Since there are Z times as many electrons as positive ions, the mean force on a positive ion resulting from these collisions is $-Z\boldsymbol{F}_{e,i}$. If in equation (21) we consider the velocity due to $\boldsymbol{F}_{e,i}$ only, we find

$$\boldsymbol{v}_\perp(1,1) = \frac{c}{eB^2}\boldsymbol{B}\times\boldsymbol{F}_{e,i}. \tag{48}$$

Since $\boldsymbol{F}_{e,i}$ is directly proportional both to the collision frequency and to the difference in the mean velocity $\boldsymbol{v}(1,0)$ between electrons and positive ions, it is clear that equation (48) gives the drift velocity in the (1, 1) approximation. This equation holds for electrons and positive ions separately, and hence also for the macroscopic velocity.

Instead of evaluating $\boldsymbol{F}_{e,i}$ directly, we first relate the quantity to more familiar concepts. As a result of the force $\boldsymbol{F}_{e,i}$, the motion of electrons through ions performs work or, more accurately, dissipates energy into heat. The work done per cubic centimeter per second is equal to $n_e\boldsymbol{F}_{e,i}\cdot(\boldsymbol{v}_i-\boldsymbol{v}_e)$. The power dissipated per cubic centimeter by a current of density $\boldsymbol{j}$ is usually expressed as ηj^2, where η is the resistivity in e.m.u. Hence, using equation (33), we obtain

$$\frac{c}{e}\boldsymbol{F}_{e,i} = \eta\boldsymbol{j}. \tag{49}$$

Equation (49) is generally valid. In the present case, we use $\boldsymbol{j}_\perp$ and $\eta_\perp$ to denote the current density perpendicular to $\boldsymbol{B}$ and the resistivity for dissipation of this current into heat. Then equation (48) becomes

$$\boldsymbol{v}_\perp(1,1) = \frac{\eta_\perp}{B^2}\boldsymbol{B}\times\boldsymbol{j}_\perp(1,0). \tag{50}$$

If the resistivity is defined in terms of energy dissipation, it is evident that this quantity depends only on microscopic collisions and is not directly dependent on $\boldsymbol{B}$. In much previous work the transverse conductivity $\sigma_\perp$ has been used as the ratio of $\boldsymbol{j}_\perp$ to $\boldsymbol{E}_\perp$. In an ideal plasma there would seem to be little justification for this procedure. As we have seen, there is no direct connection between $\boldsymbol{j}(1,0)$ and $\boldsymbol{E}$; in fact, these vectors may have quite different directions. An electrical field produces primarily a velocity at right angles to $\boldsymbol{E}$ and $\boldsymbol{B}$ and a polarization parallel to $\boldsymbol{E}_\perp$. If this velocity gives rise to a pressure gradient, currents will appear, and in certain steady conditions the ratio of $\boldsymbol{j}$ to $\boldsymbol{E}$ will equal $\sigma_\perp$. However, the physical situation is clarified if $\sigma_\perp$ is defined in terms of energy dissipation and with such a definition it appears more rational to deal with the resistivity instead of the conductivity.[10] It is evident that the primary macroscopic effect of resistivity is the appearance of the drift velocity given in equation (50).

While $\eta_\perp$ in an ideal plasma is independent of $\boldsymbol{B}$ and is closely equal to $\eta_\parallel$, the normal resistivity in the absence of a magnetic field, these two resistivities are not exactly equal. The value of η depends on how the current $\boldsymbol{j}$ is distributed among electrons of different velocities, i.e., on the detailed form of the velocity-distribution function, $f(\boldsymbol{v})$. For currents parallel and perpendicular to the magnetic field the details of these distribution functions are quite different.

To evaluate these differences, we express $\boldsymbol{j}$ and $\boldsymbol{F}_{e,i}$ in terms of f. Considering, first, the electron current only, we follow Chapman and Cowling[11] and write, for the electron distribution function,

$$f_e(\boldsymbol{w}) = f_e^{(0)}(w)\{1 + D(kw)\cos\theta\}, \tag{51}$$

[10] I am indebted to Dr. T. G. Cowling for suggesting the use of the resistivity instead of the conductivity in this connection.

[11] *The Mathematical Theory of Non-uniform Gases* (Cambridge: At the University Press, 1939).

where the polar axis is the direction in which the current is flowing, and $f_e^{(0)}(w)$ is the Maxwellian distribution function given by equation (2). The electron current density, j_e, along the polar axis is given by

$$j_e = -\frac{e}{c}\int f_e(w)\, w\cos\theta\, d\boldsymbol{w} = \frac{-4\,e n_e I_3(\infty)}{3\pi^{1/2} l_e\, c}, \tag{52}$$

where, in general,

$$I_n(\infty) \equiv \int_0^\infty x^n D(x)\; e^{-x^2} dx\,. \tag{53}$$

The force $\boldsymbol{F}_{e,i}$ may be found from the coefficient of dynamical friction, introduced by Chandrasekhar.[12] Following the notation of Cohen, Spitzer, and Routly,[13] we let $\langle \Delta_\xi \rangle$ represent the average rate of change of the electron velocity, measured in the direction along which the electron is moving. Then

$$n_e \boldsymbol{F}_{e,i} = m_e \int f_e(w) \langle \boldsymbol{\Delta}_\xi \rangle\, d\boldsymbol{w}\,. \tag{54}$$

The function $\langle \Delta_\xi \rangle$ may be taken from equations (31), (32), and (35) of Cohen, Spitzer, and Routly.[13] The quantity j in these equations refers to the quantity denoted here by l (to avoid confusion with the current density); for interactions of electrons with positive ions the quantity x occurring in these equations equals $l_i w$, where l_i is the value of l obtained when m_i, the mean mass of the positive ions, is substituted in equation (2). If the velocity of the positive ions is assumed relatively small, x is much greater than unity, and $\langle \Delta_\xi \rangle$ equals $-3L/w^2$, where, for electron-proton encounters, L is one-half its previous value.[13] The integral in equation (54) above is then readily evaluated. If we use equation (49) to express η in terms of $\boldsymbol{F}_{e,i}$, eliminating j_e and l_e by means of equations (52), and (3), we obtain

$$\eta = \frac{3\pi 6^{1/2} Z e^2 c^2 \log(qC^2)}{m_e C^3} \frac{I_0(\infty)}{I_3(\infty)}, \tag{55}$$

where $I_0(\infty)$ and $I_3(\infty)$ are defined in equation (53); C^2 is the mean-square electron velocity, equal to $3kT/m_e$; and, according to Cohen, Spitzer, and Routly,[13] q is given by

$$q = \frac{m_e}{2\,e^3 Z}\left(\frac{kT}{\pi n_e (1+Z)}\right)^{1/2}. \tag{56}$$

The problem of determining the conductivity is therefore reduced to the computation of the ratio of the integrals $I_0(\infty)$ and $I_3(\infty)$. In the general case the computation of $D(x)$ is rather complicated. In the absence of a magnetic field, or for currents parallel to the magnetic field, it may be shown that Cowling's "second approximation"[14] yields

$$\frac{I_0(\infty)}{I_3(\infty)} = 0.383\,. \tag{57}$$

This same value has also been obtained by Spitzer and Härm[15] by the use of a diffusion equation in velocity space; the earlier result by Cohen, Spitzer, and Routly,[13] is modified when all the terms in the diffusion equation are taken into account.

For currents perpendicular to a magnetic field, however, the current perpendicular

[12] *Ap. J.*, **97**, 255, 1943.

[13] *Phys. Rev.*, **80**, 230, 1950.

[14] *Proc. R. Soc. London, A*, **183**, 453, 1945; this paper considers only the first approximation in the velocity-distribution function, but represents a second approximation in the expansion of this function in terms of Laguerre (or Sonine) polynomials.

[15] In preparation.

to $\boldsymbol{B}$ is produced by a pressure gradient and, in this case, $D(x)$ is directly proportional to x. The greater w is, the farther away is the guiding center for the particle passing through a small area; since we are considering velocities on the (1, 0) approximation, we may assume a linear variation with distance for the density of guiding centers. It follows directly that the excess number of particles moving one way will be proportional to the velocity. In this case the integrals can be evaluated at once, and we have

$$\frac{I_0(\infty)}{I_3(\infty)} = \frac{4}{3\pi^{1/2}} = 0.752 . \tag{58}$$

Hence, finally, we have

$$\frac{\eta_\perp}{\eta_\parallel} = 1.96 . \tag{59}$$

This result is derived here only for the electron component of the current, but it is valid also for the current carried by the positive ions. The force on a positive ion moving through a spherical, Maxwellian distribution of electrons may again be determined from the coefficient of dynamical friction. The ratio of this force to the positive ion current is the same as in the case in which the electrons carry the current; moreover, this ratio does not depend on the kinetic temperature of the positive ions. Hence the fact that positive ions carry a large fraction of the current does not vitiate the computation of $\eta_\perp/\eta_\parallel$ from the electron current alone, and, in particular, equation (59) is generally valid for the (1, 1) approximation. In the (1, 2) approximation, however, higher terms would require consideration.

It may be noted that encounters between positive ions also produce drifts. If two ions of types 1 and 2 are interacting and each has a Maxwellian velocity distribution, with the perturbation $f^1(\boldsymbol{w})$ resulting from a linear density gradient, an evaluation of equation (54) in the more general case, together with equations (21) and (48), gives

$$\boldsymbol{v}_{1\perp}(1, 1) = \frac{4(6\pi)^{1/2} Z_1^2 Z_2^2 e^2 c^2 (m_1 + m_2) \log qC^2}{B^2 m_1 m_2 (C_1^2 + C_2^2)^{3/2}} \frac{n_2}{Z_1} \left[\frac{1}{Z_2 n_2} \nabla_\perp p_2 - \frac{1}{Z_1 n_1} \nabla_\perp p_1 \right], \tag{60}$$

where $\nabla_\perp$ denotes the component of the gradient in the plane perpendicular to $\boldsymbol{B}$. The equation for $\boldsymbol{v}_{2\perp}(1, 1)$ is obtained by interchanging the subscripts 1 and 2 in equation (60). It is evident that the total current produced by these drifts is zero. It may be noted that drifts of positive ions relative to one another will vanish in an isothermal plasma only if

$$\log (n_2)^{1/Z_2} = \log (n_1)^{1/Z_1} + \text{constant} . \tag{61}$$

Equation (61) indicates that the ions of higher Z will tend to be relatively more concentrated in regions of higher particle density.

VI. THE (2, 1) AND (3, 1) APPROXIMATIONS; DIFFUSION

The (2, 1) approximation comprises a large number of different effects. A current will be produced by the acceleration of $\boldsymbol{v}(1, 1)$. Velocities will be produced by interactions between electrons and positive ions moving with the mean velocities obtained in the (2, 0) approximation. These effects may be computed from the equations in the previous sections but will not be considered in detail here. Instead, we shall consider primarily the phenomenon of diffusion. An accurate treatment of this effect, with detailed consideration of the velocity-distribution function, would be complicated and is not attempted here. Instead, we shall compute the rate of diffusion in one extremely simple case and apply this result to obtain the order of magnitude of other diffusion rates.

Let us consider a homogeneous, uniform, infinite plasma. We take rectangular co-ordi-

nates x_1, x_2, and x_3 and assume a uniform magnetic field, parallel to the x_3-axis. In this plasma we shall consider particles, all of the same charge Ze, mass m, and particle density n. Let us suppose, now, that by some method we tag each particle either A or B, with n_A and n_B particles of each type per cubic centimeter. Other ions, of charge $Z_i e$, mass m_i, and particle density n_i will also be assumed. We now consider the rate at which particles of types A and B diffuse into each other.

We shall consider the drifts not of the particles themselves but of the guiding centers about which each particle gyrates. In the absence of encounters, each guiding center would be fixed in position under the present assumptions. If, in an encounter, the velocity of the particle changes by an amount $\Delta \boldsymbol{w}$, the position of the guiding center will also change. The vector displacement from the particle to the guiding center is given by

$$\boldsymbol{a} = \frac{m\,c}{Z\,eB^2}\,\boldsymbol{w} \times \boldsymbol{B}\,. \tag{62}$$

If we assume that the encounters occur in a region of space very small compared with the radius of gyration $\boldsymbol{a}$, then we may regard $\Delta \boldsymbol{w}$ as an abrupt change of velocity, which will produce a displacement of the guiding center given by

$$\Delta \boldsymbol{a} = \frac{m\,c}{Z\,eB^2}\,\Delta \boldsymbol{w} \times B\,. \tag{63}$$

Successive displacements of the guiding center constitute an example of random walk, as in Brownian motion; a thorough survey of such problems has been given by Chandrasekhar.[16] The net flow of guiding centers may be determined from the mean values of $\Delta \boldsymbol{a}$ and $(\Delta \boldsymbol{a})^2$. If we let F_i be the net number of guiding centers per second crossing a square centimeter perpendicular to the x_i-axis, we have, in general, the Fokker-Planck equation,

$$F_i = n\langle \Delta a_i \rangle - \frac{1}{2}\sum_j \frac{\partial}{\partial x_j}\left(n\langle \Delta a_i \Delta a_j \rangle\right), \tag{64}$$

where n is the number of particles of that type per cubic centimeter and the symbol $\langle\ \rangle$ denotes the sum of all changes in a second, averaged over all such particles, the average extending around the Larmor circle for each particle.

In the general case the computation of the diffusion co-efficients $\langle \Delta a_i \rangle$ and $\langle \Delta a_i\, \Delta a_j \rangle$ is rather involved, as the density of particles and their velocity distribution may both vary with position. Since we have here assumed that collisions with particles of type A are the same as collisions with particles of type B and that $n_A + n_B =$ a constant n, the diffusion coefficients may readily be determined. From symmetry it is evident that the mean value of $\Delta \boldsymbol{w}$, averaged over a Larmor circle, vanishes. Also, from equation (63) we obtain

$$\langle \Delta a_i \Delta a_j \rangle = \begin{cases} \dfrac{m^2 c^2}{2Z^2 e^2 B^2}\,\langle \overline{|\,\Delta \boldsymbol{w}_\perp\,|^2} \rangle & \text{if } i = j = 1 \text{ or } 2\,, \\ 0 & \text{if } i \neq j\,, \end{cases} \tag{65}$$

in which the bar denotes that an average is to be taken over all particle velocities. The velocity change $\Delta \boldsymbol{w}$ has Cartesian components Δ_ξ, Δ_η, Δ_ζ, where the ξ-axis is parallel to w, while the η-axis lies in the plane defined by $\boldsymbol{B}$ and the ξ-axis. If θ denotes the angle between $\boldsymbol{w}$ and $\boldsymbol{B}$, then

$$(\Delta w_\perp)^2 = (\Delta_\xi)^2 \sin^2\theta + (\Delta_\eta)^2 \cos^2\theta + (\Delta_\zeta)^2\,. \tag{66}$$

[16] *Rev. Mod. Phys.*, **15**, 1, 1943.

Since the distribution of velocities is isotropic, equation (65) yields, on substitution from equation (1),

$$\langle (\Delta a_1)^2 \rangle = \frac{1}{2\omega^2} \{ \tfrac{2}{3} \overline{\langle \Delta_\xi^2 \rangle} + \tfrac{1}{3} \overline{\langle \Delta_\eta^2 \rangle} + \overline{\langle \Delta_\zeta^2 \rangle} \} . \tag{67}$$

The coefficient $\langle (\Delta a_2)^2 \rangle$ equals $\langle (\Delta a_1)^2 \rangle$.

The diffusion coefficients in equation (67) may be found from Chandrasekhar[12] or from Cohen, Spitzer, and Routly.[13] Since we are here considering diffusion in physical space, the diffusion coefficients, given as a function of velocity by the above authors,[12, 13] must be averaged over a Maxwellian velocity distribution. The coefficients $\langle \Delta_\eta^2 \rangle$ and $\langle \Delta_\xi^2 \rangle$ are equal (their sum is denoted by $\Sigma[\Delta\tau_1^2]$ by Chandrasekhar),[12] and we obtain, finally,

$$K \equiv 2 \langle (\Delta a_1)^2 \rangle = \frac{4 (6\pi)^{1/2} e^2 c^2 \log (qC^2)}{3CB^2} \sum_i \frac{n_i Z_i^2}{(1 + C_i^2/C^2)^{1/2}} , \tag{68}$$

where C_i^2 is the mean-square velocity for ions of type i. Evidently, collisions with more slowly moving particles produce more rapid diffusion than do collisions with more rapid particles. Diffusion of protons, for example, is produced primarily by proton-proton collisions, with proton-electron collisions relatively unimportant. Because of the factor $1/C$ in equation (68), the heavier particles tend to diffuse more rapidly than do the lighter ones. In the argument of the logarithm in equation (68) we may take a mean value of C for all ions, since the value of this argument makes little difference. The quantity q is again determined from equation (56).

If we now assume that n_A and n_B have equal but opposite gradients along the x-axis, the rate of diffusion is given by

$$F_A = - K \frac{\partial n_A}{\partial x} = - F_B . \tag{69}$$

If this rate of flow is used to yield the mean velocity with which atoms of type A move in the x-direction, we arrive at exactly the same velocity as that obtained from equation (60), if we let atoms of types A and B correspond to types 1 and 2 in that equation and if T is assumed constant. Hence this process of autodiffusion considered here is simply another way of looking at the drift velocity in the (1, 1) approximation.

Next we may consider what happens when atoms all of a single type interact, but a density gradient is present. Since no systematic drift appears in this case in the (1, 1) approximation, one would expect autodiffusion to vanish in this same approximation. A computation of F_i in this case shows that the term in $\langle \Delta a_1 \rangle$ in equation (64) cancels the term in $\langle (\Delta a_1)^2 \rangle$, and no net drift appears. As we shall see below, collisions between identical atoms produce a net drift in the direction of the pressure gradient only in the (3, 1) approximation.

While the consideration of autodiffusion does not directly yield any new results, the diffusion coefficient K may be used to give approximate results in other problems. Let us consider the transfer of heat by diffusion. Suppose that in individual collisions each particle retained its same energy but that the position of its guiding center changed in accordance with the above results. Then the flow of heat should be given by an equation similar to equation (69), but with nkT replacing n_A. Since, as we have seen, the gradient of particle density produces no effect in this approximation when autodiffusion is considered, we may take n outside the derivative. The increase of $3nkT/2$, the internal energy of the plasma per cubic centimeter, is simply equal to minus the divergence of the heat flow, and we have, if changes in the x-direction only are considered,

$$\frac{\partial T}{\partial t} = \frac{\partial}{\partial x} \left(K \frac{\partial T}{\partial x} \right) . \tag{70}$$

Equation (70) is only approximate. To obtain an accurate expression, one must employ the detailed velocity-distribution function. When a temperature gradient is present but nT is constant, a flow of heat occurs in the direction perpendicular to ∇T and $\boldsymbol{B}$, with the more rapid atoms moving in one direction, the slower ones in the other.The effect of encounters on these two streams then produces a flow of heat in the direction of decreasing T.

Finally, we consider the viscous forces present. The transfer of lateral momentum may be treated in the same way as the transfer of heat, with the difference that the divergence of the flow of lateral momentum gives a force per unit volume. By equation (34) this force gives a current orthogonal to $\boldsymbol{B}$ and to the force. We find

$$\boldsymbol{j}_\perp = -\frac{1}{B^2}\boldsymbol{B}\times\sum_i n_i m_i \frac{\partial}{\partial x}\left(K\frac{\partial \boldsymbol{v}_\perp}{\partial x}\right). \tag{71}$$

Since $v_\perp$ is found from the (1, 0) approximation, $j_\perp$ obtained from equation (71) is of the (3, 1) approximation and is very small. This term tends to eliminate velocity gradients between different parts of the plasma, since the current will produce space charges that will tend to reduce $\partial v_\perp/\partial x$. Again, to improve the accuracy of equation (71), a detailed examination of the velocity-distribution function would be required.

INHOMOGENEOUS STELLAR MODELS. I. MODELS WITH A CONVECTIVE CORE AND A DISCONTINUITY IN THE CHEMICAL COMPOSITION*

J. B. Oke and M. Schwarzschild
Princeton University Observatory
Received April 16, 1952

ABSTRACT

A number of stellar models with a discontinuity in chemical composition have been computed through in detail. An arbitrary, but fixed, hydrogen-poor composition was used for the interior of all models, and a fixed hydrogen-rich composition was similarly used for all envelopes. The position in the star at which the change in chemical composition occurs was varied over a wide range. The computed models were found to cover well the observed red giants, as far as radii and luminosities are concerned. The masses of the theoretical red-giant models, however, fall systematically somewhat below the standard mass-luminosity relation—a circumstance not necessarily in discordance with observation.

I. INTRODUCTION

Since 1938 inhomogeneous stellar models have been investigated in a number of papers.[1] The main conclusion appears to be that inhomogeneities in the interior chemical composition may be the main cause for the large radii of the red giants. The question, however, of exactly what types of inhomogeneities are needed to explain the observed characteristics of the red giants and how these specific inhomogeneities might arise during the evolution of a red giant still appears to need further investigation.

In a recent paper[2] a series of models containing a convective core and a discontinuity in the chemical composition were computed. These computations were restricted to cases with only moderate deviations from the observed mass-luminosity relation. This restriction has been criticized[3] on the basis of the uncertainties in the few observed masses of red giants. This criticism has since gained strength by the circumstance that the mass of Capella, formerly considered a first-class datum, has recently been shown[4] to be quite uncertain.

In the present paper are given two series of models with a convective core and a chemical discontinuity—without regard to deviations from the empirical mass-luminosity law. The two series differ in the assumed variation of the absorption coefficient in the deep interior. The individual models in each series differ from one another in the percentage of the total mass contained in the hydrogen-poor interior portion of the star. All models of this paper were chosen to have the same hydrogen-poor composition in the interior and the same hydrogen-rich composition in the envelope. As in several of the

* This research was supported in part by funds of the Eugene Higgins Trust allocated to Princeton University and in part by contract with the Office of Naval Research.

[1] E. Öpik, *Pub. Obs. Tartu*, Vol. **30**, Nos. 3 and 4, 1938; **31**, No. 1, 1943; *Armagh Obs. Contr.*, No. 2, 1949; No. 3, 1951. G. Gamow, *Ap. J.*, **87**, 206, 1938. C. L. Critchfield and G. Gamow, *Ap. J.*, **89**, 244, 1939. S. Chandrasekhar and L. R. Henrich, *Ap. J.*, **94**, 525, 1941. M. Schönberg and S. Chandrasekhar, *Ap. J.*, **96**, 161, 1942. F. Hoyle and R. A. Lyttleton, *M.N.*, **102**, 218, 1942; **109**, 614, 1949. M. H. Harrison, *Ap. J.*, **100**, 343, 1944; **103**, 192, 1946; **105**, 322, 1947. G. Gamow and G. Keller, *Rev. Mod. Phys.*, **17**, 125, 1945. A. Reiz, *Ann. d'ap.*, **10**, 301, 1947. P. Ledoux, *Ap. J.*, **105**, 305, 1947; *Ann. d'ap.*, **11**, 174, 1948. Li Hen and M. Schwarzschild, *M.N.*, **109**, 631, 1949. C. M. Bondi, *M.N.*, **110**, 275, 1950. C. M. Bondi and H. Bondi, *M.N.*, **110**, 287, 1950; **111**, 397, 1951. J. G. Gardiner, *M.N.*, **111**, 102, 1951.

[2] Li Hen and M. Schwarzschild, *op. cit.*

[3] C. M. Bondi and H. Bondi, *M.N.*, **110**, 287, 1950.

[4] O. Struve, *Proc. Nat. Acad. Sci.*, **37**, 327, 1951.

earlier investigations, it was again arbitrarily assumed here that the composition in the deep interior, though hydrogen-poor, contained sufficient hydrogen to feed the nuclear energy sources in the core.

II. ASSUMPTIONS AND BASIC EQUATIONS

The models here considered consist of a hydrogen-rich envelope and a hydrogen-poor interior, the latter of which is divided into a radiative intermediate zone and a convective core. To simplify the computations, it has been assumed (*a*) that radiation pressure and degeneracy are negligible, (*b*) that electron scattering can be ignored, and (*c*) that the entire energy generation occurs within the convective core.

The computations have been carried out with help of the following definitions and equations:

Subscripts:

e, envelope; *i*, interior; *c*, center;
1, inner interface, between the convective core and the radiative intermediate zone;
2, outer interface, between the radiative intermediate zone and the envelope.

Absorption coefficient:

$$\kappa = \frac{\kappa_0}{(l/\bar{g})}\,\rho T^{-3.5} \qquad \text{with} \qquad \kappa_0 = 4\times 10^{25} Z(1+X)\,, \tag{1}$$

where the guillotine factor is given by

$$\frac{l}{\bar{g}} = \left(\frac{l}{\bar{g}}\right)_0 \left(\frac{\rho}{\rho_{2i}}\right)^a, \tag{2}$$

with $a = 0$ in the envelope of both model series and in the interior of the first model series, but with $a = 0.25$ in the interior of the second model series.

Dimensionless variables:

$$P = p\,\frac{GM^2}{4\pi R^4}\,, \qquad T = t\,\frac{\mu_e H}{k}\,\frac{GM}{R}\,, \qquad M_r = qM\,, \qquad r = xR\,. \tag{3}$$

Composition parameters:

$$l = \frac{\mu}{\mu_e} = \frac{2X_e + \frac{3}{4}Y_e + \frac{1}{2}Z_e}{2X + \frac{3}{4}Y + \frac{1}{2}Z}\,, \qquad j = \frac{Z}{Z_e}\,\frac{1+X}{1+X_e}\,\frac{\mu}{\mu_e}\,. \tag{4}$$

Appropriate relation if $Z = Z_e$: $j = l^{0.30}$.
In envelope, by definition: $l_e = j_e = 1$.
In interior, by assumption: $l_i = 2.5$, $j_i = 1.316$.

Basic equations for radiative parts:

$$\frac{dp}{dx} = -\,l\,\frac{pq}{x^2 l}\,, \qquad \frac{dq}{dx} = +\,l\,\frac{px^2}{l}\,, \tag{5}$$

$$\frac{dt}{dx} = -\,ljC\left(\frac{p_{2i}}{t_{2i}}\right)^a \frac{p^{2-a}}{x^2 l^{8.5-a}}\,, \tag{6}$$

with

$$C = \frac{3}{4ac}\left(\frac{k}{\mu_e HG}\right)^{7.5}\left(\frac{1}{4\pi}\right)^3 \frac{\kappa_0}{(l/\bar{g})_0}\,\frac{LR^{0.5}}{M^{5.5}}\,. \tag{7}$$

Homology invariants:

$$U = l\frac{px^3}{lq}, \qquad V = l\frac{q}{lx}, \qquad n+1 = \frac{1}{jC}\left(\frac{t_{2i}}{p_{2i}}\right)^{\alpha}\frac{ql^{8.5-\alpha}}{p^{2-\alpha}}. \tag{8}$$

Emden variables for convective core:

$$t = \theta t_c, \qquad p = \theta^{n+1}p_c, \qquad x = \xi\frac{x_1}{\xi_1}. \tag{9}$$

In core, by assumption: $\gamma = \frac{5}{3}$ or $n = 1.5$.

Fitting conditions at discontinuity:

$$\frac{U_{2i}}{U_{2e}} = \frac{V_{2i}}{V_{2e}} = \frac{l_i}{l_e} = 2.5, \qquad \frac{n_{2e}+1}{n_{2i}+1} = \frac{j_i}{j_e} = 1.316. \tag{10}$$

III. CONSTRUCTION OF THE MODELS

The numerical solutions needed for the three parts of the model were obtained as follows.

In the envelope where Kramers' law was assumed for the absorption coefficient ($\alpha = 0$), the differential equations (5) and (6), together with the usual boundary conditions ($p = t = 0, q = 1$ for $x = 1$), define a single-parameter family of solutions depending only on the value of C. Ten particular solutions of this family, covering a range in $\log C$ from -1 to -7, were obtained by numerical integrations.[5]

For the convective core, the one solution needed, which has no singularity at the center, is available in tabular form.[6]

For the intermediate zone, equations (5) and (6), together with the condition of a continuous fit at the boundary of the convective core, give a single-parameter family of solutions. Each particular solution of this family is characterized by a value of the independent Emden variable, ξ_1, which gives the point at which the convective core is terminated and the intermediate radiative zone is started. A method of obtaining starting values for these solutions by applying the appropriate fitting conditions at the surface of the convective core has been described previously.[2] Five particular solutions covering the necessary range in ξ_1 were obtained by numerical integration[5] under the assumption of $\alpha = 0$. These solutions were used for the construction of the first series of models. For the second series, for which $\alpha = 0.25$ was taken in the intermediate zone, a set of numerical integrations for the intermediate zone was already available.[2]

All the numerical solutions used are shown in Figure 1 in terms of the homology invariants U and V. The two halves of this figure correspond separately to the two series of models.

To complete the models, it remains to fit the intermediate zones to the envelopes under the conditions of equations (10). This fitting can conveniently be done with the help of the U–V plane, as shown in Figure 1. If one arbitrarily selects a particular solution for the intermediate zone and if, further, one selects a particular point on this solution for the outer boundary of the intermediate zone, one can read off directly U_{2i} and V_{2i}. The starting point for the corresponding envelope solution in the U–V plane (U_{2e}, V_{2e}) can then be obtained from the first of equations (10). The jump from the point (U_{2i}, V_{2i}) to the point (U_{2e}, V_{2e}) is represented in the U–V plane by a straight line pointing to the origin. In general, however, this procedure will not permit the second equation

[5] To be published in a forthcoming *Princeton U. Obs. Contr.*

[6] *Brit. Assoc. Adv. Sci., Math. Tables*, Vol. **2**, 1932.

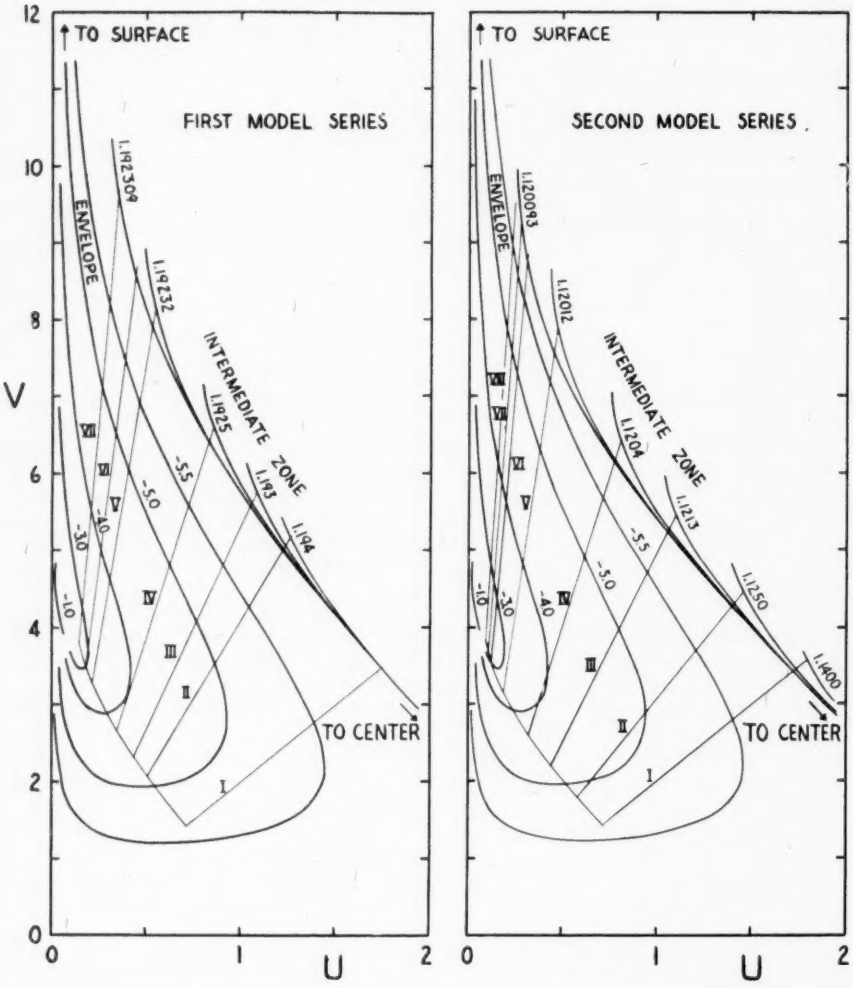

FIG. 1.—Representation of the models in terms of the homology invariants U and V. The left figure represents the first-model series, the right figure the second. The numbers on the envelope solutions denote the values of log C, the numbers on the intermediate zone solutions indicate the values of ξ_1. The various models, given in detail in Tables 1 and 2, are represented here by straight lines and are denoted by Roman numerals.

(10) to be fulfilled; the value of n_{2i} corresponding to the point (U_{2i}, V_{2i}) can be obtained from the intermediate-zone solutions (or by interpolation between them), and similarly the value of n_{2e} corresponding to the point (U_{2e}, V_{2e}) can be obtained by interpolation between the envelope solutions. In general, these two values of n will not fulfil the second condition (10) but will do so only for one specific point on each intermediate-zone solution. This specific point was determined for each of the numerical solutions for the intermediate zone by graphical interpolation, together with the corresponding point on the envelope solutions. Each such pair of points is shown in Figure 1 by a straight line connecting them. Any such jump line represents one particular model and is designated by

TABLE 1

MATHEMATICAL CHARACTERISTICS OF FIRST-MODEL SERIES

	I	II	III	IV	V	VI	VII
ξ_1	+1.21	+1.194	+1.193	+1.1925	+1.19232	+1.192315	+1.192309
U_1	+2.57	+2.582	+2.583	+2.583	+2.583	+2.583	+2.583
V_1	+1.26	+1.224	+1.222	+1.220	+1.220	+1.220	+1.220
U_{2e}	+0.720	+0.507	+0.435	+0.343	+0.218	+0.181	+0.141
V_{2e}	+1.428	+2.070	+2.306	+2.652	+3.267	+3.501	+3.844
$(n+1)_{2e}$	+3.290	+3.727	+3.839	+3.965	+4.107	+4.141	+4.174
log C	−5.37	−4.89	−4.67	−4.32	−3.44	−3.00	−2.50
log t_2	+0.150	+0.331	+0.420	+0.583	+0.995	+1.128	+0.985
log p_2	+2.635	+3.249	+3.543	+4.098	+5.487	+5.868	+5.070
log q_2	−0.857	−0.636	−0.568	−0.480	−0.313	−0.233	−0.113
log x_2	−1.162	−1.283	−1.351	−1.487	−1.822	−1.905	−1.683
log t_2/t_1	−0.17	−0.289	−0.332	−0.394	−0.505	−0.547	−0.604
log t_1	+0.32	+0.620	+0.752	+0.977	+1.500	+1.675	+1.589
log p_1	+3.10	+4.170	+4.635	+5.441	+7.284	+7.842	+7.282
log q_1	−1.35	−1.303	−1.273	−1.227	−1.103	−1.032	−0.924
log x_1	−1.37	−1.613	−1.714	−1.892	−2.291	−2.395	−2.201
log t_c	+0.43	+0.725	+0.857	+1.082	+1.605	+1.780	+1.694
log p_c	+3.37	+4.432	+4.896	+5.702	+7.545	+8.103	+7.543
$q_1=M_1/M$	+0.044	+0.050	+0.053	+0.059	+0.079	+0.093	+0.119
$q_2=M_2/M$	+0.139	+0.231	+0.270	+0.331	+0.486	+0.585	+0.771
$x_1=r_1/R$	+0.043	+0.024	+0.019	+0.013	+0.005	+0.004	+0.006
$x_2=r_2/R$	+0.069	+0.052	+0.045	+0.033	+0.015	+0.012	+0.021
log $\rho_c/\bar{\rho}$	+2.86	+3.628	+3.960	+4.541	+5.861	+6.244	+5.770

a Roman numeral. The few particular jump lines whose upper end-points do not fall on a numerical solution for the intermediate zone were obtained by interpolation between the available numerical solutions. Altogether, seven particular models were thus derived for the first series and eight for the second series, all of which are shown in Figure 1.

After the models had been completed in terms of the U–V plane, the remaining nondimensional characteristics were obtained in the following sequence. With the help of the values of U_{2e} and V_{2e}, graphic interpolation between the tabulated envelope solutions gave directly C, t_2, p_2, q_2, and x_2. Next the ratio t_2/t_1 was read from the intermediate-zone solution, since for this zone the starting point (U_1, V_1) and the end-point (U_{2i}, V_{2i}) had already been determined. This ratio, together with the previously found value of t_2, gave the value of t_1. The values of p_1, q_1, and x_1 were then determined from equations (8) with the help of the known quantities U_1, V_1, n_1, and t_1. Finally, t_c and p_c were computed with the help of the first two equations (9) by applying these equations to the inner inter-

face (subscript 1); here the values for t_1 and p_1 previously found were used, together with the value for θ_1 read from the tabulated solution for the convective core in accordance with the ξ_1 value characteristic of the particular model.

All these nondimensional quantities are listed in Table 1 for the first series of models and in Table 2 for the second series.

IV. PHYSICAL CHARACTERISTICS OF MODELS

Five of the physical characteristics of interest are completely determined by the model as derived in the previous section and do not depend on any specific properties

TABLE 2

MATHEMATICAL CHARACTERISTICS OF SECOND-MODEL SERIES

	I	II	III	IV	V	VI	VII	VIII
ξ_1	+1.1400	+1.1250	+1.1213	+1.1204	+1.12012	+ 1.120097	+ 1.120093	+ 1.120092
U_1	+2.618	+2.628	+2.631	+2.631	+2.631	+ 2.631	+ 2.631	+ 2.631
V_1	+1.112	+1.082	+1.075	+1.073	+1.072	+ 1.072	+ 1.072	+ 1.072
U_{2c}	+0.718	+0.582	+0.441	+0.324	+0.190	+ 0.127	+ 0.110	+ 0.099
V_{2c}	+1.417	+1.774	+2.181	+2.560	+3.140	+ 3.541	+ 3.690	+ 3.809
$(n+1)_{2c}$	+3.283	+3.567	+3.803	+3.962	+4.115	+ 4.173	+ 4.187	+ 4.195
log C	−5.388	−5.140	−4.793	−4.427	−3.723	− 3.000	− 2.4	− 1.5
log l_2	+0.152	+0.248	+0.390	+0.578	+1.080	+ 1.80	+ 2.4	+ 2.8
log p_2	+2.649	+2.980	+3.455	+4.107	+5.934	+ 8.66	+10.9	+12.3
log q_2	−0.866	−0.738	−0.617	−0.530	−0.422	− 0.36	− 0.3	− 0.2
log x_2	−1.169	−1.235	−1.346	−1.516	−1.999	− 2.70	− 3.3	− 3.5
log l_2/l_1	−0.182	−0.245	−0.320	−0.395	−0.515	− 0.60	− 0.6	− 0.6
log l_1	+0.334	+0.493	+0.710	+0.973	+1.595	+ 2.40	+ 3.0	+ 3.4
log p_1	+3.144	+3.706	+4.477	+5.435	+7.764	+10.86	+13.3	+14.5
log q_1	−1.422	−1.402	−1.358	−1.311	−1.233	− 1.17	− 1.1	− 1.0
log x_1	−1.404	−1.531	−1.701	−1.917	−2.460	− 3.20	− 3.8	− 4.0
log t_c	+0.429	+0.586	+0.802	+1.065	+1.687	+ 2.49	+ 3.1	+ 3.5
log p_c	+3.382	+3.938	+4.707	+5.665	+7.994	+11.09	+13.5	+14.7
$q_1=M_1/M$	+0.038	+0.040	+0.044	+0.049	+0.058	+ 0.068	+ 0.08	+ 0.11
$q_2=M_2/M$	+0.136	+0.183	+0.242	+0.295	+0.378	+ 0.44	+ 0.5	+ 0.7
$x_1=r_1/R$	+0.039	+0.029	+0.020	+0.012	+0.0035	+ 0.0006	+ 0.0002	+ 0.0001
$x_2=r_2/R$	+0.068	+0.058	+0.045	+0.030	+0.010	+ 0.002	+ 0.0005	+ 0.0003
log $\rho_c/\bar{\rho}$	+2.874	+3.273	+3.826	+4.521	+6.228	+ 8.52	+10.3	+11.1

of individual stars. These quantities are listed at the bottom of Tables 1 and 2; they are the fraction of the total mass contained in the convective core, q_1; the fraction of the total mass contained in the hydrogen-poor interior (convective core and intermediate zone), q_2; the fraction of the radius occupied by the convective core, x_1; the fraction of the radius occupied by the hydrogen-poor interior, x_2; and the ratio of central to mean density, $\rho_c/\bar{\rho}$.

The fraction of the mass contained in the hydrogen-poor interior, q_2, is the essential physical parameter which varies from model to model in each series. Tables 1 and 2 show that the computed models cover a large range in q_2, each of the two series starting with a model containing less than 14 per cent of the mass in the interior and ending with a model containing over 70 per cent in the interior.

The values listed for x_2 show that the hydrogen-poor interior, though containing in

many cases a large fraction of the mass, occupies at most a few per cent of the radius of the star. This indicates a high central concentration of these models, which is explicitly shown by the values for log $\rho_c/\bar{\rho}$ listed.

To derive further physical characteristics for the model stars here considered, it is necessary to apply the models described in the previous section to specific cases characterized by definite values for the mass, the composition, the central temperature, and the guillotine factor. Correspondingly, the subsequent computations are based on the following assumptions. The internal composition is arbitrarily taken to be $X_i = 0.01$, $Y_i = 0.97$, and $Z_i = 0.02$, while the envelope composition is assumed to be $X_e = 0.92$, $Y_e = 0.06$, and $Z_e = 0.02$. These compositions correspond to the numerical values of l_i and j_i used in the construction of the models. Further, $(t/\bar{g})_0 = 2$ has been used for the guillotine factor law given by equation (2). Finally, the central temperature was assumed to be 3×10^7 ° K throughout. This last assumption is a substitute for an accurate evaluation of the central temperature needed by the carbon cycle to produce the required energy; such computations did not seem worth while at the present state of these models and the present uncertainty in the carbon-cycle cross-sections. Finally, regarding the assumed stellar masses, the first series of models was applied only to stars of two solar masses, while the second series was applied to stars of one, two, and four solar masses.

Under these assumptions the physical characteristics were computed in the following sequence.

To start with, the radius of a particular model star could be obtained from the second of equations (3) by applying this equation to the center of the star; the radius is the only unknown quantity in this equation, since T_c, μ_e, and M are given by the above assumptions, whereas t_c can be taken from Table 1 or Table 2 for any specific model. Similarly, the luminosity could be found from equation (7). With R and L known, the effective temperature, T_e, could be obtained from its usual definition. Finally, the temperatures at the two interfaces and the densities at the center and at the two interfaces could be computed directly from the first two of equations (3)—together with the equation of state—since the nondimensional values p and t corresponding to these particular locations are listed in Tables 1 and 2.

The physical characteristics enumerated above are given in Tables 3 and 4 for models of the first and second series, respectively.

V. CHECKS ON ASSUMPTIONS

After the physical properties of the model stars were derived, it was possible to check some of the assumptions on which the computations had been based. These checks were performed on a typical case represented by model V of the first series as applied to a star of two solar masses. For this case temperatures and densities were computed for a number of points throughout the star; these are given in Table 5.

The first check concerns equation (2), the law assumed for the guillotine factor. From Morse's table of the guillotine factor for Russell mixture,[7] the guillotine factor was obtained for the temperatures and densities in question and is listed in the fifth column of Table 5. These values for the guillotine factor are also shown as a function of the density by the solid line in Figure 2. The dashed lines in the same figure represent the guillotine factor, as assumed for the models according to equation (2). The figure shows that in the envelope the assumed law is quite representative. In the interior, however, the assumption used for the models of the first series gives appreciably too low a guillotine factor, while the assumption for the second series is apparently much more representative. For future computations a still further increase in the guillotine factor for the interior seems to be indicated by Figure 2—not so much in the slope (α) as in the constant factor $(t/\bar{g})_0$.

[7] P. M. Morse, *Ap. J.*, **92**, 27, 1940.

TABLE 3

PHYSICAL CHARACTERISTICS OF FIRST-MODEL SERIES
($M/M\odot = 2$)

	I	II	III	IV	V	VI	VII
$R/R\odot$	+ 2.19	+ 4.32	+ 5.85	+ 9.82	+32.7	+49.0	+40.2
log $L/L\odot$	+ 0.87	+ 1.20	+ 1.36	+ 1.60	+ 2.22	+ 2.58	+ 3.12
log T_e	+ 3.80	+ 3.74	+ 3.72	+ 3.66	+ 3.56	+ 3.55	+ 3.74
$T_1\times10^{-6}$	+23.3	+23.6	+23.6	+23.6	+23.6	+23.6	+23.6
$T_2\times10^{-6}$	+15.7	+12.1	+11.0	+ 9.5	+ 7.4	+ 6.7	+ 5.9
log ρ_c	+ 2.29	+ 2.17	+ 2.11	+ 2.02	+ 1.77	+ 1.62	+ 1.41
log ρ_1	+ 2.13	+ 2.02	+ 1.95	+ 1.86	+ 1.61	+ 1.47	+ 1.25
log ρ_{2i}	+ 1.84	+ 1.38	+ 1.19	+ 0.91	+ 0.32	+ 0.04	− 0.36
log ρ_{2e}	+ 1.44	+ 0.98	+ 0.79	+ 0.51	− 0.08	− 0.36	− 0.76

TABLE 4

PHYSICAL CHARACTERISTICS OF SECOND-MODEL SERIES

	I	II	III	IV	V	VI	VII	VIII
	$M/M\odot=1.0$							
$R/R\odot$	+ 1.09	+ 1.57	+ 2.58	+ 4.72	+19.8	+126	+530	+1300
log $L/L\odot$	− 0.646	− 0.477	− 0.238	− 0.003	+ 0.390	+ 0.711	+ 1.000	+ 1.71
log T_e	+ 3.580	+ 3.544	+ 3.495	+ 3.423	+ 3.210	+ 2.888	+ 2.646	+ 2.63
$T_1\times10^{-6}$	+24.1	+24.2	+24.3	+24.3	+24.3	+24.4	+23	+24
$T_2\times10^{-6}$	+15.8	+13.8	+11.6	+ 9.8	+ 7.4	+ 6.1	+ 5.7	+ 6.0
log ρ_c	+ 2.91	+ 2.84	+ 2.74	+ 2.65	+ 2.49	+ 2.37	+ 2.3	+ 1.9
log ρ_1	+ 2.77	+ 2.70	+ 2.60	+ 2.51	+ 2.35	+ 2.23	+ 2.2	+ 1.8
log ρ_{2i}	+ 2.45	+ 2.22	+ 1.90	+ 1.58	+ 1.04	+ 0.63	+ 0.4	+ 0.2
log ρ_{2e}	+ 2.05	+ 1.82	+ 1.50	+ 1.18	+ 0.64	+ 0.23	+ 0.0	− 0.2
	$M/M\odot=2$							
$R/R\odot$	+ 2.18	+ 3.13	+ 5.15	+ 9.44	+39.5	+250	+1100	+2600
log $L/L\odot$	+ 0.859	+ 1.028	+ 1.268	+ 1.502	+ 1.895	+ 2.216	+ 2.501	+ 3.211
log T_e	+ 3.806	+ 3.770	+ 3.721	+ 3.648	+ 3.436	+ 3.114	+ 2.872	+ 2.858
$T_1\times10^{-6}$	+24.1	+24.2	+24.3	+24.3	+24.3	+24.4	+23	+24
$T_2\times10^{-6}$	+15.8	+13.8	+11.6	+ 9.8	+ 7.4	+ 6.1	+ 5.7	+ 6.0
log ρ_c	+ 2.31	+ 2.24	+ 2.14	+ 2.05	+ 1.89	+ 1.77	+ 1.7	+ 1.3
log ρ_1	+ 2.16	+ 2.10	+ 2.00	+ 1.91	+ 1.75	+ 1.63	+ 1.6	+ 1.2
log ρ_{2i}	+ 1.85	+ 1.62	+ 1.30	+ 0.98	+ 0.43	+ 0.03	− 0.2	− 0.4
log ρ_{2e}	+ 1.45	+ 1.22	+ 0.90	+ 0.58	+ 0.03	− 0.37	− 0.6	− 0.8
	$M/M\odot=4$							
$R/R\odot$	+ 4.37	+ 6.27	+10.3	+18.9	+79.1	+500	+2100	+5100
log $L/L\odot$	+ 2.364	+ 2.533	+ 2.773	+ 3.007	+ 3.400	+ 3.721	+ 4.010	+ 4.716
log T_e	+ 4.031	+ 3.996	+ 3.946	+ 3.875	+ 3.661	+ 3.340	+ 3.098	+ 3.084
$T_1\times10^{-6}$	+24.1	+24.2	+24.3	+24.3	+24.3	+24.4	+23	+24
$T_2\times10^{-6}$	+15.8	+13.8	+11.6	+ 9.8	+ 7.4	+ 6.1	+ 5.7	+ 6.0
log ρ_c	+ 1.70	+ 1.63	+ 1.54	+ 1.44	+ 1.29	+ 1.17	+ 1.1	+ 0.7
log ρ_1	+ 1.56	+ 1.49	+ 1.40	+ 1.31	+ 1.15	+ 1.03	+ 1.0	+ 0.6
log ρ_{2i}	+ 1.25	+ 1.01	+ 0.70	+ 0.37	− 0.17	− 0.57	− 0.8	− 1.0
log ρ_{2e}	+ 0.85	+ 0.61	+ 0.30	− 0.03	− 0.57	− 0.97	− 1.2	− 1.4

The second check refers to the neglect of electron scattering. The sixth column in Table 5 gives the ratio of the absorption coefficient here used, according to equations (1) and (2), to the absorption coefficient arising from electron scattering. The values given are computed for the same typical case used in the first check. The tabulation shows that—except in the convective core, where the absorption coefficient has no effect on the conditions—electron scattering provides less absorption than photoionization. However, electron scattering is not much less important than photoionization, at least in the inner portions of the star. Nevertheless, for the typical case represented by Table 5, the error

TABLE 5

GUILLOTINE FACTOR, ELECTRON SCATTERING, AND RADIATION PRESSURE IN TYPICAL MODEL STAR

r/R	M_r/M	log T	log ρ	log $(t/\bar{g})$	κ/κ_e	P_g/P_r
0.0	+0.00	+7.477	+1.77	+1.07	+0.8	+ 54
x_1=0.005	+0.08	+7.372	+1.61	+0.90	+1.3	+ 78
x_{2i}=0.015	+0.49	+6.867	+0.32	+0.47	+3.8	+130
x_{2e}=0.015	+0.49	+6.867	−0.08	+0.40	+1.5	+130
0.1	+0.78	+6.16	−2.26	+0.24	+3.0	+110
0.2	+0.91	+5.83	−3.28	.....	+4.1	+100
0.3	+0.96	+5.60	−4.00	.....	+5.0	+ 98
0.4	+0.98	+5.42	−4.62	.....	+5.1	+ 81
0.5	+0.99	+5.24	−5.18	.....	+6.0	+ 78
0.6	+1.00	+5.07	−5.75	.....	+6.4	+ 68
0.7	+1.00	+4.88	−6.38	.....	+6.9	+ 59

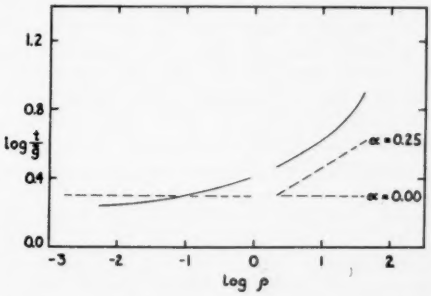

FIG. 2.—The guillotine factor through the star as a function of density. The solid line is the value as determined for the typical case of model V of the first series for a star of 2 solar masses. The dashed lines are the assumed representations for the models. In the interior, the dashed line marked "$\alpha = 0$" represents the first-model series, while the line "$\alpha = 0.25$" denotes the second-model series.

produced by neglecting electron scattering does not appear serious and is partially compensated for by the use of too small a guillotine factor, as discussed above. For heavier giants, however, the relative importance of electron scattering increases (proportional to M^2), and an appropriate combination of photoionization and electron scattering will eventually have to be taken into account.

The third check refers to the neglect of radiation pressure. The last column of Table 5 gives the ratio of gas pressure to radiation pressure for the typical case used above. The tabulation shows that radiation pressure plays virtually no role throughout the body of the star considered. Since the relative importance of radiation pressure varies with M^2,

a red giant has to have a mass of 10 solar masses or more if radiation pressure is to become really important.

The fourth check refers to the neglect of degeneracy. If in a diagram[8] showing the log T − log ρ plane, the demarcation line between degeneracy and nondegeneracy is drawn and if, in the same diagram, the data of the third and fourth columns of Table 5 are plotted, it is found that the entire typical model star represented by Table 5, including its center, falls in the nondegenerate region. The same is found to be essentially true for all the other model stars here considered, as can be seen from the ρ_c values of Tables 3 and 4.

The final check concerns the assumed central temperature of 3×10^7° K. Again choosing the same typical model, an integration of the energy generation law for the carbon cycle shows that the assumed temperature cannot be much in error if the recent estimates[9] of the rate of the carbon cycle are essentially correct.

In summarizing these checks, it appears that the actual physical conditions in stars possessing the assumed composition discontinuity are satisfactorily represented by the second series of models as long as these models are not applied to too heavy giants. The first series of models appears to underestimate the guillotine factor in the deep interior; however, the comparison of this first series with the second series is useful in showing which of the results depend sensitively on the detailed behavior of the absorption coefficient in the deep interior.

VI. HERTZSPRUNG-RUSSELL DIAGRAM

To facilitate the comparison between the present model stars and observations, the model stars described above are presented in Figure 3 in terms of the Hertzsprung-Russell diagram.

Each case of Tables 3 and 4 is plotted in Figure 3 according to its values for the luminosity and the effective temperature. Each of the three heavy lines in the center and right-hand portions of the diagram represents all the models of the second series as applied to a definite stellar mass; the bottom line corresponds to 1 solar mass, the middle line to 2 solar masses, and the top line to 4 solar masses. Each of the dashed lines crossing the solid lines corresponds to a particular model of the second series as applied to various stellar masses. Since each model has a definite fraction of the total mass in the hydrogen-poor interior, the dashed lines indicate the progression of hydrogen exhaustion; at the lower left the mass fraction in the hydrogen-poor interior is small, whereas in the upper right portion it is large.

For comparison the locations of actually observed giants, subgiants, and main-sequence stars are very approximately indicated by the shaded areas.

Figure 3 shows that the models here considered amply cover the territory in the Hertzsprung-Russell diagram occupied by the red giants. Indeed, the most extreme models of the second series give effective temperatures probably lower than that of any observed star.

How sensitively the effective temperature of a star, i.e., its radius, depends on the exact run of the absorption coefficient in the deep interior is shown by the thin solid line which represents the first series of models as applied to stars of 2 solar masses. According to this series, a star of 2 solar masses reaches its lowest effective temperature at about 3500° K, while the same star, according to the second series, can reach an effective temperature below 1000° K. Therefore, to predict accurately the position in the Hertzsprung-Russell diagram of an inhomogeneous star, it will be necessary not only to specify in detail the character of the chemical inhomogeneity but also to represent the absorption coefficient in the interior with appreciable accuracy.

[8] G. W. Wares, *Ap. J.*, **100**, 158, 1944.

[9] I. Epstein, *Ap. J.*, **112**, 207, 1950.

To indicate the great difference in location in the Hertzsprung-Russell diagram between chemically homogeneous and inhomogeneous stars, the position of homogeneous stars with central temperatures of $3 \times 10^{7\,\circ}$ K is indicated by a set of lines in the left-hand part of Figure 3. Here again each solid line connects all points corresponding to a given stellar mass, while each dashed line corresponds to a given degree of hydrogen exhaustion. For the homogeneous models the degree of hydrogen exhaustion is given directly by the hydrogen abundance (assumed constant throughout the star) which decreases from 92 per cent near the middle of Figure 3 to 1 per cent near its left edge.

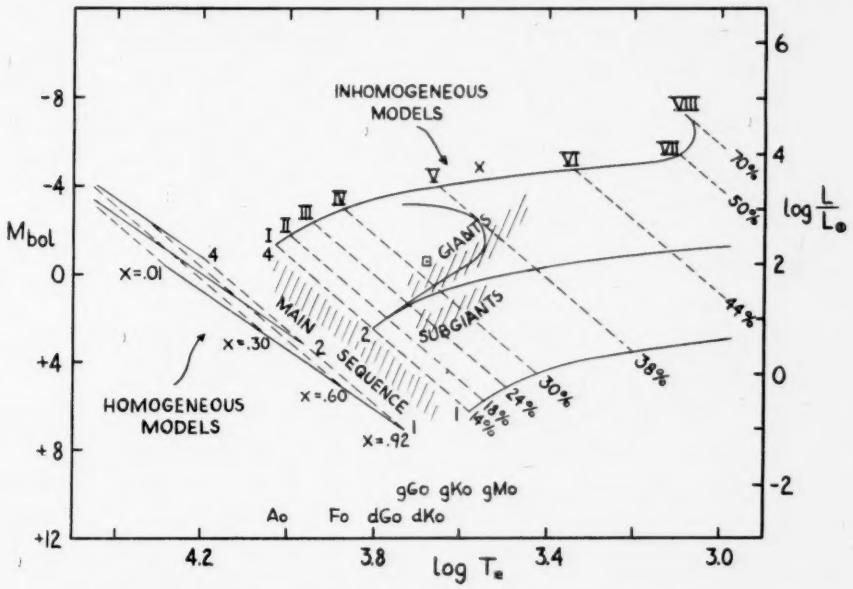

FIG. 3.—The Hertzsprung-Russell diagram for the models in terms of bolometric magnitude and effective temperature. The three heavy lines marked *1*, *2*, and *4* in the right part of the diagram represent the models of the second series applied to stars of 1, 2, and 4 solar masses. (The extra thin solid curve shows, for comparison, the line for 2 solar masses for the first-model series.) Each dashed line represents a specific model, which is marked by its Roman numeral and its percentage of the total mass in the hydrogen-poor interior. The solid and dashed lines to the left denote the corresponding homogeneous models. The hatched areas represent, approximately, the normal observed Hertzsprung-Russell diagram. The square and cross represent, respectively, the observed positions of Capella and ζ Aurigae.

Figure 3 permits a rough estimate of the possible evolutionary track of a bright star through the upper portions of the Hertzsprung-Russell diagram. A star of, say, 2 solar masses will start approximately as an F0 star with a bolometric absolute magnitude of about +3. If this star contains strong mixing mechanisms and correspondingly remains chemically homogeneous throughout its life, it will evolve along the middle one of the solid lines in the left-hand part of Figure 3 and thus increase in both absolute magnitude and effective temperature. If, however, the same star contains only a limited mixing mechanism, which only successively reaches through larger and larger fractions of the stellar mass, then the star will evolve along the middle one of the solid lines in the right-hand portion of Figure 3. It will thus, while slowly increasing in luminosity and be-

coming redder and redder, reach a minimum in the effective temperature, after which it will increase its effective temperature again and, passing through the supergiant region, end as a bright-blue star—assuming that no new physical phenomena set in before the star has essentially exhausted all its hydrogen. The great difference in the evolutionary track through the Hertzsprung-Russell diagram for homogeneous and inhomogeneous stars shows that the strength and character of the internal mixing mechanisms play a decisive role in the apparent evolution of bright stars.

It is tempting to compare Figure 3 with the Hertzsprung-Russell diagram for a globular cluster under the assumption that the cluster stars are built according to the inhomogeneous models here considered. To derive for each star its present position along its evolutionary track, one has to take account of the difference in speed of evolution for stars of different luminosity or mass. Thus a star of 1 solar mass may still be essentially homogeneous; a star of 2 solar masses may already have developed the hydrogen-poor core containing, say, 15 per cent of the total stellar mass; and a star of 3 solar masses may already have extended its hydrogen-poor core to over 70 per cent of its total mass. If one draws a line through the three corresponding points in Figure 3, one obtains a curve which has some resemblance to the main branch of the Hertzsprung-Russell diagram of a globular cluster. It does, however, not seem warranted to follow this speculation at present into further detail, mainly because of the arbitrariness with which the character of the chemical inhomogeneity has been selected for the models here investigated.

VII. MASSES OF RED GIANTS

In the preceding section the present stellar models were compared with observations in terms of absolute magnitudes and effective temperatures. It remains to compare the theoretical models with observed stellar masses.

The direct observational data on masses of red giants appear to be still very restricted and uncertain. The best available data seem to be those for Capella and Zeta Aurigae. The red components of these two binaries are indicated in the Hertzsprung-Russell diagram of Figure 3 by a square and a cross, respectively. By interpolating in this diagram between the heavy lines which represent various stellar masses, one can read off mass values for the two stars. One thus obtains approximately 2.5 and 5 solar masses for the red components of Capella and Zeta Aurigae, respectively. These theoretical mass values, derived under the assumption that the present inhomogeneous models are applicable to the stars considered, are to be compared with the observational values.

For the red component of Capella the earlier observational value of 4 solar masses has recently been shown to be possibly too high. The new observations[10] give, with much uncertainty, a mass around 2.7 solar masses, which is in satisfactory agreement with the above theoretical value.

For the red component of Zeta Aurigae a mass of 15 solar masses or more has been derived from the observational data.[11] The discrepancy between this value and our theoretical value of 5 solar masses is very large indeed. The question arises whether the observational value could possibly be greatly in error. The observational mass is based on the determination of the mass function and the mass ratio. The mass function was derived from radial-velocity measurements of the K component, which has many sharp lines, on spectrograms which covered the entire orbit; accordingly, the mass function seems fairly secure. On the other hand, the mass ratio is derived from radial-velocity measurements of the B component, which has few and broad lines, on a small number of spectrograms, which in each of the three investigations in question covers only one

[10] Struve, *loc. cit.*

[11] W. Christie and O. Wilson, *Ap. J.*, **81**, 426, 1935.

particular phase of the orbital cycle. Accordingly, the mass ratio for Zeta Aurigae appears to be extremely uncertain. Instead of using the uncertain mass ratio, one might use the assumption that the B component of Zeta Aurigae falls on the mass-luminosity relation applicable for main-sequence stars. Thus one would get, for a bolometric magnitude of -1.4,[12] a mass of 5 solar masses for the B component. The latter value, together with the observed mass function, would give 6 solar masses for the mass of the K component. This empirical value would be in excellent agreement with the theoretical value derived above. Whether, however, this interpretation of the observational data on Zeta Aurigae is correct can be decided only after a set of spectrograms covering the B component around an entire orbital cycle has been obtained.

In addition to the use of individual binaries with red-giant components, statistical data for whole groups of such binaries may be used to derive averaged masses of red giants.[13] Such averaged mass determinations for red giants appear, however, at present still very uncertain, as is indicated by the appreciable difference in the result, depending on whether trigonometric or spectroscopic parallaxes are used.

Besides the direct method of determining stellar masses from binaries, two indirect methods may be used for gaining information regarding the masses of red giants.

As a first method the period-density law for pulsating stars may be applied to cepheids. Since for cepheids the periods are very well known and the radii can be determined with fair accuracy from absolute magnitudes and effective temperatures, the theoretical period-density law can be used to determine the masses of cepheids. The resulting masses are, by a factor of approximately 3, smaller than those which are obtained if the mass-luminosity relation of main-sequence stars is applied to the cepheids.[14] This discrepancy has in the past been interpreted as indicating that the numerical coefficient in the theoretical period-density law must differ appreciably from the value thus far derived from pulsation theory. Now, however, it appears at least equally likely that one should interpret this discrepancy as indicating that the masses of cepheids are, in fact, appreciably smaller than had been inferred from the application of the mass-luminosity relation for main-sequence stars to cepheid variables.

As a second indirect method, one may derive the gravitational acceleration in the atmosphere of a star by a detailed analysis of the line strengths in its spectrum. When this method was first applied to giants and supergiants, values were found for the gravitational acceleration which were smaller by large factors than those derived from the mass-luminosity relation. This large discrepancy has since been greatly diminished, first, by introducing the H^- absorption, which increased the mean absorption coefficient, and, second, by introducing the turbulent velocities as deduced from line profiles, which increased the total kinetic temperature.[15] Nevertheless, the gravitational accelerations now derived are still smaller than those obtained from the mass-luminosity law of main-sequence stars by a factor of the order of 3. Perhaps this may be taken as further indication that the masses of the red giants are indeed somewhat smaller than those implied by the standard mass-luminosity relation.

In summarizing the observational data regarding the masses of red giants, one may conclude that the indirect evidence somewhat favors the relatively low masses required by the present inhomogeneous models and that the direct evidence does not necessarily contradict these low values.

[12] P. Wellmann, *A.N.*, **279**, 257, 1951.

[13] H. N. Russell and C. E. Moore, *The Masses of the Stars* (Chicago: University of Chicago Press, 1940).

[14] I. Epstein, *Ap. J.*, **112**, 6, 1950.

[15] O. C. Wilson, *Ap. J.*, **107**, 126, 1948; M. Schwarzschild, B. Schwarzschild, and W. S. Adams, *Ap. J.*, **108**, 207, 1948.

VIII. SUMMARY

The inhomogeneous models described in detail in Sections III and IV and compared with observations in Sections VI and VII appear to cover well the observed ranges for red-giant stars, as far as luminosities and radii, i.e., position in the Hertzsprung-Russell diagram, are concerned.

The present models give masses for red giants which are smaller than those given by the mass-luminosity relation of main-sequence stars by factors of from 1.5 to about 3. The limited observational evidence on the masses of red giants, though in itself not suggesting a deviation from the regular mass-luminosity relation, still does not seem to be in direct discordance with these relatively low masses.

The two series of inhomogeneous models here described indicate that the evolutionary track of a bright star through the Hertzsprung-Russell diagram does depend sensitively both on the precise character of any chemical inhomogeneity and on the detailed run of the absorption coefficient in the deep interior. For stars with weak mixing mechanisms and an absorption law not too different from that of Kramers, the present models indicate an evolution which starts at the main sequence, passes through phases of increasing radius until a maximum size is reached, when the hydrogen-poor interior and the hydrogen-rich envelope are comparable in mass, and ends in a return toward the main sequence.

Stellar models like the present ones must still be considered as exploratory, owing to the arbitrariness with which the character of the chemical inhomogeneity is assumed. If, indeed, a chemical inhomogeneity is an essential feature in the internal structure of the red giants, as now appears likely, it will be possible to derive definite models for red giants only after the physical mechanisms which govern the degree and character of the internal mixing have been determined.

THE SPECTRUM AND RADIAL VELOCITIES OF W VIRGINIS

ROSCOE F. SANFORD
MOUNT WILSON AND PALOMAR OBSERVATORIES
CARNEGIE INSTITUTION OF WASHINGTON
CALIFORNIA INSTITUTE OF TECHNOLOGY
Received April 25, 1952

ABSTRACT

Twenty-three coudé spectrograms of W Virginis have been used to study changes of the spectrum and of radial velocity with change of light. Phases were found to be satisfactorily represented by

$$T \text{ max.} = \text{JD } 2432687.0 + 17^{d}.26944E \text{ (G.M.T.)}.$$

The spectral class varies from about F2 at maximum light to about G6 at minimum light. For an interval $0.15P$ around maximum light most spectrograms showed at least some double absorption lines. There are large changes of relative intensities with phase between lines of the ionized elements and ground-state lines of neutral elements, such as *Fe* I. The spectral class of W Vir is somewhat earlier at its light-minimum than that of X Cygni at the same phase. Hydrogen emission lines are present from light-minimum to $0.1P$ past light-maximum (an interval of $0.45P$), about as found by Joy.

The absorption-line radial velocities follow a single curve covering an interval of $1.15P$. This curve starts at phase $0.95P$, with minimum at phase $0.0P$, and maximum thereafter at phase $0.9P$, and then ends at phase $0.1P$. There is an overlap of successive cycles for $0.15P$. The behavior of the absorption-line velocities of W Vir finds at least a qualitative explanation by a shock wave that traverses its reversing layer.

Velocities from the hydrogen absorption lines agree with those from the other absorption lines, the correspondence being with the longer component of these other absorption lines if they are double. The velocities given by the hydrogen emission lines measured on microphotometer tracings vary from about -70 km/sec at phase $0.65P$ to about -100 km/sec from phase $0.94P$ to $0.10P$. Emission hydrogen lines have an average width of about 2.3 A.

W Vir differs from ordinary cepheids in having a high galactic latitude, a large systemic velocity, a light-curve quite unlike that of ordinary cepheids of the same period, a large velocity amplitude, and at times double absorption lines and emission components of the hydrogen absorption lines.

The cepheid variable W Virginis, with a galactic latitude of 57°.6, differs greatly from ordinary cepheids, which lie mostly near the galactic equator. The shape of its light-curve is quite different from that of most other cepheids of like period. One-prism spectrograms[1] have shown that the systemic velocity, -66 km/sec, given by its absorption lines is unusually high and that, from minimum to maximum of light, the hydrogen lines are in both emission and absorption. W Vir is considered to be a member of Baade's stellar population II. These characteristics set this variable apart from the ordinary cepheid variables and make it important to study its spectrum with the highest practicable dispersion. It was found possible to obtain spectrograms of W Vir of fair density, even at light-minimum, with the 32-inch coudé spectrograph at the 100-inch telescope (10 A/mm). This required the use of a slit-width somewhat greater than that for optimum definition. The resultant spectrograms served very well for the determination of radial velocities but were somewhat lacking in sharpness of detail.

The writer obtained thirteen spectrograms in the interval from January, 1948, to July, 1949. The phases of these spectrograms were well distributed over the cycle of light-change. These thirteen spectrograms were to have been used by the writer in studying the velocity variation, the relation of velocity variation to light-variation, the change of spectrum with phase, and in a cursory comparison of the spectrum of W Vir with that of X Cyg, an ordinary cepheid of similar period. However, the addition of one spectrogram, Ce 6889, by William Buscombe and nine subsequent ones by Arthur Abt, made available

[1] A. H. Joy, *Mt. W. Contr.*, No. 607; *Ap. J.*, **89**, 3. 6, 1939.

twenty-three coudé spectrograms (Table 1) for my study as well as for a spectrophotometric investigation which Abt has under way.

THE PERIOD

Photometric observations[2] that fell within the interval covered by coudé spectrograms gave JD 2432687.0 as the epoch of maximum.

Although Gordon and Kron used the period of 17.271671 days[3] to assemble their photometric observations, they comment as follows: "Our results . . . indicate that the shape of the light curve is variable. . . . The accumulated evidence now shows that the period varies but its determination is undoubtedly complicated by the variation in the shape of

TABLE 1

RADIAL VELOCITIES OF W VIRGINIS

Plate Ce	JD 243+	Phase (P)	Phase Interval	Abs. Vel. (Km/Sec)	Hydrogen Em. Vel. (Km/Sec)
7102	3825.743	0.940		−92.8 −36.4	− 96
6207	3376.837	.951		−97.2 −42.6	− 83
5092	2599.946	.958		−40.3	−104
5616	3014.799	.981	E II	−40.9	−105
6211	3377.854	.004		−92.0 −37.0	.....
5647	3049.753	.008		−94.0 −43.1	−103
5617	3015.844	.044		−92.2 −42.2	−108
5618	3016.788	.099		−91.6 −45.6	− 89
5651	3069.747	.163		−94.9	.....
5556	2966.957	.213		−91.2	.....
5216	2725.717	.242		−89.0	.....
5058	2571.010	.283		−78.3	.....
7010	3781.793	.401		−67.1	.....
5187	2694.721	.447	A	−71.6	.....
6947	3730.956	.451		−73.9	.....
7013	3782.788	.458		−64.0	.....
7017	3783.794	.516		−59.5	.....
6965	3750.865	.604		−51.7	.....
5110	2611.883	.650		−49.2	− 70
7080	3821.754	.709		−48.6	− 72
7085	3822.751	.766	E I	−44.2	− 72
6889	3719.953	.814		−38.3	.....
7091	3823.754	0.825		−42.3	− 88

the light curve. The period would have to be shortened to 17^d26713 to make our time of minimum agree with that of the next most recent light curve." The period 17.26944 days chosen by the writer harmonizes the older one-prism velocities[1] with the coudé velocities and is approximately the mean of Gaposchkin's period and the one in the above quotation. Certainly, this intermediate period will serve amply well to relate the coudé velocities and Gordon and Kron's photometric observations within the relatively short interval of 73 cycles which covers them. Phases are in decimals of the period (Table 1) as derived from

$$T \text{ max.} = \text{JD } 2432687.0 + 17^d26944E \text{ (G.M.T.)}.$$

[2] Gordon and Kron, *Ap. J.*, **109**, 177, 1949.

[3] S. Gaposchkin, *Harvard Bull.*, No. 906, 1937.

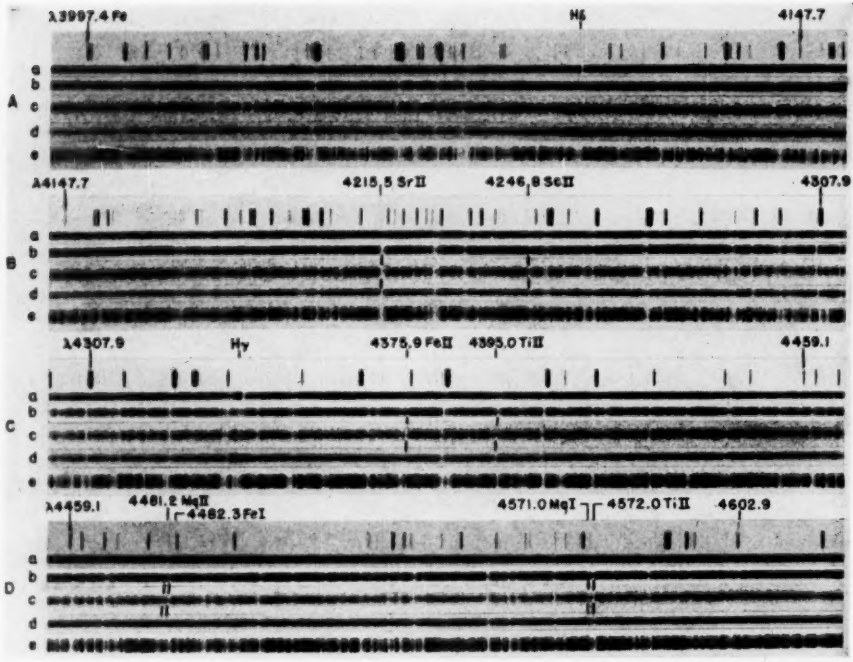

FIG. 1.—Spectrograms of W Vir and X Cyg

STAR	PLATE Ce	PHASE (P)		MAG.	VELOCITY (KM/SEC)
		From Max.	From Min.		
a W Vir	7102	+0.94	+0.34	9.5	−39 −93
b W Vir	7010	+ .40	− .20	9.7	−70
c W Vir	5110	+ .65	+ .05	10.5	−50
d W Vir	7091	+ .82	+ .22	9.9	−40
e X Cyg	5332	+0.68	+0.04	.....	.....

THE SPECTRUM

The following remarks will be clarified by Figure 1, which reproduces the spectrum of W Vir at four different representative phases and the spectrum of X Cygni at phase 0.68*P*. The latter was chosen for comparison because it is an ordinary cepheid with a period of 16.39 days, much like that of W Vir.

It is convenient to divide the spectrograms of W Vir into three groups: one group (E I), included in the phase interval 0.65*P*–0.95*P*, with spectrograms in which hydrogen has both emission and absorption lines and other elements have only single absorption lines; a second group (E II), included in the phase interval 0.95*P*–0.10*P*, with hydrogen having lines as in group E I but generally with at least some of the other elements showing double absorption components; and a third group (A), included in the phase interval .0*P*–0.60*P*, in which all elements, including hydrogen, have only single absorption lines.

Emission lines of hydrogen prevail in the phase interval from light-minimum to light-maximum and for an interval of 0.1*P* beyond, in which short interval W Vir is very little

TABLE 2

SPECTROGRAMS OF W VIRGINIS WITH DOUBLE ABSORPTION LINES

PLATE NO. Ce	PHASE (P)	ELEMENT AND RELATIVE INTENSITIES SHORTWARD TO LONGWARD COMPONENT RATIO, S:L		
		Sr II	*Ti* II	*Fe* I
7102	0.94	2:3	2:3	2:1
6207	.95	2:1	2:2	2:trace
6211	.00	3:1	2:0.5	2:0
5647	.00	1:2	1:3	1:2
5617	.04	1:1	1:1	1:1
5618	0.10	1:1	1:1	1:1

fainter than at maximum light (see Fig. 1). Each emission hydrogen line is divided into a strong shortward and a relatively weak longward part by a superposed absorption line. This difference in intensity of components increases markedly from minimum to maximum of light, so that finally the longward parts are scarcely visible.

The spectral class, as judged from the absorption lines, seems to range from about F2 at maximum to G6 at minimum of light.

Six of the eight spectrograms of group E II have a considerable number of double absorption lines; the two exceptions are Ce 5092 and Ce 5616. Even the strongest absorption lines of Ce 5092 have no resolved shortward components, but rudimentary shortward components may be evidenced by shortward wings of some of the strongest lines, as shown by microphotometer tracings. There may be a few of the strongest absorption lines of Ce 5616 with feeble shortward components, but these were unsuitable for measurement.

Table 2 gives the six spectrograms with double absorption lines in order of phase and the estimated ratio of the relative intensity of shortward (S) to longward (L) components for the three elements with the most prominent double lines. There seems to be no significant progression of the ratio S:L with phase. Double absorption lines are well shown on the reproduction of Ce 7102 (Fig. 1).

During the phase interval A, all lines of W Vir, those of hydrogen included, are in absorption only and are single. The spectrum changes in this interval from about F5 at the beginning to G6 at the end (light-minimum). Figure 1 shows that the spectrum of W Vir in the neighborhood of light-minimum is somewhat earlier than that of X Cyg near its light-minimum.

Attention is called to pairs of lines in the spectrum of W Vir (Fig. 1), each pair comprised of a line from an ionized element and one from a neutral element in the ground state. Three such pairs are shown in the accompanying tabulation. Their relative inten-

4395.0.....	*Ti* II	4375.9.....	*Fe* I
4481.2.....	*Mg* II	4482.2.....	*Fe* I
4572.0.....	*Ti* II	4571.1.....	*Mg* I

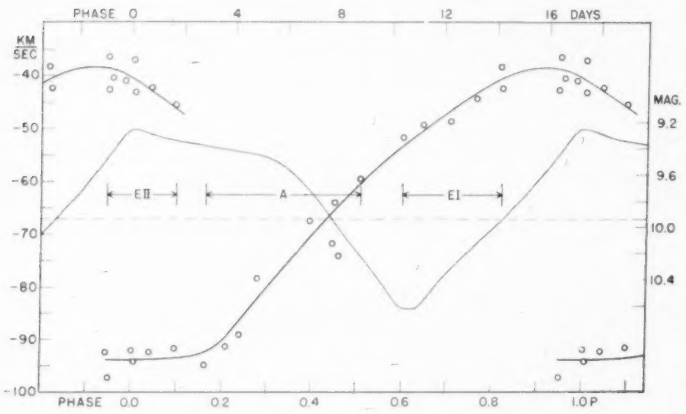

FIG. 2.—Circles are absorption-line velocities of W Vir. One complete velocity-curve is shown, together with the end of the preceding and the beginning of the following velocity cycle. Thin line is Gordon and Kron's light-curve; broken line is systemic velocity. Phase intervals *E* II, *A*, and *E* I are indicated.

sities undergo large changes; the ratios of neutral line intensities to ionized line intensities are largest at minimum light.

The strong line of *Sc* II at λ 4246.83 appears to be relatively less conspicuous in the spectrum of W Vir than in that of X Cyg. Other differences are apparent on inspection of Figure 1, but these need to be evaluated by spectrophotometry.

THE RADIAL VELOCITIES

All spectrograms in the phase interval E II except Ce 5092 and possibly Ce 5616 have at least some of their absorption lines double and hence give two radial velocities, as in the fourth column of Table 1. There is but one radial velocity for each spectrogram from absorption lines in phase intervals A and E I. The absorpion velocities and freehand curves through them are plotted in Figure 2. These velocities seem to be best represented by a curve beginning at phase $0.95P$ and continuing for an interval of $1.15P$. Thus there is an overlap of $0.15P$, during which the new cycle furnishes the shortward and the old cycle the longward components of the double lines. At the beginning of a velocity-curve

the velocity is nearly constant at −93.5 km/sec for 0.15*P*. At phase 0.10*P* the velocity starts to increase algebraically, until at phase 0.90*P* it reaches its maximum of −38.8 km/sec. There follows a drop to −46 km/sec at phase 0.10*P*.

In the phase interval 0.12*P*–0.82*P* the absorption lines are single and define a velocity-curve that changes from minimum to maximum. But in this phase interval there are two groups of velocities, each group derived from spectrograms in the same cycle. The first group is Ce 7010, 7013, and 7017 on three consecutive nights, and the second group is Ce 7080, 7085, 7091, and 7102, covering a 4-day interval. Each group shows a smooth progression of velocities within its cycle. On the other hand, the interval from 0.28*P* to 0.46*P* contains five spectrograms, no two of which belong in the same cycle, and their velocities show a considerable scatter. The consistency shown by velocities in the same cycle and the scatter of velocities from different cycles may indicate a velocity variation that changes in different cycles. It may also be inferred that cycles are not all alike in

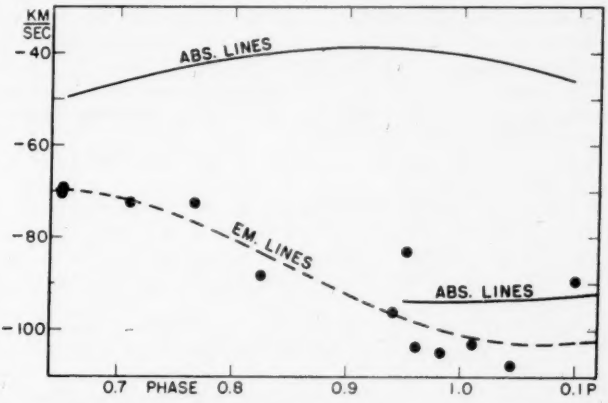

FIG. 3.—Hydrogen emission-line velocities plotted with solid circles and represented by a broken line. Solid line taken from absorption-line velocity-curve of Fig. 2.

radial-velocity changes from the fact that Ce 5092 and Ce 5616 have little evidence of double absorption lines, such as are shown by all other spectrograms in the interval E II.

The coudé spectrograms of W Vir have absorption-line radial velocities with a semi-amplitude of variation of 27.4 km/sec and a systemic velocity of −67 km/sec. Joy's values are −33.5 km/sec and −66 km/sec, respectively.

The hydrogen lines in the phase interval E I and E II are in both emission and absorption. The absorption lines give velocities which agree with the velocities from the absorption lines of the other elements if these lines are single, and with their longward components if they are double.

The superposed absorption components prevented satisfactory measures of the displacements of the hydrogen emission lines on the spectrograms themselves. However, microphotometer tracings which seemed fairly adequate for this purpose furnished the displacements from which the velocities in Table 1 were obtained. Although these velocities are liable to considerable error, they seem to give evidence of a variation, as brought out in Figure 3. The velocity trends downward from −70 km/sec at phase 0.65*P* to −100 km/sec at phase 0.95*P*, with little or no change thereafter until the disappearance of the emission lines at phase 0.10*P*. The average width of the emission hydrogen lines is at least 2.3 A.

DISCUSSION

The spectrum of W Vir is most interesting on account of the doubling of absorption lines near maximum light and the presence of emission lines of hydrogen for about half the light-cycle. The doubling of the absorption lines suggests that a violent outrush of gases from the atmosphere of W Vir starts before the gases of the preceding outburst have fallen completely back and disappeared. The lifetime of any given source of absorption seems to be somewhat ($0.15P$) greater than one cycle of light-change. In consequence, two masses of gas seem to coexist near maximum light, the one mass inrushing at its maximum rate and the other outrushing at its maximum rate.

Absorption-line velocities of W Vir and the relation of their changes to changes of light may be explained quantitatively by means of shock waves.[4] Such a shock wave is thought of as entering the reversing layer at its bottom and passing through its successive strata at the time when the reversing layer is falling in at its maximum velocity. This wave imparts a high outward velocity to successive strata, beginning at the bottom. That part of the reversing layer which has not been hit by the shock wave continues to rush rapidly inward. The Doppler effect separates the absorption lines of the inrushing from those of the outrushing gases. However, this would apparently require the relative intensities of the shortward to the longward components of the double lines to be weakest at the beginning and to grow stronger as the interval for double lines advances. This is not evidenced by the data in Table 2.

The mechanism for explaining the variations of light and velocity of W Vir must account for, or at least must not run counter to, the following: (*a*) emission lines of hydrogen are present from the time of light-minimum until $0.1P$ after maximum light; (*b*) the algebraic decrease of the velocities given by these emission lines to values not greatly different from those of the absorption lines at the beginning of a velocity cycle; (*c*) an absorption component of each hydrogen line always longward from the center of emission; and (*d*) an average emission-line width of 2.3 A.

The explanation of the emission lines of W Vir is not clear. If these lines are a product of the shock wave, it would seem that the emission lines begin in layers below the reversing layer, perhaps after the shock wave has passed by this lower level. If such a mechanism is present, it might account for the continuance of the emission lines until the shock wave has completely traversed the reversing layer.

This paper is intended primarily as a record of the radial-velocity behavior of W Vir. This has served to show that this variable star is of such exceptional interest that it merits further study of its radial velocities, as well as careful spectrophotometric consideration, before an attempt is made to provide a picture of a mechanism to explain its variations of spectrum, velocity, and light.

[4] M. Schwarzschild, *Harvard Circ.*, Nos. 429 and 431, 1938.

THE PREMINIMUM SPECTRUM OF R LEONIS

PAUL W. MERRILL
MOUNT WILSON AND PALOMAR OBSERVATORIES
CARNEGIE INSTITUTION OF WASHINGTON
CALIFORNIA INSTITUTE OF TECHNOLOGY
Received April 10, 1952

ABSTRACT

This article is based mainly on six spectrograms, dispersion 9 A/mm, taken with the 200-inch telescope, fairly well distributed over the interval from maximum light to minimum.

Various groups of bright lines have characteristic phases of greatest intensity. Lines of [*Fe* II] appear strongest at minimum and may possibly be emitted at constant brightness throughout the cycle. The behavior of the anomalous displaced bright lines of *Ca* II is described in detail. A curious fact is that the bright portion of H λ 3968 is stronger than the corresponding feature of K λ 3933. Somewhat similar asymmetrical emission occurs at *Ca* I λ 4227. Emission in the *Al* I lines λ 3944 and λ 3961 is less displaced.

The radial velocity from the dark lines changes little near maximum, but toward minimum it is slightly lower. Slight changes in the velocities from bright lines continue the trends previously observed after maximum. Lines of *H* and *Fe* II show slight acceleration outward from the star, while lines of neutral metals have accelerations in the opposite direction.

During the time of declining light, the changing intensities of certain features of the absorption spectra of Me variable stars indicate that the temperature of the reversing layer is regularly decreasing. The spectacular emission lines, however, show striking changes in intensity which bear no simple relation to the temperature of the reversing layer. The spectra of R Leonis[1, 2] and of R Hydrae[3] have previously been studied in detail for the first three or four months after maximum light, and numerous bright lines in the spectrum of χ Cygni[4] have been followed for about five months after maximum. A. H. Joy has nearly ready for publication a study of *o* Ceti in which the spectrum of the red star is followed until that of the blue companion interferes. Near minimum light very few observations[5] have been made except with low dispersion.[6, 7]

The present article describes spectrograms of R Leonis 094211 taken mainly with the 200-inch telescope, distributed fairly well over the whole interval from maximum light to minimum. The period of the variable is 313 days; magnitude range, 5.0–10.5; spectral type at maximum, M8e. The spectroscopic behavior is typical of advanced Me variables.

The recent spectrograms are listed in Table 1. The plates taken with the 100-inch telescope, dispersion 10 A/mm, are marked "Ce"; those with the 200-inch are marked "Pc," 9 A/mm, or "Pd," 18 A/mm. I am indebted to I. S. Bowen and O. C. Wilson for the 200-inch plates, most of which had long exposures, one extending over two nights. Dates of the 200-inch plates are shown on the light-curve in Figure 1.

The changing intensities of several of the more important groups of bright lines are summarized in Table 2. These estimates, in arbitrary units, reflect the line intensities with respect to the continuous spectrum on each plate; no account was taken of the

[1] P. W. Merrill, *Mt. W. Contr.*, No. 720; *Ap. J.*, **103**, 275, 1946.

[2] P. W. Merrill, *Mt. W. Contr.*, No. 743; *Ap. J.*, **107**, 303, 1948.

[3] P. W. Merrill, *Mt. W. Contr.*, No. 717; *Ap. J.*, **103**, 6, 1946.

[4] P. W. Merrill, *Mt. W. Contr.*, No. 735; *Ap. J.*, **106**, 274, 1947.

[5] R Hydrae, P. W. Merrill, *Ap. J.*, **116**, 18, 1952.

[6] Mira Ceti, A. H. Joy, *Mt. W. Contr.*, No. 311; *Ap. J.*, **63**, 281, 1926.

[7] Several stars: P. W. Merrill, *Mt. W. Contr.*, No. 539; *Ap. J.*, **83**, 272, 1936.

TABLE 1

SPECTROGRAMS OF R LEONIS

Plate	Date	Obs.	Exposure (Min.)	Seeing	Vis. Mag.*	Phase (Days)	Cont. Spect.
Ce 3316	1943 Dec. 12	P. W. M.	180	3	6.6	− 18	Strong
Ce 6091	1950 Jan. 5	P. W. M.	130	3	5.6	+ 15	V. strong
Ce 6161	Feb. 22	P. W. M.	126	4–3	7.1	+ 64	Med.
Pc 35	Nov. 28	I. S. B.	95	2–4	6.4	+ 31	Strong
Pc 40	Dec. 22	O. C. W.	180	2–0	6.9	+ 55	Strong
Pc 47	1951 Jan. 19	I. S. B.	360	1–3	7.5	+ 83	Strong
Ce 6883	Feb. 24	P. W. M.	100	3	8.6	+119	Weak
Pc 62	25	I. S. B.	270	2–3	8.6	+120	Med.
Pc 66	Mar. 21, 22	I. S. B.	860	2–4	9.2	+144	Strong
Ce 6960	27	P. W. M.	206	2–0	9.4	+150	V. weak
Pc 88	Apr. 21	O. C. W.	360	2–4	9.9	+175	Weak
Pd 96†	May 20	I. S. B.	200	1–4	9.6	+204	Med.

* To obtain magnitude in the blue-violet, add color index of about 1.8.

† Dispersion 18 A/mm; definition poor; measurements not reliable. Dispersion of all other plates 9 or 10 A/mm.

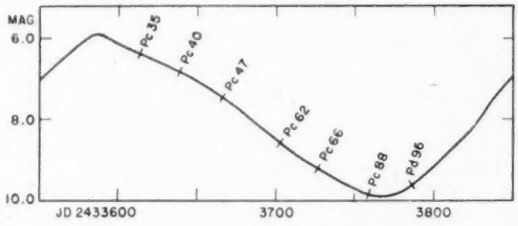

FIG. 1.—Light-curve of R Leonis showing dates of spectrograms

TABLE 2

INTENSITIES OF BRIGHT LINES

PLATE	MAG.	PHASE (DAYS)	*H*	*Fe* I	*Mg* I		*Si* I	*Sc* I	*Ga* I	*Fe* II	[*Fe* II]
					U.V.	λ 4571					
Pc 35	6.4	+ 31	30	2	5	Tr	7	1	0	2	0
40	6.9	+ 55	35	4	5	2	7	2	0	2	0
47	7.5	+ 83	20	9	5	8	7	3	Tr	2	0
62	8.6	+120	6	12	5	16	2	Tr	2	3	1
66	9.2	+144	3	10	5	20	Tr	0	3	3	3
88	9.9	+175	2	10	5	25	Tr	0	Tr	3	6
Pd 96*	9.6	+204	Tr	7	?	25	0	0	?	3	6
Approx. phase of greatest intensity	.....	.....	+50	+120	.....	(+180)	+50	+80	+140	.....	+200

* Low dispersion; estimates not reliable.

changing magnitude of the star. The behavior indicated in the first part of the table is similar to that previously observed in several variables.

The last Pc plate, dispersion 9 A/mm, was taken only 5 days before minimum light. Although the continuous spectrum is weak, estimates of intensities of the bright lines are approximately comparable with those on previous plates. Unfortunately, this is not true of the last plate, Pd 96, taken 24 days after minimum; the continuous spectrum is well exposed, but the dispersion is only 18 A/mm and the definition is imperfect. Nevertheless, the estimates on this plate, although of low accuracy, give some idea of the behavior at this otherwise unobserved phase.

The hydrogen lines are strongest at phase about +50 days. They weaken rapidly after +80 days until at minimum they are scarcely visible; during this interval they become relatively narrow, and the series tends to assume the normal Balmer decrement. When the lines reappear as the light increases after minimum, the relative intensities are highly abnormal.

Lines of *Si* I λ 3905 and λ 4103 are strong at maximum and remain without much change for about 3 months, then fade rapidly. Lines of *Fe* I are weak at maximum light; they increase in strength until about phase +120 days, after which they decrease slowly, the strongest remaining visible even at minimum light. Weaker lines of *Sc* I λ 3907.48 and of *Ca* I λ 4172.05 appear for rather short intervals, coming to greatest strength at about phase +80 and +140 days, respectively. Appearing a few weeks after maximum, λ 4571 *Mg* I strengthens slowly for 4 or 5 months, then remains outstanding through minimum. The behavior of the ultraviolet *Mg* I lines λλ 3829, 3832, and 3838 is entirely different; these lines retain nearly the same intensity throughout the whole interval from maximum to minimum light.

The lines of *Fe* II also change but little, becoming slightly more prominent as the star fades. The five strongest lines of multiplet (1) of *Fe* II between λ 3255 and λ 3303 are seen in the fourth order on the strongly exposed plate Pc 66 superposed on the third-order spectrum near λ 4370. The weaker of these lines are recognizable only because they are offset slightly, the tips of the lines being seen at one edge of the strong third-order spectrum. The displacement occurred at the slit; it was due to the dispersion of the star's light by the earth's atmosphere, an effect usually considered a nuisance in astronomy but which is sometimes helpful in stellar spectroscopy. A more complete investigation of the ultraviolet lines of *Fe* II in the spectra of variables[4] and other objects[8] is desirable.

Lines of [*Fe* II] are absent near maximum but become well marked toward minimum. This behavior is probably characteristic of Me variables. These forbidden lines may possibly remain of constant brightness while the star fades. Such behavior would be comparable to that of certain forbidden lines in the spectrum of R Aquarii, which seem to be emitted quite independently of variations in the brightness of the red variable. This is all the more remarkable because forbidden lines require low density and a large volume for their production. The [*Fe* II] lines in the spectrum of R Leonis obviously deserve careful photometric observation.

A large number of additional bright lines, many of them unidentified, were measured on plate Pc 66 and especially on Pc 88. Nearly all are included in the list previously published[4] for χ Cygni for phase +162 days. As in χ Cygni, λ 3735.3 becomes very strong, remaining visible on plate Pd 96.

The anomalous displaced emission lines connected with H and K of *Ca* II are well shown in the present series of plates. Their curious behavior is brought out by the tracings in Figure 2 and by the measurements in Table 3. These bright lines remain visible on plate Pd 96, where their displacement is about the same as on Pc 88. The striking asymmetry may possibly be due to a circulation of calcium atoms in the star's extensive atmosphere, the rising atoms emitting strongly, while the cooler descending atoms, mostly

[8] G. Herzberg, *Ap. J.*, **107**, 94, 1948.

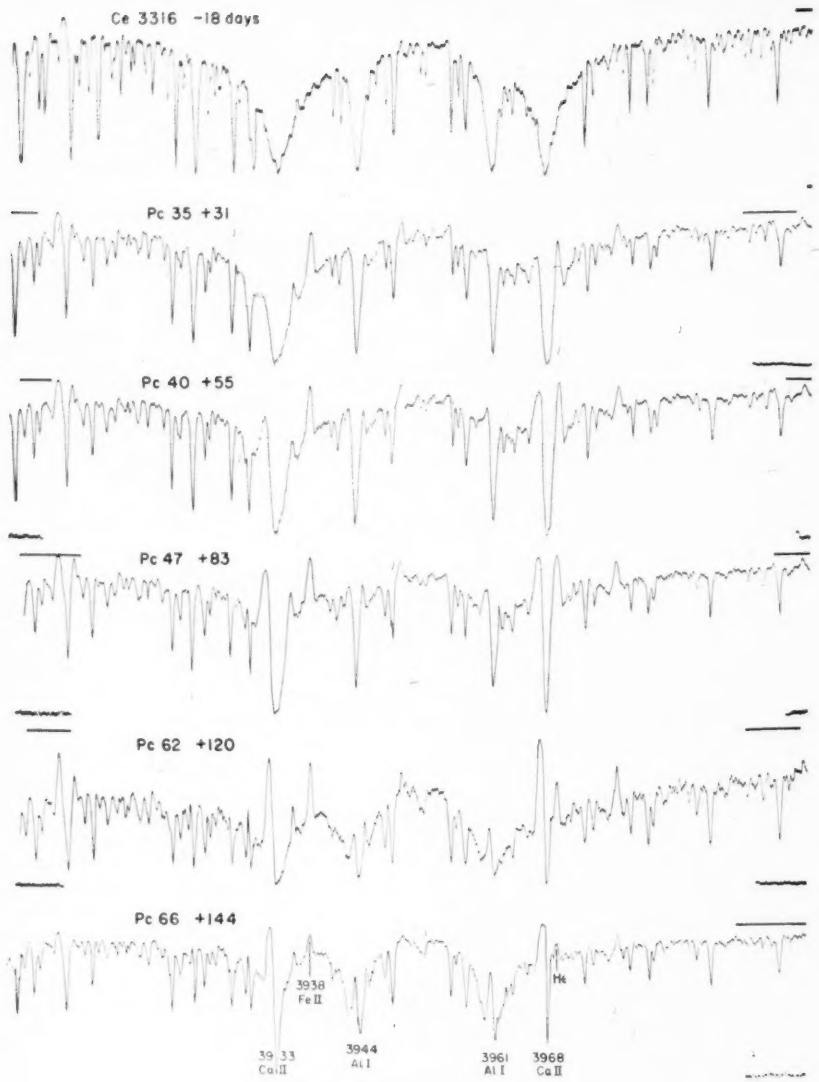

FIG. 2.—Tracings of the region of H and K of *Ca* II in the spectrum of R Leonis

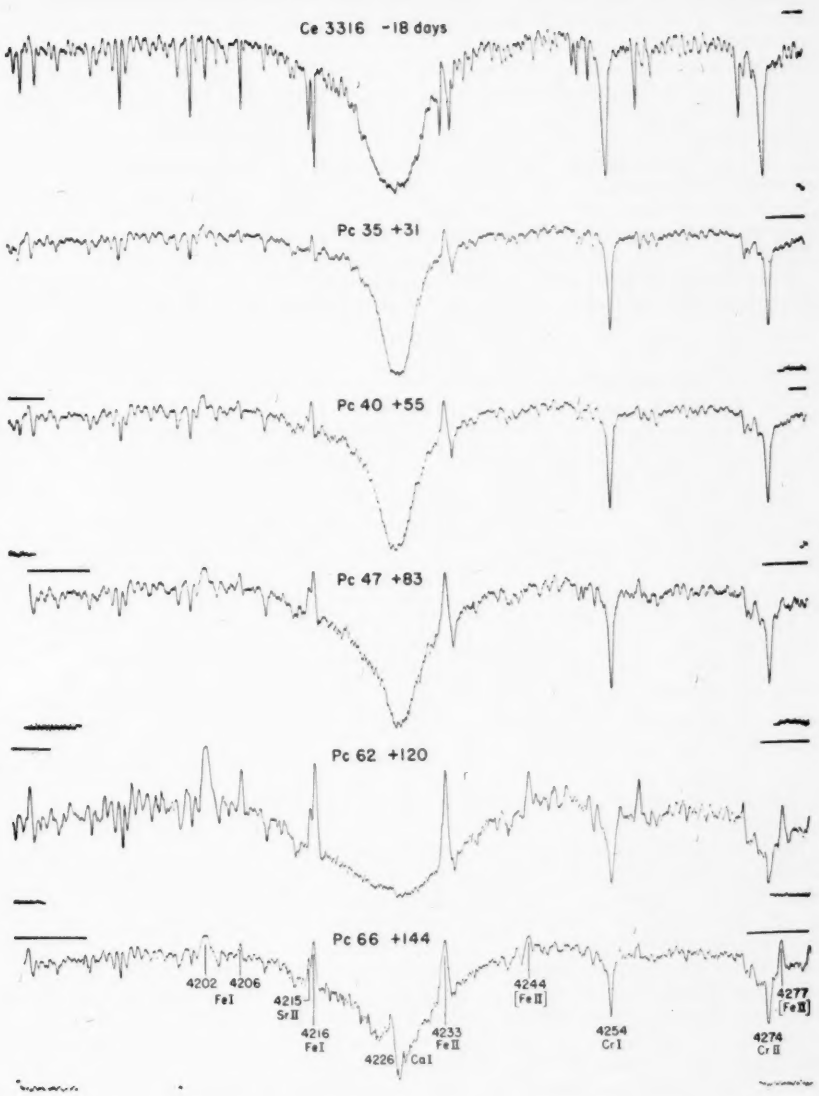

FIG. 3.—Tracings of the region of λ4226 of *Ca* I in the spectrum of R Leonis

in the ground level, are the more powerful absorbers. The largest negative velocities are measured from the emission lines at the earliest phases. As the phase advances, the "center of gravity" of the emission has a smaller negative displacement; this may represent a slowing-down of atoms ejected radially outward. The velocities in Table 3 are those directly measured without any corrections, except for the orbital motion of the earth; to make them comparable with velocities in previous tabulations of R Leonis[1] and R Hydrae,[3] a correction of −11 km/sec should be added. Actually, all three sets of data agree fairly closely, showing that the displacements and their changes are recurrent phenomena characteristic of Me variables. The circumstance, well established by observation of several stars, that the bright portion of H λ 3968 is regularly stronger than the corresponding feature of K λ 3933 is difficult to explain. Comparable observations of the infrared *Ca* II lines λλ 8498, 8542, and 8662 might throw light on the matter.

Asymmetrical emission within the broad absorption *Ca* I line λ 4227, weaker than that of H and K but otherwise rather similar, is shown clearly on plate Pc 66 (see Fig. 3).

TABLE 3

RADIAL VELOCITIES MEASURED FROM LINES OF *Ca* II AND *Al* I
(KM/SEC)

PLATE	PHASE (DAYS)	*Ca* II EM.		*Al* I EM.		*Al* I ABS.	
		λ 3933	λ 3968	λ 3944	λ 3961	λ 3944	λ 3961
Ce 3316	− 18	.....	.....	.....	.....	+ 9	+ 8
Ce 6091	+ 15	.....	.....	.....	.....	+13	+10
Ce 6161	+ 64	.....	−77	.....	.....	.....	.....
Pc 35	+ 31	.....	−90	.....	.....	+13	+11
Pc 40	+ 55	−87	−71	.....	.....	+10	+12
Pc 47	+ 83	−70	−49	−35	−38	+17	+18
Ce 6883	+119	−52	−38	.....	.....	.....	.....
Pc 62	+120	−47	−34	−16	−12	+31	+28
Pc 66	+144	−37	−33	− 7	− 8	+37	+34
Pc 88	+175	−33	−25	.....	.....	.....	.....

The effect, so far as I know not previously observed in this line, obviously parallels that at H and K.

Weak displaced emission seems to develop also in the great *Al* I lines λ 3944 and λ 3961, but it is more nearly central than in the *Ca* lines (see Fig. 2 and Table 3).

The radial velocities measured from various groups of lines are recorded in Table 4 and are summarized in Table 5. Near maximum light the velocity from the absorption lines changes very little; toward minimum there appears a slight tendency toward lower velocities. A velocity of −2 km/sec was obtained on the low-dispersion plate Pd 96, but it is feared that this result is unreliable. More observations near minimum are needed. In general, it appears that differences in velocity from one cycle to another may be as large as the changes within any one cycle. Thus the hypothesis of volume pulsation finds little support in the measured displacements of the dark lines. In view of the long period, a pulsation of moderate velocity amplitude is, of course, not precluded.

Similarly, measurements of the bright lines can scarcely be used as evidence of pulsation. In general, the slight changes in velocity recorded in Tables 4 and 5 show a continuation of the trends indicated at earlier phases by previous observations with high dispersion.[1] Various lines behave differently. Lines of *Fe* I show a decided correlation with excitation potential, those of higher excitation potential having algebraically greater velocities. A similar correlation was found previously among the absorption lines of

various elements. Bright lines of *Fe* II regularly yield a velocity intermediate between the dark-line velocity and that from the *H* lines. With advancing phase, lines of *H* and of *Fe* II appear to show slight accelerations outward from the star, while lines of neutral metals have accelerations in the opposite direction. Some of these differential effects might arise if electric or magnetic forces were involved in the motions.

TABLE 4

RADIAL VELOCITIES DERIVED FROM VARIOUS GROUPS OF LINES (KM/SEC)

PLATE	PHASE (DAYS FROM MAX.)	ABS.		EMISSION LINES									
				H		*Fe* I		*Mg* I		*Fe* II		[*Fe* II]	
		Vel.	No.	Vel.	No.	Vel.	No.	Vel.	No.	Vel.	No.	Vel.	No.
Ce 3316	− 18	+11.5	135	+3.2	2	.....	.....	.....	.....	.....	.....	.....	.....
Ce 6091	+ 15	+12.2	38	.....	.....	.....	.....	.....	.....	.....	.....	.....	.....
Ce 6161	+ 64	+12.0	26	−1.1	17	−0.7	31	−3	3	+2	5	.....	.....
Pc 35	+ 31	+11.2	60	−3.1	7	−6.1	5	−6	3	+5	2	.....	.....
Pc 40	+ 55	+11.1	61	−4.0	12	−5.8	9	−7	4	+2	3	.....	.....
Pc 47	+ 83	+12.4	46	−2.6	10	−0.6	22	−6	4	+2	5	.....	.....
Ce 6883	+119	+ 7.6	18	−2.4	11	+0.3	19	−2	4	+1	6	+2	7
Pc 62	+120	+10.8	27	−2.9	5	+2.5	24	0	4	+3	13	+5	9
Pc 66	+144	+ 7.3	18	−8.	1	−2.2	25	−6	4	−2	18	−1	12
Ce 6960	+150	.....	.....	.....	.....	0.	4	−4	1	−5	1	−3	2
Pc 88	+175	+ 6.9	24	0.	1	−1.8	13	−2	4	0	9	+1	16

TABLE 5

RADIAL-VELOCITY SUMMARY (KM/SEC)

LINES	PHASE (DAYS)			LINES	PHASE (DAYS)		
	< +100	> +100	All		< +100	> +100	All
Absorption	+11.8	+8.2	+10.2	*Si* I	− 1.2	+5.4	+ 1.0
Emission	.....	.....	.....	*Sc* I	− 1.0	+5.2	+ 1.0
H	− 2.7	−3.3	− 3.0	*Sr* II	− 1.6	−1.1	− 1.3
Fe I	− 3.3	−0.2	− 1.6	*Fe* II	+ 1.7	+0.3	+ 1.0
Mg I	− 5.5	−2.8	− 4.0	[*Fe* II]	.....	+0.8	+ 0.8

The closely similar behavior in various Me spectra of many complicated details is remarkable. In these stars it appears that long series of involved spectroscopic phenomena naturally follow some recurring disturbance originating, probably, below the photosphere.

The recent spectrograms show that under favorable circumstances the 200-inch telescope could follow the spectrum of R Leonis with dispersion of 9 A/mm right through minimum light. It remains important to obtain more extensive data at this phase.

MEASUREMENTS IN THE SPECTRA OF FOUR LONG-PERIOD VARIABLE STARS OF CLASS Me

PAUL W. MERRILL
MOUNT WILSON AND PALOMAR OBSERVATORIES
CARNEGIE INSTITUTION OF WASHINGTON
CALIFORNIA INSTITUTE OF TECHNOLOGY
Received May 16, 1952

ABSTRACT

This paper describes short series of spectrograms, dispersion 9 A/mm, taken with the 200-inch telescope, of the following long-period Me variables: T Cas, R LMi, W Hya, and T Cep. Radial velocities from both bright and dark lines at various phases and intensities of several groups of bright lines are recorded. With minor variations, the behavior of the bright lines, including the displaced *Ca* II lines, in all four stars conforms to the complex pattern previously observed in o Ceti and R Leonis. The forces involved, possibly in part electric or magnetic, must be highly specialized. The radial velocities are in good agreement with those determined for the same stars many years ago.

The remarkable cyclical changes in the spectra of long-period variable stars are fairly well known, but further observation is needed to ascertain the nature and extent of variations in the pattern from star to star and from cycle to cycle in the same star. These variations may perhaps be compared to those of the weather from year to year. Observations with high dispersion, 10 A/mm, of only seven or eight Me variables have as yet been published and most of these have been limited to phases near maximum light. Hence it may be worth while to record data derived from short series of spectrograms of the four variables listed in Table 1.

Nearly all the spectrograms used in this study (Table 2) were obtained with the 200-inch telescope by I. S. Bowen and O. C. Wilson, to whom I am much indebted for this valuable material. The dispersion, in the third order of a plane grating ruled by H. W. Babcock, is 9.1 A/mm. On some of the plates, wave lengths from about 3700 A to 4050 A are measurable also in the fourth order, dispersion 6.8 A/mm.

The photometric data for R Cas, R LMi, and T Cep in Table 2 were kindly supplied by Mrs. Margaret W. Mayall, of the Harvard College Observatory. Data for W Hya were supplied through the courtesy of Mr. Frank M. Bateson, of the Royal New Zealand Astronomical Society.

Radial velocities derived from the dark lines and from several of the more important groups of bright lines are in Table 2. Estimated intensities of various groups of bright lines are in Table 3.

T Cassiopeiae.—The *TiO* bands and the low-temperature lines of *K* I, *Ca* I, and *Cr* I are strong, indicating an advanced spectral type, M8e, but the bright lines in general are not so intense as in some other variables. With the exception of λ 3852, the bright lines of *Fe* I appear decidedly weaker (and less numerous) than normal; possibly they become stronger later in the cycle.

R Leonis Minoris.—The absorption spectrum is one of the most advanced M-type spectra yet observed, and the bright lines are unusually intense. Note the differences in the relative intensities of certain bright lines on the first two plates taken at nearly the same phase in successive cycles. The low dark-line velocity on plate Ce 5525 at phase +145 days, about 85 days before minimum, requires confirmation; it differs greatly from the result yielded by the stronger plate Pc 48, phase +104 days.

TABLE 1

DATA CONCERNING FOUR LONG-PERIOD VARIABLE STARS

Star	Desig.	Mag. Range	Period (Days)	Spectrum at Max.
T Cas	001755	8–12	445	M8e
R LMi	093934	7–13	372	M8e
W Hya	134327	7–10	386	M8e
T Cep	210868	6–11	388	M7e

TABLE 2

JOURNAL OF OBSERVATIONS

Plate	Obs.	Date 1951	Exp. Min.	See-ing	Vis. Mag.*	Phase (Days)	Cont. Spect.	Radial Vel. (Km/Sec) Abs.	No.	*H*	*Mg*	*Fe* II	*Fe* [II]
						T Cassiopeiae							
Pc 147	I.S.B.	Aug. 21	270	2–4	8.2	+ 38	Med.	−12.1	55	−24	−27	−15	.....
Pc 155	I.S.B.	Sept. 16	310	2–4	8.8	+ 64	Med.	−12.3	56	−23	−27	−14	.....
Pc 195	I.S.B.	Oct. 17	306	1–2	9.7	+ 95	Weak	−15.6	17	−30	−24	−15	−19
						R Leonis Minoris							
Ce 5525	P.W.M.	Feb. 5†	350	4–2	10.6	+145	Weak	− 0.6	11	− 5	− 7	− 2	− 3
Ce 6156	P.W.M.	Feb. 21‡	300	2–1	11.6	+144	V. weak	.....	...	− 3	− 3	− 1	.....
Pc 34	I.S.B.	Nov. 28‡	285	5–3	9.4	+ 51	Med.	+ 8.5	28	− 5	− 8	+ 3	.....
Pc 42	O.C.W.	Dec. 23‡	425	0–3	10.1	+ 76	Strong	+ 7.9	28	− 5	− 6	0	.....
Pc 48	I.S.B.	Jan. 20	630	2–4	10.8	+104	Strong	+ 9.0	50	− 5	− 4	0	.....
						W Hydrae							
Pc 61	I.S.B.	Feb. 24	345	2–3	8.4	+121	Weak	+40.0	15	+27	+35	+35	+39
Pc 71	I.S.B.	Mar. 24	440	1–3	9.4	+180	Weak	+36.7	28	+24	+34	+30	+31
Pc 87	O.C.W.	Apr. 20	240	2–4	9.7	+207	Weak	.....	...	.....	+28	....	(+18)
Pc 104	I.S.B.	May 24	275	1–3	(9.7)	+241	Weak	+38.4	19	.....	+29	.....	.....
						T Cephei							
Pc 105	I.S.B.	May 24	90	2–3	6.4	− 36	Strong	−10.8	82	−24	−28	−13	.....
Pc 138	I.S.B.	Aug. 9	90	2–3	7.3	+ 51	Strong	−14.0	19	−24	−27	−18	.....
Pc 160	O.C.W.	Sept. 21	210	2–4	8.6	+ 84	Strong	−15.4	44	−25	−28	−21	−18
Pc 194	I.S.B.	Oct. 17	300	2–4	9.3	+110	V. strong	−17.6	45	−27	−27	−21	−21

* To obtain magnitude in the blue-violet, add color index of about 1.8.

† 1949.

‡ 1950.

TABLE 3

INTENSITIES OF BRIGHT LINES

Star Plate	Vis. Mag.	Phase (Days)	*H*	*Fe* I	*Mg* I		*Si* I	*Fe* II	[*Fe* II]
					U.V.	λ 4571			
T Cas:									
Pc 147	8.2	+ 38	15	3	2	2	2	1	0
Pc 155	8.8	+ 64	12	5	2	5	2	1	0
Pc 195	9.7	+ 95	5	6	?	6	2	1	1
R LMi:									
Ce 5525	10.6	+145	5	10	5	20	2	3	4
Ce 6156	11.6	+144	2	4	5	5	5	2	0
Pc 34	9.4	+ 51	25	2	5	0	7	2	0
Pc 42	10.1	+ 76	25	5	5	2	7	2	0
Pc 48	10.8	+104	20	8	5–6	7	7	2	0
W Hya:									
Pc 61	8.4	+121	6	8	?	12	3	2	tr
Pc 71	9.4	+180	3	8	?	15	2	2	1
Pc 87	9.7	+207	0	3	?	7	(1)	tr	1
Pc 104	(9.7)	+241	0	1	?	3	(0)	(0)	(0)
T Cep:									
Pc 105	6.4	− 36	20	2	2	0	4	2	0
Pc 138	7.3	+ 51	20	5	3	3	4	3	0
Pc 160	8.6	+ 84	15	10	4	12	3	4	1
Pc 194	9.3	+110	6	12	4	25	2	3	2

TABLE 4

DISPLACEMENTS OF BRIGHT LINES OF *Ca* II (IN KM/SEC)*

Star	Plate	Phase (Days)	λ 3933	λ 3968
T Cas	Pc 147	+ 38	.....	−85
	Pc 155	+ 64	− 97	−74
R LMi	Ce 5525	+145	− 57	−48
	Ce 6156	+144	.....	(−48)
	Pc 48	+104	− 87	−72
W Hya	Pc 61	+121	− 48	−45
	Pc 71	+180	− 51	−37
T Cep	Pc 138	+ 51	−106	−89
	Pc 160	+ 84	− 78	−60
	Pc 194	+110	− 58	−47

* Referred to absorption-line velocities (see Table 2).

W Hydrae.—The absorption spectrum is an advanced one, and the bright lines on the first two plates are moderately strong for the phases at which the plates were taken. The incomplete light-curve available to me indicates that the last plate, Pc 104, was taken about at minimum light. The intensity of the bright line *Mg* I λ 4571 at this phase is unexpectedly low; perhaps the maximum intensity of this line comes earlier in the cycle than in most Me variables. One-prism spectrograms obtained in the 1920's appear to bear out this suggestion. The amplitude of the mean light-curve is decidedly less than normal for the period and spectral type.

T Cephei.—The type is almost as advanced as that of the other stars, and the bright lines are very intense. The dark-line velocity seems to become algebraically less by a few kilometers per second as the phase advances, but the velocities from the bright lines show little change.

With minor variations, the behavior of the bright lines in all four stars conforms to the pattern previously observed in *o* Ceti, R Leonis, and other Me variables.

The general behavior of the anomalous bright lines of *Ca* II resembles that of these lines in the spectra of R Leonis and R Hydrae, and the displacements (Table 4) are much the same at corresponding phases. In attempts at physical interpretation of these variables, the emphasis would seem to belong on conformity rather than on individual variation. It is clear that a well-defined spectroscopic pattern, with all its bizarre and complicated sequences, is set going by the same forces that produce the typical variations in total brightness. These forces are probably highly specialized because the characteristic spectroscopic phenomena are limited so closely to red variables with long periods and large changes in light.

The radial velocities are in good agreement with those determined with low dispersion for these same stars many years ago,[1] thus raising a strong presumption that there are no secular variations in velocity.

Some of the differential effects in the velocities derived from the bright lines which in R Leonis[2] seemed to point to the action of electric or magnetic forces are clearly present in the data for the stars discussed in this paper. For example, on almost every plate the velocity derived from the bright lines of *Fe* II is intermediate between the dark-line velocity and that derived from the bright lines of hydrogen. In all four stars the high-excitation bright lines of *Fe* I yield algebraically greater velocities than the low-excitation lines.

For future work on the spectra of long-period variables at their fainter phases, the following stars might be strategic: R Leo, R Cas, T Cep, χ Cyg, R And, and R Cyg.

[1] P. W. Merrill, *Pub. Astr. Obs. U. Michigan*, **2**, 45, 1916; *Mt. W. Contr.*, No. 264; *Ap. J.*, **58**, 215, 1923; *Mt. W. Contr.*, No. 649; *Ap. J.*, **94**, 171, 1941.

[2] P. W. Merrill, *Ap. J.*, **116**, 337, 1952; *Mt. W. and P. Reprint*, No. 72.

THE CEPHEID VARIABLE S SAGITTAE

I. THE RADIAL-VELOCITY VARIATION*

G. H. HERBIG AND J. H. MOORE†
Lick Observatory, University of California
Received April 28, 1952

ABSTRACT

A study of the radial velocity of the cepheid variable S Sagittae, as determined from 95 Michigan one-prism and 121 Lick three-prism spectrograms, has confirmed the earlier result of Aldrich that the normal velocity of the cepheid pulsation undergoes a cyclic variation with a period of 1.8 years. The resolution of the observed radial velocity into its two components has resulted in accurate radial velocity-curves for both. There is some evidence that the short-period velocity-curve undergoes a periodic displacement during the long-period cycle, but the effect is marginal, and its reality is open to question. Mount Wilson coudé plates of S Sagittae were studied spectrophotometrically in the ultraviolet in an attempt to detect traces of an early-type companion star. No evidence of such a companion was found. A lower limit could be placed on the magnitude difference between the cepheid (at minimum light) and an early-type companion: at λ 3780, $\Delta m \geq 2.4$ mag. At λ 4500, it is estimated that $\Delta m > 1.5$ mag., if the companion is of late type. Pulsation seems to be ruled out as the agent responsible for the long-period velocity variation, and it is concluded that the available evidence favors an interpretation in terms of simple binary motion. Inferences can be made as to the magnitude and spectral type of the companion if it is a normal star and obeys the mass-luminosity relationship and if the cepheid obeys the mass-luminosity and period-luminosity relations: the companion star must be a giant of spectral type G or later, with $M_{vs} > +0.2$. The departures of S Sagittae from the color range versus period, light-range versus period, and velocity range versus light-range relationships defined by other cepheids are apparently characteristic of the star itself, for they are not due to the contribution of the companion to the total light of the system.

I. INTRODUCTION

The first observations with a slit spectrograph of the bright cepheid variable S Sagittae were made by R. H. Curtiss[1] in 1903 and 1904 at the Lick Observatory. He obtained seven spectrograms with a one-prism spectrograph and a 16-inch camera attached to the 36-inch refractor; this instrument produced a dispersion of 57 A/mm at $H\gamma$. Curtiss' observations demonstrated the variation of radial velocity now known to accompany the 8-day period of the cepheid variation. In 1906 J. D. Maddrill obtained thirty-two additional spectrograms with the same equipment. The velocities from Maddrill's plates were later discussed by J. Hellerich,[2] who discovered that the systemic velocity of the 8-day variation is not constant but is subject to a slow variation. Hellerich represented the γ-velocity by a constant plus a linear term in the time. It might be mentioned here that the slope of the long-period variation, determined by Hellerich from this limited amount of material of low precision, is in good agreement with that predicted for the epoch of those observations by the accurate elements derived later in this paper.

An extensive investigation by J. A. Aldrich,[3] based on 124 Michigan one-prism plates (dispersion 40 A/mm at $H\gamma$) obtained in 1913–1923, served to separate the short-period

* *Contributions from the Lick Observatory*, Ser. II, No. 41.

† At the time of his death on March 15, 1949, Dr. Moore had carried his study of the radial velocity of S Sagittae to the point where preliminary curves were available for the two components of the velocity variation. Except for these results, the computations upon which they were based, and the velocities themselves, Dr. Moore left no notes or manuscript on the subject. In order to carry this work onward, all this material was re-examined and checked by Dr. Herbig, who is responsible also for the detailed discussion of the velocities, the obtaining and tracing of the coudé plates, the writing of the text, and the conclusions drawn therein.—C. D. SHANE.

[1] *Ap. J.*, **20**, 231, 1904; *Lick Obs. Bull.*, **3** (No. 62), 40, 1904.

[2] *A.N.*, **210**, 65, 1919.

[3] *Pop. Astr.*, **32**, 218, 1924; *Pub. Obs. U. Mich.*, **4**, 75, 1932.

(cepheid) velocity variation from the long-period cycle and resulted in the following orbital elements for the latter:

$P = 682$ days, $\omega = 195°25'$,
$K = 14.6$ km/sec, $T = \text{JD } 2420279.0$,
$\gamma = -12.3$ km/sec,[4] $a \sin i = 136.4 \times 10^6$ km,
$e = 0.165$, $f(m) = 0.218 m_\odot$.

A series of fifty-one spectrograms obtained at the Lick Observatory with the Mills three-prism spectrograph (dispersion 11 A/mm at λ 4500) in 1921–1927 was discussed by T. S. Jacobsen;[5] he improved the short-period velocity-curve by empirically removing the long-period change in the γ-axis. In 1938, 1939, 1940, 1947, and 1948 the Mills spectrograph was used by and under the direction of J. H. Moore to obtain seventy-six additional plates of S Sagittae. It is the purpose of this paper to discuss the new material, to combine it with earlier observations in order to derive definitive information on both the short- and the long-period velocity variations, and to describe spectrophotometric measurements of Mount Wilson coudé plates made with the aim of detecting the presence of a second star.

II. THE RADIAL VELOCITIES

The plates of S Sagittae taken in 1938–1948 with the Mills spectrograph were superior in quality to the earlier series, in that the availability of faster emulsions and (in 1947–1948) of coated optics permitted the use of a narrower slit and shorter exposures. The slit-width, projected on the plate, of the 1921–1927 series was 38μ, which was reduced to 28μ in 1938–1940 and to 19μ in 1947–1948. The dependence on slit-width of the flexure correction, due to the departure from collimation caused by flexure in the telescope tube, was taken into account in the reductions. The shorter exposures improved the quality of the velocities, since there was, proportionately, less opportunity for temperature variation in the spectrograph during the exposure.[6] The plates were measured in a Hartmann spectrocomparator against a standard spectrogram of the sky; the 1939 series was measured by Miss Doris Roosen-Raad, and all others by Moore. The observed velocities, corrected for flexure and for the earth's motion, are given in Table 1.

In order to disentangle the short- and long-period velocity-curves, the assumption was made that the two variations proceed entirely independently of each other. In that case the velocity of the system at any time, which is the algebraic sum of the short- and long-period variations, may be computed by considering one component without regard for the other. This assumption was tested at a later stage in the analysis. It was also assumed that the period of the short-period velocity variation is identical with the period of the light-variation of the cepheid. The period derived by H. Schneller[7] and adopted by B. Kukarkin and P. Parenago in the 1948 *General Catalogue of Variable Stars* was employed throughout; phases in the short-period cycle were computed from

$$\text{JD } 2429090.000 + 8^d.3821723E\,. \qquad (1)$$

[4] This γ corresponds to −10.0 km/sec on the system of the 1938–1948 Lick observations. The systematic correction of +2.3 km/sec to Aldrich's velocities is discussed later in this paper.

[5] *Lick Obs. Bull.*, **13** (No. 393), 112, 1928.

[6] A small change in the internal temperature of the Mills spectrograph can take place, despite the operation of the thermostatic control, in the presence of a large variation of the outside temperature. The internal change is caused by a time delay in the supply of a compensating quantity of heat; this lag occurs when there is a large local loss of heat via the metal supporting members of the spectrograph that pass through the temperature jacket.

[7] *Kl. Veröff. Berlin-Babelsberg*, No. 20, 1938.

TABLE 1*

SPECTROSCOPIC OBSERVATIONS OF S SAGITTAE, 1938–1948

No.	Plate	JD	Observed Velocity (Km/Sec)	Short-Period Phase (Days)	Long-Period Phase (Days)
		1938 2429000+			
1	25584	092.760	−36.6	2.760	92.8
2	25590	093.885	−31.7	3.885	93.9
3	25594	095.864	−24.2	5.864	95.9
4	25602	098.927	−29.6	0.545	98.9
5	25609	099.930	−40.0	1.548	99.9
6	25622	102.918	−32.6	4.536	102.9
7	25629	104.930	−14.8	6.548	104.9
8	25644	112.906	−18.9	6.142	112.9
9	25645	113.753	− 7.6	6.989	113.8
10	25646	114.752	− 2.4	7.988	114.8
11	25652	115.883	−30.8	0.736	115.9
12	25657	117.852	−33.4	2.705	117.9
13	25673	120.872	−20.0	5.725	120.9
14	25682	122.890	− 1.9	7.743	122.9
15	25687	123.834	−16.4	0.305	123.8
16	25688	124.841	−35.3	1.312	124.8
17	25695	125.704	−34.2	2.175	125.7
18	25713	126.861	−30.2	3.332	126.9
19	25735	128.701	−25.6	5.172	128.7
20	25744	130.861	− 1.7	7.332	130.9
21	25745	131.857	− 3.8	8.328	131.9
22	25772	143.804	−25.0	3.511	143.8
23	25779	147.818	+ 3.1	7.525	147.8
24	25785	150.680	−30.8	2.005	150.7
25	25786	151.826	−26.0	3.151	151.8
26	25789	152.794	−21.0	4.119	152.8
27	25807	153.680	−21.3	5.005	153.7
28	25831	154.790	− 9.9	6.115	154.8
29	25836	156.752	+ 3.1	8.077	156.8
30	25841	158.786	−27.4	1.729	158.8
		1939			
31	26397	447.941	+ 2.6	5.890	447.9
32	26453	475.740	+ 9.1	0.160	475.7
33	26454	476.883	−15.2	1.303	476.9
34	26456	477.838	−14.3	2.258	477.8
35	26512	499.844	+18.3	7.500	499.8
36	26514	502.840	−17.5	2.114	502.8
37	26519	506.759	+ 1.8	6.033	506.8
38	26524	509.820	− 7.7	0.711	509.8
39	26531	512.716	− 9.1	3.607	512.7
40	26534	513.722	− 9.6	4.613	513.7
41	26538	514.698	− 5.1	5.589	514.7
42	26542	521.745	−10.3	4.254	521.7

* The following spectrograms were measured but rejected because of poor quality or large residuals:

Plate	JD 2429000+	Observed Velocity (Km/Sec)	Short-Period Phase (Days)	Long-Period Phase (Days)
25579	091.760	−43.8	1.760	91.8
26390	446.946	− 2.9	4.895	446.9
27040	795.914	−34.1	1.812	119.7
27049	800.940	− 6.3	6.838	124.7

According to Schneller, maximum light occurs at phase 1.48 days on this phase system.

The most extensive group of observations, made in 1938, was used for determining a first approximation to the short-period velocity-curve. When the 1938 observations were plotted against phase, each successive cycle was seen to be shifted in the velocity co-ordinate with respect to the previous curve. This shift, due to the long-period variation, took place at the rate of about 0.15 km/sec/day at that time, and the observed velocities were first reduced to a standard epoch by removing this shift, which was as-

TABLE 1—*Continued*

No.	Plate	JD	Observed Velocity (Km/Sec)	Short-Period Phase (Days)	Long-Period Phase (Days)
		1940			
		2429000+			
43	27027	793.877	− 3.0	8.157	117.7
44	27033	794.805	−31.1	0.703	118.6
45	27043	796.954	−33.1	2.852	120.8
46	27044	797.833	−29.4	3.731	121.6
47	27050	801.939	+ 0.4	7.837	125.7
48	27051	802.893	−20.3	0.408	126.7
49	27054	803.944	−37.0	1.459	127.7
50	27055	804.807	−33.6	2.322	128.6
51	27064	807.949	−21.3	5.464	131.7
52	27065	808.945	−11.7	6.460	132.7
53	27066	810.944	− 5.7	0.077	134.7
54	27084	817.942	− 3.4	7.075	141.7
55	27100	824.861	−17.2	5.612	148.7
56	27119	832.914	−20.1	5.283	156.7
		1947			
		2432000+			
57	31822	376.745	−33.5	0.933	671.9
58	31824	380.755	−29.2	4.943	676.0
59	31825	380.811	−29.7	4.999	676.0
60	31864	396.887	−30.0	4.311	15.9
61	31865	396.964	−29.7	4.388	16.0
62	31868	398.851	−16.5	6.275	17.9
63	31869	399.865	− 5.3	7.289	18.9
64	31872	402.798	−41.9	1.840	21.8
65	31876	404.882	−30.9	3.924	23.9
66	31889	410.849	−41.7	1.509	29.8
67	31898	413.883	−32.8	4.543	32.9
68	32146	495.656	−35.7	2.494	114.7
69	32234	522.660	−25.0	4.352	141.7
		1948			
70	32598	686.937	−11.0	0.985	305.9
71	32610	696.933	− 8.5	2.599	315.9
72	32614	697.910	− 4.5	3.576	316.9

sumed to vary linearly with the time over the 1938 season. The first-approximation short-period curve so obtained was then improved by a determination of the correction required to reduce each individual observation to the curve, after which these corrections were plotted against the time and a smooth curve was drawn through the resulting points. Corrections read from this curve were applied to the observed velocities, and the second approximation velocity-curve was constructed by drawing it, freehand, through the plotted points. A further improvement in this freehand curve resulted from the construction of a plot of the residuals between the curve and the observed velocities (with the long-period change removed) as a function of short-period phase. These residuals

were then smoothed and the freehand curve corrected accordingly. The result was the "1938 short-period curve," whose γ-velocity was the velocity in the long-period cycle at the 1938 mean epoch.

The 1940 velocities were then compared with the 1938 curve, and by the same procedure the march of the long-period cycle was removed. The "1938, 1940 curve" was obtained by combining the two sets of corrected velocities. The 1939 velocities were treated by comparison with this curve in the same way as were those of 1940. Finally, the three velocity-curves were combined, after the proper zero-point corrections, into a master "1938, 1939, 1940 curve." The master-curve was then used to remove the effect of the short-period variation from all the observations, both Michigan and Lick. Each observed velocity in this way yielded a value of the long-period component of the velocity. To simplify the work, the individual observations were gathered into small groups of from 1 to 20 velocities; the data on these groups are given in Table 2. The final systematic corrections to Aldrich's and Jacobsen's velocities, described in a later paragraph, have been applied to the velocities in Table 2. It was found that the errors of the early Lick one-prism velocities measured by Curtiss and by Maddrill are so large that they are incapable of contributing anything of value to this study. Consequently, those observations will not be considered here.

It was soon evident that Aldrich's one-prism velocities required an appreciable correction to bring them into agreement with the Lick three-prism results; a preliminary examination indicated that a correction near +2.1 km/sec was necessary.[8] Aldrich assigned weights ranging from 1 to 10 to each of his plates. For the present discussion this scale was compressed by giving Aldrich's 9 and 10 a weight of 3; his 6, 7, and 8 a weight of 2; his 3, 4, and 5 a weight of 1; all plates to which he had assigned weights of 1 and 2 were rejected. Furthermore, a Michigan plate (dispersion 40 A/mm) of the highest weight was given one-third the weight of a Mills spectrogram (11 A/mm). The Mills plates were all considered to have the same weight of 9, although it will be seen later that the 1921–1927 velocities are somewhat less reliable than those of 1938–1948.

Examination of the velocities after the short-period change had been removed showed that the remaining variation was cyclic, with a period slightly shorter than that found by Aldrich (682 days); a value near 675 days was definitely better. With the period determined provisionally, it was possible to reduce all the observations to a single long-period cycle, to draw a smooth curve through them, to use this curve to improve the hitherto piecemeal removal of the long-period variation from the observed velocities, and thus to obtain a superior short-period velocity-curve. This short-period curve was constructed by using only the 1938–1948 Mills observations. The new curve made it possible to derive better long-period velocities, which were then examined closely in order to obtain a final value for the period. A value of 676.2 days was adopted, orbital elements of the long-period curve were computed, normal points were formed, and the elements were adjusted by least squares (see Table 3). Residuals between the predicted velocity [= V (short period) + V (long period)] and the observed velocity were then obtained in order to determine better values for the systematic corrections to be applied to the Michigan and to the 1921–1927 Lick velocities to reduce them to the system of the 1938–1948 Lick observations. These corrections were introduced, the entire process was repeated, and the systematic corrections again were evaluated. They are:

$$V\text{ (Moore)} - V\text{ (Jacobsen)} = -0.9 \pm 0.1\text{ (p.e.) km/sec},$$

$$V\text{ (Moore)} - V\text{ (Aldrich)} = +2.3 \pm 0.2\text{ (p.e.) km/sec}.$$

[8] Moore found (*Pub. Lick Obs.*, **18**, xii, Table III, 1932) a correction of +1.8 km/sec to the Michigan radial velocities of F5–G4 stars as the result of a study of far less extensive material than that available here.

TABLE 2

GROUPING OF OBSERVATIONS FOR STUDY OF THE LONG-PERIOD VARIATION

MEAN JD	MEAN PHASE* (DAYS)	MEAN LONG-PERIOD VELOCITY† (KM/SEC)	WEIGHT	NO. OF SPECTROGRAMS	RESIDUAL‡ (KM/SEC)	NORMAL POINT NO.	IDENTIFICATION OF PLATES IN GROUP§
			Michigan (Aldrich) Observations				
2419976.1	442.9	+ 0.1	3	3	+0.2	5	2–4
2420010.9	477.7	− 0.8	15	11	+0.9	5	6–12, 15, 16, 18, 19
0047.4	514.2	− 3.9	14	11	+0.2	6	21–23,–25–32
0071.5	538.3	− 7.1	6	6	−1.0	6	34–39
0116.8	583.6	−10.7	3	3	−0.1	7	40–42
0286.8	77.4	−29.8	2	1	−1.6	1	43
1037.8	152.2	−17.2	14	5	0.0	2	46–50
1071.1	185.5	−11.4	16	11	−0.4	3	51–57, 59–61, 63
1106.0	220.4	− 5.4	22	13	+0.4	3	65–69, 72, 73, 75, 77–81
1386.7	501.1	− 4.0	1	1	−0.8	6	82
1450.7	565.1	− 8.1	32	20	+0.6	7	83–88, 90–93, 95–99, 101–105
1477.7	592.1	−12.6	10	5	−1.0	7	109–111, 113, 114
1801.9	240.1	− 7.2	5	4	−3.6	3	116–118, 120
3521.8	607.6	−17.0	1	1	−3.6	7	123
			Lick (Jacobsen) Observations				
2422913.2	675.2	−22.3	81	9	+0.5	8	6, 10, 13, 14, 15, 17, 20, 25, 27
2930.1	15.9	−25.0	81	9	0.0	8	2, 4, 5, 8, 11, 21, 24, 28, 30
2954.7	40.5	−27.8	9	1	−0.3	8	22
3976.7	386.3	+ 1.0	54	6	−0.4	4	1, 9, 12, 16, 19, 26
3988.0	397.6	+ 2.0	36	4	+0.7	4	3, 7, 23, 29
4704.1	437.5	+ 0.8	45	5	+0.6	5	31, 34, 37, 38, 40
4742.6	476.0	− 2.6	36	4	−1.0	5	32, 33, 35, 39
4770.4	503.8	− 3.4	45	5	−0.1	6	36, 42, 45–47
4802.4	535.8	− 6.5	36	4	−0.6	6	41, 43, 44, 48
5073.4	130.6	−21.3	18	2	+0.1	2	50, 51
			Lick (Moore) Observations				
2429096.3	96.3	−26.7	45	5	0.0	1	1–5
9109.9	109.9	−24.8	45	5	0.0	1	6–10
9120.3	120.3	−23.0	45	5	+0.1	1	11–15
9127.4	127.4	−21.7	45	5	+0.2	2	16–20
9145.2	145.2	−18.4	45	5	0.0	2	21–25
9155.4	155.4	−15.7	45	5	+0.8	2	26–30
9447.9	447.9	− 0.8	9	1	−0.5	5	31
9476.8	476.8	− 1.8	27	3	−0.2	5	32–34
9504.8	504.8	− 3.0	36	4	+0.4	6	35–38
9515.7	515.7	− 4.2	36	4	0.0	6	39–42
9795.8	119.6	−23.8	36	4	−0.5	1	43–46
9803.4	127.2	−22.0	36	4	0.0	2	47–50
9809.2	133.0	−20.3	27	3	+0.5	2	51–53
9825.2	149.0	−18.2	27	3	−0.5	2	54–56
2432379.4	674.6	−23.9	27	3	−1.1	8	57–59
2398.1	17.1	−24.4	36	4	+0.7	8	60–63
2408.1	27.1	−27.0	36	4	−0.8	8	64–67
2495.7	117.5	−24.5	9	1	−0.9	1	68
2522.7	144.5	−19.7	9	1	−1.1	2	69
2693.9	312.9	+ 1.2	27	3	+0.3	4	70–72

* Phases in the long-period orbit are referred to JD 2429000.0 and are computed with a period of 676.2 days.

† The mean long-period velocity is the observed velocity with systematic corrections of +2.3 km/sec applied to Aldrich's observations and −0.9 km/sec to Jacobsen's and with the short-period velocity variation removed.

‡ The residual is the mean long-period velocity of the third column *minus* the velocity predicted for that phase by the long-period orbital elements given in Table 4.

§ The numbers in the last column refer to plates listed by Aldrich in his Table 8 (*Pub. Obs. U. Michigan*, **4**, 75, 1932), by Jacobsen in his Table II, and in Table 1 of this paper. In the cases of Aldrich's and Jacobsen's observations, their plates have been given numbers from 1 to 124 and 1 to 51, respectively, simply in the order in which they occur in those tables. The numbers assigned to Moore's 1938–1948 series are those appearing in the first column of Table 1 of this paper.

These corrections were employed in the adjustment of the observed velocities, and the whole solution was made again. Since no change in these corrections resulted from the new approximation, the above values are regarded as final. The orbital elements of the long-period cycle obtained in the last approximation were adopted; they are given in Table 4. The use of the above systematic corrections served to reduce the sum of the weighted squares of the residuals from 66.3 (km/sec)^2, for the solution where +2.1 km/sec was applied to the Michigan velocities and 0.0 km/sec to the 1921-1927 Lick series, to 14.0 (km/sec)^2. The residuals between the grouped observed velocities (freed of the short-period variation) and the velocities predicted by the elements of Table 4 are given

TABLE 3

NORMAL PLACES FOR THE LONG-PERIOD CYCLE

Normal No.	Mean Phase* (Days)	Normal Velocity (Km/Sec)	Weight	Number of Plates			Residual (O−C) (Km/Sec)
				Aldrich	Jacobsen	Moore	
1	111.0	−24.80	182	1	0	20	−0.13
2	140.0	−19.38	266	5	2	26	+ .10
3	209.8	− 7.62	43	28	0	0	− .39
4	372.8	+ 1.69	107	0	10	3	+ .10
5	460.9	− 0.85	135	14	9	4	.00
6	515.1	− 4.24	174	18	9	8	− .05
7	573.0	− 9.38	46	29	0	0	+ .05
8	11.6	−24.43	270	0	19	11	+0.01
Total†				95	49	72	

* Phases in the long-period cycle are reckoned from JD 2429000.0 and are based on a period of 676.2 days.

† The discrepancies between these totals and the figures given in the text for numbers of plates result from the rejection of spectrograms of low weight or with abnormally large residuals.

TABLE 4

ORBITAL ELEMENTS OF THE LONG-PERIOD CYCLE AND THEIR PROBABLE ERRORS

$P = 676^d2$ (assumed)	$\omega = 202°.28 \pm 0°.91$
$K = 15.03 \pm 0.06$ km/sec	$T =$ Phase $89^d.7 \pm 1^d.3$
$\gamma = -10.0$ km/sec	$a \sin i = 135.5 \times 10^6$ km
$e = 0.246 \pm 0.004$	$f(m) = 0.217 m_\odot$

in the last column of Table 3. The usual check on the importance of the neglected higher-order terms in the unknowns of the least-squares solution was made by comparing the residuals for the normal points as obtained, on the one hand, from representation by the corrected orbital elements and, on the other, from substitution of the unknowns back into the observation equations. The maximum disagreement between the two sets of residuals was 0.02 km/sec, which demonstrates the unimportance of the higher-order terms.

The velocity-curve resulting from the elements of Table 4, as well as the observed velocities in Table 2, is plotted in Figure 1. The probable errors of the elements in Table 4 were computed on the assumption that the residuals between observed velocities and those taken from the final long- and short-period curves could properly be regarded as arising equally from uncertainties in the two curves, as well as from errors of observa-

tion. That is to say, the two components of the observed velocity variation are observable with equal accuracy. The probable errors of the long-period elements that would result from the assumption that the residuals are due entirely to errors in those elements and to the errors of observation are $\sqrt{2}$ times those given in Table 4.

Co-ordinates of the final short-period curve, which is based only on Moore's 1938–1948 velocities, are given in Table 5, and the curve and individual observations are plotted in Figure 2. The adopted curve was obtained from the individual velocities by taking sliding means of four points at a time, and then by smoothing these means by inspection. The curve is adjusted so that the areas above and below the 0.0 km/sec axis

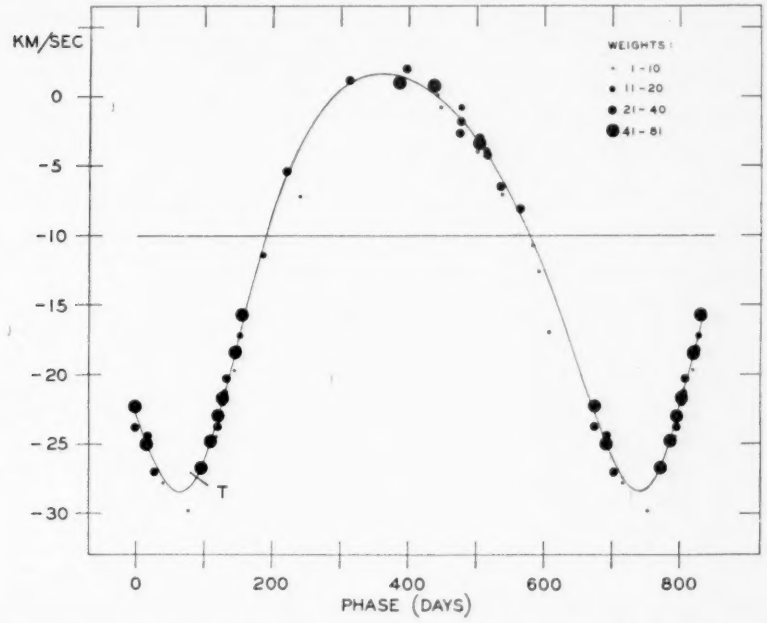

FIG. 1.—The long-period velocity-curve of S Sagittae. This curve represents the periodic variation of the center-of-mass velocity of the cepheid. The solid line corresponds to the orbital elements of Table 4.

are equal. Aldrich fitted to the short-period velocity variation two superimposed velocity-curves of periods 8.38 and 4.19 days. The "secondary oscillation" of period 4.19 days is a mathematical fiction that may be used if one wishes to represent the observed velocity-curve, with its hump on the rising branch, by means of ordinary orbital elements.

With the adoption of long- and short-period velocity-curves and the determination of the necessary systematic corrections for reduction to the system of the 1938–1948 observations, it is possible to compute the accidental probable errors and weights of the three series of velocities. The mean weight of the Michigan plates used in this discussion (when those of low weight are rejected, as described earlier) is 1.52 on the weight scale of 1 to 9 used in this paper. The probable error of the velocity from a single plate with this mean weight is ± 1.94 km/sec. The probable error of a velocity determined by Jacobsen with the Mills spectrograph is ± 0.80 km/sec, and of one determined by Moore ± 0.61 km/sec. If these probable errors are reduced to relative weights, they correspond to weights of 1.0:8.8:15.4 for an Aldrich plate of weight 1, a spectrogram obtained by

TABLE 5

CO-ORDINATES OF SHORT-PERIOD VELOCITY-CURVE

Phase (Days)	Velocity (Km/Sec)	Phase (Days)	Velocity (Km/Sec)	Phase (Days)	Velocity (Km/Sec)
0.10	+13.1	2.60	−10.7	5.80	+ 2.4
0.20	+ 9.7	2.90	− 9.3	6.10	+ 5.7
0.30	+ 6.3	3.20	− 8.0	6.40	+ 9.1
0.40	+ 2.4	3.50	− 6.7	6.70	+12.5
0.50	− 1.0	3.80	− 5.4	7.00	+16.0
0.60	− 3.5	4.00	− 4.8	7.30	+19.2
0.70	− 5.7	4.10	− 4.8	7.50	+20.8
0.85	− 8.6	4.20	− 4.9	7.70	+21.6
1.00	−10.9	4.40	− 5.5	7.80	+21.6
1.20	−13.0	4.60	− 6.1	7.90	+21.5
1.40	−14.1	4.70	− 6.2	8.10	+20.2
1.60	−14.3	4.80	− 6.1	8.20	+19.0
1.80	−14.0	5.00	− 5.5	8.30	+17.4
2.00	−13.5	5.20	− 4.0	8.40	+15.2
2.30	−12.2	5.50	− 0.9	8.50	+12.5

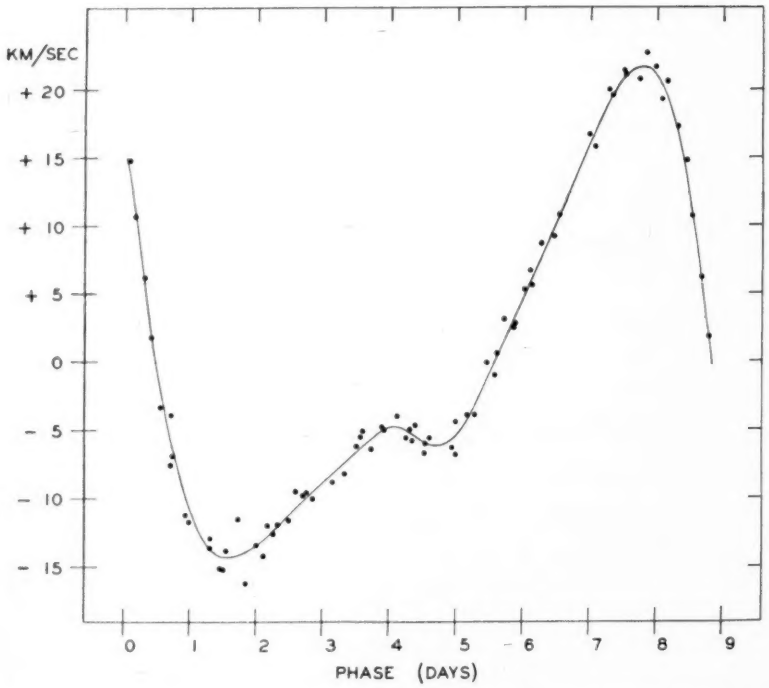

FIG. 2.—The short-period velocity-curve of S Sagittae. This component of the velocity variation is that proceeding in synchronization with the light-variation of the cepheid. Co-ordinates of the solid line are given in Table 5.

Jacobsen, and one obtained by Moore, respectively. The weights actually used in the discussion were 1:9:9; they were taken as approximately inversely proportional to the dispersions. The reasons for the superiority of the velocities obtained in 1938–1948 with the Mills spectrograph over those of 1921–1927 have already been mentioned.

In 1950 and 1951, a number of spectrograms of S Sagittae were obtained with the coudé spectrograph of the 100-inch telescope at Mount Wilson; the dispersion was 10 A/mm. The 1950 plates were taken with the primary purpose of investigating the contribution of a companion star to the light of the cepheid, and they are discussed from that point of view in Section III. Five of these spectrograms, as well as three exposures of the supergiants β Aquarii and 9 Pegasi, have been measured for radial velocity. The velocities are based on the MIT wave lengths of twenty-two *Fe* I lines in the wave-length interval λλ 3820–3983, chosen on the basis of freedom from serious blends. The results are given in Table 6. It will be seen that a systematic correction of −2.1 km/sec is required to reduce the coudé velocities to the system of the S Sagittae results, which is close to the Lick system. The origin of this discrepancy is unknown. It appears that, aside

TABLE 6

MOUNT WILSON COUDÉ SPECTROGRAMS OF S SAGITTAE, β AQUARII, AND 9 PEGASI

Star	Plate	Date (U.T.)	Measured Velocity (Km/Sec)	Adopted Velocity* (Km/Sec)	*V* (Adopted) *minus* *V* (Measured)
S Sge	Ce 6641	1950 Nov. 1, 2^{h}00^m	− 9.2	−11.0	−1.8
S Sge	6704	Nov. 30, 1 47	+16.0	+13.2	−2.8
S Sge	6708	Dec. 1, 2 05	+ 4.2	+ 1.2	−3.0
S Sge	6711	Dec. 2, 2 49	−21.8	−21.1	+0.7
S Sge	7631	1951 Nov. 9, 1 48	+19.6	+16.4	−3.2
β Aqr	6648*a*	1950 Nov. 2, 4 08	+ 8.6	+ 6.8	−1.8
β Aqr	6648*b*	Nov. 2, 4 16	+ 9.1	+ 6.8	−2.3
9 Peg	6712	Dec. 2, 4 04	−19.7	−22.3	−2.6

* The adopted velocities for S Sagittae are those computed from the long-period orbital elements of Table 4 and the short-period velocity-curve of Table 5. The adopted velocities of β Aquarii and 9 Pegasi are taken from *Pub. Lick Obs.*, Vol. **16**, 1928.

from this instrumental correction, the coudé velocities of 1950–1951 are not in disagreement with the velocity elements of S Sagittae derived from the 1913–1948 material.

The residuals were next examined for any evidence that the short- and long-period variations were not completely independent, as was originally assumed. Strong concentrations of Mills observations made three regions of the long-period cycle particularly suitable for this purpose (the Michigan velocities were not considered because of their relatively large probable error). These regions were the phase intervals from 664–41 days, 77–159 days, and 383–544 days. The residuals of all the Mills observations in each of these intervals were plotted against short-period phase. These diagrams are shown in the first three panels of Figure 3, where Jacobsen's and Moore's observations are distinguished from one another only by the length of the vertical lines, which represent twice the corresponding probable errors (±0.8 km/sec for Jacobsen's observations and ±0.6 km/sec for Moore's).

Any dependence of the shape of the short-period velocity-curve upon phase in the long-period cycle would cause systematic departures of the residuals from the 0.0 km/sec axis in these plots; furthermore, these departures would differ from one diagram to the next. The general scatter of the points about the axis of zero residuals in Figure 3 is quite in harmony with their probable errors, as it should be, since the plotted residuals

represent a considerable portion of the material from which the probable errors were determined. There seems, however, to be a certain tendency for the residuals to depart from the 0.0 km/sec axis in a systematic way, particularly in the 77–159- and 383–544-day panels. These departures are small, and their reality is not at all certain, so that it is necessary to examine the residuals in an objective way because of the possibility that the apparent "runs" are simply an accidental phenomenon. The data were first studied by several rather general statistical methods that required no knowledge of the form of the suspected variation of the 8-day cycle over the 676-day period. These tests will not be described here, since the results were inconclusive, presumably because of the non-

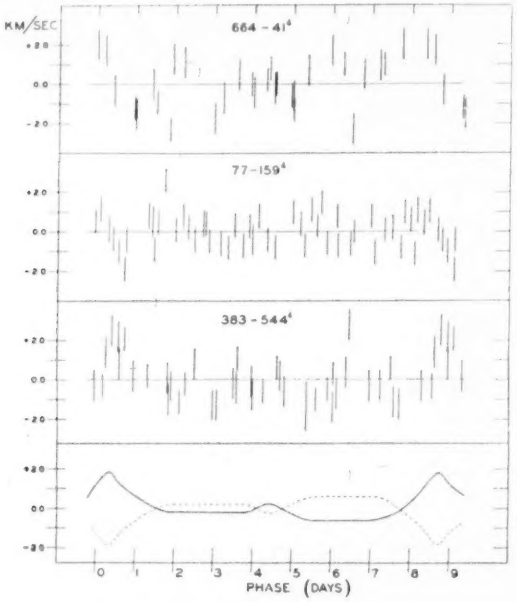

FIG. 3.—*First three panels:* Residuals between observed velocities (with long-period variation removed) and the short-period curve of Fig. 2, in three regions of the long-period cycle. *Bottom panel:* Residuals to be expected if the instantaneous short-period curve were shifted by 0.05 day in the direction of greater phase (*solid line*), and by 0.05 day in the opposite direction (*dashed line*). These predicted curves are to be compared with the progressions of residuals in the first three panels of the figure.

committal nature of the approach. The procedure finally adopted was as follows: first, the material was carefully examined to see if any simple modification of the short-period velocity-curve could produce the apparent "runs" in Figure 3. Second, the behavior of this modification throughout the long-period cycle was studied; it was assumed that it varied smoothly and in synchronization with the 676-day period. Third, the effect was removed from each observation on the basis of the results of this study. Fourth and finally, the reality of the entire effect was then judged by the result of its removal upon the residuals: if the improvement is statistically significant, then one can state that the effect probably is real. As will appear, the improvement of the residuals is *not* statistically significant within the framework of the assumptions that went into the correction of the observations. Although the phenomenon does not seem to be a real one, the chance that

it may be real justifies a condensed description of the technique of study and testing, and of the results.

The first step, as described above, began with the observation that the general run of the residuals in the second and third panels of Figure 3 suggests that a shift along the time axis of the "instantaneous" short-period velocity-curve with respect to the mean curve of Figure 2 might be, to a considerable extent, the responsible effect. In the fourth panel of Figure 3 is shown (solid line) the curve of residuals that would be produced by a simple horizontal shift of the instantaneous curve in the direction of *greater* short-period phase by 0.05 day with respect to the mean curve, as well as the residual curve (dashed line) that would result from a shift of the same amount in the direction of *lesser* phase. The sign convention adopted is that this shift, S, is reckoned as positive is the former case. A certain similarity to these predicted curves is seen in the distribution of residuals in the 77–159- and 383–544-day panels of Figure 3. It is then possible, if one assumes that we are observing the effect of an oscillatory shift of the short-period velocity-curve, to obtain the amount of this shift that corresponds to a given residual. This is most easily done by constructing a family of predicted curves corresponding to different shifts, S, and reading off the value of S for each residual by interpolating between these curves. Weights that were proportional to the amplitude of one of the predicted residual curves at the proper phase were assigned to the values of S obtained from each residual, since the regions of greatest slope of the velocity-curve should figure most importantly in the determination of any horizontal displacement. In practice, only observations lying in the short-period phase intervals 8.0–1.3 days, 2.0–3.5 days, and 5.0–7.4 days were considered at all, since residuals in the other regions were of very small weight. Weights were also assigned according to whether the value of S was derived from a Jacobsen or a Moore observation.

The second step, to determine the variation of S throughout the long-period cycle, began with the plotting of the individual values of S against long-period phase; this diagram is shown in Figure 4. It will be seen that there is a tendency for the points in Figure 4 to fall on or below the $S = 0^d0$ axis in the phase interval 664–159 days, and to lie high in the 383–544-day region. The simplest functional form that this apparent variation of S could take would be that of a sine wave of the type

$$S = A + B \sin [\mu (t - t_2) + \phi] , \qquad (2)$$

where μ is the mean angular daily motion in the long-period cycle and $t - t_2$ is the long-period phase in days. The disposable parameters A, B, and ϕ were fitted to the S-values of Figure 4 by least squares, and the sine wave shown there thus obtained. The values found for these quantities, together with their probable errors, are:

$$A = +0.008 \pm 0.006 \text{ day} , \qquad B = 0.029 \pm 0.006 \text{ day} , \qquad \phi = 206° \pm 18° .$$

The possibility that this periodic shift is due to the light-time effect in the long-period orbit is immediately ruled out by the large value of the semiamplitude: $B = 0.029$ day; the value due to light-time would be only 0.005 day. The two effects disagree in phase by about 100 days as well, but the reality of this discordance is not so convincing as that of the amplitudes because of the uneven distribution of the observations over the long-period cycle.

The most obvious explanation of such a varying shift of the instantaneous velocity-curve with respect to the mean curve is that the 8-day period is slightly variable and that it oscillates about its mean value in the long period of 676 days. The phase shift, S, would then be the result of the accumulation of the difference in periods over a number of (short-period) cycles. Let us assume, in order to relate the variation of S found from

the observations to such a period change, that the time scale of the short-period velocity variation oscillates with time and that at any instant, t, is given by

$$1 + a \sin [\mu (t - t_2) + \psi] \tag{3}$$

in terms of its mean value, where $t - t_2$ is the long-period phase.[9] Then, for any time t, one may obtain the short-period velocity from Figure 2, not by using as argument $t - t_1$, where t_1 is the origin of the short-period phase, but rather $\tau - t_1$, which is given by

$$\tau - t_1 = (t - t_1) - \frac{a}{\mu} \{\cos [\mu (t - t_2) + \psi] - \cos \psi\} . \tag{4}$$

Since S has been defined as $\tau - t$, then

$$S = \frac{a}{\mu} \sin \left[\psi + \frac{\pi}{2}\right] - \frac{a}{\mu} \sin \left[\mu (t - t_2) + \psi + \frac{\pi}{2}\right] , \tag{5}$$

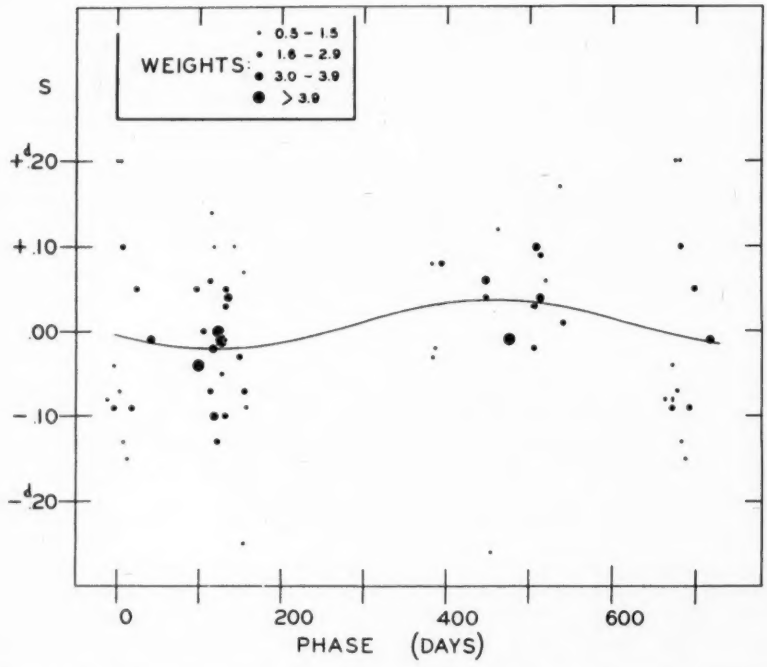

FIG. 4.—The variation of the phase shift, S, throughout the long-period cycle. The sine wave is that represented by the least-squares corrected parameters given in the text.

[9] Throughout this discussion, the subscript 1 will be attached to short-period quantities, and the subscript 2 to long-period quantities.

so that a and ψ of equation (3) can be identified by comparing equations (2) and (5). This procedure gives, when applied to the second terms of equations (2) and (5) and when one uses the numerical values of B and ϕ obtained from the residuals,

$$a = -\mu B = -0.00027\,, \qquad \psi = \phi - \frac{\pi}{2} = 116°\,.$$

The semiamplitude of the phase variation of the short period is aP_1, or 0.0023 day. These elements correspond to a variation of the short period from a minimum value of 8.380

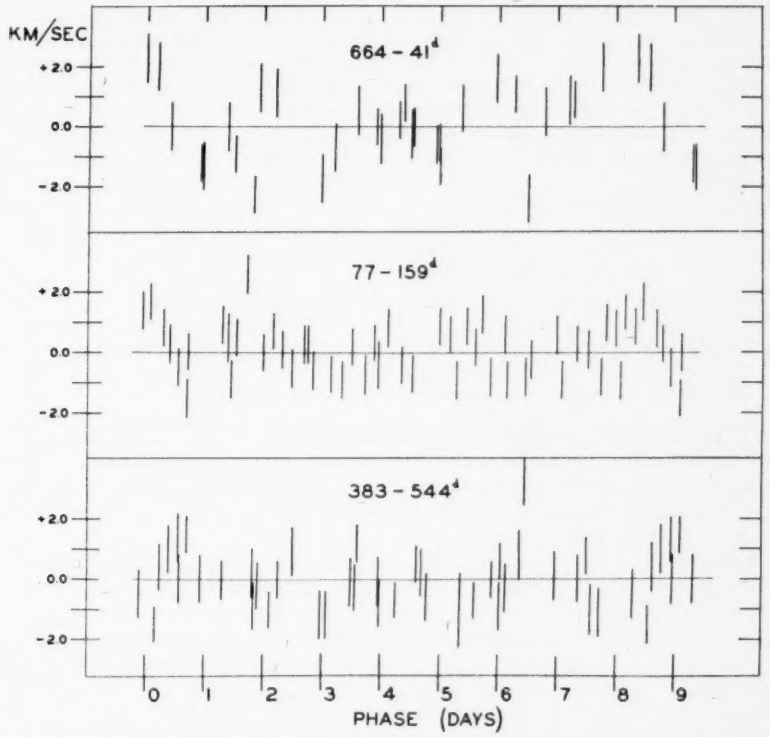

FIG. 5.—These panels correspond to the first three panels of Fig. 3, except that the phase-shift effect, described in the text, has now been removed.

days near long-period phase 630 days, to a maximum value of 8.384 days a half-cycle later.

The third step in the process of testing the reality of the S-variation is the removal of the effect from the Mills velocities. This removal was effected by reading the S predicted for the time of each observation from the sine wave of Figure 4; this value of S was then converted into a correction to the velocity. The new residuals obtained in this way are plotted in Figure 5 in the same manner as the original residuals are shown in Figure 3. The new residuals show a more uniform scatter with phase, but one would hesitate to pronounce them a significant improvement, because of the large general dispersion

The final step is to determine whether the improvement is statistically significant. Let A represent the hypothesis that the observed velocities can be represented completely by the long- and short-period variations, where the former is characterized by the six independent orbital elements of Table 4 and the latter by the curve of Figure 2 and Table 5. The short-period curve can be represented, formally, as the sum of two orbital curves with periods P_1 and $P_1/2$. Since P_1 is not determined from the velocities and since the observations give the sum of the γ-velocities of the three components of the variation and not their individual values, it can be seen that eight more independent elements or parameters determined from the observations are required to specify the short-period variation. Therefore, fourteen parameters that determine the shape of the predicted velocity variation are involved in hypothesis A, plus two other quantities: the ratio of the weights of the 1921–1927 and 1938–1948 observations and the systematic correction required to reduce the 1921–1927 velocities to the system of those obtained in 1938–1948. Now let B represent the hypothesis that the observed velocities contain, in addition to these long- and short-period variations, a component of the type proposed in the preceding discussion to account for the phase shifts S. This discussion included the determination from the observations of three additional parameters. If one now defines the quantities

$$s_A^2(I) = \sum_{i=1}^{N(I)} [V_i - V_i^{(A)}]^2$$

and

$$s_B^2(I) = \sum_{i=1}^{N(I)} [V_i - V_i^{(B)}]^2,$$

where $V_i^{(A)}$ represents the velocity predicted for the time of the ith observation under hypothesis A, and $V_i^{(B)}$ the same quantity under hypothesis B, and where V_i is the corresponding observed velocity (all for observations of series I, where I refers to Jacobsen's 1921–1927 observations and II to those of Moore in 1938–1948), then the quantity

$$F = \frac{\{[w(I)\, s_A^2(I) + w(II)\, s_A^2(II)] - [w(I)\, s_B^2(I) + w(II)\, s_B^2(II)]\}/f_1}{[w(I)\, s_B^2(I) + w(II)\, s_B^2(II)]/f_2} \quad (6)$$

provides a measure of the probability that the improvement in the weighted residuals of hypothesis B over those of hypothesis A is a real one.[10] In equation (6), $w(I)$ and $w(II)$ are the relative weights of the two series of observations, which are 0.36 and 0.64, as may be seen from the probable errors already quoted. The quantity f_2 is the number of degrees of freedom corresponding to hypothesis B: the total number of observations (118) minus the number of independent parameters (19); f_1 is the number of additional parameters involved in hypothesis B over those in A (3).

Computation shows that $F = 1.75$. Mood[11] tabulates F as a function of f_1 and f_2 for various values of α, the probability of obtaining the improvement simply as a result of chance. Extrapolation from the data of Mood's table gives $\alpha = 0.17$. In other words, the improvement in the residuals that resulted from the introduction of the sine-wave approximation for S would be expected to occur seventeen times out of one hundred trials as a result of pure chance. Statisticians generally require that α be less than 0.05 for the result to be "significant"; therefore, hypothesis B is statistically untenable, de-

[10] J. Neyman, *Year Book Amer. Phil. Soc.*, p. 141, 1944. See also A. M. Mood, *Introduction to the Theory of Statistics* (New York: McGraw-Hill, 1950), sec. 14.2.

[11] *Op. cit.*, Table V.

spite the success of the correcting process in making the revised residuals look more satisfactory to the eye than did the old ones.

The question may arise whether some part of the *S*-variation might not be due to an error in the adopted value of the short period or to a secular change in its length.[12] No evidence that this is the case has been uncovered. The *S*-values were examined for indications of such an effect. None were found, nor were any shown by the times of maximum light, for the years 1921–1949, which could be found in the literature. The *S*-values determined from the velocities are not well distributed in time for the detection of an oscillatory phase shift, concentrated as they are in seven observing seasons over a period of 26 years. It is unlikely, however, that any systematic effect could have been missed that gave rise to a change in phase shift, either progressive or variable with a long period, with an amplitude of much more than 0.1 day over the interval 1921–1940. Certainly, there is no evidence of any period change during these years of the size obtained by A. Severny[13] from a discussion of a large number of photometric observations made in the years 1886–1931: he found both erratic and secular changes in the times of maximum and minimum light that amounted to as much as 0.5 day on either side of the values predicted on the basis of a constant period.

Schneller's value for the length of the short period, which was used throughout this investigation, was based on photometric material available to him in 1938; he did not state whether all material published since the discovery of the variability of the star was considered, but one may assume that a considerable interval of time was used. There is no convincing evidence that Schneller's period fails to represent the earliest Mills observations used in the investigation of the *S*-effect, made in 1921, 1924, and 1926, or photometric observations back to 1921. In the other direction there is less opportunity for such checks, but in that case the time interval over which the ephemeris had to be extrapolated—that is, over which the correctness of Schneller's period had to be assumed—was not, effectively, a long one. This is because, of the fifty-five values of *S* discussed here, fifty-two were derived from Mills velocities obtained between 1921 and 1940; only three were based on 1947 observations.

To conclude this section, one may say that the reality of the *S*-effect is in serious doubt, but the possibility that it is not entirely without meaning is large enough that it is here made a matter of record, so that it can be kept in mind by future investigators of S Sagittae. It would hardly seem wise to pursue this matter, or the similar one of the light-time effect, any further by radial-velocity observations, at least of the accuracy available for this study. Extensive photoelectric observations of the light-variation offer more promise of yielding information on these questions with a great deal less labor and with far more modest equipment.

III. THE SPECTROPHOTOMETRY

It was felt that a considerable effort directed toward the detection of the spectrum of a companion of S Sagittae would be justified, since it would be of considerable importance if one could establish directly that the long-period velocity variation is due to orbital motion. Since there is no sign in the λ 4500 region of any doubling or filling-in of the lines of the cepheid, it was decided to make a thorough search at shorter wave lengths. The near ultraviolet seemed the most favorable region for several reasons: (1) according to O. J. Eggen,[14] the departure of S Sagittae from the period versus color amplitude and period versus light amplitude relationships obeyed by other cepheids can be explained by the contribution of a companion about 1.9 mag. fainter photographically than the variable at minimum light and with a color index of about zero, corresponding to a late B- or early A-type star; (2) the examples of other G- and K-type super-

[12] This possibility was suggested by Dr. Martin Schwarzschild (private communication).

[13] *A.J.U.S.S.R.*, **10**, 190, 1933. [14] *Ap. J.*, **113**, 367, 1951; *Lick Obs. Contr.*, Ser. II, No. 32.

giants (e.g., ζ Aur, 31 Cyg, 32 Cyg, 52 Per, etc.) show that B- or A-type companions are common among such stars, although their predominance may be an observational effect; (3) although the difference of magnitude between such a blue companion and the variable would decrease with decreasing wave length, the near ultraviolet (about λλ 3700–3800) seemed more favorable than somewhat shorter wave lengths, since the confluence of the Balmer wings in a late B- or early A-type companion would cause the actual energy distribution just longward of the Balmer limit to fall well below the distribution appropriate to the color temperature at longer wave lengths. To the shortward of λ 3646, furthermore, the depression of the continuum of the companion by continuous Balmer absorption would have a similar effect. Investigation of the region just to the longward of the atmospheric cutoff, where Balmer absorption would be small, was not practicable for instrumental reasons. In view of these considerations, the spectral region λλ 3775–3787, between *H*10 and *H*11, was chosen for examination.

The spectrograms used for this portion of the investigation were taken in November and December, 1950, when S Sagittae was at phases 529–531 days and 558–560 days in the long-period cycle. Since the two velocity-curves cut the γ-axis at phase 578 days, the relative displacement of the spectral lines of the two stars on these plates would be expected to be very small. The plates were obtained with the coudé spectrograph of the 100-inch telescope at Mount Wilson. The 32-inch camera was used, together with a plane grating ruled by H. W. Babcock; the dispersion in the third-order ultraviolet is 10 A/mm. The emulsion used was Eastman IIa-O, baked for about 2 days at 50° C. The spectrograms were heavily overexposed in the ordinary photographic region in order to obtain satisfactory densities at λλ 3600–3800. Calibration spectra were impressed on the plates during the stellar exposure, and in no case did the effective stellar exposure time exceed the calibration exposure time by a factor greater than 3. Seven spectrograms of S Sagittae were obtained, as well as four exposures of the standard supergiants β Aqr and 9 Peg.

Visual examination of the plates of the variable taken in the vicinity of minimum light revealed no evidence of the spectrum of an early-type companion in the ultraviolet. In order to strengthen and make quantitative this observation, however, three of the best spectrograms of the variable, exposed at strategic phases in the 8-day cycle, as well as three of the exposures of β Aqr and 9 Peg, were traced with the modified Moll microphotometer of the Lick Observatory with a magnification of 190 times. The continuum was drawn in a consistent fashion on all the tracings, and the central intensities of 10 lines (mostly due to *Fe* I) in the λλ 3775–3787 region were derived in the usual way.

While it was appreciated that a cepheid cannot be regarded as a normal supergiant at any time in its light-cycle, it was hoped that a comparison of the central intensities of S Sagittae at minimum light with those in β Aqr and 9 Peg would make possible a statement on the amount of filling-in by the hypothetical companion. (It is in the neighborhood of minimum that the spectra of cepheids are known to resemble, more closely than at any other phase, those of normal I*b* supergiants.) These two stars were chosen as representatives, among normal objects, of the spectral type of the variable when faint. S Sagittae has been found by A. D. Code[15] to vary in spectral type between F6 I*b* and G5 I*b*. The types of β Aqr and 9 Peg on the same system are G0 I*b* and G5 I*b*, respectively. The familiar variation with phase of the line strengths in the cepheid was well shown by the observed central intensities; that is, the lines of S Sagittae strengthened greatly toward minimum light, with the cores of the strongest subordinate lines showing a tendency to approach a residual intensity of slightly less than 0.10, because of saturation. The central intensities near minimum light in S Sagittae, however, were consistently less than those in the comparison stars. One can, therefore, set only an upper limit to the contribution of a companion in this region by making the assumption that the centers of the strong lines saturate at zero central intensity and that the finite cen-

[15] *Ap. J.*, **106**, 309, 1947.

tral intensity actually observed (about 0.10) is due entirely to the continuum of the companion. The instrumental central intensities of the absorption lines of the cepheid certainly are greater than zero, because of the presence of a small but unknown quantity of energy there plus a certain amount artificially introduced by instrumental and photographic effects. The assumption that the companion is entirely responsible for the filling-in to a residual intensity of 0.10 would therefore be expected to yield a high upper limit for the relative brightness of the companion with respect to the cepheid at λ 3780. This assumption gives the result that m(companion) − m(cepheid at minimum) = +2.4 mag. The use of the Planck formula and Eggen's data on the properties required of the hypothetical companion predict that $\Delta m = +1.3$ mag. at λ 3780. The fact that the central intensities indicate $\Delta m \geq +2.4$ mag. at that wave length demonstrates that the departure of S Sagittae from Eggen's relationships cannot be ascribed to the contribution of a blue companion.

IV. DISCUSSION AND CONCLUSIONS

The evidence bearing on the nature of the long-period velocity variation of S Sagittae will now be considered. There are many objects among the RR Lyrae variables known to undergo changes in their light-curves, but there are only two stars[16] for which information is available on the accompanying modifications of the velocity-curves. In these two stars the most conspicuous effect is a variable phase shift of the short-period cycle; this shift is apparent in both light- and velocity-curves. It is accompanied by some change in the shape and amplitude of the velocity-curves, but any variation in the mean velocity is small and uncertain.[17]

This situation differs markedly from the case of S Sagittae, where the long-period variation in the mean velocity of the cepheid is comparable in range with the variation due to pulsation. It is true that there may be in S Sagittae a small variation in the phase of the short-period curve accompanying the long-period cycle, but this effect is very definitely a secondary effect if it is real. Clearly, the 676-day cycle of mean velocity in S Sagittae differs fundamentally from the periodic changes in the light- and velocity-curves of the RR Lyrae variables, and it is therefore quite a different phenomenon.

This dissimilarity in itself does not eliminate the possibility that the long-period velocity variation in S Sagittae is due to a radius change, but two other facts indicate that the long-period variation is not due to a slow pulsation. The first of these is that there is no evidence of any light-variation accompanying the 676-day cycle of velocity variation. The best photometric evidence bearing on this last point is that of Eggen.[18] His photoelectric observations of S Sagittae were made in 1948 (between long-period phases 392 and 411 days) and in 1949 (phases 46–150 days). The photoelectric observations of A. L. Bennett[19] were all made in an interval of 205 days in 1939, between long-period phases 13 and 218 days, so that they are entitled to less weight in this connection. But neither series shows any indication of a slow change in the short-period light-curve.

The second argument against interpretation of the 676-day cycle in this way involves consideration of the dimensions of such a pulsation. Numerical integration of the velocity-curve[20] yields the relative displacement of the atmosphere if the velocity is regarded

[16] RR Lyrae: O. Struve and A. Blaauw, *Ap. J.*, **108**, 60, 1948; R. F. Sanford, *Ap. J.*, **109**, 208, 1949. XZ Cygni: O. Struve and A. Van Hoof, *Ap. J.*, **109**, 215, 1949.

[17] No detailed spectroscopic observations have as yet been made of those classical cepheids known to show departures from a mean light-curve. Likewise, no information is available on possible light-changes accompanying the observed variation in the velocity-curves of certain classical cepheids.

[18] *Op. cit.*, Table 14. [19] *Ap. J.*, **90**, 289, 1939.

[20] Allowance must be made here for limb darkening and for the fact that the observed velocity is the result of an instrumental integration over one hemisphere of the star. A darkening coefficient of 0.6 was used in these computations, but the conclusions would not be affected by any reasonable variation of this quantity.

as due to a change in radius. This calculation shows that a radius variation is demanded during the 676-day cycle of 2×10^8 km in either direction from the mean radius. Since the mean radius of the star is only about 0.4×10^8 km, it is clear that such a pulsation is impossible.

It would be very desirable to make accurate photometric observations of S Sagittae in order to test the reality of the *S*-variation (see Sec. II) as well as to detect the light-time effect in the long-period orbit. The light-time effect—if one regards the elements of Table 4 as due to binary motion—would amount to 15 minutes between the points of maximum and minimum distance from the earth. A total shift of the cepheid light-curve by this amount with respect to a mean light-curve would therefore be expected. The light-curve is steepest on the rising branch; the change in photographic light at that time amounts to about 0.55 mag. per day. The light-time effect would therefore act to make the cepheid appear about 0.006 mag. brighter near the time of that conjunction when it is nearest the earth in the 676-day orbit than at the same short-period phase at the other conjunction. It can be determined only by observation if the shape of the short-period light-curve is stable enough through individual cycles to make this test feasible. Furthermore, the light-time effect would have to be disentangled from the presumably larger *S*-variation. A positive detection of the light-time effect would be very strong evidence in favor of the binary motion interpretation, and consequently an attempt at this test by someone with the proper equipment is strongly urged.

It is concluded that the evidence available at this time favors the binary interpretation of the long-period velocity variation of S Sagittae. No unambiguous sign of the presence of another star has been discovered, but, on the other hand, no information is available that is in disagreement with the binary hypothesis. Pulsation, in particular, seems to be ruled out as the responsible agent.

With the likelihood of binary motion in the 676-day cycle thus established, it is possible to employ the observational data to investigate the nature of the invisible companion. The mass function

$$f(m) = \frac{m_2^3}{(m_1 + m_2)^2} \sin^3 i \qquad (7)$$

has been found to be $0.217\ m_\odot$. Since $\sin^3 i$ can be no larger than unity, then if the mass of the cepheid component of S Sagittae (m_1) can be taken from the mass-luminosity relation, we can obtain a lower limit to the mass of the companion (m_2). From this quantity and the observed lower limits to the difference of magnitude at λ 3780 and at λ 4500, some inferences can be made as to the magnitude and spectral type of the companion star.

Apart from the usual doubt as to the applicability of the mass-luminosity relation to the cepheid variables, we have here the additional question as to how much confidence may be placed in results obtained from it as well as from the period-luminosity relation in the case of S Sagittae, which all the evidence shows to be a somewhat abnormal cepheid (see below). Furthermore, we can proceed only by making the assumption that the companion is a normal star and obeys the mass-luminosity relation. The fainter components of some spectroscopic binaries are known to be anomalous in these respects, and hence this assumption may be incorrect. These serious questions must be kept in mind when weighing the results now to be derived.

Shapley's period-luminosity relation[21] gives a median bolometric[22] absolute magnitude

[21] *Proc. Nat. Acad. Sci.*, **26**, 541, 1940.

[22] The bolometric corrections and effective temperatures used in this discussion are those given by G. P. Kuiper (*Ap. J.*, **88**, 429, 1938). The color temperatures are those on the T_1 scale of Stebbins and Whitford (*Ap. J.*, **102**, 318, 1945).

of -2.9 for S Sagittae. This value corresponds to $m_1 = 7.1\ m_\odot$, according to Kuiper's mass-luminosity relation.[23] Equation (7) can then be solved for m_2:

$$m_2 \geq 2.8 m_\odot , \qquad \text{and hence} \qquad M_{\text{bol}}\ (\text{companion}) \leq +0.3 .$$

First consider the situation where M_{bol} (companion) $= +0.3$, which would be the case for $i = 90°$. If the companion is a normal object, this would mean that it could be either (1) an early A-type main-sequence star or (2) a giant of type G. These two possibilities will now be examined in detail, as well as the situation when $i < 90°$.

Possibility 1: Companion an early A-type dwarf.—Such a star would have $M_{\text{pg}} = +0.9$, so that $\Delta m_{\text{pg}} = M_{\text{pg}}$ (companion) $- M_{\text{pg}}$ (S Sge at minimum) $= +0.9 - (-1.3) = +2.2$ at λ 4400. The assumption of black-body radiation for both stars leads to $\Delta m = +1.4$ at λ 3780. But it has already been shown that $\Delta m \geq +2.4$ at λ3780. Consequently, the companion cannot be an early-type star if $i = 90°$. If $i < 90°$, the mass of the companion must be greater and its absolute magnitude brighter, but this hypothesis makes still worse the disagreement with the spectrophotometric lower limit to Δm. An identification of the companion with a main-sequence or high-luminosity O-, B-, or A-type star is, therefore, not feasible.

Possibility 2: Companion a G-type giant.—Such a star would have $M_{\text{pg}} = +1.0$ to $+1.5$, so that $\Delta m_{\text{pg}} = +2.3$ to $+2.8$. At λ 3780, this would correspond to the same Δm, since the color temperatures of the two stars would be very nearly the same. A companion of this type would be very difficult to detect spectroscopically. If $i < 90°$, the mass of the companion would be larger, the absolute magnitude brighter, and the spectral type later (if we confine attention to the giants).[24] The coudé plates were taken near the time of conjunction in the long-period orbit, when the lines of the two stars would be nearly superimposed, and no duplicity of the lines would be expected. The Mills spectrograms upon which the 1938–1948 velocities are based were, however, taken through the entire 676-day cycle. A careful comparison of several pairs of plates, both spectrograms of each pair having been taken near minimum light of the cepheid, but at opposite nodes in the long-period orbit, revealed no evidence of the spectrum of another star in the λ 4500 region. It is estimated that if the companion were a late-type star and were no more than 1.5 mag. fainter than the cepheid in this region, its spectrum would have been detected. This fact demonstrates that

$$M_{\text{pg}}\ (\text{companion}) > +0.2 ,$$

which is of no help in settling the spectral type of the fainter star, since the mean photographic absolute magnitudes of normal stars lying on the giant branch depart only slightly from $M_{\text{pg}} = +1.3$ between G and M0. We can be certain only that the companion is not a supergiant. If the spectral type is quite late, its spectrum might be detectable in the red or infrared.

It is concluded that, to the extent that the fundamental assumptions made in the above calculations are valid, the observational evidence suggests that the companion of S Sagittae is a giant star of spectral type G or later.

The possibility that S Sagittae may be an eclipsing binary deserves brief mention. There is nothing in the present observations to suggest that such is the case, but the matter deserves a photometric test. The orbital elements of Table 4 predict a minimum projected separation between the two stars (companion in front of the cepheid) at long-period phase 607 days. This phase will next occur on November 24, 1952, and October 1, 1954, but the first date will find the star not well placed for observation, although acces-

[23] *Ap. J.*, **88**, 472, 1938.

[24] The observed limiting Δm at λ 3780 is inapplicable here, since it was obtained under the assumption that the spectrum of the secondary is continuous at that wave length. If the companion is a G-, K-, or M-type star, this is not the case.

sible. Reasonable assumptions as to the radii and masses of the two stars lead to an eclipse duration of about 2 weeks if $i = 90°$.

It has been shown in Section III that the departure of S Sagittae from the photometric relationships obeyed by many other cepheids cannot be caused by the contribution of a companion star of early type, and in the present section it was demonstrated that this fact is understandable in view of mass and luminosity considerations. The photometric discrepancy extends also to the light-range versus velocity-range relationship defined by other cepheids. S Sagittae seems, therefore, to be a somewhat peculiar cepheid, although, in the absence of adequate information on other variables of the same period and type, one cannot decide whether the peculiarities are a property of just this one star or whether they occur in all cepheids of a certain kind.

TABLE 7

CEPHEIDS WITH VARIABLE SYSTEMIC VELOCITIES

Star	Period (Days)	Remarks and References
α UMi	3.97	Long period = 29.6 years: J. H. Moore, *Pub. A.S.P.*, **41**, 254, 1929
FF Aql	4.47	R. F. Sanford, *Ap. J.*, **81**, 132, 1935; **114**, 335, 1951
Y Sgr	5.77	J. C. Duncan, *Ap.J.*, **56**, 340, 1922; P. ten Bruggencate, *Harvard Circ.*, No. 351, 1930; this star is under observation at Mount Hamilton
S Sge	8.38	Long period = 1.85 years: this paper

It is appropriate to recall here that variation of the normal velocity is not unknown among other cepheids. Table 7 lists those stars for which the evidence is strongest for changes in the systemic velocity; several other cepheids are known for which the evidence is not so convincing. It may be that, upon further study, long-period variations like that of S Sagittae will be found to be fairly common, since a respectable fraction of the cepheids for which extensive and accurate radial-velocity material is available have turned out to possess velocity variations in addition to that accompanying the pulsation.

Acknowledgment is made of the large amount of valuable advice given by Miss Elizabeth L. Scott, of the Statistical Laboratory of the University of California, in connection with the statistical tests employed in Section II of this paper. The kindness of Dr. I. S. Bowen, director of the Mount Wilson and Palomar Observatories, in making it possible for one of us to obtain the coudé spectrograms discussed in Section III, is greatly appreciated.

THE CEPHEID VARIABLE S SAGITTAE

II. THE EMISSION LINES*

GEORGE H. HERBIG
Lick Observatory, University of California
Received April 28, 1952

ABSTRACT

Emission components have been found in the H and K lines of the cepheid variable S Sagittae (P = 8^d4, spectral type F6 *Ib*–G5 *Ib*); they are present for 1.0–1.6 days on the rising branch of the light-curve. The bright lines are displaced shortward with respect to *Fe* I absorption lines by −68 km/sec. Profiles have been obtained from a Mount Wilson coudé plate; the lines are sharp on their longward edges, but the shortward sides are diffuse. The emission lines shift with the absorption spectrum in the pulsation cycle, and it is clear that they are not associated with the invisible component of the binary system. Intensity measurements on plates of low dispersion (53 A/mm) show that the bright K line appears about 0.6 day after minimum light, increases in strength during the time when it is present, but disappears between 0.5 and 0.9 day before maximum light. These and other facts, as well as a close parallelism with the structure and behavior of the bright *Ca* II lines observed in long-period variables after maximum light, indicate that the observed emissions are only the shortward wings of broad bright lines that originate low in the atmosphere of S Sagittae, the remainder being obliterated by overlying *Ca* II absorption. The shortward displacement of the underlying bright line with respect to the absorption spectrum indicates that the emitting layers are rising. The observed increase of intensity of the emission may be the result of upward motion, except that the weakening of the overlying *Ca* II absorption line must also act to increase the observed intensity of the emission.

I. INTRODUCTION

Apparently the first published announcement of the presence of bright lines of *Ca* II in a classical (Baade's population type I) cepheid variable was that of W. S. Adams and A. H. Joy,[1] who discovered emission in the H and K lines of ζ Geminorum (P = 10^d2). They stated that "emission components on the sides of the strong absorption cores [of H and K] are seen for about two days during the time of rapid change from negative to positive velocity." Joy and R. E. Wilson,[2] in their list of stars with bright H and K, describe the emission in this star as double and broad, with the shortward component considerably stronger than the longward. The shortward H and K emission is present on the upper portion of the rising branch of the light curve and through the time of maximum light. I am indebted to Drs. Joy and Merrill for the opportunity to examine the Mt. Wilson spectrograms of ζ Geminorum.

In 1948, A. Van Hoof[3] discovered emission components in the H and K lines of the cepheid X Cygni (P = 16^d4). These bright lines appeared at two phases during the 16-day cycle: at a "still-stand" on the rising branch of the light-curve, and shortly after maximum light; they were very faint between these phases and were absent at other times. The emission was always displaced shortward by about −85 km/sec with respect to the *Fe* I absorption lines in the spectrum. Joy and Wilson[2] found the emission to be double, with the shortward component wide and much stronger than the longer, but they gave no details.

The star η Aquilae (P = 7^d2) is described by Joy and Wilson as having H and K emission; the bright lines are double, with the shortward component broad and much the stronger of the two. Attention was specifically called to the *Ca* II emission in η Aquilae by T. S. Jacobsen,[4] who observed it on a Victoria plate taken near mid-ascending branch of

* *Contributions from the Lick Observatory*, Ser. II, No. 42.

[1] *Pub. A.A.S.*, **9**, 254, 1939.

[2] *Ap. J.*, **109**, 231, 1949.

[3] *Ap. J.*, **108**, 160, 1948.

[4] *Pub. A.S.P.*, **62**, 269, 1950.

the light-curve. Jacobsen found the emission displaced shortward with respect to the weaker absorption lines in the spectrum by −42 km/sec. The shortward-displaced emission in η Aquilae is well seen on a Lick plate (of dispersion about 20 A/mm) taken by F. L. Whipple on October 16.17, 1930, U.T., at a time when the star was beginning its rise to maximum light. The emission is not mentioned in Whipple's study of this star[5] on a series of spectrograms of which this plate is a member. A Mount Wilson coudé plate of η Aquilae, obtained by the writer on November 9, 1951, shows weak *central* bright lines in H and K as well as the strong shortward emissions.

Emission lines of *Ca* II have been found in the cepheid T Monocerotis ($P = 27^{d}0$) by R. F. Sanford,[2] but no details are available except that the bright lines are wide and are displaced shortward.

Emission lines in the cepheid variable S Sagittae ($P = 8^{d}4$) were found by the writer on a spectrogram (of dispersion 10 A/mm) obtained with the coudé spectrograph of the 100-inch telescope at Mount Wilson on December 1, 1950, U.T. (= JD 2433616.6). This plate was one of a series (listed in Table 1) taken with this instrument with the purpose

TABLE 1

MOUNT WILSON COUDÉ SPECTROGRAMS OF S SAGITTAE

Plate Ce	JD 2433000+	Phase (Days)	Remarks
	1950		
6641	586.583	3.74	
6647	587.642	4.80	
6653	588.620	5.78	Underexposed
6704	615.574	7.58	
6708	616.587	8.60=0.21	
6711	617.617	9.63=1.24	
	1951		
7625	958.617	6.96	Visual region; 2 exposures
7626	958.651	6.99	Visual region; 2 exposures
7631	959.575	7.92	
7632	959.620	7.96	Visual region; 3 exposures

of investigating the possible contribution to the light of the cepheid by a faint companion star.[6] Since the center of the region being studied lay at λ 3780, the plates were overexposed at H and K. This proved to be a fortunate circumstance, because the peak intensity of the emission components of H and K is less than 0.2 of the flux in the continuous spectrum drawn over the absorption line at that wave length, and hence the emissions would not be conspicuous on a spectrogram properly exposed for the continuum in that region. On this plate (Ce 6708), the bright lines are conspicuously asymmetrical. Displaced shortward of the centers of the absorption H and K lines, the emission components are very sharp on their longward edges and reach a maximum intensity very near those edges (see Fig. 3). From their peaks, they fade away gradually shortward and merge with the broad underlying *Ca* II absorption wings. They appear very similar to the bright lines on the spectrograms of X Cygni and η Aquilae reproduced by Van Hoof and by Jacobsen, when allowance is made for the different dispersions in the three cases.

The bright lines in S Sagittae are transitory features. A coudé spectrogram taken 1.0 day before the plate on which they were discovered shows what may be a faint trace of emission in the form of a suspicious abruptness of the shortward side of the absorption

[5] *Lick Obs. Bull.*, **16** (No. 442), 1, 1932.

[6] G. H. Herbig and J. H. Moore, *Ap. J.* [preceding paper], 1952; *Lick Contr.*, Ser. II, No. 41.

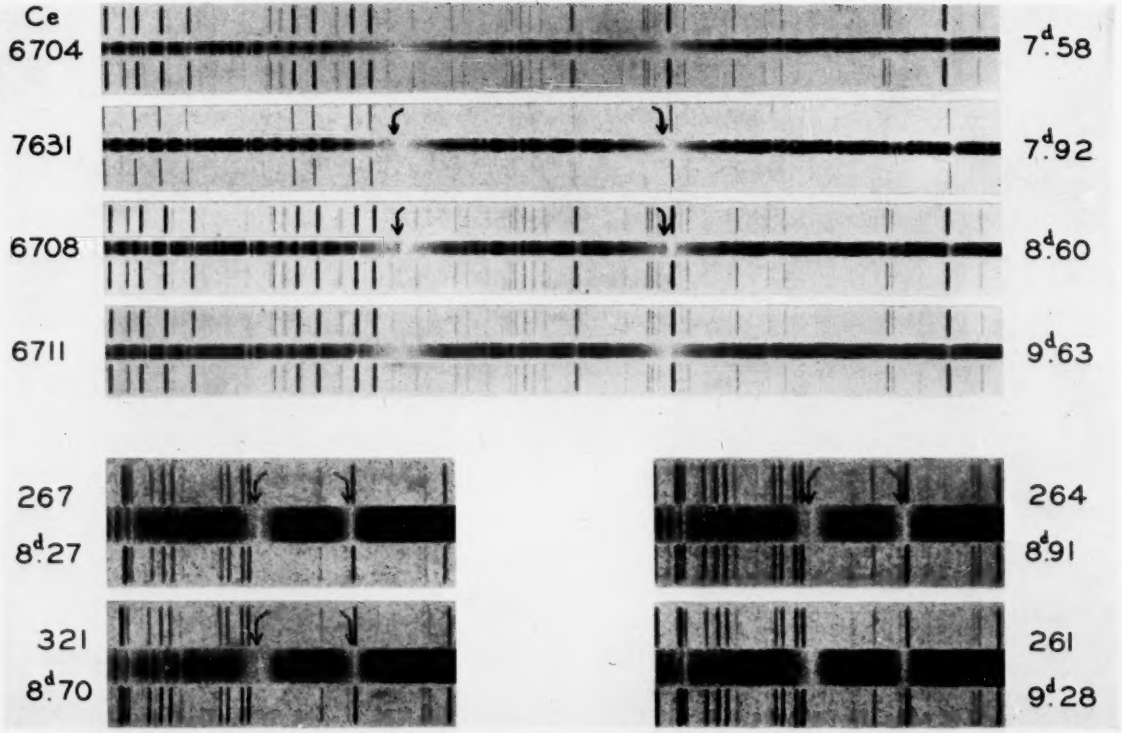

FIG. 1.—The H and K lines of S Sagittae before, during, and after the brightline stage. The four upper spectrograms were obtained with the coudé spectrograph of the 100-inch Mount Wilson telescope. The four low-dispersion plates reproduced below were taken with the Lick 36-inch refractor. Plate numbers and phases are indicated beside each spectrogram; arrows point to the bright H and K lines on those plates where they are present.

core, but a plate exposed 1.0 day after Ce 6708 shows no sign of them. The H and K regions of these three spectrograms are reproduced in Figure 1, as well as another coudé plate, obtained one year later, that shows the emission lines weakly. Figure 2 is a plot of Eggen's photoelectric light-curve of S Sagittae,[7] upon which are marked the phases[8] of all available spectrograms that cover the H and K lines adequately. No *Ca* II emission has been observed with certainty except on those plates exposed between phases 7.9 and 8.9 days, on the rising branch of the light-curve, but weak shortward emission is suspected on two coudé plates (Ce 6641 and 6647) exposed at phases 3.7 and 4.8 days, on the descending branch of the light-curve. All sufficiently exposed plates taken between phases 7.9 and 8.9 days show the bright lines, so that their appearance seems to be a normal phenomenon recurring each cycle. No emission has been found associated with other absorption lines in the region λλ 3600–4000 (the plates are very dense at longer wave

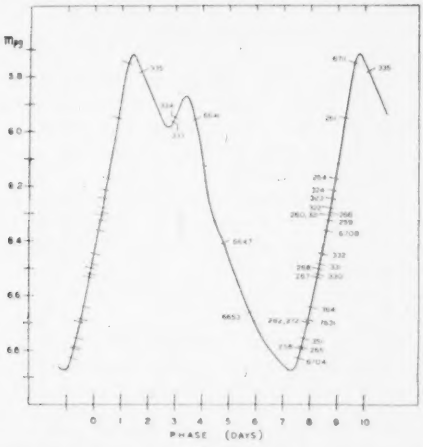

FIG. 2.—The photographic light-curve of S Sagittae, determined photoelectrically by O. J. Eggen. The plate numbers of spectrograms appear next to the lines that cross the light-curve at the phases when the plates were exposed. Three-digit plate numbers correspond to low-dispersion (53 A/mm) Lick spectrograms; four-digit numbers refer to Mount Wilson coudé plates (dispersion 10 A/mm).

lengths). Several coudé exposures (with dispersion 15 A/mm) were made of the visual region at phase 7.96 days, at which time weak emission was present in the H and K lines, but no sign of bright components was seen at *Hα* or the D lines. Two spectrograms of the same region were obtained (with the 36-inch refractor and a two-prism spectrograph with a 16-inch camera, which produces a dispersion of 60 A/mm at the D lines) at phase 8.5 days, when the bright *Ca* II lines are stronger; but the results were again negative.

It was important to obtain a considerable number of additional observations of the emission lines in S Sagittae in order to study their behavior more closely than was possible on the small number of coudé plates. Additional spectrograms for this purpose were obtained at the Lick Observatory with the 36-inch refractor. Because of the low transmission of the 36-inch objective at H and K, it was necessary to employ low dispersion. A 6-inch camera was used, together with two light flint prisms set for minimum deviation

[7] *Ap. J.*, **113**, 367, 1951; *Lick Contr.*, Ser. II, No. 32.

[8] All phases of S Sagittae in this paper are computed from the same formula as was used previously for the "short-period phase":

$$\text{Phase } 0^d000 = \text{JD } 2429090.000 + 8^d3821723E.$$

at λ 3950; this combination gives a dispersion of 53 A/mm at λ 3950. In good seeing, with a slit-width of 0.08 mm, a spectrogram of S Sagittae at photographic magnitude 6.3, widened to 0.3 mm and well-exposed near the centers of H and K, could be obtained with an exposure time of 80 minutes. Eastman II*a*-O plates were used altogether. Twenty-three satisfactory plates were secured with this spectrograph; they are listed in Table 2 and plotted on the light-curve in Figure 2. Some of these spectrograms are shown in Figure 1.

TABLE 2

LICK SPECTROGRAMS OF S SAGITTAE

Plate	JD 2433000+	Phase* (Days)	V_{abs} (Km/Sec)	Predicted V_{abs}† (Km/Sec)	V_{em} (Km/Sec)	Weight of V_{em}	V_{em} *minus* V_{abs} (Km/Sec)	Relative Intensity of K Emission
258	733.016	7.68	.....	.....	.....	.....	.....	<0.01
259	734.009	8.67=0.29	− 8	−16	− 65	2.0	− 57	.035
260	734.044	8.70=0.32	−10	−18	− 75	2.0	− 65	.06
261	743.001	9.28=0.90	.....	.....	.....	.....	.....	< .01
262	750.001	7.90	.....	.....	.....	.....	.....	‡
264	751.017	8.91=0.53	−12	−27	− 72	2.0	− 60	.09
265	774.951	7.70	.....	.....	.....	.....	.....	‡
266	775.971	8.72=0.34	−14	−23	− 64	2.0	− 50	.06
267	783.905	8.27	− 2	−10	− 86	1.5	− 84	.01
268	783.956	8.32	+ 1	−11	−100	1.0	−101	.035
272	791.918	7.90	+ 3	− 7	−104	1.0	− 87	.045
280§	800.909	8.51=0.13	.....	.....	.....	.....	.....	.....
281§	800.949	8.55=0.17	.....	.....	.....	.....	.....	.....
321	901.681	8.70=0.32	− 2	− 8	− 77	2.0	− 75	.09
322	901.734	8.75=0.37	− 9	−10	− 59	2.0	− 50	.055
323	901.789	8.81=0.42	.....	.....	.....	.....	.....	(.015)
324	901.846	8.86=0.48	− 7	−14	− 92	1.3	− 85	.055
330	909.655	8.29	+10	+ 5	− 63	1.0	− 73	.....
331	909.724	8.36	+10	+ 4	− 48	1.3	− 58	.015
332	909.799	8.43=0.05	+ 6	+ 2	− 64	1.0	− 70	.....
333	912.669	2.92	.....	.....	.....	.....	.....	< .01
334	912.742	2.99	−16	−21	.....	.....	.....	< .01
335	936.659	1.76	−18	−22	.....	.....	.....	< .01
351	942.668	7.77	.....	.....	.....	.....	.....	<0.01
364	959.693	8.03	.....	.....	.....	.....	.....	‡

* This is the "short-period phase" of the preceding paper.

† Predicted from the elements of the preceding paper.

‡ The spectrogram is underexposed, and hence weak emission would not be visible.

§ These two spectrograms cover the visual region.

II. THE LINE DISPLACEMENTS

The positions of the intensity peaks of the asymmetrical emission lines in H and K were measured on Ce 6708; the traces of emission seen on two other coudé plates were too faint for reliable measurement. The maximum of intensity on Ce 6708 was displaced shortward by −48 km/sec with respect to the mean of a group of twenty-two relatively unblended *Fe* I-lines[9] in the interval λλ 3820–3983. The centers of gravity of the emission lines, which would be measured on spectrograms of low dispersion, lie roughly 10 km/sec still farther shortward.

The bright lines were measured also on thirteen spectrograms of the low-dispersion

[9] The radial velocity of S Sagittae was also derived from these measurements. For details and results see the preceding paper (n. 6).

series obtained with the 36-inch refractor; the results from the individual plates are given in Table 2. The absorption-line velocity of S Sagittae was measured on these plates by the use of five lines, mainly due to *Fe* I, chosen from those measured on the coudé spectrograms. These lines have the wave lengths λλ 3895.66, 3903.00, 3922.91, 3927.92, and 3961.46. The wave lengths of the second and fifth lines are not the laboratory values but were obtained from the coudé measurements. The absorption-line velocities also are contained in Table 2. A comparison with the velocities of S Sagittae predicted from the elements of the preceding paper shows immediately that the low-dispersion velocities are always algebraically more positive than predicted. The mean correction required to reduce these velocities to the system of the Mills three-prism spectrograph, for the seven plates taken between March and May, 1951 (before JD 2433795), is -10 ± 1 (p.e.) km/sec; for the eight plates taken in September and October (after JD 2433795), the correction is -5 ± 1 (p.e.) km/sec. It probably is significant that, in the interval between these two groups of observations, certain mechanical modifications were made in the collimating arrangements of the spectrograph. These modifications, or the accompanying disturbances of the instrument apparently affected the amount of the systematic correction; it may be that the error arises from some misalignment of the spectrograph. The explanation cannot be that the collimation was faulty, since that adjustment was checked in May and found to be satisfactory; the spectrograph was recollimated in August after the modifications were completed. The fact that several plates of bright supergiants, taken during those periods with the same adjustments and measured in the same way, require a similar correction to their velocities is evidence that the error cannot be a property of S Sagittae alone. In any case, the absorption-line velocities in Table 2 require these corrections, and it is assumed that the emission-line velocities need them as well. If this assumption is correct, the presence of the systematic correction is of no consequence in the determination of the displacement of the bright H and K lines with respect to the absorption spectrum.

The following conclusions can be drawn from the measurements of line displacement: (1) There is no convincing evidence of any variation of the relative displacement of bright and dark lines through the time when the emission is present, although the dispersion of the measured emission-line velocities is rather large and a moderate change could well be masked by this scatter. The question is an important one, and it should be studied on plates of considerably higher dispersion than those available for this part of the investigation. It is clear, however, that, at least to a first approximation, the emission lines shift together with the absorption spectrum along the steep descending branch of the velocity-curve. The weighted mean value of the shortward displacement of the centers of gravity of bright H and K with respect to the *Fe* I lines is -68 ± 3 (p.e.) km/sec, if one combines the values from all the plates on which the lines are seen. (2) The data show clearly that the emitting region shares the motion of the cepheid in its long-period orbit: there is nothing in the velocities of H and K to indicate any association with the fainter component of the binary system.

III. THE EMISSION-LINE PROFILES AND INTENSITIES

The profiles of the absorption H and K lines on four coudé plates (Ce 6704, 6708, 6711, and 7631) have been derived from tracings made with the modified Moll microphotometer of the Lick Observatory. The first three plates were properly exposed for somewhat shorter wave lengths, as already mentioned; their calibration spectra, as well, were of proper density at λλ 3700–3800 but were overexposed at H and K. Consequently, the toes of the characteristic curves of these three spectrograms were not defined, and so the densities of the deepest portions of the profiles of absorption H and K could not be converted into relative fluxes. If one defines r as F/F_c, the ratio of the flux in the line at wave length λ to the flux at λ in the hypothetical undisturbed continuum drawn over the

line, then this cutoff of the lower end of the characteristic curve has the effect of leaving undetermined that part of the profile with $r < 0.08$–0.10, depending upon the spectrogram in question. The profiles of the K line derived from the first three plates mentioned above are shown in Figure 3; the cores are not drawn in for the reason just mentioned. No allowance has been made in these profiles for instrumental broadening or for scattered light in the spectrograph. The profiles from Ce 6704 and 6711 are entitled to less weight than that from Ce 6708, since those two spectrograms were not so uniformly widened as the latter, and consequently a shorter slit had to be used when they were traced in the microphotometer, with increased grain fluctuations. The profiles of the H line reveal little that is not present at K, and so are not shown.

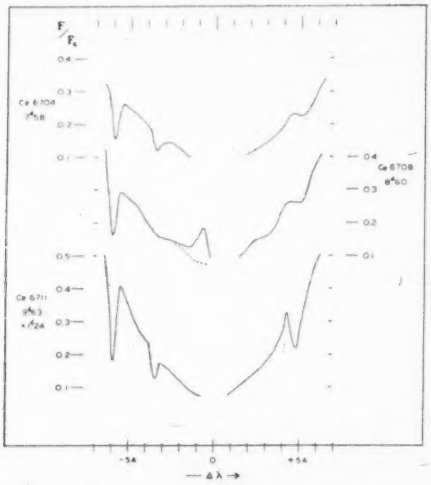

FIG. 3.—The profile of the K line of *Ca* II in S Sagittae: just after minimum light (from plate Ce 6704), midway up the rising branch of the light-curve (Ce 6708), and just before maximum light (Ce 6711). These profiles were derived from the first, third, and fourth coudé plates shown in Fig. 1. The phase when each spectrogram was taken is marked under the plate number. The core of the line is not shown because of inadequate plate calibration for the low densities, as explained in the text. The hypothetical contour of the absorption line, if emission was absent, is indicated by the dashed line in the second profile. The unit of the ordinates is the flux in the continuum drawn over the absorption line.

The profiles show that the bright lines on Ce 6708 are, in reality, not very intense: their peak r's are only 0.18 for both H and K; allowance for instrumental broadening would, of course, increase these values. This intensity is less than one might guess from a visual inspection of the plates. The discrepancy is due to the great extent of the wings of the H and K absorption lines, which the eye fails to appreciate.

As S Sagittae rises toward maximum light, the H and K absorption lines become weaker; because of saturation in the cores, this effect is most apparent in the wings and is strikingly shown by the profiles in Figure 3. In order to free the bright lines from the contribution of the underlying absorption wing, it is necessary to obtain the absorption profile from other spectrograms taken at near-by phases when the emission lines are absent. (The reflected profile of the other wing of the line on the same plate was not used, because it was not certain that weak emission was absent to longward. It was later found that there was no certain evidence of longward emission, so that this caution was unnecessary for the K line. In the H line, however, it would be unsafe to use the reflected profile

because of the contribution of $H\epsilon$.) The phase differences between the plates were used to obtain the profiles of the undisturbed absorption lines on Ce 6708 and 7631 by simple linear interpolation between those of Ce 6704 and those of 6711. The faint emission suspected on Ce 6704 was too faint to affect the results. This hypothetical profile for the K line is indicated by a dashed line beneath the emission in Figure 3. The results of the subtraction of this hypothetical absorption profile from the absorption plus emission profiles of Ce 6708 are shown in Figure 4. The approximate nature of the method of in-

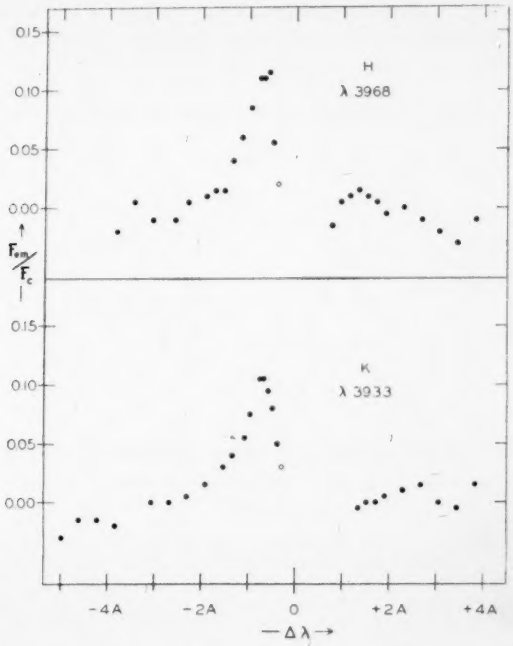

FIG. 4.—The profiles of the H and K emission lines on Ce 6704, obtained by subtracting from the observed profiles the contribution of the underlying absorption lines. The unit of the ordinates is, as in Fig. 4, the flux at that wave length in the continuum drawn over the absorption lines. The open circle represents a point of low weight.

terpolation, combined with errors in the profiles, has resulted in a zero-point error, probably variable across the diagram, of as much as 0.02 in F (emission)$/F_c$.

The profiles of the bright lines in Figure 4 resemble the self-reversed lines observed in laboratory sources having a large temperature gradient. They suggest that in S Sagittae the emission lines originate below the level where the cores of the H and K lines reach a large optical thickness, but not necessarily below all the levels in which the wings are formed. The sharp longward edge of the emission is, in this picture, the result of the concealment of all but the shortward wing of a symmetrical emission line by the powerful absorption in the overlying cores of H and K. It is clear that, if the cores of the H and K absorption lines are asymmetrical with respect to the wings, the observations show only that the emission is displaced shortward relative to the cores.[10] That is, the emitting

[10] The asymmetrical self-reversal sometimes observed in the laboratory is believed to be due to a differential pressure effect (see R. D. Cowan and G. H. Dieke, *Rev. Mod. Phys.*, **20**, 451, 1948).

region must be rising with respect to the higher layers in which the line centers are formed; how it is moving with respect to the deeper layers in which the H and K wings originate is unknown. Adams and Joy[1] have actually shown for ζ Geminorum that this asymmetry must exist, because the velocity-curve determined by them from the centers of H and K differs in shape and phase from that defined by weaker lines. It is therefore reasonable to expect a similar effect in S Sagittae. The present coudé material is not well suited for the detection of such an effect, since only four plates, adequately exposed for the cores of the *Ca* II lines, remain after those with emission are excluded. Measurement of these four plates indicates that discrepancies of as much as 10 km/sec exist between the two kinds of line, but the variation of this quantity with phase cannot be determined from such scanty material.

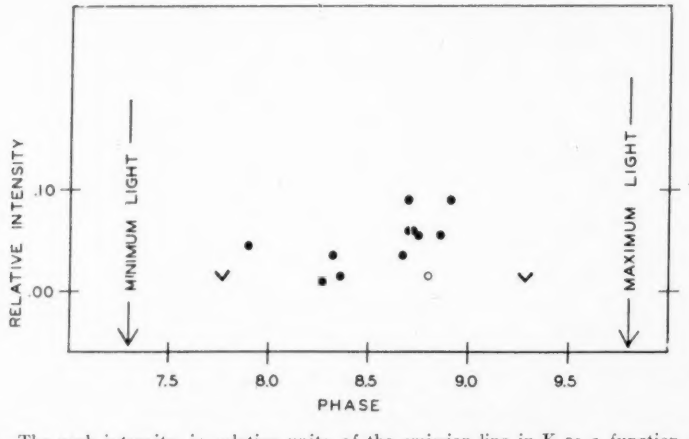

FIG. 5.—The peak intensity, in relative units, of the emission line in K as a function of phase, determined from the Lick low-dispersion spectrograms. The unit is a variable one, the flux at that wave length in the continuum drawn over the absorption K line at the phase when each plate was taken. The open circle represents the intensity on a plate on which the photometry was confused by an emulsion flaw. The carets indicate plates on which the emission in the K line is invisible.

The intensities of the emission lines were obtained also from the low-dispersion plates but a simplified photometric procedure was employed, in which the longward wing of the absorption line was used as a scale of intensity. Microphotometer tracings permitted selection of the point in the wing at which the deflection was equal to that at the peak of the emission line, as blurred by the instrumental profile. The wave length of this point was then determined from a Hartmann formula fitted to near-by *Fe* I lines, and the value of F/F_c for this wave length and the proper phase was then read from the curves of that quantity constructed from the profiles determined from the four coudé plates. This procedure gives the value of F (emission + absorption)$/F_c$ for the bright line; a constant 0.08 was subtracted from this sum in order to free it from the contribution of the background. Only the intensity of the K line was determined, for several reasons: the emission in H occurs at a point where the density of the absorption wing is changing very rapidly, which makes photometry with low dispersion very difficult; the longward wing of H is confused with $H\epsilon$, whose variation with phase is opposite to that of H, so that the variation of the combined F/F_c is more complicated than that at K; there is a possibility that weak emission is present on the longward wing of H.

The relative intensities of the emission line in K, obtained in this way, are listed in

Table 2 and are plotted in Figure 5. The unit is the flux at λ 3933 in the continuum drawn over the line. Since this unit changes in value as the star varies in light and color, it is necessary to remove this effect in order to obtain the K intensities on an absolute basis. This elimination was accomplished by use of the colors and magnitudes[7] of S Sagittae and the effective wave lengths[11] determined by Eggen. The Planck formula, with the proper color temperature calculated from the photoelectric colors, gives the ratio of fluxes at λ 3933 and at the effective wave length of the Pg_p magnitude at any phase. The light-curve yields the variation of flux at the effective wave length, so the correction factor that reduces relative intensities to absolute intensities follows immediately. The unit adopted for the absolute intensities is the flux in the (undisturbed) continuum at λ 3933 when the variable is at phase 7.7 days, not long after minimum light. In Figure 6

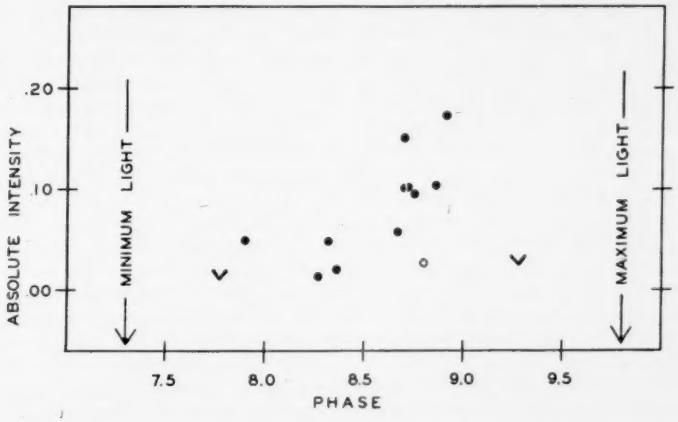

FIG. 6.—The peak intensity, in an absolute unit, of the emission line in K as a function of phase, determined from the Lick spectrograms. The points are the same as those plotted in Fig. 5, but they are now expressed in a unit that is independent of the variation in magnitude and color of the variable. The unit is the flux in the hypothetical continuum at λ 3933 when the variable is at phase 7.7 days. The open circle represents the intensity on a plate of low weight. The carets indicate plates on which the emission is invisible.

are plotted the absolute intensities obtained in this way. The carets at each end of Figures 5 and 6 indicate the nearest plates on which the emission lines were not visible; it is estimated that the intensity of the bright K line at those times must have been less than that indicated by the carets. The scatter of the points in Figures 5 and 6 is not believed to be real; photometric inaccuracies may be expected to cause accidental errors of that magnitude.

Figures 5 and 6 show that the bright line in K makes its appearance, on the Lick low-dispersion spectrograms, about 0.6 day after (photographic) minimum light; its presence is suspected, however, on a coudé plate exposed 0.28 day after minimum. It grows steadily stronger, at least until phase 8.9 days, but it has disappeared by phase 9.3 days, or 0.5 day before maximum light. The increase in intensity takes place both with respect to the continuum and in absolute units, although the rise in brightness and color temperature with phase across Figures 5 and 6 makes this increase more marked in the latter case. The emission in the K line is, therefore, present on the Lick spectrograms for at

[11] *Ap. J.*, 111, 68, 1950; *Lick Contr.*, Ser. II, No. 25.

least 1.0 day, but for less than 1.6 days on the rising branch of the light-curve. It is unfortunate that no observations were obtained between phases 8.91 and 9.28 days; attempts to fill this gap failed repeatedly on account of bad weather.

IV. DISCUSSION

It has already been mentioned that the structure of the bright *Ca* II lines in S Sagittae strongly suggests that they are the result of the mutilation by overlying absorption of shortward-displaced emission lines that originate low in the atmosphere. This proposal can be strengthened by an interesting comparison that is possible between the bright H and K lines in S Sagittae and those which appear in the shortward wings of the H and K lines in long-period variables about $0.1P$ after maximum light. The best data on these latter stars are those obtained with high dispersion by P. W. Merrill on the Me-type variables R Hydrae[12] and R Leonis,[13] the Me star with S-type characteristics χ Cygni,[14] and the Se variable R Andromedae.[15] The following points of similarity are to be noted: (1) Structurally, the bright H and K lines in the long-period variables closely resemble those in S Sagittae: in both kinds of star, the bright lines are diffuse, are displaced shortward, and are sharp on the longward sides. (2) The bright lines in S Sagittae become stronger as the phase advances. This is certainly true for the relative intensities in the long-period variables, but it is not known how the absolute intensities behave in those stars. (3) Merrill has commented on the fact that in the red variables the emission in H is stronger than in K, which is opposite to what one would expect from the relative transition probabilities. This is an exaggeration of the effect found in S Sagittae, where the two lines have equal peak intensities. (4) Finally, Merrill's measurements show that the shortward displacement of the bright component of K is always greater than that of the line in H and that this difference decreases as the variables become fainter and the bright lines stronger. In S Sagittae the eight low-dispersion plates on which both lines are well measurable indicate a shortward displacement of bright K with respect to H of 4.5 ± 1.6 (p.e.) km/sec, a discrepancy so small that it might not be taken too seriously if it were not for the parallelism with the long-period variables. No change in the displacement of the bright lines in S Sagittae, with respect to the absorption spectrum, has been detected in the low-dispersion velocities reported in this paper. This is only what one would expect if the change in displacement, *per day*, was no larger in S Sagittae than in the long-period variables, for the bright lines in the cepheid are measurable for only one day while those in the late-type variables studied by Merrill were observable for 50 to 100 times as long, and hence a small daily change in the latter stars has a greater opportunity to accumulate.

There is strong evidence (quite independent of the bright lines in H and K) that, in long-period variables, the regions responsible for the bright lines lie below the layers that produce the absorption spectrum and that, as the cycle advances, the emitting regions effectively rise up through the absorbing layers. In the case of the *Ca* II lines, the effect of actual change in the relative position of the two layers is entangled with the decrease of optical depth in the absorption line due to the diminishing ionization of calcium as the stars become fainter. (In S Sagittae, the absorption lines weaken as the star becomes *brighter*.) Both processes act to diminish the effective amount of self-absorption by the overlying layers, but there is no need to distinguish the two effects for the present purpose. Now it is striking that every one of the four properties of the bright *Ca* II lines in the long-period variables that are mentioned in the previous paragraph can be understood in terms of the phenomenon of self-absorption (or in terms of a decreasing amount

[12] *Ap. J.*, **103**, 6, 1946; see esp. Pl. I and p. 12.

[13] *Ap. J.*, **103**, 275, 1946; see esp. Pl. XII and p. 287.

[14] *Ap. J.*, **106**, 274, 1947; see esp. Fig. 2 and p. 282.

[15] *Ap. J.*, **105**, 360, 1947; see esp. Fig. 6 and pp. 372–373.

of self-absorption), a process whose presence is readily understandable if the relative position of the emitting and absorbing regions is that indicated at the beginning of this paragraph.

The fact that each of these four properties of the *Ca* II emission lines in the red variables is shared by the bright lines of S Sagittae (or, if absent, its absence is understandable) encourages one to think that a similar phenomenon is taking place in both cases: namely, at very definite phases in the light-cycles of the two kinds of star, high-temperature material appears low in the atmosphere and subsequently seems to move upward, both as a result of actual relative movement as well as diminishing absorption at higher levels.

Despite this similarity between the *Ca* II emission in S Sagittae—and the observations of bright H and K in other cepheids demonstrate that the presence of these lines may be of rather common occurrence in such stars—and the long-period variables, there are important differences between the phenomena in the two kinds of objects. In the late-type variables the emission lines are present on the descending branch of the light-curve; in the cepheids they have been observed on the ascending branch and through maximum, in different stars. Furthermore, in the long-period variables the bright lines in H and K seem to be stronger than in S Sagittae, and they are accompanied by many emission lines of other elements; in the cepheid, no other bright lines have been found.

The self-absorption process may also account, in an entirely natural way, for a long-standing anomaly in the spectra of the Me-type variables. Merrill has noted[16] that the infrared *Ca* II triplet (λλ 8498, 8542, 8662) appears in emission in the long-period variables *o* Ceti and R Hydrae around the time of maximum light, while H and K remain in absorption, despite the fact that the two multiplets have common upper levels. This apparent anomaly may come about in the following way: since the upper levels are the same, the ratios of the numbers of downward transitions contributing to the two multiplets are fixed by the transition probabilities, and they are independent of the excitation. But the emission lines are formed low in the atmosphere and hence suffer absorption by overlying *Ca* II vapors, and for this process the situation is different for the infrared multiplet than for the H and K lines. H and K have the ground state, 4^2S, as a lower level, while the infrared triplet arises, in absorption, from 3^2D, which has an excitation potential of 1.69 volts. At the temperature of *o* Ceti at maximum light, about 2900°, the populations of $3^2D_{5/2}$ and $3^2D_{3/2}$ in thermodynamic equilibrium will be 3×10^{-3} and 2×10^{-3}, respectively, that of the ground state. The *f*-value of the K line is about thirteen times that of λ 8542, the strongest line of the infrared triplet,[17] which causes the effective number of atoms contributing to λ 8542 in absorption to be about 2×10^{-4} as many as are effective in the K line. These facts show that the conditions for the appearance of emission, when self-absorption is present, are considerably more favorable for the infrared triplet than for H and K, although the violet lines would be much the stronger in emission if self-absorption were absent. Corroboratory evidence for the interpretation in terms of different self-absorption is furnished by the appearance of infrared emission much earlier in the cycle than H and K, and by the observation that in R Hydrae, at about the same phase, the shortward displacements of the infrared emission lines are considerably less than those of the emission components in H and K.

This inversion of the normal intensities of emission lines formed in the presence of self-absorption, while qualitatively plausible under the conditions described above, is best understood if an idealized model of such a stellar atmosphere is examined; the extreme example of a long-period variable near maximum light will be used for purposes of illustration. Consider a homogeneous layer of gas producing an emission spectrum; within

[16] *Ap. J.*, **79**, 183, 1934; *Trans. I.A.U.*, **6**, 443, 1938.

[17] D. R. Hartree and W. Hartree, *Proc. R. Soc., London, A*, **164**, 184, 1938, give the total *f*-values for these multiplets. The LS-coupling intensity rules enable one to compute the fraction contributed by each transition within the multiplets.

this layer there exists local thermodynamic equilibrium characterized by a temperature T_E. Let this emitting region lie beneath a cooler layer which acts only to extinguish the energy passing through it: there is assumed to be no appreciable re-emission or scattering of energy back into the beam by this material. Local thermodynamic equilibrium exists in this layer as well, but at a temperature T_A, where $T_A < T_E$. If t_λ denotes the optical depth at any wave length in the emitting layer, then the profile of an emission line produced in that layer will be given by

$$F_\lambda = B_\lambda (T_E) \cdot [1 - e^{-t_\lambda}], \tag{1}$$

where $B_\lambda(T_E)$ represents the Planck function with temperature T_E at λ. At that wave length, the extinction produced by the absorbing layer is

$$e^{-\tau_\lambda}, \tag{2}$$

where τ_λ is the optical depth at λ in the absorbing layer, so that the profile of the emission line, as observed from outside the star, is the result of multiplying these two expressions. Now consider an atom having three energy levels: the ground level 0, a somewhat higher state 1, and a high level 2. We are interested in the ratio of intensities, at corresponding points[18] in the two lines, of the lines resulting from the transitions $0 \leftrightarrow 2$ and $1 \leftrightarrow 2$ in the presence of self-absorption. If

$$I_\lambda = \frac{F_\lambda}{B_\lambda (T_E)}, \tag{3}$$

and if the λ subscripts are now dropped but with the understanding that the results still refer to definite points in each line, then

$$\frac{I_{21}}{I_{20}} = \frac{1 - e^{-t_{21}}}{1 - e^{-t_{20}}} \cdot \frac{e^{-\tau_{21}}}{e^{-\tau_{20}}}. \tag{4}$$

Now, if it is permissible to write

$$\frac{t_{21}}{t_{20}} = \frac{\lambda_{21}}{\lambda_{20}} \frac{f_{21}}{f_{20}} \frac{g_1}{g_0} e^{-\epsilon_{10}/kT_E} \tag{5}$$

and

$$\frac{\tau_{21}}{\tau_{20}} = \frac{\lambda_{21}}{\lambda_{20}} \frac{f_{21}}{f_{20}} \frac{g_1}{g_0} e^{-\epsilon_{10}/kT_A}, \tag{6}$$

where the f's are the oscillator strengths, the g's are the statistical weights, and ϵ_{10} is the energy difference in ergs between states 0 and 1, we may compute from equation (4) the ratio of intensities to be expected under a given set of conditions. Consider the case where the transition $0 \leftrightarrow 2$ represents the K line of *Ca* II and the transition $1 \leftrightarrow 2$ produces λ 8542. In the case of a long-period variable, $T_A = 2900°$ near maximum light. T_E is unknown; it will be assumed to be 10,000°. The Boltzmann terms in equations (5) and (6) are then 0.42 and 3.5×10^{-3}, respectively. The oscillator strengths are $f_{20} = f_{\lambda\,3933} = 0.8$ and $f_{21} = f_{\lambda\,8542} = 0.06$. The values of $I_{\lambda\,8542}/I_{\lambda\,3933}$ that result from the use of these parameters in equation (4) are unrealistic in the sense that the intensities within each line are expressed in units of the value of the Planck function for $T_E = 10{,}000°$ at the lines. In practice, spectrograms on which the intensities of these lines were to be compared would be given exposures such that the continuous spectrum at the two wave lengths would appear equally strong on both plates. Since the distribution of energy in the continuous spectrum is roughly that of a black body at 2900°, the units of equation

[18] By "corresponding points" is meant points whose distances from the line centers are the same when measured in units of the Doppler width appropriate to each line.

(4) should be changed from B_λ ($T = 10{,}000°$) to B_λ ($T = 2900°$) for comparison with observation. This has been done for the values given in Table 3, which contains intensity ratios obtained from equation (4) for various values of $t_{\lambda\ 3933}$ and $\tau_{\lambda\ 3933}$.

The values given in the table show how the overlying layer, by producing an increased weakening of the K line while leaving λ 8542 little affected, can actually invert the expected relative intensity at corresponding points in the two lines. The foregoing is not, however, a demonstration that the peak intensities or the total intensities of actual lines will be inverted; comparison of such a theory with observation must await a more detailed development. If an accurate theory bears out the present suggestions, it will

TABLE 3

COMPUTED VALUES OF THE RATIO OF $F_{\lambda\ 8542}/B_{\lambda\ 8542}$ (T_A) TO $F_{\lambda\ 3933}/B_{\lambda\ 3933}$ (T_A) AT CORRESPONDING DISTANCES FROM THE CENTER OF EACH LINE, AS A FUNCTION OF OPTICAL DEPTH IN THE EMITTING LAYER ($t_{\lambda\ 3933}$) AND IN THE ABSORBING LAYER ($\tau_{\lambda\ 3933}$)

$t_{\lambda\ 3933}$	$\tau_{\lambda\ 3933}$					
	0.0	0.5	1.0	2.0	5.0	7.5
0.0*	0.007	0.011	0.018	0.048	0.96	11.7
0.5	.008	.013	.022	.060	1.2	15
1.0	.010	.016	.027	.074	1.5	18
2.0	.014	.023	.038	.104	2.1	25
5.0	.028	.046	.076	.20	4.1	50
20	.071	.12	.19	.52	10.5	128
∞	0.095	0.16	0.26	0.70	14	172

* The line for $t_{\lambda\ 3933} = 0.0$ contains the limiting values as $t_{\lambda\ 3933} \to 0$.

eliminate the need for an explanation of the behavior of the violet and infrared calcium lines in terms of a fluorescent process, such as that suggested by A. B. Wyse.[19]

It may be appropriate to mention here that the bright *Ca* II lines observed in M-type dwarfs seem to have a different origin from those in the M giant long-period variables. Three pieces of evidence indicate that the emission in dMe stars does not originate below the absorption spectrum: first, the bright *Hβ* line in late-type dMe stars is not suppressed by *TiO* absorption as in the gMe variables; second, the bright *Ca* II lines in the dwarfs give the same radial velocity as the absorption lines; third, the bright *Hε* line in the dwarfs is essentially unaffected by its superposition upon the H absorption line of *Ca* II.

I am indebted to Dr. I. S. Bowen, director of the Mount Wilson and Palomar Observatories, for the opportunity to use the 100-inch telescope in order to obtain the coudé spectrograms described in this paper, and to Dr. M. Schwarzschild for a helpful discussion.

[19] *Pub. A.S.P.*, **53**, 184, 1941.

A PHOTOELECTRIC LIGHT-CURVE OF DY PEG

BRAULIO IRIARTE
Yerkes Observatory
July 14, 1952

The variable star DY Pegasi has a period of only 105 minutes. Its spectral type varies from A3 at maximum to A9 at minimum light.[1] The light-curve is typical of its class, with a rapid increase in brightness of approximately 0.7 mag. photographically and a slower decline.

In the testing of observing techniques in 1948, Hiltner obtained two runs of this star. The runs were continuous in one color except for occasional interruptions for the observation of a comparison star. The receiving element consisted of an RCA 1P21 with a Corning 3385 filter. The effective wave length is near λ 5500. The output of the cell was delivered to a DC amplifier, which, in turn, actuated a Brown recorder. In the reductions, the

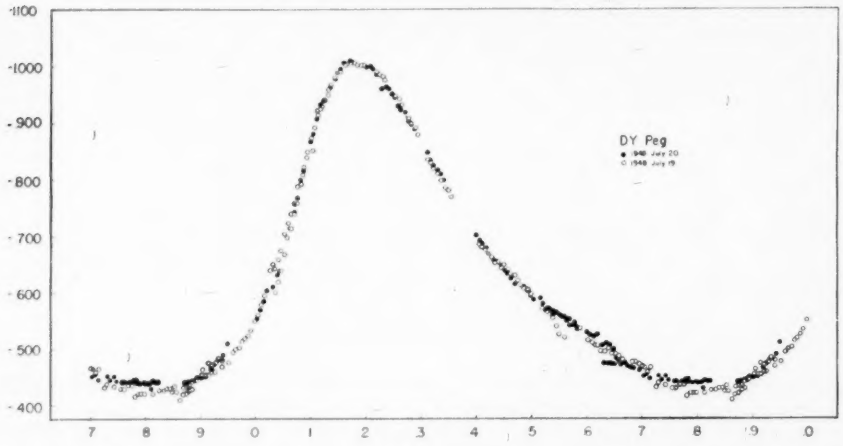

FIG. 1

continuous records were divided into intervals of approximately 40 seconds, and the deflections were read for these intervals. The deflections for a comparison star were plotted against time, and each deflection of DY Peg was compared with the comparison star, assuming a linear interpolation between comparison-star observations. The interval between comparison observations varied from 15 to 45 minutes. No correction for extinction was required because of the nearness of the comparison star to the variable and similarity in color.

The observations are recorded in Tables 1 and 2. The first column gives the Julian Day, the second column the phase computed from the equation given by Steinmetz:[2]

$$\text{Phase} = (\text{JD} - 2430000) / 13.712468.$$

The third column gives the difference in magnitude of DY Peg and that of the comparison star. These observations are plotted in Figure 1. The amplitude at this effective wave length is 0.58 mag. The light-curve does not seem to repeat in all details, especially near minimum light, where the scatter in the observations appears greater than at maximum. The median magnitude on the rising branch occurred at phase 0.06, in good agreement with the ephemeris.

[1] W. P. Bidelman, *Ap. J.*, **106**, 135, 1947. [2] C. H. D. Steinmetz, *B.A.N.*, **10**, 178, 1946.

TABLE 1

Photometric Observations of DY Peg

1948 July 19

JD (Helio.) 2430000+	Phase	Δ Mag	JD (Helio.) 2430000+	Phase	Δ Mag	JD (Helio.) 2430000+	Phase	Δ Mag
2751.8552	.726	-0.431	2751.8961	.287	-0.892	2751.9330	.793	-0.420
.8555	.730	-0.437	.8965	.292	-0.880	.9334	.798	-0.420
.8564	.743	-0.434	.8978	.310	-0.836	.9339	.813	-0.419
.8573	.755	-0.429	.8982	.316	-0.829	.9371	.849	-0.423
.8579	.763	-0.429	.8956	.321	-0.819	.9375	.855	-0.423
.8582	.767	-0.436	.8991	.328	-0.810	.9380	.862	-0.410
.8588	.776	-0.436	.8996	.335	-0.798	.9384	.867	-0.417
.8624	.825	-0.426	.9000	.343	-0.786	.9389	.874	-0.421
.8630	.833	-0.426	.9005	.347	-0.781	.9393	.879	-0.426
.8634	.839	-0.429	.9009	.353	-0.769	.9398	.886	-0.439
.8639	.845	-0.429	.9046	.404	-0.685	.9403	.893	-0.444
.8644	.852	-0.434	.9050	.409	-0.681	.9411	.904	-0.463
.8656	.869	-0.431	.9055	.416	-0.675	.9415	.910	-0.453
.8660	.874	-0.434	.9059	.422	-0.668	.9419	.915	-0.474
.8664	.880	-0.436	.9063	.427	-0.662	.9423	.921	-0.471
.8668	.885	-0.441	.9067	.433	-0.652	.9428	.927	-0.476
.8673	.892	-0.444	.9011	.438	-0.654	.9432	.933	-0.483
.8681	.903	-0.454	.9076	.445	-0.643	.9437	.940	-0.478
.8685	.909	-0.450	.9080	.450	-0.648	.9445	.951	-0.476
.8690	.915	-0.453	.9084	.456	-0.639	.9450	.958	-0.494
.8693	.920	-0.457	.9088	.461	-0.631	.9454	.963	-0.499
.8698	.926	-0.459	.9093	.468	-0.627	.9459	.970	-0.502
.8707	.939	-0.467	.9097	.474	-0.619	.9463	.975	-0.513
.8750	.998	-0.549	.9102	.480	-0.611	.9467	.981	-0.518
.8754	.003	-0.561	.9106	.486	-0.605	.9471	.986	-0.524
.8759	.010	-0.579	.9111	.493	-0.603	.9475	.991	-0.533
.8763	.016	-0.596	.9114	.497	-0.595	.9506	.034	-0.601
.8770	.025	-0.640	.9130	.519	-0.570	.9510	.040	-0.619
.8776	.033	-0.643	.9136	.527	-0.564	.9514	.045	-0.639
.8780	.039	-0.659	.9140	.532	-0.560	.9518	.051	-0.668
.8784	.044	-0.675	.9144	.538	-0.553	.9522	.056	-0.697
.8789	.051	-0.705	.9149	.545	-0.538	.9526	.062	-0.714
.8793	.057	-0.724	.9152	.549	-0.524	.9530	.067	-0.740
.8798	.063	-0.745	.9159	.559	-0.517	.9534	.073	-0.757
.8802	.069	-0.758	.9191	.602	-0.513	.9539	.080	-0.792
.8806	.074	-0.787	.9196	.609	-0.509	.9543	.085	-0.822
.8812	.083	-0.807	.9200	.615	-0.504	.9548	.091	-0.839
.8819	.092	-0.849	.9204	.620	-0.505	.9555	.102	-0.852
.8824	.099	-0.874	.9207	.624	-0.494	.9561	.110	-0.922
.8828	.105	-0.893	.9213	.633	-0.494	.9565	.115	-0.925
.8833	.111	-0.914	.9218	.639	-0.499	.9470	.122	-0.944
.8837	.117	-0.929	.9222	.645	-0.490	.9575	.129	-0.959
.8841	.122	-0.941	.9227	.652	-0.489	.9579	.134	-0.967
.8845	.128	-0.951	.9231	.657	-0.486	.9583	.140	-0.981
.8909	.216	-0.991	.9236	.664	-0.479	.9587	.145	-0.987
.8913	.221	-0.986	.9249	.682	-0.476	.9591	.151	-0.991
.8917	.227	-0.983	.9259	.696	-0.472	.9596	.158	-1.002
.8920	.231	-0.976	.9262	.700	-0.467	.9600	.163	-1.005
.8935	.251	-0.947	.9266	.705	-0.464	.9604	.169	-1.006
.8939	.257	-0.943	.9270	.711	-0.457	.9609	.176	-1.006
.8943	.262	-0.932	.9274	.716	-0.464	.9613	.181	-1.002
.8947	.268	-0.919	.9322	.782	-0.416	.9617	.187	-1.002
.8952	.275	-0.908	2751.9326	.788	-0.420	2751.9621	.192	-1.002
2751.8956	.280	-0.900						

TABLE 2

Photometric Observations of DY Peg

1948 July 20

JD (Helio.) 2430000+	Phase	Δ Mag	JD (Helio.) 2430000+	Phase	Δ Mag	JD (Helio.) 2430000+	Phase	Δ Mag
2752.8608	.516	-0.587	2752.9963	.002	-0.553	2752.9260	.410	-0.686
.8612	.521	-0.577	.8967	.008	-0.570	.9265	.417	-0.679
.8618	.529	-0.570	.8972	.014	-0.586	.9269	.422	-0.667
.8021	.533	-0.563	.8976	.020	-0.604	.9274	.429	-0.658
.8626	.540	-0.560	.8984	.031	-0.611	.9277	.433	-0.655
.8633	.550	-0.558	.8988	.037	-0.632	.9286	.445	-0.646
.8639	.558	-0.556	.8992	.042	-0.639	.9290	.451	-0.636
.8644	.565	-0.551	.9006	.061	-0.714	.9294	.456	-0.631
.8648	.570	-0.551	.9010	.067	-0.743	.9298	.462	-0.623
.8653	.577	-0.544	.9015	.074	-0.768	.9303	.469	-0.613
.8657	.583	-0.533	.9018	.079	-0.799	.9312	.481	-0.610
.8661	.588	-0.533	.9023	.085	-0.816	.9316	.486	-0.608
.8669	.599	-0.527	.9032	.097	-0.867	.9320	.492	-0.600
.8674	.606	-0.523	.9036	.103	-0.882	.9324	.497	-0.593
.8678	.612	-0.520	.9041	.109	-0.907	.9328	.503	-0.586
.8682	.617	-0.524	.9045	.115	-0.932	.9345	.526	-0.566
.8690	.628	-0.504	.9049	.120	-0.937	.9349	.532	-0.569
.8695	.635	-0.507	.9058	.133	-0.962	.9354	.539	-0.565
.8700	.642	-0.504	.9064	.141	-0.978	.9359	.545	-0.563
.8704	.647	-0.497	.9067	.145	-0.987	.9363	.551	-0.557
.8708	.653	-0.482	.9071	.151	-0.995	.9367	.556	-0.556
.8765	.731	-0.451	.9075	.156	-1.006	.9372	.563	-0.547
.8769	.736	-0.444	.9083	.167	-1.010	.9376	.569	-0.540
.8774	.743	-0.450	.9086	.171	-1.007	.9381	.576	-0.540
.8785	.758	-0.443	.9105	.197	-0.997	.9385	.581	-0.538
.8791	.767	-0.441	.9110	.204	-0.999	.9389	.587	-0.534
.8795	.772	-0.441	.9114	.209	-0.995	.9392	.591	-0.533
.8800	.779	-0.444	.9119	.216	-0.986	.9423	.633	-0.474
.8804	.784	-0.445	.9126	.226	-0.960	.9427	.639	-0.473
.8814	.998	-0.440	.9131	.233	-0.963	.9431	.644	-0.472
.8817	.802	-0.439	.9135	.238	-0.959	.9436	.651	-0.471
.8821	.808	-0.439	.9139	.244	-0.951	.9441	.658	-0.476
.8825	.813	-0.443	.9143	.249	-0.945	.9444	.662	-0.471
.8829	.819	-0.442	.9148	.256	-0.929	.9449	.669	-0.474
.8833	.824	-0.442	.9151	.260	-0.923	.9453	.674	-0.468
.8868	.872	-0.440	.9157	.268	-0.918	.9457	.680	-0.465
.8872	.878	-0.442	.9162	.275	-0.903	.9461	.685	-0.464
.8877	.884	-0.443	.9166	.281	-0.897	.9469	.696	-0.461
.8881	.890	-0.443	.9170	.286	-0.888	.9474	.703	-0.451
.8885	.895	-0.448	.9187	.310	-0.848	.9478	.709	-0.454
.8890	.902	-0.447	.9191	.315	-0.833	.9483	.715	-0.446
.8902	.919	-0.465	.9195	.321	-0.824	.9521	.768	-0.441
.8906	.924	-0.472	.9200	.327	-0.816	.9525	.773	-0.436
.8910	.930	-0.477	.9205	.334	-0.807	.9529	.779	-0.439
.8915	.937	-0.481	.9209	.340	-0.797	.9533	.784	-0.440
.8919	.942	-0.489	.9252	.399	-0.701	.9538	.791	-0.438
2752.8924	.943	-0.509	2752.9257	.406	-0.692	2752.9552	.810	-0.428

THE SPECTROSCOPIC ORBIT OF 26 AQUILAE*

K. L. FRANKLIN
Leuschner Observatory, University of California
Received April 28, 1952

ABSTRACT

Elements have been determined for 26 Aquilae from fifty-one Mills spectrograph observations covering a 20-year interval. This single-line system is of special interest because of its high orbital eccentricity, 0.833. The period is 266.544 days, and the primary component has a spectral type of G8 III–IV. Photoelectric observations were made to test for eclipses, but the results are not conclusive. Probable dimensions of the components are derived.

OBSERVATIONS AND VELOCITY-CURVE

The variability of the radial velocity of 26 Aquilae[1] was suspected by Joseph Lunt[2] from three observations (designated as Nos. 1, 2, and 4 in Table 1) made at the Cape Observatory and was confirmed by W. W. Campbell[3] on the basis of three Lick observations (Nos. 3, 5, and 7, Table 1). With the exception of two plates, one (No. 6) taken at the southern station of the Lick Observatory, no further observations of this system were made for 21 years. In 1942–1943, six Lick spectrograms, obtained over an interval of nearly 450 days, showed a slow change in the radial velocity. This fact reinforced the findings of Lunt and Campbell and demonstrated as well that the period might be long. Other observations were made in the period 1944–1947, but no systematic attempt was made to study this star until 1949–1950. In September, 1949, this star was placed on the observing program of the Mills three-prism spectrograph, with the purpose of studying the velocity variation in detail. A total of fifty-three Lick spectrograms are now available for this study.

To assure homogeneity of the data, only those plates were used that were taken with the Mills spectrographs at the Lick Observatory. All plates of the new series were measured on a Hartmann spectrocomparator against a standard plate of α Arietis, of spectral type K2 III. All but five of the older Lick spectrograms were remeasured against this standard plate. Full or half-weight was assigned to each plate at the time of measurement, according to its quality. All velocity reductions and subsequent residuals were carried to hundredths of a kilometer per second, as listed in the accompanying tables. These values have been used throughout the calculations, although the last decimal is not significant.

Of the five spectrograms not remeasured, one was generally underexposed and half of the comparison spectrum was missing; it was not used in this study. The other four had been taken with the original Mills spectrograph. The published velocities[4] for these plates were adopted here, but they were assigned half-weight.

A control on the recent measures was furnished by the observation of standard-velocity stars of similar spectral type. No appreciable systematic deviation from the I.A.U. standard-velocity system[5] was found.

The radial velocities, referred to the sun, were plotted against phases obtained from a

* *Contributions from the Lick Observatory*, Ser. II, No. 43.

[1] 26(f) Aquilae ($\alpha = 19^h15^m2$, $\delta = -05°31'$ [1900]) = BD−5°4936 = HR 7333 = HD 181391 (5.1, G5) = GC 26669

[2] *Ann. Cape Obs.*, **10**, 16E, 1921.

[3] *Pub. A.S.P.*, **34**, 169, 1922.

[4] *Pub. Lick Obs.*, **16**, 284, 1928.

[5] *Trans. I.A.U.*, **3**, 171, 1928.

TABLE 1

OBSERVATIONS

Obs. No.	Plate No.	Date (JD)	Helioc. Vel. (Km/Sec)	O−C (Km/Sec)	Wt.	Phase (*P*)
1	Lunt	2421844.297	−19.5	−6.87	0	0.5704
2	Lunt	2212.324	−12.6	+1.54	0	.9511
3	11422*	2531.832	−25.4	−2.27	0.5	.1498
4	Lunt	2559.390	−22.5	−3.92	0	.2532
5	11505*	2584.665	−17.1	−0.93	0.5	.3480
6	8335†	2833.88	−19.4	−1.68	0	.2830
7	11932*	2951.695	−11.1	−0.15	0.5	.7250
8	15997	5435.861	−38.92	−0.36	0.5	.0449
9	28083	2430538.891	−20.70	+0.26	1.0	.1901
10	28122	0555.820	−18.11	+0.46	1.0	.2536
11	28155	0575.732	−15.72	+0.88	1.0	.3283
12	28183	0597.810	−15.17	−0.21	1.0	.4111
13	28271	0648.639	−12.00	+0.25	0.5	.6018
14	29003	0908.668	−10.03	+0.20	1.0	.8475
15	29621‡	1253.968	.....	.....	0	.8729
16	29653	1276.865	−15.73	−0.05	1.0	.9588
17	29684	1294.817	−47.09	+1.43	0.5	.0261
18	29820	1341.671	−20.21	+0.23	0.5	.2019
19	29864	1355.658	−19.14	−0.60	1.0	.2544
20	30555	1614.966	−18.57	+0.88	1.0	.2272
21	30594	1637.857	−14.98	+1.97	0.5	.3131
22	30614	1658.886	−15.50	−0.20	1.0	.3920
23	30641	1677.815	−13.83	+0.28	1.0	.4630
24	30664	1691.749	−13.00	+0.35	0.5	.5153
25	31250	2015.821	−10.74	+0.15	1.0	.7311
26	31279	2036.833	−09.07	+1.25	1.0	.8100
27	31323	2065.778	−11.30	−0.02	1.0	.9186
28	31875	2404.770	−20.27	+0.66	1.0	.1906
29	31888	2410.765	−20.42	−0.43	1.0	.2129
30	31897	2413.813	−19.04	+0.52	1.0	.2243
31	31946	2432.705	−17.91	−0.52	1.0	.2952
32	33129	3167.743	−35.31	+0.64	1.0	.0528
33	33135	3171.677	−32.63	−0.32	1.0	.0676
34	33146	3177.735	−29.58	−1.15	1.0	.0903
35	33162	3182.662	−26.56	−0.60	1.0	.1088
36	33177	3189.655	−24.36	−0.21	1.0	.1350
37	33178	3195.640	−22.63	+0.02	1.0	.1575
38	33208	3215.619	−18.78	+0.49	1.0	.2324
39	33323	3372.024	−10.87	−0.59	0.5	.8192
40	33344	3384.015	−11.77	−1.50	1.0	.8642
41	33353	3390.995	−11.37	−0.86	1.0	.8904
42	33363	3397.984	−10.72	+0.48	1.0	.9166
43	33372	3414.008	−23.09	+0.40	1.0	.9767
44	33374	3416.916	−36.65	+0.29	1.0	.9877
45	33383	3418.974	−55.98	−0.37	1.0	.9954
46	33384	3420.976	−69.21	+0.51	1.0	.0029
47	33385	3422.940	−65.10	−0.13	1.0	.0103
48	33386	3423.968	−60.55	−0.26	1.0	.0141
49	33393	3424.940	−57.05	−1.00	1.0	.0178
50	33396	3426.974	−48.71	+0.35	1.0	0.0254

TABLE 1—*Continued*

Obs. No.	Plate No.	Date (JD)	Helioc. Vel. (Km/Sec)	O−C (Km/Sec)	Wt.	Phase (*P*)
51	33399	2433428.990	−43.79	+0.22	1.0	0.0330
52	33400	3430.952	−39.88	+0.53	1.0	.0403
53	33403	3432.986	−37.22	+0.28	1.0	.0479
54	33415	3438.873	−31.75	+0.09	1.0	.0700
55	33428	3451.839	−26.42	−0.94	1.0	.1187
56	33496	3474.890	−21.18	−0.88	1.0	0.2052

* Observation with original Mills spectrograph. Not remeasured.

† Two-prism observation from Santiago, Chile.

‡ Underexposed; not measurable on the Hartmann spectrocomparator.

provisional period derived by J. H. Moore from the 1920–1947 observations. The method of Lehmann-Filhés was used to obtain a good set of preliminary elements.

Since a correction to the period was included among the unknowns to be found by least squares,[6] the establishment of normal points was seriously restricted. Only those observations were combined that fell close together in time within the same cycle or in phase within two adjacent cycles. The normal points and their residuals with respect to the final elements are listed in Table 2.

All the observations and normal points were then represented by the preliminary elements, and the residuals of the normal points were used in a least-squares correction of the preliminary elements. The large eccentricity made it necessary for the corrections to the elements to be small, in order that higher-order terms could be neglected. Two least-squares solutions were necessary to obtain satisfactorily small residuals. The normal points were recomputed with the second set of elements before proceeding with the second improvement. Dispersion of the observations about the final velocity-curve (Fig. 1) indicates a probable error of ±0.47 km/sec for an observation of unit weight. The final elements of 26 Aquilae are listed in Table 3, together with the elements[7] of the three systems having the highest known eccentricities, σ Piscium, β Arietis, and BD+31°2540.

The spectrum of 26 Aquilae has been variously assigned to types between G5 and K0. Miss Nancy G. Roman, of the Yerkes Observatory, has very kindly classified the spectrum on the system of Morgan, Keenan, and Kellman.[8] She assigns a classification of G8 III–IV to 26 Aquilae.

DISCUSSION

Some statements can be made about the properties of the components of 26 Aquilae if we supplement the observational data with the following assumptions:

[6] *Pub. Allegheny Obs.*, **1**, 35, 1906. The term containing m, the correction to the mean motion, is given by Schlesinger as $(\beta \sin u)(t - T)m$. It is important to notice that $t - T$, where t is the date of observation and T is the epoch of perihelion passage, is in days, while β and u are cyclic variables involving the phase and hence repeat each period. Since $(t - T)$ can become inconveniently large, we can make the substitution $m' = nm$, where n is a convenient factor (a power of 10, say) and carry out the solution for m', reconverting to m at the end. This makes it possible to reduce the coefficient of m' to a number of the order of unity.

[7] J. H. Moore and F. J. Neubauer, *Lick Obs. Bull.*, **20**, 1 (No. 521), 1948.

[8] *An Atlas of Stellar Spectra* (Chicago: University of Chicago Press, 1943).

a) That both components obey the mass-luminosity relation as deduced by Russell and Moore:[9]

$$\log \mathfrak{m} = -0.1048\,(M_{\text{bol}} - 5.23)\,, \tag{1}$$

where $\mathfrak{m}$ is the mass in solar units.

b) That the relation between temperature, T,[10] and photoelectric color, C_p, is that given by O. J. Eggen:[11]

$$C_p = \frac{7200^\circ}{T} - 0^{\text{m}}.71\,. \tag{2}$$

TABLE 2

NORMAL POINTS

Phase (P)	Observations (No. in Table 1)	Wt.	Helioc. Vel. (Km/Sec)	O−C (Km/Sec)
0.0029	46	1.0	−69.21	+0.51
.0103	47	1.0	−65.10	−0.13
.0141	48	1.0	−60.55	−0.26
.0178	49	1.0	−57.05	−1.00
.0254	50	1.0	−48.71	+0.35
.0261	17	0.5	−47.09	+1.43
.0330	51	1.0	−43.79	+0.22
.0449	8	0.5	−38.92	−0.36
.0557	32, 33, 52, 53, 54	5.0	−34.89	+0.24
.0903	34	1.0	−29.58	−1.15
.1208	35, 36, 55	3.0	−25.73	−0.44
.1984	37, 38, 56	3.0	−20.71	−0.13
.2307	28, 29, 30, 31	4.0	−19.26	+0.07
.2464	18, 19, 20, 21	3.0	−18.37	+0.43
.2489	3, 5	1.0	−20.24	−1.52
.2958	9, 10, 11, 12	4.0	−17.03	+0.35
.4451	22, 23, 24	2.5	−14.29	+0.11
.6018	13	0.5	−12.00	+0.25
.7250	7	0.5	−11.1	−0.15
.8199	25, 26, 27	3.0	−09.81	+0.47
.8475	14	1.0	−10.03	+0.20
.8802	39, 40, 41, 42	3.5	−10.99	−0.61
.9588	16	1.0	−15.73	−0.05
.9767	43	1.0	−23.09	+0.40
.9877	44	1.0	−36.65	+0.29
0.9954	45	1.0	−55.98	−0.37

[9] *The Masses of the Stars* (Chicago: University of Chicago Press, 1940), p. 112, eq. 113. However, a recent empirical mass-luminosity law, deduced by Z. Kopal and C. G. Treuenfels from eclipsing-binary data (*Harv. Circ.*, No. 457, Fig. 3, June, 1951), indicates smaller masses for the components of 26 Aquilae, approximately 1.8 and 0.8 in solar units for primary ($M_{\text{bol}} = +2.2$) and secondary $M_{\text{bol}} = +4.9$), respectively.

[10] The temperature, T, is as given by Keenan and Morgan, *Astrophysics* (New York: McGraw-Hill, 1952), chap. i.

[11] *Ap. J.*, **113**, 410, 1951; *Lick Obs. Contr.*, Ser. II, **2**, 44 (No. 32), 1951.

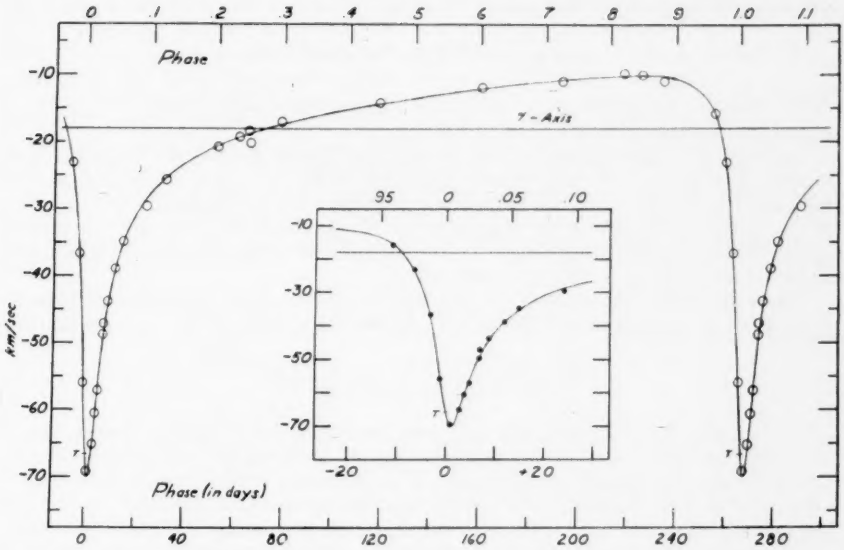

FIG. 1.—Velocity-curve of 26 Aquilae, computed from the final elements. The circles are the normal points listed in Table 2. There is no significance in their size. The insert shows the region near periastron (T) with $0.5X$ ordinate and $2X$ abscissa of the complete figure. The probable error of an observation of unit weight is ± 0.47 km/sec.

TABLE 3

COMPARISON OF ELEMENTS OF HIGHLY ECCENTRIC SYSTEMS

System m_v, HD Sp.	26 Aql 5.10, K0	σ Psc* 5.46, B9	β Ari* 2.72, A5	BD+31°2540* 6.55, F5
P (days)	266.544 ± 0.013	81.12	106.9973	39.28
T (JD)	2433420.207 ± 0.044	2431308.667	2428010.944	2428711.847
ω	152°.65 ± 0°.38	345°.2	24°.17	326°.7
e	0.833 ± 0.0017	0.898	0.892	0.786
K (km/sec)	29.86 ± 0.19	{54.27 60.00}	37.63	43.22
γ (km/sec)	−18.00	+10.40	−03.68	−08.22
$a \sin i \times 10^{-6}$ (km)	60.57	{26.6 29.5}	25.027	14.432
$f(m)$	0.1249	.....	0.0547	0.0778
$m \sin^3 i$	.....	{0.56 0.51}	.....	.....

* Data are from the *Fifth Catalogue of the Orbital Elements of Spectroscopic Binary Stars* (see n. 7).

c) That the radii can be computed by the use of the Planck formula and the photoelectric color through the relation:[12]

$$\log \frac{R}{R_\odot} = 0.82C_p - 0.2M_v + 0.56 . \tag{3}$$

d) That M_{pg} for a K0 subgiant[13] can be obtained from Eggen's result[14] that M_{pg} is essentially constant at +3.6 for all subgiants.

Application of the color index, +0.8 mag. (eq. [2] with $T = 4650°$[10]), and the bolometric correction,[15] −0.3 mag., results in a value of $M_{bol} = +2.5$. If the trigonometric parallax,[16] $\pi = 0''.027 \pm 0''.005$, and $m_v = 5.1$, as determined at Harvard, are used, then $M_v = +2.3$ and $M_{bol} = +2.0$, which is in good agreement with that derived from the spectroscopic absolute magnitude.[13] The calculations were therefore carried through for three values of $M_v = +2.8$, $+2.5$, and $+2.3$.

The value of m_1, the mass of the brighter component, was then obtained from the mass-luminosity relation (eq. [1]) and inserted into the expression for the mass function,

$$f(m) = \frac{m_2{}^3 \sin^3 i}{(m_1 + m_2)^2} = 0.1249 , \tag{4}$$

which contains two unknowns, $\sin^3 i$, and m_2. Additional information, however, may be obtained from an estimate of the mass ratio, m_1/m_2. Since the spectrum of the secondary is not visible on the Mills spectrograms, it is estimated conservatively that $M_{pg,2} - M_{pg,1} \geq 1^m.3$. This difference sets a lower limit on m_1/m_2, while equation (4) yields an upper limit, since $\sin^3 i \leq 1$. In this manner, it was found that $90° \geq i \geq 52°$. Values of the masses, radii, magnitudes, and temperatures of both components, computed for the two extreme values chosen for M_v and for the limiting values of the inclination, are given in Table 4, which contains in its columns two sets of data, in roman and italic type, that are mutually consistent.

If the inclination is near 90°, the values of $a \sin i$, ω, and the parallax would indicate a total displacement of the brighter component on the sky of $0''.02$. This is almost the limit of accuracy of the observations needed to derive an astrometric orbit for 26 Aquilae. If the inclination is not 90°, the astrometric problem is correspondingly less difficult, though never easy.

If the inclination is near 90°, eclipses will occur. To estimate the circumstances of a possible eclipse, calculations were carried out with representative values of the dimensions of the system. The results for central transit (secondary star in front) indicate an eclipse depth of no more than about 0.05 mag., while, for occultation (primary in front), the maximum depth would be about 0.15 mag. These configurations could last approximately 1 day for transit eclipse centered around phase $0.9893P$, and 2 days for occultation eclipse around phase $0.0409P$.

In order to test for the possibility of eclipses, 26 Aquilae was observed, on several nights before and during the critical phases, with photoelectric equipment attached to the 12-inch refractor and the Crossley reflector of the Lick Observatory. Since the star was low in the southwest at sunset, conditions were unfavorable for photometric work

[12] Russell, Dugan, and Stewart, *Astronomy* (Boston: Ginn & Co., 1938), **2**, 738.

[13] *Ap. J.*, **81**, 187, 1935; *Mt. W. Contr.*, No. 511. This spectral classification was used for all numerical work, since that supplied by Miss Roman arrived after the completion of the calculations. The slightly different type does not seriously affect the results shown in Table 4. The Mount Wilson observers assigned a spectroscopic absolute magnitude of $M_v = +2.3$ to 26 Aquilae.

[14] *Ap. J.*, **112**, 141, 1950; *Lick Obs. Contr.*, Ser. II, **1**, 433 (No. 30), 1950.

[15] G. P. Kuiper, *Ap. J.*, **88**, 452, Fig. 2, 1938.

[16] *General Catalogue of Stellar Parallaxes*, F. Schlesinger (Yale, 1935).

during the end of October and the beginning of November, 1951. Although every care was taken to determine the extinction during each run from stars near 26 Aquilae, the nightly variations at the large zenith distances could not be adequately taken into account. As a result, the observations are inconclusive regarding the occurrence of an eclipse; the occultation could not be observed because of inclement weather.

If eclipses of appreciable depth can be observed, the system of 26 Aquilae should furnish a value of the dimensions of a late-type subgiant. There also exists the possibility of finding reflection effects during and shortly after periastron. Since the expected drop in light during transit would be of the order of a few hundredths of a magnitude, a good value for the constant light is very important. Thus the system should be observed over a period of several days *before* the transit phase, because reflection effects shortly after eclipse could give a spurious value for the constant light. Obviously, a good value of this

TABLE 4

DESCRIPTIONS OF COMPONENTS*

	Primary	Secondary	
i	.....	90°	52°
	.....	*90°*	*55°*
M_v	+2.3	+4.9	+3.6
	+2.8	*+5.2*	*+4.1*
$R/R_\odot$	5.70	1.11	1.44
	4.53	*1.03*	*1.26*
m†	2.18	1.10	1.52
	1.93	*1.03*	*1.35*
T‡	4650°	5630°	6540°
	4650°	*5500°*	*6250°*

* In each column, numbers in roman and in italic type are mutually consistent (see the remark in n. 13).

† From eqs. (1) and (4). Bolometric corrections are from Kuiper (n. 15); secondary component is assumed to be on main sequence.

‡ See n. 10.

parameter is necessary to detect any reflection that may occur, regardless of eclipses. Occultation would not present such serious difficulties.

In such highly eccentric systems as described in Table 3, one might expect some unusual phenomena to occur, such as some form of reflection effect or perhaps tidal distortions of the figures of the components. As can be seen from the velocity-curve for 26 Aquilae (Fig. 1), there were two observations made near periastron. These (and others) were critically compared on the Hartmann spectrocomparator with other observations made far from periastron. No changes, however, could be noted in the spectrum in the limited region between $H\beta$ and $H\gamma$. Since the sudden change in velocity occurred unexpectedly, no preparations were made to observe the system in other spectral regions.

On low-dispersion plates taken throughout the cycle by Dr. G. H. Herbig, faint, narrow central emission components appear in the H and K lines of *Ca* II.

In the summer of 1952, 26 Aquilae is very favorably situated for observations near periastron, since it is in opposition near the critical phases. The next equally favorable observing period will occur at the end of June, 1955, although those occurring in April, 1953, and October, 1954, will be accessible.

The predicted times of the most important configurations of 26 Aquilae, for the periastron passages occurring in 1954 and 1955, are shown in the accompanying tabulation.

	Configuration		
	Transit Phase = 0.9893P	Periastron Phase = 0.0000P	Occultation Phase = 0.0409P
1954 U.T.	Oct. 1.119	Oct. 3.971	Oct. 14.873
JD	2435016.619	2435019.471	2435030.373
1955 U.T.	June 24.663	June 27.515	July 8.417
JD	2435283.163	2435286.015	2435296.917

The system of 26 Aquilae is a very interesting one and deserves further study by both spectroscopic and photometric methods, not only to learn more about the system itself, but to provide additional information on subgiants.

It is a pleasure to express my gratitude to Drs. Hermann Haupt, George H. Herbig and Gibson Reaves, of the Lick Observatory, for making the photometric observations. I wish especially to thank Dr. Herbig, who suggested this problem, made numerous observations of the system, and guided the work throughout.

Note added in proof.—In July and August, 1952, comparisons were made between 26 Aquilae and HD 180086 (6.56 mag., F0) with the 12-inch Lick refractor and a photometer using an E.M.I. type 5659 photomultiplier cell and Corning filters 5543 and 3385. No significant changes in 26 Aquilae were detected during periastron passage as compared with the light and color obtained at other phases. Clouds prevented observations of both mid-eclipse phases, but no change was observed as late as 0.038P. This phase would correspond to 4 hours after second contact of the occultation eclipse, if $i = 90°$. Although eclipses probably are not present, the only conclusions permissible at present are (1) $i \neq 90°$, and (2) the companion is not bright enough to cause a reflection effect.

PHOTOELECTRIC OBSERVATIONS OF NU ERIDANI

MERLE F. WALKER
Berkeley Astronomical Department, University of California
Received May 13, 1952

ABSTRACT

The photometric observations of ν Eridani in January and February, 1951, December, 1951, and January, 1952, can be satisfied by the spectroscopic period, $P_2 = 0.1735089$ day. One outstanding discrepancy with the spectroscopic observations remains: the beat period determined from the photometric observations of December, 1951, and January, 1952, is $P_3 = 8.7$ days, while the spectroscopic $P_3 = 6.9808$ days. This disagreement and also the observations in January and February, 1951, suggest that both the period and the amplitude of the beat-curve are variable. For the December, 1951, and January, 1952, observations, $P_1 = 0.1770$ day, and the values of the light-variations associated with P_1 and P_2 are $R_1 = 0.067$ mag. and $R_2 = 0.114$ mag., respectively.

Photoelectric observations of ν Eridani in two colors, covering an interval of 29 days from December 21, 1951, to January 19, 1952, have been carried out with the 12-inch refractor of the Lick Observatory. ν Eridani has been listed as a doubtful member of the β Canis Majoris class for many years. The results obtained by the earlier observers had suggested that the period was variable and that, for this reason, the star should not be classed with the other β Canis Majoris stars. In 1921 F. Henroteau obtained a period of 0.23667 day for the variation in radial velocity.[1] This period predicted either a maximum or a minimum of the velocity-curve. In 1927 he was unable to verify this period or to find any other which would represent the observations.[2] About this same time R. H. Baker discovered that the light of the star was variable and derived a period of 0.15430 day.[3] Subsequently it was found by Zessewitch[4] and independently by the author[5] that Henroteau's observations can be represented by a period of 0.17351 day. This strongly suggested that the period is constant.

It was therefore planned to carry out a series of simultaneous spectroscopic and photometric observations of ν Eridani during the 1951–1952 season, similar to the program adopted for 16 Lacertae.[6,7] Unfortunately, weather conditions did not permit the program to be carried out completely; simultaneous observations were secured on only two nights. The nine photometric runs which were obtained form the basis of the present paper.

The photometer, filters, and recording system employed were the same as those used for 16 Lactertae.[7] The primary comparison star used was μ Eridani. Observations of ω Eridani and of HD 28749 were also obtained as a check on the constancy of μ Eridani. So far as could be determined, there was no significant variation in any of the comparison stars.

The observations have been reduced to no atmosphere, using extinction coefficients determined each night from the comparison stars. The magnitudes and colors have been left on the system defined by the telescope–filter-cell combination. The individual light- and color-curves are shown in Figures 1 and 2. The dots represent blue-magnitude differences and the circles color differences, ν Eridani minus μ Eridani. The abscissae of the

[1] *Pub. Dom. Obs. Ottawa*, Vol. **5**, No. 3, 1921.
[2] *Ibid.*, Vol. **9**, No. 4, 1927.
[3] *Pub. A.S.P.*, **38**, 86, 1926.
[4] *A.J. U.S.S.R.*, **21**, 94, 1944.
[5] *Pub. A.S.P.*, **63**, 176, 1951.
[6] O. Struve, D. H. McNamara, R. P. Kraft, S. M. Kung, and A. D. Williams, *Ap. J.*, **116**, 81, 1952.
[7] M. F. Walker, *Ap. J.*, **116**, 106, 1952.

curves are heliocentric Julian dates. Each symbol represents a single deflection of about 1-minute duration registered on a Brown recorder. It was necessary to change battery boxes and photomultiplier cells during the course of the observations on January 18, so that the light-curve may be somewhat uncertain.

As in the case of 16 Lacertae, there is no evidence of a variation in color. In order to determine whether variations of temperature occur, it will be necessary to observe the star with a very long color base line.

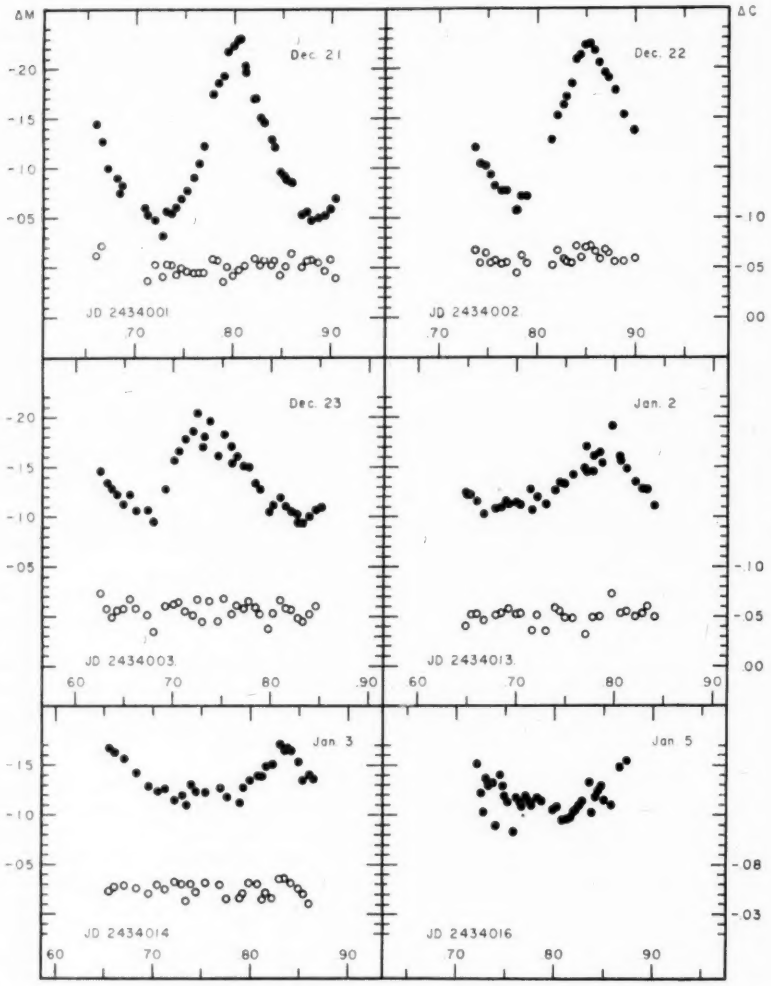

FIG. 1.—Photometric observations of ν Eridani in 1951 and 1952. The dots represent blue-magnitude differences, and the circles color differences, ν Eridani minus μ Eridani, reduced to no atmosphere. Each symbol represents a single deflection of about 1-minute duration registered on a Brown recorder.

The observations show the existence of a very large beat phenomenon; the light-range varies at least between 0.181 and 0.048 mag., while the value of the mean light remains essentially constant. The values of the light-variation observed in December, 1951, and January, 1952, together with those observed in January and February, 1951,[5] are listed in Table 1. The present observations are best represented by a period of $P_3 = 8.7$ days, as shown in Figure 3; the phases have been arbitrarily computed from zero phase =

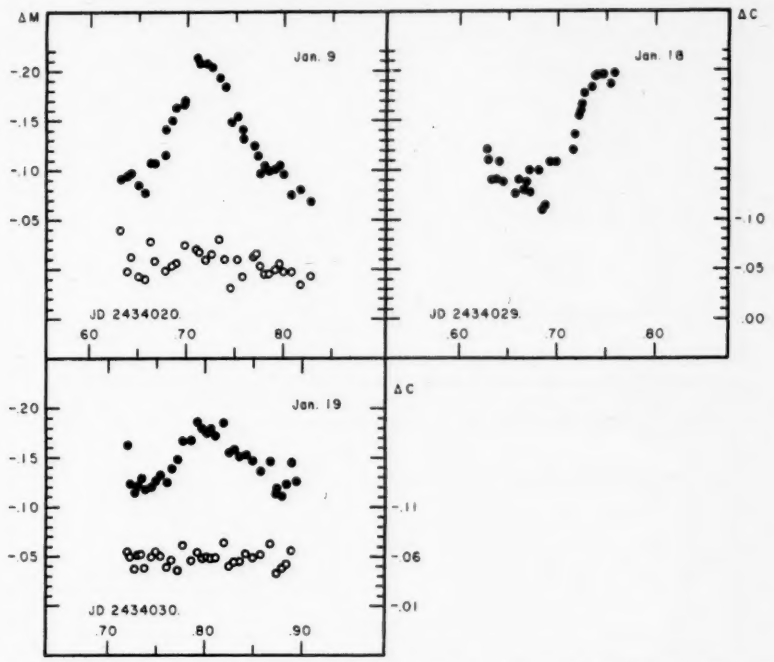

FIG. 2.—Photometric observations of ν Eridani in 1952. Ordinates and symbols as in Fig. 1

TABLE 1

OBSERVED LIGHT-VARIATIONS OF ν ERIDANI

JD	Light-Range R (Mag.)	Phase (P=8.7 Days)	JD	Light-Range R (Mag.)	Phase (P=Days 8.7)
2433			2434		
670.7	0.122		003.7	0.092	0.22
671.6	.098		013.8	.054	.38
672.7	.088		014.8	.048	.49
677.7	.075		016.8	.060*	.72
679.7	.088		020.7	.130	.17
2434			029.7	.107	.21
001.8	.181	0.00	030.8	0.060	0.33
002.8	0.154	0.12			

* Low weight; probable error ± 0.02 mag.

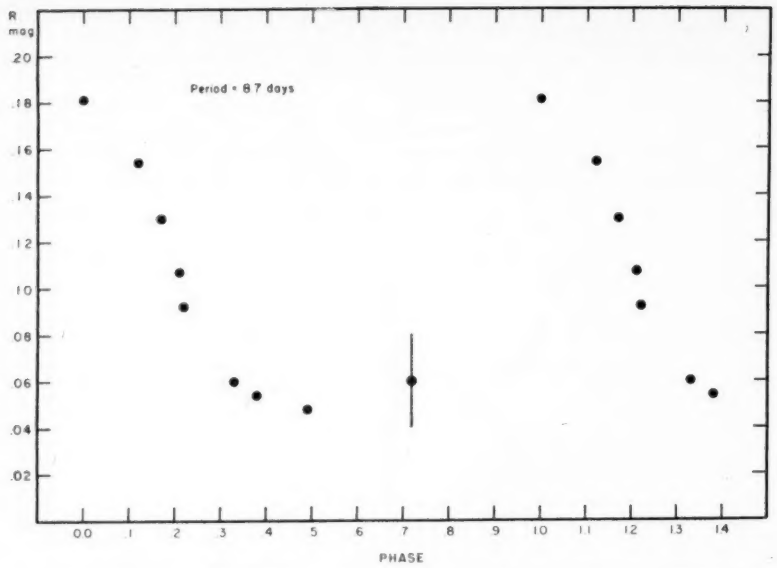

FIG. 3.—The beat period in the amplitudes of the light-curves observed in December, 1951, and January, 1952. The ordinate is the light-variation, the abscissa is the phase computed from zero phase = JD 2434001.8 + 8.7E days. The vertical line indicates the uncertainty in the observation of January 5.

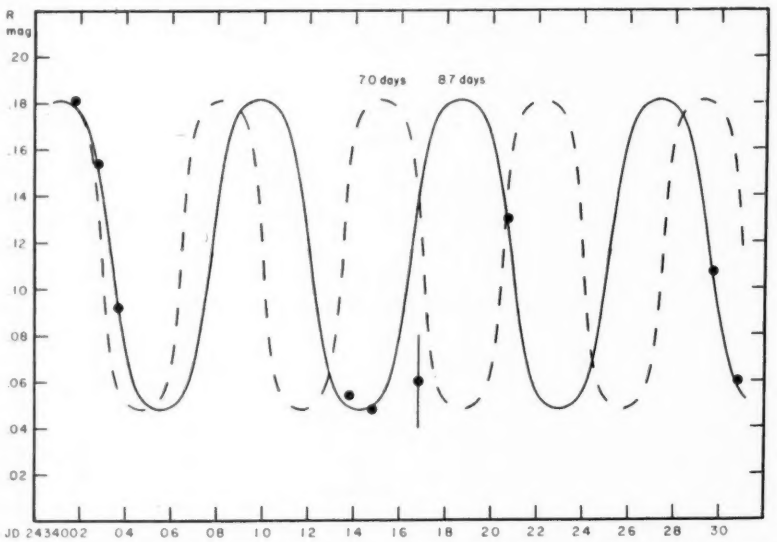

FIG. 4.—Amplitudes of the light-curves observed in December, 1951, and January, 1952. Ordinate and symbols as in Fig. 3. The abscissa is the Julian date. Curves having periods of 7.0 and 8.7 days have been drawn to illustrate the difficulty of fitting the observations to a 7-day period. The curves are only for purposes of illustration and are not intended to be curves of best fit.

JD 2434001.8 + 8.7E days. This 8.7-day period is at variance with the beat period of 6.9808 days derived by O. Struve *et al.*[8] The observed values of the light-variation are plotted against Julian date in Figure 4. Their distribution would seem to rule out any possibility of representing the observations with the 7-day period. All the spectroscopic observations, both Henroteau's and Struve's, can be represented by the 7-day period. However, during the interval covered by the recent photoelectric observations, only two complete velocity-curves were obtained. It is therefore not possible to ascertain whether the radial velocities obeyed the 7-day or the 9-day period during this one-month interval.

The most likely explanation would seem to be that the length of the beat period is variable in some manner. The light-variations observed in January and February, 1951, shown in Figure 5, appear to bear out this supposition. They apparently will not fit either the 7-day or the 9-day period but require a still longer one of around 12 days, although this is very uncertain, since there are so few observations. The general appearance of the curve, incomplete though it is, suggests that the amplitude of the beat-curve was smaller at that time than in the more recent set of observations. In a general way, this agrees with the spectroscopic results,[8] which also indicate that there are changes in the ampli-

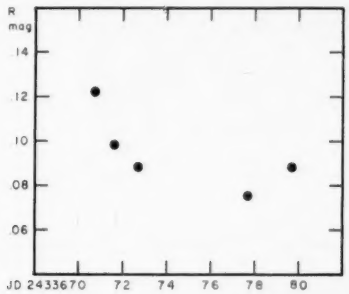

FIG. 5.—Amplitudes of the light-curves observed in January and February, 1951, plotted against Julian date. The ordinate is the light-variation.

tude of the beat-curve and suggest that it was passing through a minimum at about that time. This difference in the values of the beat period shows again the desirability of obtaining simultaneous spectroscopic and photometric observations.

There is obviously not enough photometric material as yet available to attempt an accurate determination of the short, 4-hour period. About all that can be said at the present time is that the photometric observations can be represented by the spectroscopic period. The observed times of maximum light of ν Eridani are listed in Table 2, together with the residuals between the observed maxima and those computed from the formula:

$$\text{Helioc. max.} = \text{JD } 2433670.731 + 0.1735089E \text{ day.}$$

The epoch has been arbitrarily chosen as the time of the first observed maximum. The residuals for December, 1951, and January, 1952, have been combined with the 8.7-day period according to the formula: Zero phase = JD 2434001.8 + 8.7E days. Because of the uncertainty in the value of the beat period, no attempt has been made to include the earlier observations. Figure 6 shows that they exhibit a variation in the 9-day period. The exact amplitude and form of the residual curve cannot be determined, since there are observations only over half the cycle. However, it appears that the amplitude is of the same

[8] O. Struve, D. H. McNamara, S. M. Kung, R. P. Kraft, and A. D. Williams, *Ap. J.*, **116**, 398, 1952.

order of magnitude as for the corresponding curve of residuals of times of minimum velocity found by Struve.[8]

If, following Struve's notation, we call $P_2 = 0.1735089$ day and $P_3 = 8.7$ days, then, since the residuals tend to become more positive after the time of maximum light-variation,[6,7]

$$\frac{1}{P_3} = \frac{1}{P_2} - \frac{1}{P_1},$$

TABLE 2

OBSERVED MAXIMA OF ν ERIDANI
(Max. Light = Helioc. JD 2433670.731 + 0.1735089E Day)

Helioc. JD	O−C (Day)	Phase (P=8.7 Days)	Helioc. JD	O−C (Day)	Phase (P=8.7 Days)
2433			2434		
670.731	0.000		002.854	+0.027	0.12
671.784	+ .012		003.732	+ .037	.22
672.663	+ .023		013.794	+ .036	.38
677.681	+ .010		014.832	+ .033	.49
679.774	+ .021		020.719	+ .021	.17
2434			029.755*	+ .034	.21
001.801	+0.015	0.00	030.798	+0.036	0.33

* Low weight.

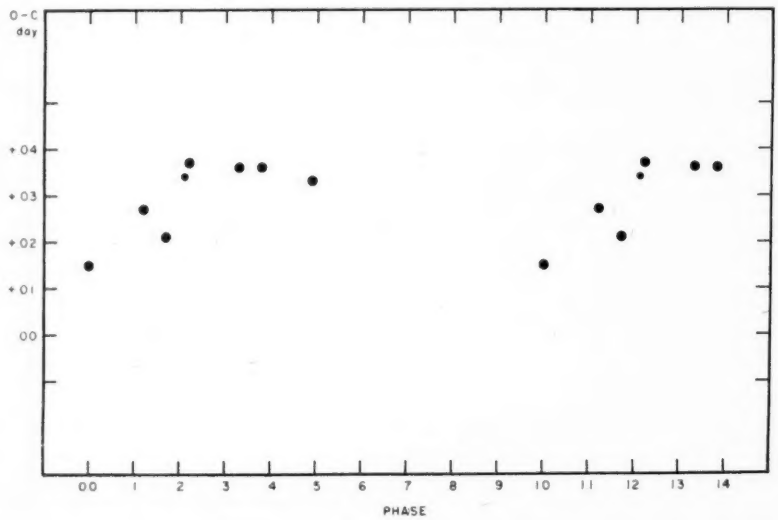

FIG. 6.—Periodic variations in the time of maximum light. The ordinate is the residual, observed maximum minus maximum predicted from the formula: Helioc. max. = JD 2433670.731 + 0.1735089E day. The phases are computed from Zero phase = JD 2434001.8 + 8.7E days. Only the observations of December, 1951, and January, 1952, have been included. The small symbol indicates low weight.

and therefore $P_1 = 0.1770$ day. Whether or not this period is correct depends upon the correctness of the beat period. It is probably significant, however, that the residuals, like the beat amplitudes during the period covered by the observations, fit the 9-day period and not the 7-day period and that they, like their spectroscopic counterparts, indicate that $P_1 > P_2$.

The light-variations associated with P_1 and P_2 are $R_1 = 0.067$ mag. and $R_2 = 0.114$ mag., respectively. The ratio of $R_2/R_1 = 1.7$. Since the value of $2K$ observed by McNamara on December 21 was about 76 km/sec, we may assume that K_1 was near its maximum value of 15 km/sec,[8] so that the ratio of $K_2/K_1 = 1.6$. Thus it appears that in ν Eridani, unlike 16 Lacertae,[7] the ratios of the light- and velocity amplitudes are approximately the same.

TABLE 3

SIMULTANEOUS OBSERVATIONS OF LIGHT AND VELOCITY

JD	Light-Range R (Mag.)	$2K$ (Km/Sec)	ΔT^* (Day)	
			1	2
2433				
671.6	0.098	48	−0.005	−0.003
672.7	.088	55	+ .005	− .020
2434				
001.8	.181	76	− .004	0.000
030.8	0.060	22	−0.008	.....

* 1, Maximum light minus gamma velocity; 2, minimum light minus gamma velocity.

So far we have simultaneous spectroscopic and photometric observations of ν Eridani on only four nights. Thus there are not enough data profitably to discuss the relationships between the light- and velocity-curves. The existing material has been collected in Table 3.

I am indebted to Dr. C. D. Shane for permission to use the facilities of the Lick Observatory and to the members of the staff for their kind interest and co-operation.

THE RADIAL VELOCITY OF NU ERIDANI*

O. STRUVE, D. H. MCNAMARA, S. M. KUNG, R. P. KRAFT, AND A. D. WILLIAMS
Berkeley Astronomical Department, University of California
Received May 13, 1952

ABSTRACT

Individual velocity-curves were obtained on 15 nights from 220 Mount Wilson and Lick spectrograms. These curves are represented as the sum of three components: (1) a harmonic oscillation with $P_1 = 0.1779$ day, $K_1 = 11$ km/sec; (2) a harmonic oscillation with $P_2 = 0.1735089$ day, $K_2 = 24.5$ km/sec; and (3) an additional, and probably variable, variation of K_1 between 8 and 15 km/sec. The absorption lines vary in profile and are most often sharp on the lower half of the ascending branch of the velocity-curve. The beat period, $P_3 = 6.9808$ days, is sometimes distorted by the variation of K_1.

Although ν Eridani has long been known as a B-type star of variable radial velocity[1] and although F. Henroteau had observed it extensively with the spectrograph at Ottawa,[2] interest in its peculiar variations has been recently revived by the photoelectric and radial-velocity observations by M. Walker.[3] He not only confirmed R. H. Baker's discovery of the variability in the light of this star[4] but also succeeded in deriving a reliable period which is close to one given by V. P. Zessewitch on the basis of Henroteau's radial velocities.[5]

TABLE 1

LIST OF STAR LINES

λ	Element	Plate*	λ	Element	Plate*
3933.66	*Ca* II	γ	4340.47	*Hγ*	γ
3964.73	*He* I	γ	4387.93	*He* I	γ
4009.27	*He* I	γ	4471.48	*He* I	γ, L
4026.19	*He* I	γ	4481.23	*Mg* II	γ, L
4069.79	*O* II	γ	4552.65	*Si* III	L
4101.74	*H δ*	γ	4567.87	*Si* III	L
4120.81	*He* I	γ	4574.78	*Si* III	L
4143.76	*He* I	γ	4590.97	*O* II	L
4267.17	*C* II	γ	4596.18	*O* II	L

* γ indicates the spectrograms taken with the Mount Wilson 60-inch reflector and Cassegrain spectrograph with 18-inch camera. "L" indicates the spectrograms taken with the Lick 36-inch refractor and Mills spectrograph.

The present paper deals with a new series of radial velocities, obtained from spectrograms secured, respectively, by O. Struve with the single-prism spectrograph attached to the Mount Wilson 60-inch telescope (Ser. γ in Table 1) and by D. H. McNamara with the three-prism Mills spectrograph attached to the 36-inch refractor of the Lick Observatory (Ser. L in Table 1).[6]

The measurements were carried out in the same manner as for 16 Lacertae. The spectral types of these two stars are similar, but the lines of ν Eridani are usually stronger and easier to measure than those of 16 Lacertae.

Table 1 gives a list of the star lines used in the present work. The *Ca* II line was found

* The observational material used in this investigation was obtained at the Mount Wilson and Lick Observatories.

[1] E. B. Frost and W. S. Adams, *Ap. J.*, **17**, 151, 1903.

[2] *Pub. Dom. Obs., Ottawa*, Vol. **5**, No. 3, 1921; Vol. **9**, No. 4, 1927.

[3] *Pub. A.S.P.*, **63**, 176, 1951.

[4] *Pub. A.S.P.*, **38**, 93, 1926.

[5] *A.J. U.S.S.R.*, **21**, 94, 1944.

[6] See also D. H. McNamara, *Pub. A.S.P.*, **64**, 76, 1952.

TABLE 2

MINIMUM AT JD 2423709.816 + 0.1735089*E*

Plate	JD	Phase (Day)	Radial Velocity (Km/Sec)	Plate	JD	Phase (Day)	Radial Velocity (Km/Sec)
	2433				2433		
γ.....	937.953	0.134	−18.3	γ.....	962.974	0.170	− 1.8
	.970	.151	−24.4		.983	.006	− 2.2
	.987	.168	−26.7		.993	.016	+ 4.9
	938.003	.011	−17.7		963.002	.025	+11.0
	.019	.027	− 2.9		.011	.034	+15.8
	.035	.043	+15.8		.868	.023	+ 6.0
	.917	.057	+19.2		.878	.033	+13.1
	933	.073	+31.4		.888	.043	+18.9
	.949	.089	+43.7		.898	.053	+27.9
	.965	.105	+56.3		.907	.062	+33.7
	.982	.122	+45.0		.917	.072	+39.1
	.998	.138	+17.0		.926	.081	+44.6
	939.014	.154	− 6.1		.935	.090	+44.8
	.031	.171	−14.8		.946	.101	+39.4
	.047	.014	−19.4		.956	.111	+29.1
	901	000	−14.0		.965	.120	+11.4
	.917	.016	−12.9		.975	.130	+ 4.9
	.933	.032	−12.6		.985	.140	− 5.8
	.950	.049	− 0.4		.994	.149	−12.8
	.965	.064	+10.2		964.004	.159	− 9.0
	.983	.082	+26.9		.824	.111	+36.5
	.999	.098	+31.0		.833	.120	+25.7
	940.015	.114	+42.9		.843	.130	+ 6.4
	.032	.131	+42.4		.853	.140	− 5.9
	.049	.148	+19.8		.862	.149	−14.3
	961.818	.055	+31.7		.872	.159	−17.9
	.828	.065	+32.4		.881	.168	−19.6
	.837	.074	+29.5		.892	.006	−18.2
	.846	.083	+27.3		.901	.015	−11.9
	.856	.093	+20.4		.910	.024	− 4.6
	.866	.103	+14.2		.919	.033	+ 4.2
	.876	.113	+10.5		.930	.044	+12.7
	.886	.123	+ 5.0		.939	.053	+18.0
	.896	.133	+ 1.9		.948	.062	+27.3
	.906	.143	+ 1.6		.960	.074	+34.5
	.915	.152	+ 6.7		.972	.086	+42.0
	.925	.162	− 1.1		.980	.094	+43.4
	.935	.172	+ 4.3		.990	.104	+39.8
	.944	.008	+ 7.8		.999	.113	+38.2
	.953	.017	+ 8.2		965.008	.122	+23.9
	.963	.027	+10.6		.813	.059	+25.2
	.973	.037	+17.7		.822	.068	+32.9
	.982	.046	+19.0		.830	.076	+34.6
	.992	.056	+22.5		.838	.084	+44.3
	962.866	.062	+36.3		.847	.093	+42.5
	.876	.072	+35.4		.856	.102	+50.3
	.885	.081	+40.8		.864	.110	+42.8
	.895	.091	+39.3		.872	.118	+39.4
	.904	.100	+28.0		.880	.126	+35.1
	.914	.110	+16.2		.888	.134	+23.0
	.923	.119	+ 5.4		.897	.143	+ 9.7
	.933	.129	+ 0.7		.906	.152	− 2.2
	.942	.138	− 4.0		.917	.163	− 9.7
	.955	.151	− 8.3		.926	.172	− 9.5
	.964	0.160	− 5.3		.935	0.008	− 9.3

TABLE 2—*Continued*

Plate	JD	Phase (Day)	Radial Velocity (Km/Sec)
	2433		
γ	965.943	0.016	− 7.5
	.951	.024	− 2.0
	.961	.034	+ 9.3
	.970	.043	+13.2
	.979	.052	+20.4
	.988	.061	+21.1
	966.811	.016	− 8.0
	.819	.024	−10.1
	.827	.032	− 4.3
	.835	.040	+ 2.7
	.844	.049	+ 7.9
	.851	.056	+10.9
	.860	.065	+21.4
	.869	.074	+22.1
	.876	.081	+27.9
	.884	.089	+28.1
	.892	.097	+31.4
	.899	.104	+37.3
	.908	.113	+38.8
	.917	.122	+36.3
	.924	.129	+32.6
	.933	.138	+28.4
	.942	.147	+19.2
	.951	.156	+ 6.1
	.960	.165	− 0.2
	.969	.001	− 3.1
	.978	.010	−10.1
	.988	.020	− 1.4
	2434		
L	001.648	.152	−16.8
	.662	.166	−21.4
	.677	.007	−17.3
	.701	.031	− 2.2
	.712	.042	+ 9.6
	.722	.052	+17.7
	.733	.063	+31.0
	.745	.075	+43.7
	.756	.086	+53.6
	.772	.102	+51.7
	.786	.116	+38.6
	.804	.134	+ 7.8
	.813	.143	− 3.5
	.822	.152	−16.5
	.835	.165	−22.4
	.849	.006	−21.0
γ	030.641	.169	+ 5.4
	.649	.003	+ 4.6
	.657	.011	+ 0.5
	.665	.019	+ 0.7
	.674	.028	− 1.0
	.683	.037	+ 3.8
	.691	.045	+ 6.6
	.699	.053	+ 8.2
	.707	.061	+ 8.9
	.716	.070	+ 9.2
	.724	0.078	+12.8
	2434		
λ	030.733	0.087	+14.1
	.742	.096	+16.1
	.750	.104	+21.7
	.759	.113	+17.7
	.767	.121	+21.7
	.775	.129	+26.8
	.783	.137	+19.7
	.791	.145	+18.6
	.799	.153	+17.6
	.808	.162	+10.3
	031.609	.096	+23.9
	.618	.105	+28.6
	.627	.114	+24.9
	.636	.123	+20.3
	.644	.131	+19.5
	.652	.139	+16.4
	.660	.147	+11.0
	.669	.156	+12.1
	.677	.164	+ 6.5
	.685	.172	+ 6.3
	.693	.006	+ 3.8
	.701	.014	+ 7.7
	.710	.023	+ 6.5
	.719	.032	+ 7.1
	.728	.041	+11.3
	.735	.048	+13.1
	.743	.056	+17.0
	.752	.065	+23.7
	.760	.073	+27.5
	.769	.082	+19.3
	.777	.090	+15.3
	.785	.098	+18.7
	.793	.106	+13.4
	.801	.114	+14.2
	.809	.122	+15.9
L	049.614	.056	+16.2
	.627	.063	+25.4
	.642	.078	+36.8
	.655	.091	+47.2
	.678	114	+47.4
	.697	133	+ 8.8
γ	053.609	.060	+28.8
	.619	070	+29.9
	.690	.141	+ 8.6
	.700	.151	+ 8.3
	.710	.161	+ 8.7
	.729	.006	+19.5
	.738	.015	+25.7
	.747	.024	+22.0
	.757	.034	+19.9
L	056.606	.107	+48.0
	.619	.120	+31.3
	.631	.132	+ 1.0
	.649	.150	−18.3
	.708	0.036	− 2.1

to be partly interstellar and was not included in forming the means. The mean *Ca* II velocity is +12.8 km/sec. Table 2 gives the individual radial velocities for 220 spectrograms, between October 18, 1951, and February 14, 1952. No heliocentric corrections were applied to the dates or the phases. Figures 1–3 show the individual velocity-curves on 15 nights. An inspection of these curves reveals at once that (*a*) there is a marked, and probably periodic, change in $2K$; (*b*) there is no change in $\gamma = +14.0$ km/sec; and (*c*) the precision of determining $2K$ from the individual curves is unusually great—of the order of ± 2 km/sec for a complete curve containing at least one maximum and one minimum.

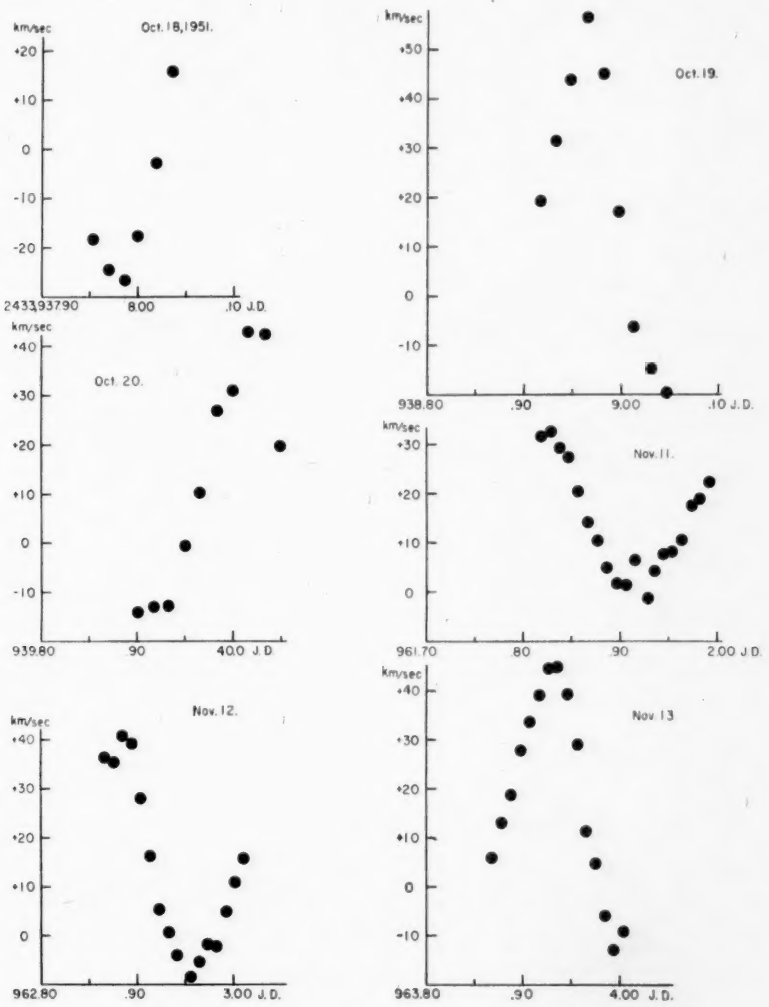

FIG. 1.—Individual radial velocity-curves of ν Eridani

Zessewitch[5] had derived a period of $P = 0.1735073$ day for the radial velocity of ν Eridani. With the epoch for minimum radial velocity at JD 2423709.816, October 16, 1923, it covers reasonably well a range of 46,453 cycles, or 8060 days, from December 18, 1902, to January 11, 1925. However, it does not fit the 1951 and 1952 observations, as is shown in Table 3; the differences between the observed and calculated phases at minimum velocity amount to about half the period. With the same epoch as given by Zessewitch, a slight change of the period has to be made in order to fit the 1951 and 1952

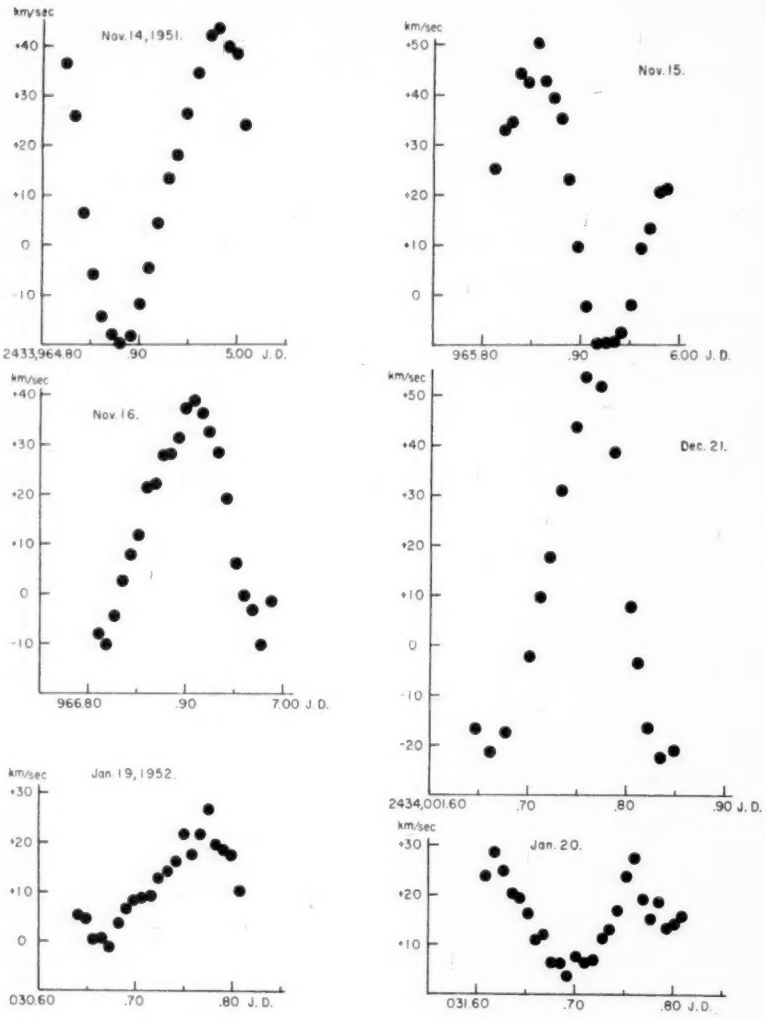

FIG. 2.—Individual radial velocity-curves of ν Eridani

observations. The best fit is obtained with a period $P_2 = 0.1735089$ day. The table shows that it covers a range of 76,112 cycles or 13,206 days, from December 18, 1915, to February 14, 1952, but it does not represent the two early observations on December 10, 1912, and October 26, 1906. From this discussion the change of the period of the radial velocity, although small, seems to be real. The beat period, if it exists, must also change, owing to this change of the radial-velocity period. The phases given in Table 2 were computed from the formula:

$$\text{Minimum radial velocity} = \text{JD } 2423709.816 + 0.1735089E\,. \qquad (1)$$

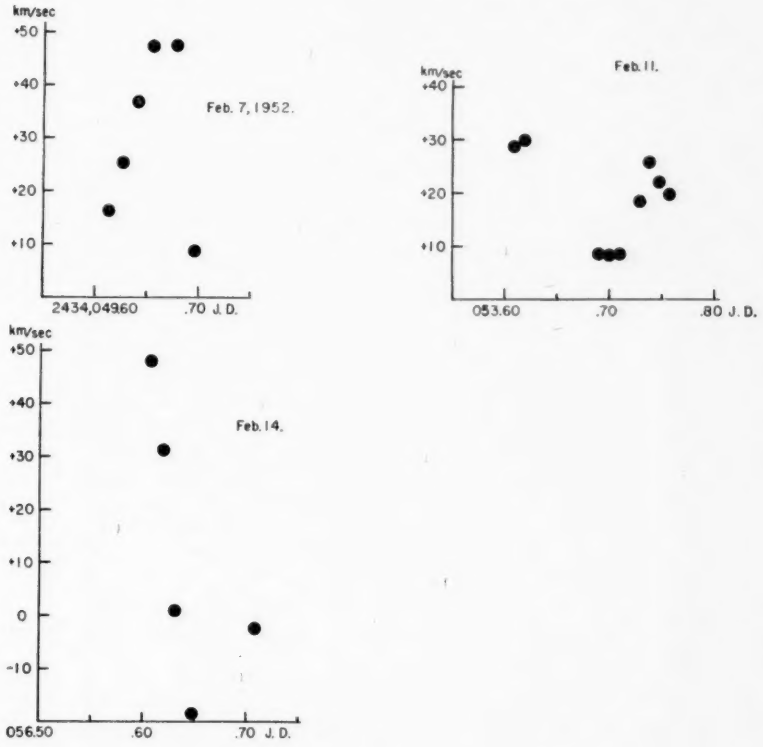

FIG. 3.—Individual radial velocity-curves of ν Eridani

In Tables 4 and 5 are listed the observed values of $2K$, estimated from Henroteau's[2] observations and from our own set of observations. A close examination of the dates and values of $2K$ of Henroteau's observations, beginning with JD 2424062.8, indicates that the minimum values of $2K$ appear to occur in intervals of 7 days. This is supported by our own February observations, which give two large values of $2K$ separated by an interval of 7 days and a very small value of $2K$ falling approximately halfway between them.

TABLE 3

DETERMINATION OF THE PRINCIPAL PERIOD, P_2

E	Observed Minimum Velocity		O−C	
	Date	JD	$P=0^d.1735073$	$P=0^d.1735089$
−43843	Dec. 18, 1902	2416102.700	-35×10^{-3}	$+5\times10^{-3}$
35728	Oct. 26, 1906	17510.753	+6	+63
22837	Dec. 10, 1912	19747.476	+46	+83
16479	Dec. 18, 1915	20850.595	+6	+32
6357	Oct. 8, 1920	2606.837	+7	+17
6346	10	608.738	−1	+9
6335	12	610.671	−24	+34
6288	20	618.783	−19	−9
6277	22	620.710	−1	+9
− 6139	Nov. 15	644.646	−9	+1
0	Oct. 16, 1923	2423709.816	0	0
6	17	710.870	+13	+13
29		714.837	−11	−11
34	21	715.710	−5	−5
35	22	.880	−9	−9
57	26	719.730	+24	+24
75	29	722.802	−27	−27
92	Nov. 1	725.790	+11	+11
161	13	737.740	−11	−11
213	22	746.783	+10	+10
230	25	749.706	−17	−17
310	Dec. 9	763.587	−16	−17
311	9	763.769	−8	−8
322	11	765.680	−5	−6
339	14	768.650	+15	+14
356	17	771.589	+4	+4
357		.751	−7	−8
368	19	773.688	+21	+21
391	23	777.638	−19	−20
454	Jan. 3, 1924	788.596	+8	+7
477	7	792.550	−29	−30
569	23	808.556	+14	+13
2023	Oct. 1	2424060.834	+13	+9
2034	3	062.752	+22	+19
2046	5	064.812	0	−3
2063	8	067.758	−4	−7
2069	9	068.804	+1	−2
2075	10	069.850	+6	+3
2086	12	071.753	+1	−3
2092	13	072.787	−6	−10
2127	19	078.858	−8	−11
2167	26	085.780	−26	−29
2179	28	087.884	−4	−7
2184	29	088.753	−3	−6
2248	Nov. 9	099.859	−1	−5
2264	12	102.651	+14	+11
2265		.824	+14	+10
2288	16	106.788	−13	−16
2293	17	107.670	+2	−2
2351	27	117.743	+11	+8
2391	Dec. 4	124.690	+18	+14
2431	11	131.620	+8	+4
2449	14	134.720	−15	−19
2546	31	151.560	−6	−10
2610	Jan. 11, 1925	162.660	−10	−14
57414	Jan. 25, 1951	2433671.653	+89(−85)	−3
57420	26	672.700	+95(−79)	+3
58590	Oct. 18	937.987	−89(+85)	−10

TABLE 3—*Continued*

E	Observed Minimum Velocity		O−C	
	Date	JD	$P=0^d.1735073$	$P=0^d.1735089$
59087	Nov. 11, 1951	2433961.920	-5×10^{-3}	-16×10^{-3}
59093	12	962.953	+71	−24
59099	13	963.994	+70	−24
59104	14	964.881	+90(−84)	−5
59110	15	965.923	+91(−83)	+8
59115	16	966.819	+119(−55)	+24
59317	Dec. 21	2434001.835	+86	−8
59483	Jan. 19, 1952	030.670	+123(−51)	+24
59489	20	031.693	+101(−73)	+6
59616	Feb. 11	053.700	+43	−23
59634	14	056.660	+72	−12

TABLE 4

Amplitudes of Radial Velocity-Curves (Henroteau)

Julian Day	$2K$ (Km/Sec)	Julian Day	$2K$ (Km/Sec)	Julian Day	$2K$ (Km/Sec)
2422295.7	26	2423765.6	52	2424072.8	47
606.8	50	768.6	28	075.8	27
608.8	44	771.6	54	076.7	23
610.8	30	773.6	30	078.8	50
618.8	42	777.7	50	082.8	36
620.8	70	786.5	65	083.8	22
644.8	35	788.6	65	085.8	38
2423708.8	32	792.5	32	086.8	54
709.8	58	806.5	60	087.8	70
710.8	42	808.5	40	088.8	63
714.8	31	2424060.8	52	099.8	51
715.8	60	061.8	40	102.7	25
719.7	24	062.8	22	106.8	60
725.7	62	064.8	45	107.7	72
726.7	42	066.8	60	124.7	31
732.7	70	067.8	49	151.7	52
746.7	21	068.8	36	162.6	64
749.7	60	069.8	28		
763.7	24	071.8	42		

TABLE 5

Variation of $2K$ in 48 ν Eridani (1951–1952)

Date	JD	Phase (Days)	$2K$ (Km/Sec)	Date	JD	Phase (Days)	$2K$ (Km/Sec)
1951				1951			
Oct. 18	2433937.91	0.6	78	Nov. 16	2433966.91	1.7	49
19	938.96	1.7	75	Dec. 21	2434001.76	1.7	76
20	940.02	2.7	56	1952			
Nov. 11	961.83	3.6	32	Jan. 19	030.78	2.8	23
12	962.88	4.7	48	20	031.62	3.6	22
13	963.93	5.7	56	Feb. 7	049.66	0.7	70
14	964.98	6.8	63	11	053.62	4.6	21
15	965.86	0.7	59	14	056.60	0.6	73

The best-determined epochs of maximum values of $2K$ from Henroteau's observations are JD 2423709.8 and JD 2424087.8. These dates give a difference of 378 days. In order to retain a period near 7 days, this difference corresponds to periods of 6.873, 7.00, and 7.132 days, depending upon the number of cycles. If we adopt as our epoch JD 2433965.2 for the maximum value of $2K$, we find that periods near 6.873 and 7.132 days are inconsistent with our own data. Referring to Table 6, we find that periods of 6.9808 and 6.9905 days give almost the same residuals. It is interesting to note that a period of 6.85 days was found by Zessewitch. It is evident that there is no way to distinguish which is the most reliable period. The net result is that the exact beat period cannot be found with the present data.

TABLE 6

TIME OF MAXIMUM VALUES OF $2K$, OBSERVED AND COMPUTED

$2K$ Max. Obs.	$P_3 = 6.9808$ Days		$P_3 = 6.9905$ Days	
	$2K$ Max. Calc.	O−C	$2K$ Max. Calc.	O−C
JD				
2422299.2	2422300.3	−1.1	2422298.1	+1.1
620.8	621.4	−0.6	619.6	+1.2
2423709.8	2423710.4	−0.6	2423710.1	−0.3
715.8	717.4	−1.6	717.1	−1.3
732.7	731.3	+1.4	731.1	+1.6
750.0	752.3	−2.3	752.1	−2.1
787.5	787.2	+0.3	787.0	+0.5
806.5	808.1	−1.6	808.0	−1.5
2424066.8	2424066.4	+0.4	2424066.7	+0.1
073.2	073.4	−0.2	073.6	−0.4
080.0	080.4	−0.4	080.6	−0.6
087.8	087.4	+0.4	087.6	+0.2
107.7	108.3	−0.6	108.6	−0.9
2433937.9	2433937.3	+0.6	2433937.2	+0.7
965.2	965.2	0.0	965.2	0.0
2434001.8	2434000.1	+1.7	2434000.2	+1.6
056.6	056.0	+0.6	056.1	+0.5

We shall adopt the period $P_3 = 6.9808$ days for the purpose of illustration. Table 7 gives the time of observed maximum of $2K$, the calculated time of maximum of $2K$, and the difference (O − C). The maximum values of $2K$ were calculated with the aid of the formula:

$$\text{Max. of } 2K = 2433965.2 + 6.9808 \text{ days} .$$

These results are plotted in Figure 4. There is no doubt that the maximum values of $2K$ vary from one cycle of the beat period to the next, since the November 11–16 observations clearly pass through a maximum with $2K = 64$ km/sec. Yet we have $2K$ values in excess of 75 km/sec.

The values of K_1 and K_2 can be found from the minimum and maximum values of $2K$. We have, first, for the extensive ranges in K:

$$K_2 + K_1 = 40 \text{ km/sec} , \qquad K_2 - K_1 = 10 \text{ km/sec} ,$$

from which we find $K_2 = 25$ km/sec and $K_1 = 15$ km/sec. From the November 11–16 set of observations we find

$$K_2 + K_1 = 32 \text{ km/sec} ; \qquad K_2 = 24 \text{ km/sec} ;$$
$$K_2 - K_1 = 16 \text{ km/sec} ; \qquad K_1 = 8 \text{ km/sec} .$$

These results indicate that K_1 is variable.

In Table 8 we have listed the times of the observed maxima of the short-period variation. We have also calculated the maximum with the aid of the equation

$$\text{Vel. max.} = 2433965.857 + 0.1735089E \ .$$

The period is the same as that of formula (1), but the epoch corresponds to the time when maximum velocity was actually observed on November 15, 1951. This epoch does not precisely differ by $(n + \frac{1}{2})P_2$ from the epoch of formula (1), because the velocity-curves

TABLE 7

TIMES OF MAXIMUM RADIAL VELOCITY, OBSERVED AND COMPUTED, WITH $P_2 = 6.9808$ DAYS

Date	Max. Obs.	Max. Calc.	O−C (Days)	Phase (Days)
1951				
Jan. 25	2433671.750	2433671.759	−0.009	6.7
26	672.621	672.627	− .006	0.6
Oct. 19	938.965	938.963	+ .002	1.7
20	940.020	940.004	+ .016	2.7
Nov. 12	962.887	962.907	− .020	4.7
13	963.933	963.948	− .015	5.7
14	964.980	964.989	− .009	6.8
15	965.857	965.857	.000	0.7
16	966.908	966.898	+ .010	1.7
Dec. 21	2434001.765	2434001.773	− .008	1.7
1952				
Jan. 19	030.775	030.749	− .026	2.7
20	031.628	031.617	+ .011	3.6
Feb. 7	049.667	049.662	+0.005	0.7

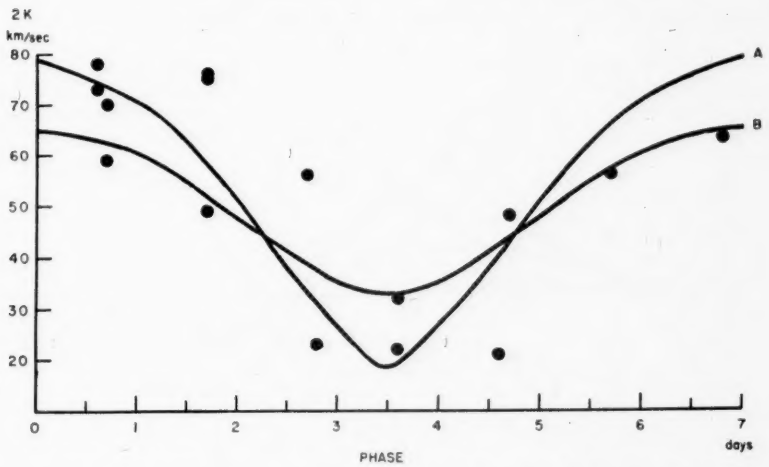

FIG. 4.—Variation of $2K$ in ν Eridani. Curve A is based on $K_2 = 24.5$ km/sec, and $K_1 = 15$ km/sec. Curve B is based on $K_2 = 24.5$ km/sec, and $K_1 = 8$ km/sec (see *Ap. J.*, **112**, 537, 1950, for the theoretical expression).

are slightly unsymmetrical. The differences (O − C) are given in the fourth column of Table 8 and the phases of the maximum, in terms of the beat period, are given in the fifth column. We have included two maxima taken from Walker's[3] 1951 observations of ν Eridani. The results are presented graphically in Figure 5. They show the same behavior as the (O − C) points in 16 Lacertae. It is interesting to note that Walker's observations agree with the present ones. Our period predicts a maximum between his two radial velocity-curves. This would indicate that the maximum amplitude of $2K$ can be as low as the 54 km/sec indicated by his velocity-curve in one cycle of the beat period. Since

TABLE 8

LINE WIDTHS OF 48 ν ERIDANI*

Position on Radial Velocity-Curve		1951										1952				
		Oct. 18	Oct. 19	Oct. 20	Nov. 11	Nov. 12	Nov. 13	Nov. 14	Nov. 15	Nov. 16	Dec. 21	Jan. 19	Jan. 20	Feb. 7	Feb. 11	Feb. 14
Descending branch	Top				B											
	Bottom	Bc	Bc							Bc						
	Upper											Bc				
	Middle												B			
	Lower											Bc				
Ascending branch	Upper			Bc	B			A B	A Bc							
	Middle		Bc				A	A B	Bc				A B			
	Lower	A			A	A B	A B	A	A B	A Bc	S	A				S

*"S" means "sharp," as given by McNamara, who based his estimates on all lines of the Lick Mills plates. "A" means "sharp," as given by Kraft, who based his estimates on the five lines λ λ3964, 4101, 4267, 4340, and 4471 of the Mount Wilson plates. "B" means "sharp," as given by Kung, who based his estimates on the three lines λ λ 4101, 4120, and 4143 of the Mount Wilson plates. "Bc" means "comparatively sharp," i.e., less conspicuous, as given by Kung.

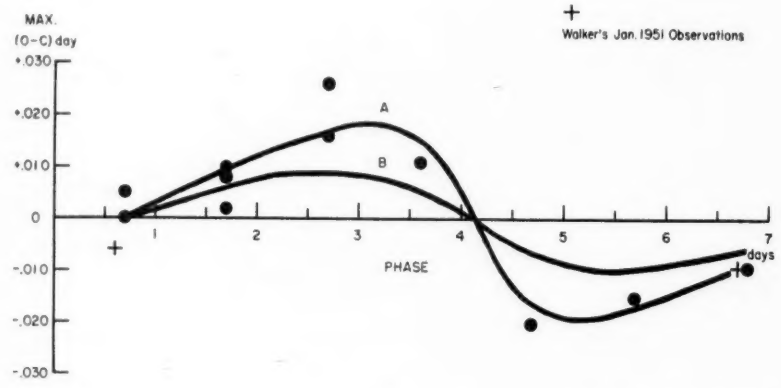

FIG. 5.—Variation in the times of maximum radial velocity. Curve A is based on $K_2 = 24.5$ km/sec, and $K_1 = 15$ km/sec. Curve B is based on $K_2 = 24.5$ km/sec, and $K_1 = 8$ km/sec (see *Ap. J.*, **112**, 537, 1950, for the theoretical expression).

$2K_2 = 48$–50 km/sec, K_1, which seems to be the variable, can be as small as 2–3 km/sec. If this is the case, we should expect very little variation in the velocity-curve from one night to the next. Walker's light- and velocity-curves appear to show little or no variation from January 24 through January 26.

There is some uncertainty about the designations P_1 and P_2, and the corresponding semiamplitudes K_1 and K_2. In other stars we have used the subscript 1 to designate that oscillation which is not accompanied by a change in line profile. In β CMa the distinction was clear, and $P_2 > P_1$, $K_1 > K_2$, but in all other stars the variation in line profile was found to be associated with the larger velocity amplitude: $K_2 > K_1$.

Our material is not very suitable for a study of the line profiles, because the Mount Wilson spectrograms were obtained with small dispersion (32 A/mm). The variation found by McNamara on the Lick plates, which have a dispersion of 10 A/mm, was large, but the number of Lick plates is too small for an exhaustive study. Nevertheless, an attempt was made to estimate the character of the lines on all spectrograms.

All the measurers were impressed by the apparent change in the sharpness of the same spectral lines, especially $H\gamma$ and $H\delta$, in a sequence of spectra. For the Mount Wilson plates a comparator was used, in order to match each spectrum of a selected plate with the spectra of the other plates. The line quality was designated arbitrarily 1, 2, 3, 4, according to the degree of increasing diffuseness. The result, based upon estimates by several persons, is shown in Table 8 and appears to indicate that the sharp-line stage falls mostly upon the ascending branch of the radial velocity-curve, especially its lower part. This justifies our designation of P_2 and K_2 as corresponding to the larger value of amplitude, $K_2 > K_1$. But it should be noted that in β CMa, 12 Lac, etc., it was always K_2 that was found to vary, not K_1, which varies in ν Eridani. The two interfering oscillations are as follows:

$$P_1 = 0.1779 \text{ day} \; ; \qquad K_1 < 8 \text{ to } 15 \text{ km/sec} \; ;$$

$$P_2 = 0.1735089 \text{ day} \; ; \qquad K_2 = 24.5 \text{ km/sec} \; .$$

The principal conclusion from this work is that a beat period is discernible, but that its clear-cut effect is partly obliterated by large, and perhaps irregular, variations of K_1. Such variations may at times reinforce the beat effect of the $2K$ and the (O − C) curves (Figs. 4 and 5) and may also, at times, distort the beat period P_3. We believe that this may be the most reasonable explanation of the difference in P_3 found by us from the radial velocities and the value found by Walker from the photoelectric observations. We already know that in 16 Lac the ratio $\Delta m_1/\Delta m_2 \neq K_1/K_2$. Hence the degree of distortion caused by a change in Δm_1 may not be the same as that caused by a change in K_1.

THE CURVE OF LINE-WIDTH CORRELATION AND DOPPLER VELOCITIES IN STELLAR ATMOSPHERES*

I. DELTA CANIS MAJORIS

SU-SHU HUANG† AND OTTO STRUVE
Berkeley Astronomical Department, University of California
Received April 18, 1952

ABSTRACT

A new method of studying Doppler velocities in stellar atmospheres is proposed. It depends upon a relation between the equivalent widths and the half-widths of the absorption lines. Turbulent velocities of both large and small eddies can be determined by this method. Applying it to δ Canis Majoris, we find that the turbulent velocities of large eddies are practically constant with respect to the strengths of the absorption lines and that the turbulent velocities of small eddies increase very rapidly with the increase of line intensities. A general discussion is given of the interrelationship between the turbulent spectrum and the Doppler broadening of absorption lines, but no attempt has been made to explain the physical nature of the large eddies.

I. INTRODUCTION

As was mentioned in a previous communication,[1] the curve of growth represents one of the most powerful methods employed in astrophysical research. But, unfortunately, it involves some uncertainties and difficulties. The uncertainties lie in the position of the continuum determined in the stellar spectrum from which the equivalent widths of spectral lines are obtained and in the *f*-values used in the actual plotting of the observed curve of growth, while the difficulties lie in the interpretation of the results derived by this method. This latter difficulty is more or less formal. Indeed, in the paper mentioned above we have succeeded in giving a meaning to the values of the physical quantities derived by comparison of the observed curve of growth with a theoretical one calculated independently by D. H. Menzel[2] and A. Unsöld.[3] But, for the time being at least, we can see no way to eliminate or to reduce the uncertainties, which can easily lead one to doubt the results obtained from the curve of growth. A recent example is K. O. Wright's relation[4] between turbulent velocities and excitation potentials for the small eddies.[5] Hence it is very desirable to formulate a method which can determine some of the physical quantities in the same manner as the curve of growth but which avoids these uncertainties. We hope the method introduced here may fill this requirement.

Theoretically, the present method is extremely simple. It is a natural result of studying the turbulent velocities of large eddies[6] as well as of small eddies, and it is based on a relation between the equivalent width and the half-width (defined as the width at half-depth) of the spectral lines. Because the number of effective absorbing atoms is eliminated, we need no longer any uncertain *f*-value in order to get an observed curve.

* The observational material used in the present investigation was obtained at the Mount Wilson Observatory.

† John Simon Guggenheim Memorial Foundation Fellow.

[1] S. S. Huang, *Ap. J.*, **115**, 529, 1952.

[2] *Ap. J.*, **84**, 462, 1936.

[3] *Physik der Sternatmosphären* (Berlin: J. Springer, 1938), pp. 266–269.

[4] *J.R.A.S. Canada*, **41**, 49, 1947; R. B. King and K. O. Wright, *Ap. J.*, **106**, 224, 1947; K. O. Wright and E. Van Dien, *J.R.A.S. Canada*, **43**, 15, 1949; L. Goldberg and K. A. Pierce, *O.N.R. Project M720-5*, Ann Arbor, October, 1947; D. H. Menzel and B. Bell, *O.N.R. Project M720-5*, Ann Arbor, June, 1948.

[5] E.g., A. Unsöld and O. Struve, *Ap. J.*, **110**, 455, 1949; S. S. Huang, *Ap. J.*, **112**, 399 and 418, 1950.

A small depression (or lifting) of the continuum in the spectrum will decrease (or increase) the equivalent width and the half-width at the same time. This is equivalent to making the line a little stronger (or weaker) than that corresponding to the real value. Hence, in the present method, the position of the continuum has only a secondary effect upon the observed curve. Moreover, as both the equivalent width and the half-width are considered here, we should expect to derive the turbulent velocities both of small eddies and of large eddies.[6] This is indeed possible, as we shall see in the next section.

On the other hand, the present method has its own defects. First of all, a high-dispersion spectrogram must be used in order that the half-width can be measured. The method is therefore somewhat limited in its applications. Next, the number of effective absorbing atoms does not enter into the final relation, and consequently the excitation temperature is beyond the reach of this method. Finally, although we can estimate the damping constant, it does not give as good an approximation as that given by the curve of growth. The reason for this latter point becomes apparent in Section II. This method can therefore be regarded as an aid to the study of the Doppler velocities in stellar atmospheres only; and in this respect it is obviously much superior to the curve-of-growth method.

In Section II the relations between equivalent width and half-width are first calculated on the basis of an interpolation formula introduced by M. Minnaert.[7] The relations are then plotted on a logarithmic scale, just as for the curve of growth, and are used as a standard for comparison with observed curves. In Section III a general discussion is given of the interrelationship between the sizes of eddies and the formation of spectral lines of different intensities. Some qualitative predictions as to the turbulent broadening of spectral lines are thereby given. Finally, in the last two sections the spectrum of δ Canis Majoris is analyzed, and turbulent velocities of both large eddies and small eddies are derived. Wright's relation between excitation potentials and turbulent velocities of the small eddies is verified. On the other hand, we find that the turbulent velocities of the large eddies do not vary much with the excitation potentials.

II. THE THEORETICAL CURVE OF LINE-WIDTH CORRELATION

As in the calculation of the theoretical curve of growth, we have first to choose a line-profile formula, in order to compute a relation between equivalent widths and half-widths. Different line-profile formulae have been written down,[8] but the one which suits our purpose best is an interpolation formula[7] given by Minnaert. The reason for using this interpolation formula has been fully discussed in a previous paper[1] in connection with a critical study of the curve-of-growth method and therefore will be omitted here. Let N be the number of effective absorbing atoms per unit optical thickness in the continuum and α_ν be the atomic absorption coefficient. Writing x_ν as a certain mean value[9] (defined in the previous paper[1]) of $N\alpha_\nu$, we have, for the depth of an absorption line R,

$$R = \frac{R_c x_\nu}{R_c + x_\nu}, \tag{1}$$

where R_c is the limiting depth of very strong lines and is nearly equal to 1. Following the standard notation,[3] we introduce the Doppler width $\Delta\lambda_D = \xi\lambda/c$ and the damping constant a (in units of the Doppler width) and change the scale in the usual way:

$$v = \frac{\lambda - \lambda_0}{\Delta\lambda_D},$$

[6] E.g., S. S. Huang, *Ap. J.*, **112**, 418, 1950.

[7] *Zs. f. Ap.*, **10**, 40, 1935.

[8] For a survey of line-profile formulae see, e.g., S. S. Huang, "On the Absorption Lines Formed in Stellar Atmospheres" (to appear elsewhere).

[9] It should be noted here that in defining x_ν in this way we have avoided using the concept of the reversing layer.

where λ_0 represents the center of the line. If A_λ is the equivalent width (in angstrom units), we have

$$\frac{A_\lambda}{2R_c\Delta\lambda_D} = \int_0^\infty \frac{aZH(v, a)\,dv}{aZH(v, a) + 1}, \tag{2}$$

where

$$a = \frac{2\pi^{3/2}e^2}{mc} = 9.354 \times 10^{-2}, \qquad Z = \frac{Nf}{R_c\Delta\omega_D}, \tag{3}$$

and

$$H(v, a) = \frac{a}{2\pi}\int_{-\infty}^{\infty} \frac{e^{-y^2}dy}{(a/2)^2 + (v-y)^2}.$$

The relations between $\log [A_\lambda/(2R_c\Delta\lambda_D)]$[10] and $\log Z$ for different values of a obtained from equation (2) are usually understood as the curve of growth based on the Schuster-Schwarzschild model, because the concept of the reversing layer has been used in order to define x_ν in equation (1). On the other hand, equation (1) is not a solution of the equation of transfer for the Schuster-Schwarzschild model but is true for any model with local thermodynamic equilibrium. Moreover, as we have redefined x_ν without using the concept of the reversing layer,[1] it seems to us that equation (2) should be better designated as the curve of growth for local thermodynamic equilibrium.

In a similar manner we can derive a relation between the half-width and the quantity Z. Let D_λ be the half-width in angstrom units and let, for the sake of simplicity,

$$v' = \frac{D_\lambda}{2\Delta\lambda_D}.$$

From the definition of half-width we obtain

$$H(v', a) = \frac{H(0, a)}{2 + aZH(0, a)}. \tag{4}$$

Plotting $\log v'$ against $\log Z$ as obtained from equation (4), we derive another kind of curve of growth. We might appropriately call it "the curve of growth of the second kind." It may be used for all the purposes for which an ordinary curve of growth is used. But as the determination of the half-width is less accurate than that of the equivalent width, while all the uncertainties involved in the plotting of an observed curve of growth remain in the plotting of an observed curve of growth of the second kind, the latter has no practical value.

But the result of eliminating Z from equations (2) and (4) gives a relation of a quite different nature from either curve of growth, because

$$\frac{A_\lambda}{2R_c\Delta\lambda_D} = \int_0^\infty \frac{H(v, a)\,dv}{H(v, a) + [H(0, a)\,H(v', a)]/[H(0, a) - 2H(v', a)]}, \tag{5}$$

which will be called "the curve of line-width correlation," is a relation between two directly observable quantities $A_\lambda/\Delta\lambda_D$ and $D_\lambda/\Delta\lambda_D$. The integration involved in equation (5) is quite complicated and cannot be put into a finite form. It is much easier to compute the curve of line-width correlation directly from equations (2) and (4), because we can then use the results already computed by Unsöld[3] and by Menzel[2] for equation (2) and because equation (4) is not difficult to solve numerically.

Before we give the final result of our computation, it is profitable to consider the asymptotic behavior of the curve of line-width correlation. First we shall consider the damping branch with large Z and with large a, such that

$$aZH(0, a) \gg 2, \tag{6}$$

[10] In this paper we shall consistently use $\ln x$ to denote the natural logarithm of x, and $\log x$ to denote the common logarithm of x.

and v' is already on the damping wing of the absorption line. We have, therefore, approximately

$$H(v', a) = \frac{1}{aZ}. \tag{7}$$

The asymptotic behavior of $H(v, a)$ is well known,[3] and equation (7) reduces to

$$v' = \frac{D_\lambda}{2\Delta\lambda_D} = \frac{(a\,aZ)^{1/2}}{2^{1/2}\pi^{1/4}}. \tag{8}$$

On the other hand, the equivalent widths of spectral lines on the damping branch of the curve of growth are given by[3]

$$\frac{A_\lambda}{2R_c\Delta\lambda_D} = \frac{\pi^{3/4}(a\,aZ)^{1/2}}{2^{3/2}}. \tag{9}$$

It follows from equations (8) and (9) that

$$\log\frac{A_\lambda}{2R_c\Delta\lambda_D} = \log\frac{\pi}{2} + \log\frac{D_\lambda}{2\Delta\lambda_D}, \tag{10}$$

which is independent of a. For this reason the damping constant a cannot be accurately determined by the present method.

Next, we consider the limiting case in which Z is large and a is small, such that equation (7) holds true while v' is on the Doppler core of the absorption lines. It can be easily shown that

$$v'^2 = \ln(aZ). \tag{11}$$

On the other hand, $A_\lambda/(2R_c\Delta\lambda_D)$ in the present case has a well-known asymptotic behavior,[3] hence

$$\frac{A_\lambda}{2R_c\Delta\lambda_D} = v'\left\{1 - \frac{0.4112}{v'^4} - \frac{1.776}{v'^8} - \cdots\right\}. \tag{12}$$

Approximately, we have

$$\log\frac{A_\lambda}{2R_c\Delta\lambda_D} = \log\frac{D_\lambda}{2\Delta\lambda_D}.$$

In the last case the asymptotic behavior of the curve of line-width correlation for weak lines will be considered. If

$$aZH(0, a) \ll 2,$$

and damping is small, we have

$$\exp(-v'^2) = \tfrac{1}{2} - \frac{aZ}{4} + \frac{a^2Z^2}{8} - \frac{a^3Z^3}{16} + \cdots, \tag{13}$$

and[3]

$$\frac{A_\lambda}{2R_c\Delta\lambda_D} = \frac{\sqrt{\pi}}{2}aZ\left\{1 - \frac{aZ}{\sqrt{2}} + \frac{a^2Z^2}{\sqrt{3}} - \frac{a^3Z^3}{\sqrt{4}} + \cdots\right\}. \tag{14}$$

Equations (13) and (14) give the relation between $D_\lambda/(2\Delta\lambda_D)$ and $A_\lambda/(2R_c\Delta\lambda_D)$ in a parametric form. If we neglect a^2Z^2 and higher-order small quantities, they can be combined into the following form:

$$v'^2 = \ln 2 + \frac{A_\lambda}{2R_c\Delta\lambda_D\sqrt{\pi}}. \tag{15}$$

As the equivalent width, $A_\lambda/\Delta\lambda_D$ approaches zero, $v'^2 \to \ln 2$, i.e., no matter how weak the line is, the half-width, v', will never be smaller than $(\ln 2)^{1/2}$. The final result is plotted in Figure 1, which will be used as the standard for comparison with observed curves. Going from the left to the right, the five curves in Figure 1 represent five cases of damping, i.e., $a = 10^{-1}$, $a = 10^{-2}$, $a = 10^{-3}$, $a = 10^{-4}$, and $a = 0$.

III. PROBLEMS OF TURBULENT VELOCITIES IN STELLAR ATMOSPHERES AND APPLICATIONS OF THE CURVE OF LINE-WIDTH CORRELATION

In a previous paper[6] we have divided the eddies, for convenience in describing observational results, into two kinds according to the manner in which they broaden the absorption line: the "large eddies" with linear dimensions greater than, and the "small

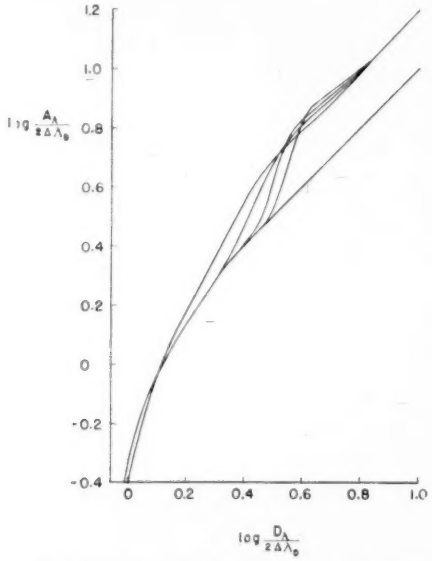

FIG. 1.—The curve of line-width correlation. The curve shows the relative growth of the equivalent width, A_λ, and of the half-width, D_λ. The line widths are measured in units of the Doppler width, $\Delta\lambda_D$.

eddies" with linear dimensions smaller than, the thickness of the reversing layer. The large eddies broaden the absorption lines without increasing their equivalent widths, while the small eddies both broaden the lines and increase their equivalent widths. In this manner we can expect quite naturally that supergiant stars will show high turbulent velocities in the curve of growth, while haziness of absorption lines in dwarf stars may sometimes be attributed to the effect of turbulent velocities of large eddies, as well as to the Stark effect and to axial rotation.

The difficulty of the previous definition of the "large eddies" and the "small eddies" lies in the fact that the reversing layer itself is not a well-defined physical entity. If we understand the reversing layer as that part of a stellar atmosphere in which the absorption line is formed, the thickness of the reversing layer is different for lines of different intensities and, worst of all, different at different frequencies for the same line. In this manner we can see how complicated is the broadening of absorption lines by turbulence. It is therefore impossible to disentangle broadening by one kind of turbulence from that

by the other. In order to give some physical meaning to the observational results that have been reached or that could be reached, we must make some approximations. This can be done by assigning an average thickness of the reversing layer to each of the absorption lines, i.e., we take an average with respect to the frequency in the same manner as we have done in a previous paper.[1] In this way we can speak about "large (or small) eddies with respect to a certain line (or a certain group of lines)" instead of simply about "large (or small) eddies." This description is somewhat more exact than the previous one.

Since the reversing layer for a weak line is much thicker than that for a strong line, the latter is broadened more by velocities of large eddies than is the weak line. At the same time, the strong line is broadened less by velocities of small eddies than is the weak line. This can be easily seen from a diagram of the turbulent spectrum. In Figure 2 the velocity is plotted against the size of the eddies. The vertical lines AB and $A'B'$ represent the thicknesses of the reversing layers τ_1 and τ_2 of two absorption lines; the one is evidently stronger than the other. Similarly, for each absorption line there should be a corre-

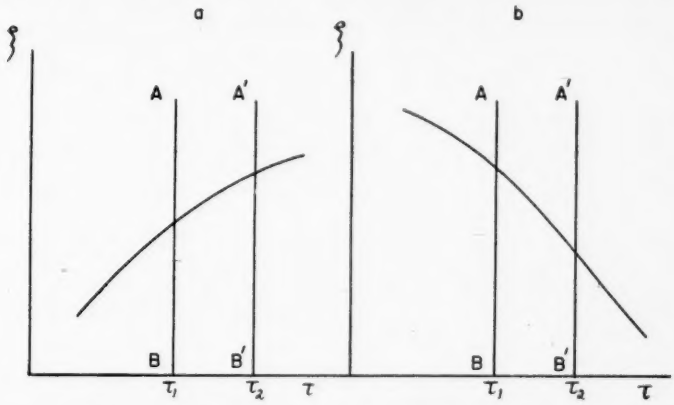

FIG. 2.—The turbulent spectrum and the definition of the large eddies and of the small eddies. The curves are drawn only for illustration and therefore do not have any quantitative significance.

sponding vertical line to represent the thickness of the reversing layer for that particular absorption line. And all eddies having sizes falling to the left (right) of a vertical line are therefore small (large) eddies with respect to the absorption line to which this particular vertical line corresponds. Hence an eddy with a definite size can be a small eddy with respect to one absorption line, while at the same time it is a large eddy with respect to a stronger absorption line. In the case of curve *a* in Figure 2, the velocities of small eddies increase as the lines become weaker, while the velocities of large eddies remain the same. (Note that we have considered only the fastest-moving eddy,[6] which is responsible for the observational results.) In the case of curve *b*, the velocities of large eddies decrease as the lines become weaker, while the velocities of small eddies remain the same. All these considerations would hold true, provided only that the turbulent spectrum were the same at every point in the stellar atmospheres. The observational results tell us, however, that the strong lines show larger velocities for the small eddies; the turbulent spectrum must, therefore, depend on the height in the atmosphere. Or among the small eddies the fastest-moving ones must have a higher velocity in an upper layer of the atmosphere than at a deeper layer.

Consider now the curve of line-width correlation. For the equivalent widths, velocities

of small eddies only (including thermal motion, for simplicity) are responsible, while, for the half-width, velocities of both kinds of eddies are responsible. Thus, for the equivalent width, the Doppler width should be

$$(\Delta\lambda_D)_1 = \frac{\xi_1 \lambda}{c}, \tag{16}$$

while for the half-width the Doppler width should be

$$(\Delta\lambda_D)_2 = \frac{\xi_2 \lambda}{c}, \tag{17}$$

where ξ_1 is the turbulent velocity which should be derived from the curve of growth (i.e., thermal motion and motion of small eddies); and ξ_2 is the turbulent velocity which should be derived from the line profiles (i.e., thermal motion and motion of both kinds of eddies). If we assume the Gaussian distribution of velocities of both kinds of eddies and denote the random velocity of small eddies by ξ_s and that of large eddies by ξ_l, it follows that[11]

$$\xi_1 = \xi_s \quad \text{and} \quad \xi_2^2 = \xi_s^2 + \xi_l^2. \tag{18}$$

Plot $\log (A_\lambda/\lambda)$ against $\log (D_\lambda/\lambda)$ from the analysis of a spectrogram, and compare this observed curve to the theoretical curve of line-width correlation given in Section II, so that a good fit is obtained; the shift in the abscissa gives $\log (2\xi_2/c)$ and the shift in the ordinate gives $\log (2\xi_1/c)$. Hence ξ_1 and ξ_2, and consequently ξ_s and ξ_l, are determined.

It should be noted that, in determining the horizontal shift, we have automatically made some assumptions regarding the nature of broadening by large eddies. As a matter of fact, we have assumed that, owing to the existence of large eddies, the line-profile formula given by equation (1) changes only by a scale factor. This is obviously an approximation and is open to further study.

Concluding this section, we should mention that in the present investigation we emphasize only the kinematic nature in stellar atmospheres of the *observable Doppler motion*, which we call "turbulence."[12] We present here only a method of analysis for studying Doppler motion in stellar atmospheres, without committing ourselves as to the physical or dynamical nature of "turbulence."

IV. THE OBSERVED DATA IN THE SPECTRUM OF δ CANIS MAJORIS

For a study of the velocities of both large eddies and small eddies, δ Canis Majoris is one of the most suitable stars, because we have already pointed out in a previous paper[13] that the line-widths of the absorption lines are much wider than the value that is consistent with the curve of growth.[14] A coudé spectrogram (a print of which is reproduced in Fig. 3) was taken on October 21–22, 1951, at Mount Wilson by one of us (O. S.). A photometric tracing of the complete spectrogram was then made at the Lick Observa-

[11] Because we have used the half-width instead of the root-mean-square width, the second equation in (18) holds only approximately. Thus ξ_l determined in the present paper should be subject to some uncertainty (see *Ap. J.*, **112**, 418, 1950).

[12] In this sense even the stellar rotation is included in the definition of "turbulence." As a matter of fact, we can determine the velocity of stellar rotation by the method presented in this paper. But to distinguish stellar rotation from the other kinds of mass motion in stellar atmospheres will be the subject of further investigations. Moreover, as stars of high luminosity rarely show appreciable rotation, we might exclude the possibility of rotation in the present paper, where a supergiant star is considered.

[13] O. Struve, *Ap. J.*, **104**, 138, 1946.

[14] *J.R.A.S. Canada*, **41**, 49, 1947.

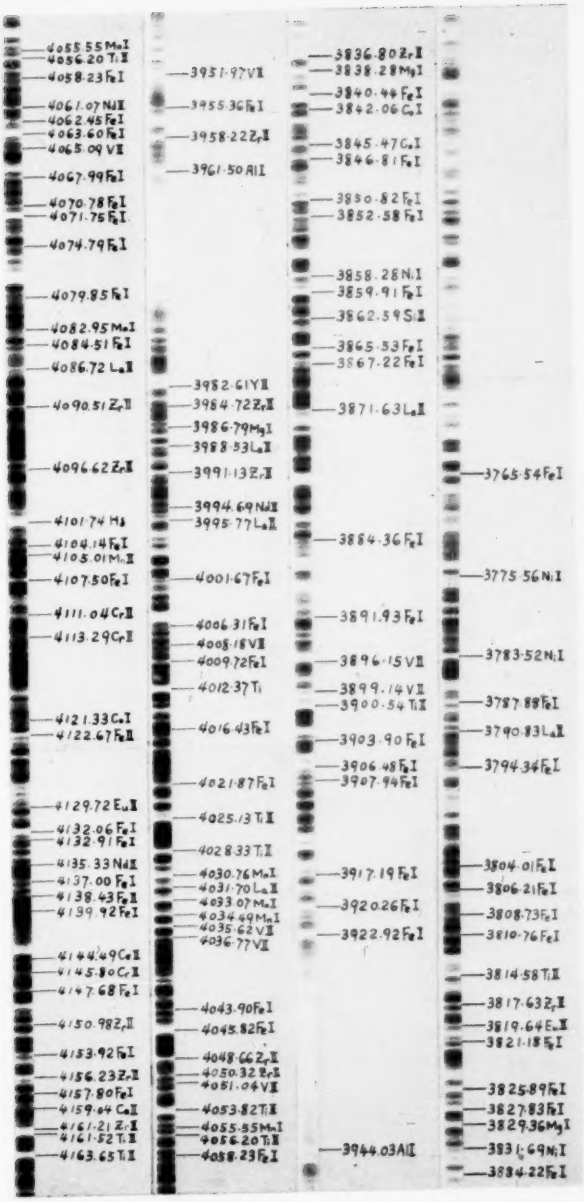

FIG. 3*a*.—The spectrum of δ Canis Majoris, from a coudé spectrogram taken at the Mount Wilson Observatory.

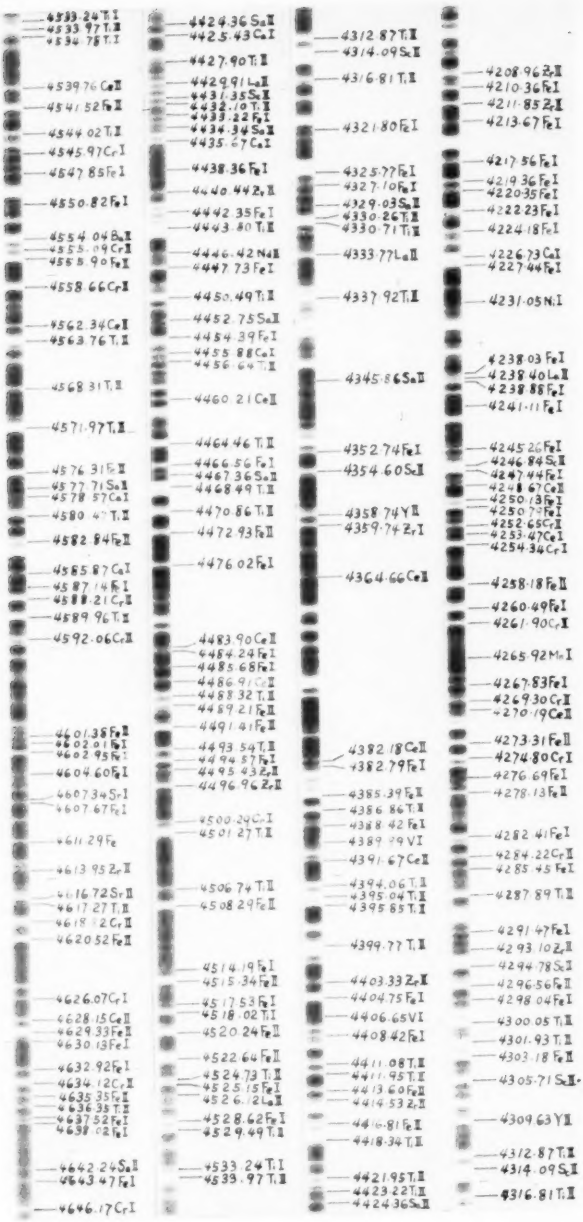
4533.24 Ti I
4533.97 Ti I
4534.78 Ti I
4539.76 Ce II
4541.52 Fe II
4544.02 Ti I
4545.97 Cr I
4547.85 Fe I
4550.82 Fe I
4554.04 Ba II
4555.09 Cr I
4558.9 Fe I
4558.66 Cr I
4562.34 Ce I
4563.76 Ti I
4568.31 Ti II
4571.97 Ti II
4576.31 Fe II
4577.71 Sc II
4578.57 Ca I
4580.47 Ti II
4582.84 Fe II
4585.87 Ca I
4587.14 Fe I
4588.21 Cr I
4589.96 Ti II
4592.06 Ce II
4601.38 Fe II
4602.01 Fe I
4602.95 Fe I
4604.60 Fe I
4607.34 Sr I
4607.67 Fe I
4611.29 Fe
4613.95 Zr II
4616.72 Sr II
4617.27 Ti II
4618.82 Cr II
4620.52 Fe II
4626.07 Cr I
4628.15 Ce II
4629.33 Fe II
4630.13 Fe I
4632.92 Fe I
4634.12 Cr I
4635.35 Fe I
4636.33 Ti II
4637.52 Fe I
4638.02 Fe I
4642.24 Sc II
4643.47 Fe I
4646.17 Cr I
4424.36 Sc II
4425.43 Ca I
4427.90 Ti II
4429.91 La II
4431.35 Sc II
4432.10 Ti II
4433.22 Fe I
4434.34 Sc II
4435.67 Ca I
4438.36 Fe I
4440.44 Zr II
4442.35 Fe I
4443.80 Ti II
4446.42 Nd II
4447.73 Fe I
4450.49 Ti II
4452.75 Sc II
4454.39 Fe I
4455.88 Ca I
4456.64 Ti II
4460.21 Ce II
4464.46 Ti II
4466.56 Fe I
4467.36 Sc II
4468.49 Ti II
4470.86 Ti II
4472.93 Fe II
4476.02 Fe I
4483.90 Ce II
4484.24 Fe I
4485.68 Fe I
4486.91 Cr II
4488.32 Ti II
4489.21 Fe II
4491.41 Fe II
4493.54 Ti II
4494.57 Fe I
4495.43 Zr II
4496.96 Zr II
4500.29 Cr I
4501.27 Ti II
4506.74 Ti II
4508.29 Fe II
4514.19 Fe I
4515.34 Fe II
4517.53 Fe I
4518.02 Ti I
4520.24 Fe II
4522.64 Fe II
4524.73 Ti II
4525.15 Fe I
4526.21 La II
4528.62 Fe I
4529.49 Ti II
4533.24 Ti I
4539.97 Ti II
4312.87 Ti II
4314.09 Sc II
4316.81 Ti II
4321.80 Fe I
4325.77 Fe I
4327.10 Fe I
4329.03 Sc II
4330.26 Ti II
4330.71 Ti II
4333.77 La II
4337.92 Ti II
4345.86 Sc II
4352.74 Fe I
4354.60 Sc II
4358.74 Y II
4359.74 Zr I
4364.66 Ce II
4382.18 Ce II
4382.79 Fe I
4385.39 Fe II
4386.86 Ti II
4388.42 Fe I
4389.29 V I
4391.67 Ce II
4394.06 Ti II
4395.04 Ti II
4395.85 Ti II
4399.77 Ti II
4403.33 Zr II
4404.75 Fe I
4406.65 V I
4408.42 Fe I
4411.08 Ti II
4411.95 Ti II
4413.60 Fe I
4414.53 Zr II
4416.81 Fe I
4418.34 Ti II
4421.95 Ti II
4423.22 Ti II
4424.36 Sc II
4208.96 Zr II
4210.36 Fe I
4211.85 Zr I
4213.67 Fe I
4217.56 Fe I
4219.36 Fe I
4220.35 Fe I
4222.23 Fe I
4224.18 Fe I
4226.73 Ca I
4227.44 Fe I
4231.05 Ni I
4238.03 Fe I
4238.40 La II
4238.88 Fe I
4241.11 Fe I
4245.26 Fe I
4246.84 Sc II
4247.44 Fe I
4248.67 Ce II
4250.13 Fe I
4250.79 Fe I
4252.65 Cr I
4253.47 Ce I
4254.34 Cr I
4258.18 Fe II
4260.49 Fe I
4261.90 Cr I
4265.92 Mn I
4267.83 Fe I
4269.30 Cr II
4270.19 Ce II
4273.31 Fe II
4274.80 Cr I
4276.69 Fe I
4278.13 Fe II
4282.41 Fe I
4284.22 Cr II
4285.45 Fe I
4287.89 Ti II
4291.47 Fe I
4293.10 Zr II
4294.78 Sc II
4296.56 Fe II
4298.04 Fe I
4300.05 Ti II
4301.93 Ti II
4303.18 Fe II
4305.71 Sc II
4309.63 Y II
4312.87 Ti II
4314.09 Sc II
4316.81 Ti II

FIG. 3*b*.—Same

tory. The reduction follows the usual way, while the correction of the instrumental broadening of the half-width has been carried out only in a certain approximation.

Let the instrumental broadening function be a Gaussian one. For weak lines, it follows from equation (1) that $R \rightarrow_a ZH(v, a)$. The damping wing is not important in the weak line of a supergiant star. We have therefore a Gaussian function broadened by another Gaussian function. If v_o is the observed half-width of an absorption line; v_i, the half-width of the instrumental broadening function; and v_t the true half-width of the absorption line, we have

$$v_o^2 = v_i^2 + v_t^2 . \tag{19}$$

Equation (19) is no longer true for strong lines. The deviation from equation (19) increases with the strength of the spectral line. But as v_t becomes wider and wider, the percentage error which is important in the plotting of log v_t will not increase greatly. Thus with a certain approximation we can still apply equation (19) to strong lines. Two average values of v_i^2 (0.0090 and 0.0108) have been determined from the tracing of the weak comparison lines[15] for the regions λλ 3765–4158 and λλ 4210–4648, respectively.

Absorption lines of *Fe* I in the region between λ 3765 and λ 4648 A have been selected for the purpose of plotting the observed curves of line-width correlation. They are identified with the aid of T. Dunham, Jr.'s, tables[16] of the wave lengths in the spectrum of α Persei. The lines chosen are believed to have no serious blends. The results of the measures, after proper reduction, are given in Table 1, which lists the wave length, the excitation potential in e.v., the equivalent width, A_λ, in angstrom units, the half-width, D_λ, in angstrom units, log $(10^6 A_\lambda/\lambda)$, and log $(10^6 D_\lambda/\lambda)$.

V. DOPPLER VELOCITIES AS DERIVED FROM THE SPECTRUM OF δ CANIS MAJORIS

We now divide the absorption lines listed in Table 1 into four groups according to the excitation potentials of their lower levels. The first group includes all lines with excitation potential 0.000–1.007 e.v., the second group 1.008–2.3 e.v., the third group 2.3–3.1 e.v., and the fourth group 3.1–3.9 e.v. For each group we plot an empirical curve of line-width correlation and compare it with the theoretical curve given in Figure 1 (with $R_c = 1$). Thus we obtain the velocity ξ_1 as derived from the curve of growth and the velocity ξ_2 as derived from line profiles according to the method described at the end of Section III. The velocities ξ_t and ξ_s, respectively, of large eddies and of small eddies follow immediately from equation (19). The comparison of the theoretical curve with the observed curve of line-width correlation is shown in Figure 4, and the numerical values thus determined are given in Table 2, in which the mean excitation potential of each group is the mean of the two limits but is not the average of all lines in the group. It is of interest to note that, for lines of low excitation potentials, the observed points are less scattered than for lines of higher excitation potentials. This is not surprising, because the profiles of lines arising from high levels cannot be well represented by a single interpolation formula such as the one we have used.[1] It is therefore an advantage to use the present statistical method in studying the half-widths of lines instead of investigating individual lines.

The turbulent velocities of small eddies thus determined are higher than Wright's determination[14] based on J. O'Keefe's measurement.[17] But the general behavior of the relation between ξ_s and the mean excitation potential χ has the same form in both determinations. In connection with the turbulent velocities of large eddies we have found

[15] J. L. Greenstein, *Ap. J.*, **95**, 161, 1942.

[16] See *Contr. Princeton U. Obs.*, No. 9, 1929, for the photographic region; an unpublished list for the ultraviolet region.

[17] H. R. Steel, *Ap. J.*, **102**, 429, 1945.

TABLE 1

Fe I LINES IN THE SPECTRUM OF δ CANIS MAJORIS

λ	Excitation Potential (e.v.)	Equivalent Width, A_λ (A)	Half-Width D_λ (A)	log $(10^5 A_\lambda/\lambda)$	log $(10^5 D_\lambda/\lambda)$
3765.54	3.22	0.640	0.673	2.230	2.251
3787.88	1.007	0.848	0.956	2.350	2.401
3790.10	0.986	0.708	0.829	2.271	2.338
3804.01	3.318	0.200	0.268	1.720	1.848
3805.35	3.29	0.428	0.666	2.050	2.243
3806.21	3.40	0.176	0.285	1.665	1.875
3820.43	0.855	0.951	1.025	2.396	2.428
3821.18	3.25	0.464	0.601	2.083	2.196
3825.89	0.911	0.865	0.946	2.354	2.393
3827.83	1.551	0.705	0.831	2.265	2.336
3834.22	0.954	0.928	1.044	2.384	2.435
3840.44	0.986	0.764	0.848	2.299	2.343
3841.05	1.601	0.612	0.713	2.202	2.268
3846.81	3.354	0.416	0.568	2.034	2.169
3849.97	1.007	0.832	0.915	2.334	2.376
3850.82	0.986	0.524	0.645	2.134	2.223
3852.58	2.167	0.480	0.673	2.096	2.242
3859.22	2.394	0.568	0.762	2.167	2.295
3859.91	0.000	0.792	0.915	2.312	2.375
3865.53	1.007	0.604	0.653	2.193	2.227
3867.22	3.004	0.336	0.474	1.938	2.087
3884.36	2.68	0.276	0.434	1.851	2.047
3891.93	3.40	0.436	0.653	2.049	2.225
3899.71	0.087	0.656	0.794	2.226	2.308
3903.90	2.977	0.252	0.450	1.810	2.061
3906.48	0.110	0.676	0.864	2.238	2.344
3907.94	2.75	0.272	0.507	1.842	2.112
3917.19	0.986	0.456	0.641	2.065	2.214
3920.26	0.121	0.696	0.843	2.250	2.332
3922.92	0.051	1.017	1.206	2.415	2.489
3951.17	3.26	0.304	0.544	1.887	2.139
3952.61	2.681	0.480	0.739	2.084	2.272
3955.36	3.269	0.280	0.544	1.850	2.138
3983.96	2.716	0.472	0.754	2.074	2.277
3985.39	3.29	0.088	0.187	1.344	1.672
3986.18	2.977	0.196	0.376	1.691	1.974
4001.67	2.167	0.356	0.605	1.949	2.179
4006.31	3.25	0.216	0.438	1.732	2.038
4007.28	2.747	0.172	0.314	1.632	1.895
4009.72	2.213	0.296	0.450	1.868	2.049
4021.87	2.747	0.512	0.727	2.104	2.257
4043.90	2.716	0.264	0.499	1.816	2.091
4044.62	2.819	0.256	0.474	1.802	2.069
4045.82	1.478	1.049	1.285	2.415	2.502
4058.23	3.197	0.104	0.198	1.408	1.689
4062.45	2.833	0.376	0.588	1.966	2.160
4063.60	1.551	0.865	0.991	2.328	2.387
4067.99	3.197	0.268	0.467	1.819	2.060
4070.78	3.227	0.232	0.442	1.756	2.035
4071.75	1.601	0.565	0.633	2.142	2.191
4072.52	3.415	0.188	0.421	1.664	2.014
4074.79	3.034	0.160	0.322	1.593	1.898
4084.51	3.318	0.212	0.425	1.716	2.017
4100.75	0.855	0.432	0.711	2.022	2.238
4104.14	2.819	0.212	0.503	1.713	2.088
4107.50	2.819	0.216	0.385	1.720	1.972

TABLE 1—*Continued*

λ	Excitation Potential (e.v.)	Equivalent Width, A_λ (A)	Half-Width D_λ (A)	log $(10^6 A_\lambda/\lambda)$	log $(10^6 D_\lambda/\lambda)$
4121.81	2.819	0.108	0.233	1.418	1.752
4132.06	1.601	.656	.875	2.201	2.326
4132.91	2.833	.256	.517	1.792	2.097
4137.00	3.40	.200	.417	1.684	2.003
4147.68	1.478	.244	.415	1.769	2.000
4157.80	3.402	.240	.467	1.761	2.050
4210.36	2.471	.389	.554	1.966	2.118
4213.67	2.83	.179	.305	1.628	1.860
4235.95	2.415	.636	.816	2.176	2.285
4238.03	3.402	.282	.498	1.823	2.070
4238.88	3.382	.373	.535	1.944	2.101
4240.37	3.53	.099	.275	1.369	1.813
4245.26	2.846	.234	.395	1.742	1.969
4246.09	3.63	.226	.437	1.726	2.012
4248.23	3.058	.151	.342	1.550	1.906
4250.13	2.458	.536	.595	2.101	2.146
4250.79	1.551	.489	.559	2.061	2.118
4260.49	2.389	.565	.696	2.122	2.212
4267.83	3.10	.139	.321	1.513	1.876
4271.17	2.439	.759	.915	2.249	2.330
4271.77	1.478	.640	.727	2.175	2.230
4276.68	3.865	.099	.346	1.364	1.908
4285.45	3.22	.206	.432	1.681	2.003
4298.04	3.034	.179	.421	1.619	1.989
4325.77	1.601	.671	.737	2.190	2.230
4343.27	3.24	.191	.501	1.644	2.062
4352.74	2.213	.365	.539	1.924	2.093
4375.93	0.000	.410	.542	1.971	2.093
4387.90	3.058	.250	.462	1.756	2.022
4388.42	3.587	.238	.453	1.734	2.013
4389.25	0.051	.151	.407	1.537	1.967
4404.75	1.551	.707	.784	2.205	2.250
4408.42	2.188	.410	.632	1.968	2.156
4427.31	0.051	.572	.748	2.111	2.227
4430.62	2.213	.358	.485	1.907	2.039
4433.22	3.64	.226	.477	1.708	2.033
4438.36	3.671	.080	.321	1.255	1.860
4442.35	2.188	.493	.636	2.045	2.156
4447.73	2.213	.350	.501	1.896	2.052
4466.56	2.819	.513	.622	2.058	2.143
4476.02	2.833	.397	.550	1.947	2.089
4484.24	3.587	.254	.424	1.746	1.975
4485.68	3.671	.143	.375	1.504	1.922
4494.57	2.188	.476	.595	2.025	2.122
4528.62	2.167	.704	.860	2.191	2.278
4547.85	3.53	.250	.622	1.740	2.136
4602.01	1.601	.111	.375	1.382	1.911
4602.95	1.478	.286	.469	1.794	2.008
4607.67	3.252	.139	.338	1.480	1.866
4611.29	3.638	.218	.462	1.675	2.000
4625.06	3.227	.365	.707	1.898	2.184
4630.13	2.269	.250	.587	1.732	2.103
4632.92	1.601	.139	.370	1.477	1.902
4637.52	3.269	.175	.421	1.576	1.958
4638.02	3.587	.127	.288	1.438	1.793
4643.47	3.638	.095	.383	1.312	1.917
4647.44	2.936	0.242	0.501	1.718	2.033

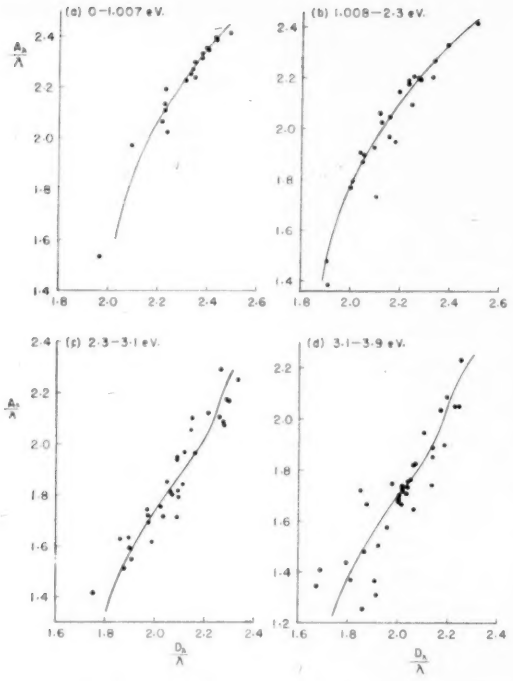

FIG. 4.—The observed curves of line-width correlation. Four groups of *Fe* I lines with different excitation potentials are used in plotting the four curves *a*, *b*, *c*, and *d*. In each curve the dots are observed points, and the solid curve is the theoretical curve translated both horizontally and vertically in such a way that a good fit with the observation is obtained. From the amount of translation, the velocities of both large and small eddies are determined.

TABLE 2

DOPPLER VELOCITIES

PRESENT DETERMINATION					WRIGHT'S DETERMINATION	
Mean Excitation Potential χ (e.v.)	Doppler Velocities (Km/Sec)				Mean Excitation Potential χ (e.v.)	Doppler Velocities (Km/Sec) $\xi_1=\xi_3$
	ξ_1	ξ_2	ξ_3	ξ_4		
0.5	15.0	16.4	15.0	6.6	1.18	8.2
1.6	10.1	11.9	10.1	6.3	2.35	6.3
2.7	5.4	8.8	5.4	6.9	3.28	5.1
3.4	3.9	7.5	3.9	6.4	4.35	4.3

a different behavior from that of the turbulent velocities of small eddies. They are practically constant for all kinds of lines (strong or weak).[11] This fits case *a* of Figure 2 discussed in Section III. In other words, the fastest-moving large eddies must have a very large size, i.e., greater than the reversing layer of very weak lines. The nature of these large eddies is beyond the scope of the present paper.[18]

Finally, we should mention that the present method of investigating Doppler velocities in stellar atmospheres should not be overemphasized, because, as we have seen, it is only an approximate method. But the approach which emphasizes the statistical study of line profiles may lead to a fruitful field of investigations in stellar astronomy.

We should like to express our sincere thanks to Dr. C. D. Shane, director of the Lick Observatory, for his hospitality and his interest in the present problem during the time when one of us (S. S. H.) was working on the photometric tracing of the spectrogram of δ Canis Majoris at the observatory. We also extend our thanks to Dr. G. Herbig, of the Lick Observatory, for instructing one of us (S. S. H.) in the use of the Lick microphotometer.

[18] O. Struve, *Pub. A.S.P.*, **63**, 138, 1951.

PRELIMINARY ANALYSIS OF THE TURBULENCE SPECTRUM OF THE SOLAR PHOTOSPHERE AT LONG WAVE LENGTHS

F. N. FRENKIEL* AND M. SCHWARZSCHILD†

Applied Physics Laboratory, Johns Hopkins University, and Princeton University Observatory

Received April 16, 1952

ABSTRACT

The available data on the velocities of granules are analyzed according to the methods of the statistical theory of turbulence. The analysis indicates that the turbulence spectrum of the solar photosphere may not be of a simple form but may have—in addition to the suspected primary maximum at wave lengths of the order of 300 km—a secondary maximum at long wave lengths of about 15,000 km.

I. INTRODUCTION

Recently, measurements have been made of Doppler shifts in a spectrum of the solar granulation.[1] From these measurements a standard deviation of the random turbulent velocity of 0.37 km/sec was found. On the other hand, one knows from the measurements of solar absorption-line profiles[2] that the standard deviation of the random velocity in the solar photosphere must be at least 1.7 km/sec. It was concluded that the larger part of the turbulent velocities in the photosphere of the sun is carried by eddies too small to be resolved on the granulation spectra. Consequently, the velocities obtained from the granulation spectrum were interpreted as referring only to relatively large eddies, i.e., as representing only the low-frequency tail of the turbulent spectrum.

From the astronomical side, a detailed analysis of the granule velocity data had not seemed promising, since they referred only to so unenergetic a fraction of the whole solar turbulence spectrum. It appeared, however, that some of the methods of statistical analysis of turbulence data used in fluid dynamics might give additional information even for such limited material. Therefore, the previously published granule velocities have now been analyzed in detail. The results of this analysis are described in this paper.

II. DERIVATION OF THE SOLAR TURBULENCE SPECTRUM

The experimental data to be analyzed here give the velocity component perpendicular to the solar surface for 340 equidistant points along a line parallel to the solar surface and 112,000 km long. According to its definition, the transverse correlation coefficient, R_y, can be derived directly from these data.

Let u_S' and u_P' denote one component of the instantaneous velocities at the two points P and S, respectively. Further, let the primes indicate that only the fluctuating part of the velocity field—after subtracting the mean stream motion—is here considered. Finally, let the line PS be perpendicular to the velocity component u. Then the transverse correlation coefficient is defined by

$$R_y(y) = \frac{\overline{u_P' u_S'}}{[\,(\overline{u_P'^2})\,(\overline{u_S'^2})\,]^{1/2}}. \tag{1}$$

* This work was supported by the U.S. Navy Bureau of Ordnance under Contract NOrd 7386.

† This work was supported, in part, by funds of the Eugene Higgins Trust allocated to Princeton University.

[1] R. S. Richardson and M. Schwarzschild, *Ap. J.*, **111**, 351, 1950.

[2] C. W. Allen, *M.N.*, **109**, 343, 1949; H. C. van de Hulst, *B.A.N.*, **10**, 79, 1946.

To derive R_y with help of equation (1), the averages occurring on the right-hand side have to be computed. Time averages cannot be used in the present case, since all the available data refer to one and the same moment. With the spatial averages here available, equation (1) becomes

$$R_y(y) = \frac{\sum_1^{N-m} u'_n u'_{n+m}}{\sum_1^{N-m} u'^2_n}. \tag{2}$$

Here n is the running index of the 340 equidistant points at which measurements were made, and y is given by $y = m \times 328$ km, since the distance between adjacent points corresponds to 328 km on the solar surface.

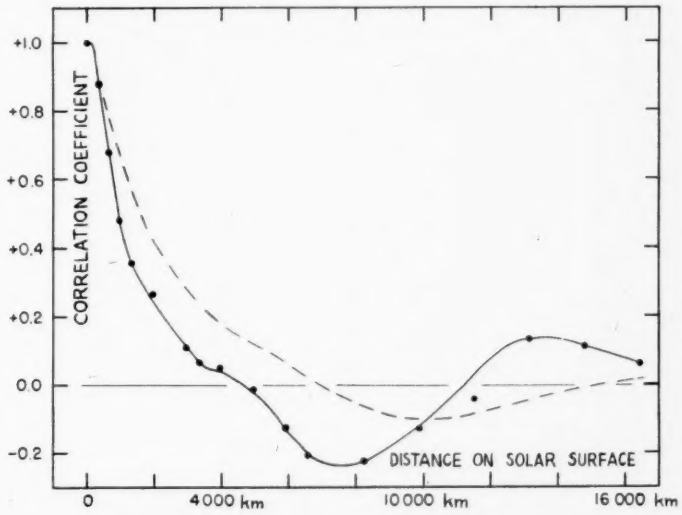

FIG. 1.—Transverse correlation coefficient (*solid line*) and longitudinal correlation coefficient (*dashed line*).

The transverse correlation coefficient, R_y, was computed according to equation (2). These computations were performed with the help of electronic punched-card machines. The results are listed in the fifth column of Table 1 and are shown in Figure 1. The limited extent of the available experimental data introduces an appreciable uncertainty into these results. The amount of this uncertainty can be estimated by comparing the R_y values in the last three columns of Table 1. The third-column values were based solely on the first half of the 340 measurements; the fourth column on three-fourths of them; and the last column on all the 340 measurements. From the comparison it appears that the data are sufficiently extensive to indicate the general shape of the correlation curve.

The curve representing the longitudinal correlation coefficient was computed with the help of the relation[3]

$$R_x(x) = \frac{2}{x^2} \int_0^x s R_y(s)\, ds. \tag{3}$$

[3] F. N. Frenkiel, *C.R.*, **222**, 473, 1946.

Since this equation holds only for isotropic, incompressible turbulence—a condition most likely not fulfilled in the solar photosphere—the curve for the longitudinal correlation coefficient should be considered only as an illustration (Fig. 1).

The transverse spectrum of turbulence was determined from the transverse correlation coefficient in accordance with the equation[4]

$$F_y(k'') = \frac{2}{\pi}\,\overline{u'^2}\int_0^\infty R_y(s)\,\cos\,(k''s)\,ds\,. \tag{4}$$

TABLE 1

TRANSVERSE CORRELATION COEFFICIENT

m	y (Km)	$R_y(y)$		
		$N=170$	$N=255$	$N=340$
0	0	+1.000	+1.000	+1.000
1	328	+0.887	+0.886	+0.880
2	656	+0.690	+0.695	+0.680
3	984	+0.491	+0.507	+0.482
4	1312	+0.356	+0.393	+0.357
6	1968	+0.277	+0.310	+0.266
9	2952	+0.067	+0.108	+0.107
10	3280	−0.015	+0.049	+0.066
12	3936	−0.081	−0.004	+0.051
15	4920	−0.176	−0.086	−0.018
18	5904	−0.265	−0.097	−0.124
20	6560	−0.311	−0.187	−0.210
25	8200	−0.288	−0.241	−0.224
30	9840	−0.131	−0.141	−0.129
35	11,480	+0.084	+0.030	−0.042
40	13,120	+0.184	+0.113	+0.131
45	14,760	+0.092	+0.089	+0.108
50	16,400	+0.008	+0.049	+0.060

TABLE 2

TRANSVERSE SPECTRUM OF TURBULENCE

k'' (Km^{-1})	$\lambda = 2\pi/k''$ (Km)	$F_y(k'')$ (Km^3/Sec^2)	k'' (Km^{-1})	$\lambda = 2\pi/k''$ (Km)	$F_y(k'')$ (Km^3/Sec^2)
0.000000	∞	97.2	0.000915	6867	47.6
.000152	41,335	44.0	.001524	4123	30.9
.000305	20,600	169.6	.002134	2944	19.9
.000457	13,748	178.0	0.003049	2060	11.8
0.000610	10,300	52.4			

The numerical computation was based, not on the individual points of the correlation coefficient given in Table 1, but on the smooth curve drawn through these points, as shown in Figure 1. This curve was extrapolated for large y-values ($y \geqq 16{,}400$ km) by an exponential curve [$R_y(y) = e^{-0.0001718y}$]. The results are listed in Table 2 and shown in Figure 2.

[4] G. I. Taylor, *Proc. R. Soc. London*, *A*, **164**, 476, 1938; and F. N. Frenkiel, *C.R.*, **222**, 367, 1946.

The range of wave numbers for which the present data give the transverse spectrum with some accuracy may be estimated as follows: The limitation at low wave numbers is directly given by the finite length L of the line covered by the measurements; significant results can clearly be obtained only for wave lengths considerably shorter than L. To formulate this limitation more quantitatively, one may consider as independent wave numbers all multiples of $2\pi/L$. Taking the mean of the energies for the lowest 16 of these independent wave numbers gives a mean point in the spectrum with a natural uncertainty in the energy of ± 25 per cent at a mean wave number of $8 \times 2\pi/L$. In the present case, with $L = 1.12 \times 10^5$ km, this lowest mean significant point falls at $k = 0.00045$ km^{-1}.

At the other end of the spectrum, at high wave numbers, the limitation is set by the resolution of the solar image from which the data were obtained. Let us assume that a point on the sun is spread out by atmospheric seeing and optical imperfections into an image with an intensity distribution given by

$$i(d) = \frac{1}{D\pi^{1/2}} e^{-d^2/D^2}. \tag{5}$$

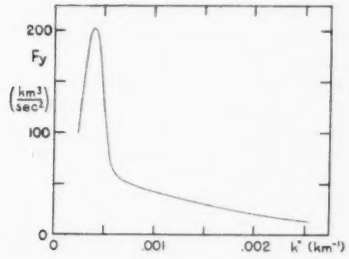

FIG. 2.—Transverse turbulence spectrum

Here D is the dispersion constant characterizing the sharpness of the solar image. Because of this washing-out of the image, the observed velocities, u_{ob}, are not equal to the true velocities u_{tr}, but are related to them by

$$u_{ob}(y) = \int_{-\infty}^{+\infty} u_{tr}(y')\, i(y' - y)\, dy'. \tag{6}$$

Here—as a first approximation—only the washing-out along the line of measurements, but not across it, has been taken into account. Introducing equation (6) into equation (2) and the resulting expression for R_y into equation (3), one finds

$$F_{yob}(k'') = F_{ytr}(k'') \exp\left(-k''^2 \frac{D^2}{2}\right). \tag{7}$$

This relation between the observed and the true spectrum shows that the washing-out affects the results very little for wave lengths $2\pi/k''$, long compared to $2\pi D$, whereas for short wave lengths, $2\pi/k'' < 2\pi D$, the observed spectrum is seriously reduced.

To apply equation (7) to the present material, the sharpness parameter D has to be estimated for the particular exposure from which the velocities were derived. From the sharpest features in the measured velocity fluctuation-curve, one can estimate as an upper limit $D < 450$ km (or $D < 0.6$ seconds of arc). From general experience with

atmospheric seeing, it does not seem likely that the actual value of D for this exposure is appreciably lower than the above upper limit. One may then conclude that the present data do not give the solar turbulence spectrum for $k'' > 1/D > 1/450$ km $= 0.0022$km^{-1} or for wave lengths shorter than 2700 km.

III. DISCUSSION OF RESULTS

The main result of the foregoing analysis is represented in Figure 2 in terms of the one-dimensional transverse turbulence spectrum. Before this result is discussed, it should be augmented by the information obtained from the absorption-line profiles. This may be done in the following way.

Figure 2 gives the frequency distribution of the turbulence energy of the resolved granules. This energy corresponds to a random velocity of 0.37 km/sec. The total turbulent energy of the solar photosphere, however, corresponds to 1.7 km/sec, as shown by the measurements of absorption-line profiles. Hence Figure 2 represents only about one-twentieth of the total turbulence energy. The main body of the solar turbulence spectrum must therefore lie at frequencies too high to be resolved on the granulation spectra—off the right-hand margin of Figure 2. From this circumstance, it had been concluded that the turbulent spectrum in the low-frequency range corresponding to the resolvable granules might be nothing but the tail end of the main turbulence spectrum. In this case, one should expect the turbulence spectrum in the observable range to decrease with decreasing frequency or, at most, be constant.

This conclusion is contradicted by the present results, which show an increase in the turbulence spectrum with decreasing frequency for most of the observable range. The details of the curve shown in Figure 2, particularly the sharpness of the maximum at $k = 0.0004$ km^{-1}, cannot be trusted, owing to the very limited observational data available. One should, however, be fairly secure if one restricts one's self to the comparison of the energies in two broad frequency bands, the first covering $k = 0.000$–0.001 km^{-1} and the second $k = 0.001$–0.002 km^{-1}. One finds that the average energy in the first band is about three times higher than in the second band. A part of this factor may be due to the fact that lack of resolution in the granule spectrum may have depressed, somewhat, the measured turbulence spectrum in the second band. But even with the worst possible assumption for the resolution, as discussed in the preceding section, one finds that the factor 3 is reduced to only 2.4.

One may then tentatively conclude that the solar turbulence spectrum may have a secondary maximum at $k = 0.0004$ km^{-1}, corresponding to a wave length of 15,000 km or eddy diameters of about 7000 km. (The term "primary maximum" is here reserved for the unobserved maximum at high frequencies, say, $k = 0.02$ km^{-1}, which presumably represents the main part of the turbulence energy.)

If, in fact, the secondary maximum exists in the turbulence spectrum of the solar photosphere, it seems likely that two separate driving mechanisms are responsible for the two maxima. The mechanism causing the primary maximum is presumably the thermal instability of the photosphere. What, then, is the cause of the secondary maximum? Two possible explanations can at present be advanced: (1) Considering the layers below the photosphere, one finds the scale height to increase with depth. Since the scale height may well determine the characteristic eddy size, i.e., the frequency of the primary maximum, one should expect the average eddy size to be larger, the lower the layer considered. Such large eddies below the photosphere may force motions on the photospheric layer of a linear scale much larger than the characteristic photospheric scale and may thus produce a secondary maximum at low frequencies. (2) There may exist free oscillations of fairly large scale in the outer layers of the sun which are randomly excited and thus appear in the turbulence analysis as a secondary maximum at long wave lengths.

Whatever the cause of the secondary maximum in the turbulence spectrum of the sun, it may well be a mild example of a phenomenon occurring with much more energy in the atmospheres of the red giants, where the turbulence is known to occur predominantly in much longer wave lengths than the characteristic length determined by the scale height of the atmosphere.

Before it seems worth while to inquire further into the cause of the secondary maximum and into its implications for the red giants, it appears necessary to verify its actual existence by further observation.

The authors wish to express their thanks to Mr. Franklyn H. Brady for his assistance in the numerical analysis and in the preparation of the data for computing on electronic punched-card machines. They are also indebted to the staff of the University of Wisconsin Computing Service for assistance in the computation.

THE DEPRESSION OF THE CONTINUUM IN A K0 DWARF

E. M. Lewis and William Liller
Observatory of the University of Michigan
Received March 27, 1952

ABSTRACT

From a study of the profiles of the λ 4227 line of *Ca* I and the K line of *Ca* II, the height of the true continuum has been calculated for the star ε Eridani. The resulting change in the total area of these lines is large and makes it apparent that any method which employs the equivalent widths of lines for the analysis of the atmospheres of late-type stars must be used with caution, especially if the lines are chosen from a wide range of wave lengths.

I. INTRODUCTION

In the blue and near ultraviolet regions of the spectra of late-type stars the absorption lines are so numerous and are crowded so close together that the wings of these lines overlap and hide the true continuum. The height of the observed continuum will then be the level of the highest visible points under the line wings. Measurements of the position of the continuum or of the equivalent widths of the lines of cool stars are therefore likely to be in error unless this depression of the continuum is taken into account.

The purpose of this study is to estimate the position of the true continuum of the near-by K0 dwarf, ε Eridani, from a study of the profiles of the λ 4227 line of *Ca* I and the K line of *Ca* II. The observed data consist of direct-intensity tracings of a plate taken with the 72-inch reflector of the Dominion Astrophysical Observatory by K. O. Wright. Dr. Wright used a two-prism spectrograph with a long focal length camera at the Cassegrain focus. The optics are of glass and give a dispersion of 6.8 A/mm at the K line; at λ 4227 the dispersion is 9.7 A/mm.

With a good knowledge of the physical conditions existing in the atmosphere of the star and with the transition probabilities of the lines, it should be possible to calculate theoretical profiles which agree closely with the observed line shapes. Unless abnormal conditions exist in the atmosphere of the star, adjustment of the height of the continuum or a change in the abundance of the ion producing the line, or both, should result in a satisfactory fit between the observed and the computed profiles. Since ε Eridani is a dwarf star, atmospheric turbulence must be small, and the effects of other abnormal conditions, such as stellar rotation or Stark or Zeeman effect, are probably negligible.

II. THE CONSTRUCTION OF THE PROFILES

Following the method described by G. Münch,[1] a model atmosphere was constructed for the star. The values for the effective temperature and for the surface gravity were taken to be 5000° K and 2.0×10^4 cm/sec^2, respectively.[2] As Münch points out, the contribution of neutral hydrogen to the opacity in the atmosphere of the sun is small, and it would be even smaller for a cooler K-type star. It was decided to neglect this source of opacity in these calculations.

[1] *Ap. J.*, **106**, 218, 1947.

[2] See L. H. Aller, "Interpretation of Normal Stellar Atmospheres," in *Astrophysics: A Topical Symposium*, ed. J. A. Hynek (New York: McGraw-Hill, 1951), p. 64.

The data used in the calculation of the line profiles are shown in the accompanying tabulation, where k_λ denotes the coefficient of continuous absorption per gram of stellar

	λ 4227	λ 3933
Summation of the Einstein A's	1.4×10^8	1.66×10^8
f-value*	2.28	0.793
$\eta_\lambda(=k_\lambda/\bar{k})$	0.70	0.64

* D. R. and W. Hartree, *Proc. R. Soc. London, A*, **164**, 161, 1938.

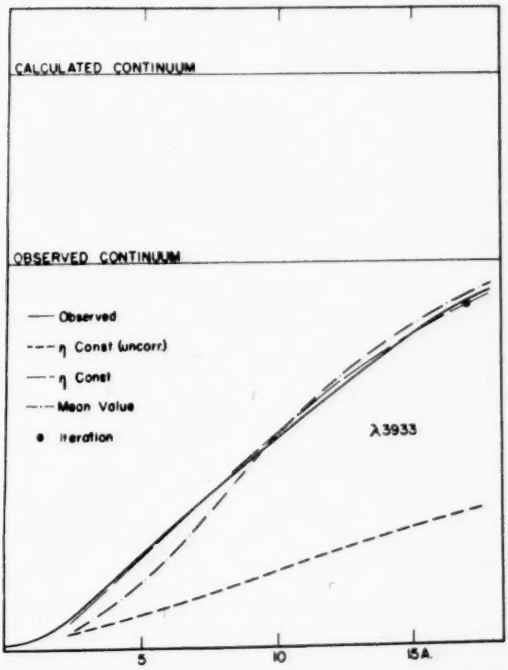

FIG. 1.—Observed and computed profiles of the K line of *Ca* II in ε Eridani

material at a wave length λ, and $\bar{k}$ the mean absorption coefficient. The adopted abundance of calcium was 1.8×10^{18} atoms per gram of stellar material. In the calculation of the collisional damping constants, a van der Waals type of force was assumed.

With these data the construction of the theoretical profiles was carried out by two methods. In the first, the ratio of the line-absorption coefficient to the continuous-absorption coefficient, η, was considered constant. The second took into account the variation of η with optical depth by use of the "mean-value" method of Strömgren. The

TABLE 1

OBSERVED AND COMPUTED PROFILES OF THE K LINE OF *Ca* II IN ϵ ERIDANI

$\lambda - \lambda_0$ (A)	Observed	η Constant (Uncorr.)	η Constant (Corr.)	Mean Value	Iteration
.3	0.118	0.050	0.106	.....	.....
.5	.248	0.089	0.237	0.176	.....
10	.545	0.204	0.557	.....	.....
12	.655	0.239	0.665	0.698	.....
17	0.910	0.346	0.895	0.921	0.891
Cont.	.....	1.0	1.5	1.5	1.5

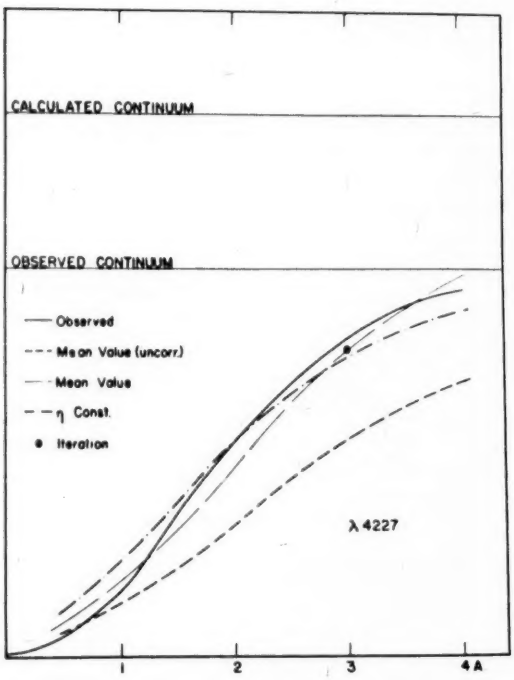

FIG. 2.—Observed and computed profiles of the λ 4227 line of *Ca* I in ϵ Eridani

iteration method of Strömgren provided a check at one point in the line. Strömgren[3] and Aller[4] have discussed these methods fully.

III. THE RESULTS

The construction of the theoretical profiles by the η-constant method was carried out first for λ 3933, and the result is shown in Figure 1, the numerical values being given in Table 1. We found that reducing the abundance by 30 per cent and raising the continuum by a factor of 1.5 would closely represent the observations. The change in the continuum height, however, alters the value of n_λ. With the aid of the theory by Chandrasekhar,[5] the new value was found to be 1.00.

TABLE 2

OBSERVED AND COMPUTED PROFILES OF THE λ 4227 LINE OF *Ca* I IN ε ERIDANI

$\lambda-\lambda_0$ (A)	Observed	Mean Value (Uncorr.)	Mean Value (Corr.)	η Constant	Iteration
0.5	0.061	0.068	0.095	0.153	.....
1	.174	0.144	0.202	0.336	.....
2	.547	0.344	0.482	0.665	.....
3	.823	0.564	0.790	0.902	0.795
4	0.948	0.705	0.987	1.054	.....
Cont.	.....	1.0	1.4	1.4	1.4

TABLE 3

EFFECT OF THE DEPRESSION OF THE CONTINUUM ON LINE INTENSITIES (A)

	Uncorrected	Corrected		Uncorrected	Corrected
Equivalent width of λ 4227	4.0	6.8	Equivalent width of λ 3933	19.0	28.9
Width at 90 per cent of continuum	7.4	15.2	Width at 90 per cent of continuum	16.8	53.4

With the changed level of the continuum, the mean-value method then gave a theoretical profile which agreed closely with the observed one. The figure also exhibits the one point determined by the iteration method.

Essentially the same procedure was carried through for λ 4227; we found that raising the continuum by a factor of 1.4 without altering the abundance of *Ca* I would represent the observations sufficiently well. The value of n_λ became 0.95. The results for λ 4227 are shown in Figure 2 and in Table 2.

IV. DISCUSSION

It is of interest to note that the above estimate of the height of the true continuum agrees qualitatively with what we should expect. At λ 3933 the average number of lines per angstrom is greater than at λ 4227; hence the smothering of the continuum by the

[3] B. Strömgren, *Festschrift für Elis Strömgren* (Copenhagen: E. Munksgaard, 1940).

[4] *Astrophysics*, Vol. I: *The Atmospheres of the Sun and Stars* (New York: Ronald Press Co., 1952), chap. viii.

[5] S. Chandrasekhar, *Radiative Transfer*, pp. 305–307 (Oxford: Clarendon Press, 1949).

overlapping lines must be more effective. As a prism spectrograph was used in obtaining these profiles, instrumental scattering, which would effectively depress the continuum, is small and was neglected in this work.

The increase in the height of the continuum will obviously affect the equivalent widths of these lines. Listed in Table 3 are these quantities, together with the widths of the lines at 90 per cent of the continuum intensity for both the corrected and the uncorrected continuum levels. These results make it clear that any method that employs the equivalent widths of lines for the analysis of the atmospheres of late-type stars must be used with caution, especially if the lines are chosen from a wide range of wave lengths. In addition, measurements of the Balmer discontinuity in late-type stars should be reexamined.

The authors are grateful to Dr. L. H. Aller for his advice and encouragement. Particular thanks are due to Dr. K. O. Wright, who supplied the observational data with which our theoretical calculations are compared.

THE AURORAL SPECTRUM IN THE WAVE-LENGTH RANGE 3300–8900 A*

W. PETRIE† AND R. SMALL‡

Physics Department, University of Saskatchewan, Saskatoon, Canada

Received March 21, 1952

ABSTRACT

Some hundred and fifty spectra of the aurora have been secured with a grating instrument which produces a linear dispersion of 85 A/mm in the first-order spectrum. The first three orders of the grating have been used in obtaining these spectra. Tables have been prepared listing those features whose origin is certain, and these data will provide useful information for a study of the excitation of the aurora. Remarks are made about any apparent anomalies in the spectra.

In 1949 a plane-grating spectrograph was constructed at the University of Saskatchewan.[1] This instrument utilized aircraft camera lenses as collimator and camera, and, although interesting preliminary results were obtained in the near infrared region of the spectrum,[2] the instrument was slow and gave poor resolution.

Early in 1951 a second grating spectrograph was constructed at the University of Saskatchewan. The optics of this instrument include a plane mirror, a paraboidal mirror collimator, a plane grating, and a flat-field Schmidt camera. The collimator has a speed of *f*4 and a focal length of 28 inches. The grating of ruled area 4 × 5 inches has 15,000 lines per inch, a blaze angle of 18°54′, and was supplied by the Bausch and Lomb Optical Company. For normal incidence on the grating the blaze falls at approximately 10,000 A in the first-order spectrum, and the concentration of radiation in this region is excellent. The flat-field Schmidt camera has a focal length of 5.5 inches and a speed of *f*0.8. This camera was constructed by A. B. Meinel, of the Yerkes Observatory, and was used in his first spectrograph built for a study of the airglow.[3]

Light from the source passes through a slit in the side of the spectrograph box, is deviated through 90° by a small plane mirror, and is incident on the collimator. This arrangement eliminates the need for off-axis optics. The plane mirror is in the collimated beam which returns to the grating and blocks about 10 per cent of the returning radiation. Part of this radiation would be lost in the camera, since the plateholder is in the beam between correcting plate and spherical mirror. These optics give a linear dispersion of approximately 85 A/mm in the first-order spectrum. The dispersion, of course, depends upon the position of the grating and the wave-length region. The spectrograph has great speed, owing to the relatively large ratio of the focal lengths of collimator and camera and to the high efficiency of the grating. In order to work on the blaze in different wave-length regions, the camera may be moved and fastened to different positions on the spectrograph bed. The bed and housing are constructed of aluminum, and the box is mounted on a simplified gun mount, which enables the operator to move the spectrograph quickly in altitude and azimuth. A light-tight shutter over the slit may be operated by remote control. The interior and exterior of the instrument are shown in Figure 1.

* This work has been supported by Contract AF 19(122)-152 with the Geophysics Research Division, Air Force Cambridge Research Centre.

† Now at Radio Physics Laboratory, Defense Research Board, Ottawa.

‡ Now at Dominion Observatory, Ottawa.

[1] *Canadian J. Res.*, *A*, **27**, 231, 1949.

[2] *J. Geophys. Res.*, **55**, 143, 1950.

[3] *Pub. A.S.P.*, **60**, 373, 1948.

OBSERVATIONAL MATERIAL

The new spectrograph has been in operation for approximately ten months, and a considerable number of spectra have been accumulated. The first three orders of the grating have been used, the dispersions in these orders being approximately 85, 42, and 28 A/mm, respectively. Suitable filters were used to avoid overlapping orders. Comparison spectra were superimposed on the earlier plates, but it soon became apparent that this procedure was unnecessary. There is a sufficient number of lines of known wave length in the auroral spectrum as reference lines.

In this paper the wave lengths and identifications of the auroral features are presented, along with certain remarks which point out any apparent anomalies in the spectra. We have listed only those features whose origin seems quite definite; weak lines of uncertain origin are not included. If there are present additional lines of atomic origin of excitation potential greater than those we have found, they must be very weak and will not have an appreciable effect on any discussion of excitation conditions. The features listed are found on all spectra of sufficient density, and these include all the major auroral forms. The results quoted here are based on an examination of some hundred and fifty spectra.

The writers feel that the identifications are reliable and that one may with confidence attempt to fit these identifications into an excitation scheme. The various features are listed in order of upper-level excitation potential, this order being most useful for a study of excitation conditions. A full discussion of the intensities will appear later. Sample spectra are illustrated in Figures 2, 3, and 4. The spectra were magnified about twenty times during the printing; the normal size of the spectrum is indicated by the contact print from the original included in Figure 4.

THE AURORAL SPECTRUM

a) The *O* I and *O* II lines present in the spectra are given in Tables 1 and 2. Included in the tables are the multiplet designations, the excitation potential of the upper level of the transition, and permitted multiplets of low energy which are missing from the spectra.

b) The *N* I and *N* II lines in the auroral spectrum are given in Tables 3 and 4.

c) Other atomic lines. The sodium D lines are on all the plates secured in the λ 5900 region. These lines belong to the aurora rather than the airglow, since they do not appear on plates of comparable exposure away from the aurora.

Similarly, the Balmer lines $H\alpha$, $H\beta$, and $H\gamma$ appear on all plates taken in the proper wave-length regions. The intensities of these lines vary greatly from one display to another and are strongest relative to other spectral features in the early part of a display and in bright active displays. These same variations have been noted by Gartlein[4] in his extensive observations. Figure 5 shows the manner in which $H\alpha$ varied throughout a display. The first two spectra were secured with the instrument pointing near the magnetic horizon, and the hydrogen line is broadened but undisplaced. The third spectrum was taken with the instrument pointing toward the magnetic zenith. $H\alpha$ is now much narrower and displaced about 10 A toward the violet end of the spectrum. As can be seen, the hydrogen line fades as the display progresses.

The magnitude of the Doppler shift of the Balmer lines is at present a debatable point. $H\alpha$ is close to the band 1 PG (7, 4) and, if shifted appreciably to the violet, will overlap this band. Furthermore, if the exposure with our instrument exceeds 3 hours, the *P* branch of the (6, 1) *OH* airglow band begins to show, and this feature overlaps the $H\alpha$ region. $H\beta$ merges with the (2, 15) VK band, and one must be careful to distinguish between these features. Finally, $H\gamma$ is bordered on both edges by *O* II lines. Since the spectrograph used for this investigation has relatively high dispersion, it is possible to sepa-

[4] *Trans. Amer. Geophys. Union*, **31**, No. 1, 7, 1950.

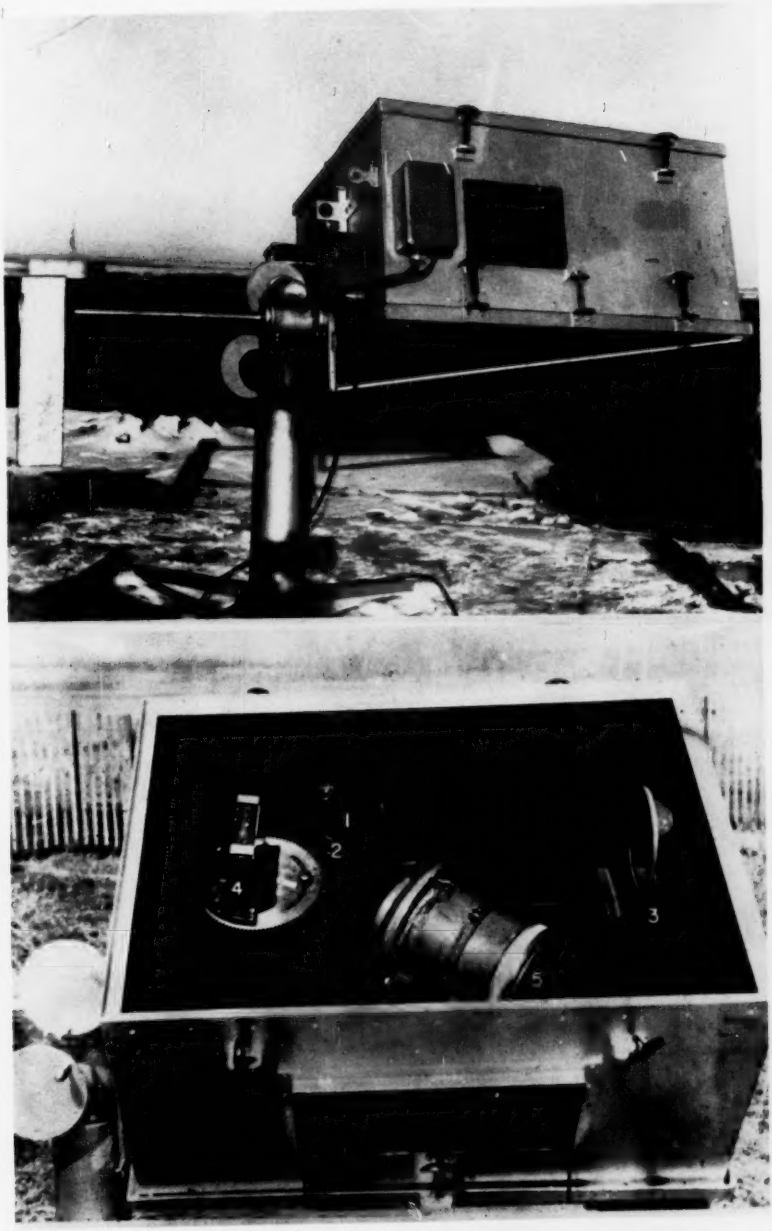

FIG. 1.—Plane grating auroral spectrograph

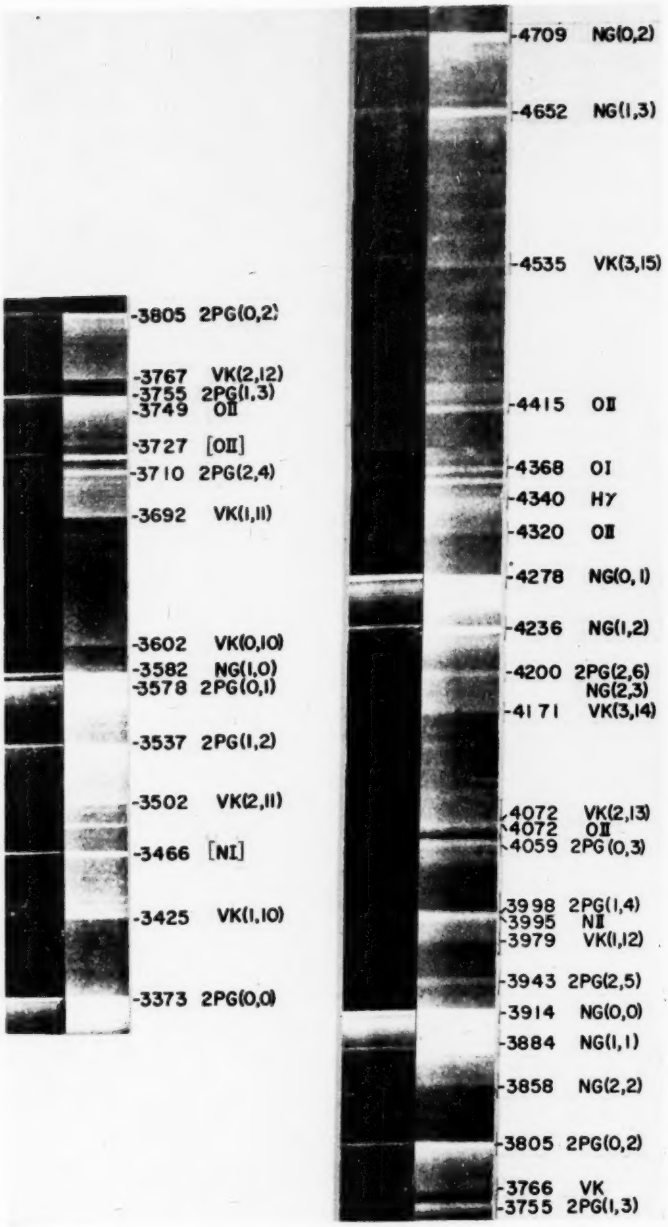

FIG. 2.—Auroral spectra

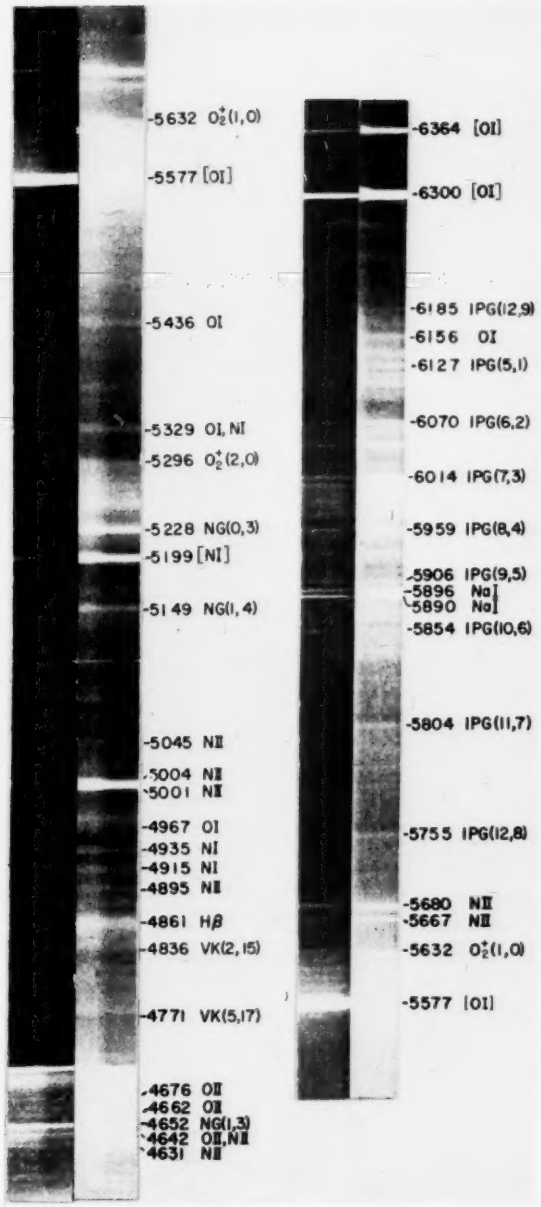

FIG. 3.—Auroral spectra

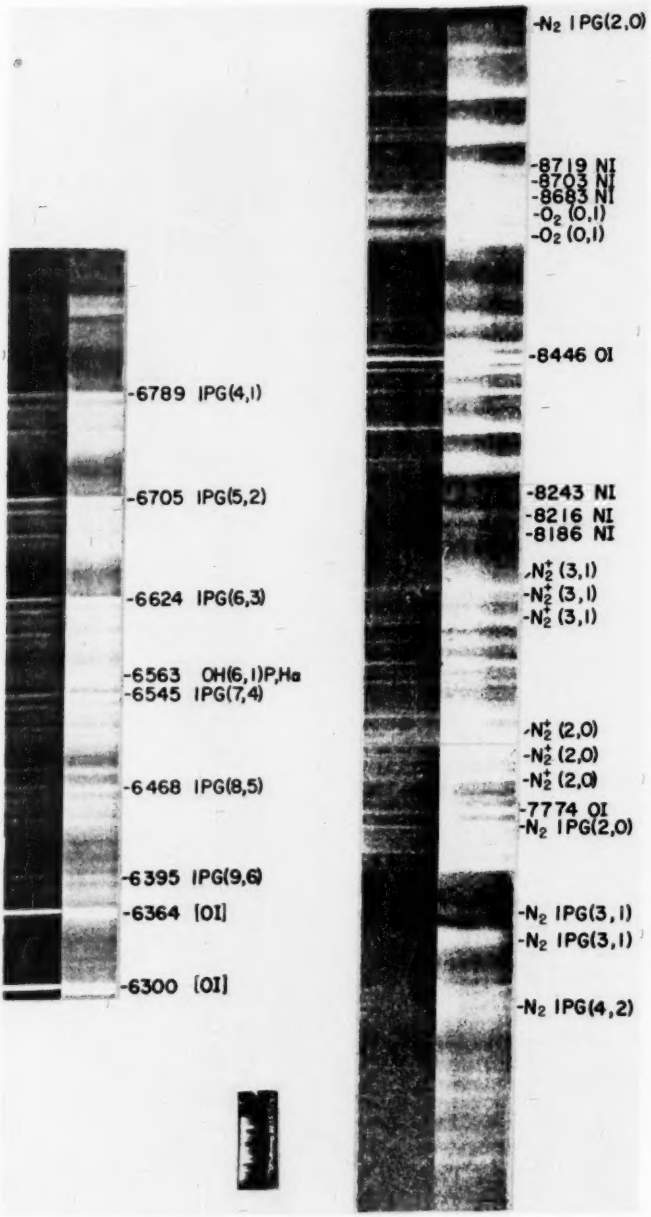

FIG. 4.—Auroral spectra

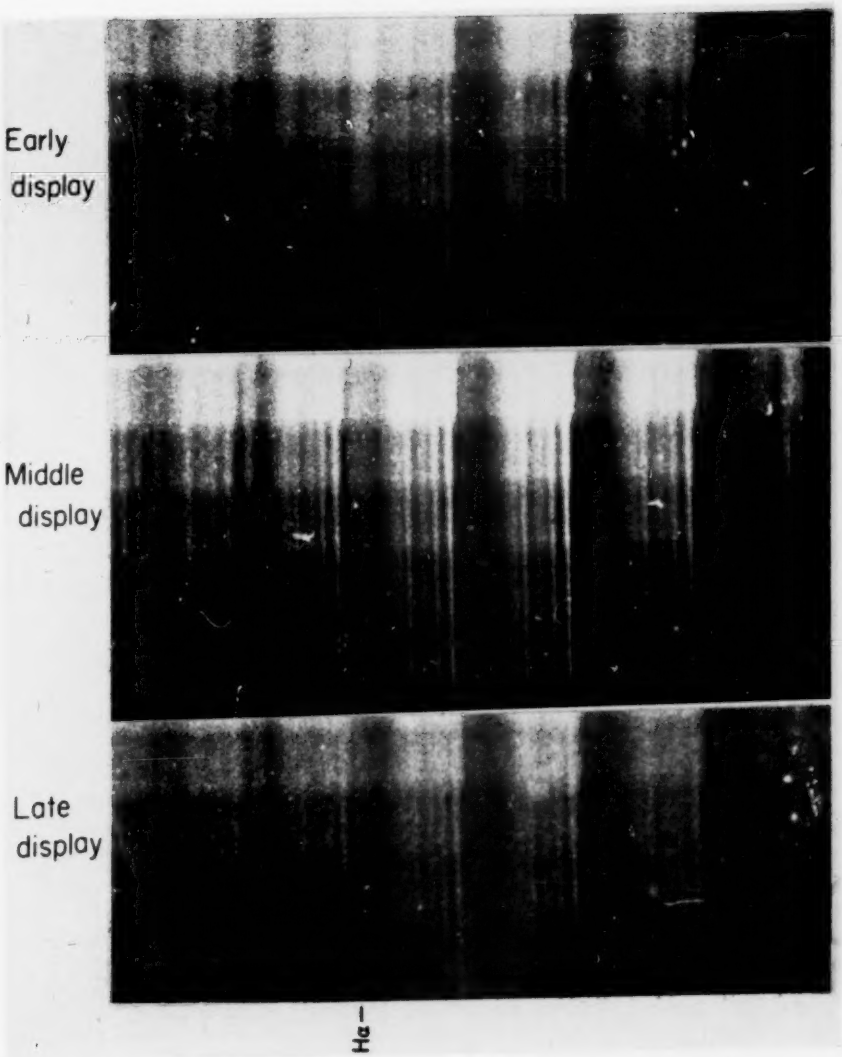

FIG. 5.—Auroral spectra

TABLE 1

O I LINES

Multiplet	Wave Length A	Excitation Potential (e.v.)	Notes
$2p^4(^3P) - 2p^4(^1D)$	6300 6364	1.96	
$2p^4(^1D) - 2p^4(^1S)$	5577	4.17	
$2p^33s(^5S^0) - 2p^33p(^5P)$	7774	10.69	
$2p^33s(^3S^0) - 2p^33p(^3P)$	8446	10.94	
$2p^33s(^3S^0) - 2p^34p(^3P)$	4368	12.31	
$2p^33p(^5P) - 2p^34d(^5D^0)$	6156	12.70	
$2p^33p(^5P) - 2p^36s(^5S^0)$	5436	12.96	
$2p^33p(^5P) - 2p^35d(^5D^0)$	5330	13.01	
$2p^33p(^5P) - 2p^36d(^5D^0)$	4968	13.18	
	Absent or Obscured Low-Level Multiplets		
$2p^33s(^5S^0) - 2p^34p(^5P)$	3947	12.23	1
$2p^33p(^3P) - 2p^33s(^3D^0)$	7995	12.49	2
$2p^33p(^5P) - 2p^35s(^5S^0)$	6456	12.61	3
$2p^33p(^3P) - 2p^35s(^3S^0)$	7254	12.64	4
$2p^33p(^3P) - 2p^34d(^3D^0)$	7002	12.70	5
$2p^33s(^3S^0) - 2p^35p(^3P)$	3692	12.82	6
$2p^33p(^3P) - 2p^36s(^3S^0)$	6046	12.98	7
$2p^33p(^3P) - 2p^35d(^3D^0)$	5958	13.01	8
$2p^33p(^5P) - 2p^37s(^5S^0)$	5020	13.15	9
$2p^33p(^3P) - 2p^37s(^3S^0)$	5555	13.16	10

NOTES TO TABLE 1

1. This line is definitely absent from our spectra; nor was it found by Barbier and Williams (*J. Geophys. Res.*, **55**, 401, 1950).
2. Absent from our spectra but present on spectra published by Meinel (*Rep. Prog. Phys.*, **14**, 121, 1951).
3. In the region 1 PG (8, 5).
4. In the region 1 PG (6, 4) and N_2^+ (4, 2).
5. Appears to be absent, although our spectra in this region are weak.
6. Absent from our spectra. Obscured by VK (1, 11).
7. In the region 1 PG (6, 2), but appears to be absent.
8. In the region 1 PG (8, 4).
9. Absent from our spectra.
10. In the region O_2^+ (3, 2).

DISCUSSION

The majority of the low-level multiplets are present in the spectrum, and others which do not appear are in the region of more prominent features. The absence of the lines at λ 3947 and λ 7995 might be considered anomalous. The former line is listed by Meinel[5] as being present, although he does not give a reference, but it is certainly missing from our spectra. Meinel[5] has found the latter line, but it is absent from some forty spectra which we have in this region. Neither does it appear in the infrared spectrum of lightning[6] nor in condensed or uncondensed discharges through air.[7] The line λ 3692 is listed by Barbier and Williams[8] but is not in our spectra. This line could be detected in the structure of the VK (1, 11) band if present.

[5] *Rep. Prog. Phys.*, **14**, 121, 1951.

[6] *Phys. Rev.*, **84**, 1263, 1951.

[7] Spectra secured in our laboratory.

[8] *J. Geophys. Res.*, **55**, 401, 1950.

TABLE 2

O II LINES

MULTIPLET	WAVE LENGTH A	EXCITATION POTENTIAL (E.V.)	NOTES
$2p^3(^4S^0)-2p^3(^2D^0)$	3726 3729	3.31	1
$2p^23s(^4P)-2p^23p(^4D^0)$	4639 4642 4662 4676	25.55	2
$2p^23s(^4P)-2p^23p(^4P^0)$	4317 4320 4349	25.74	3
$2p^23s(^2P)-2p^23p(^2D^0)$	4415	26.14	4
$2p^23s(^4P)-2p^23p(^4S^0)$	3713 3749	26.19	5
$2p^23s(^2D)-2p^23p(^2F^0)$	4591 4596	28.24	
$2p^23p(^4D^0)-2p^23d(^4F)$	4072	28.58	6
	Absent or Obscured Low-Level Multiplets		
$2p^3(^2D^0)-2p^3(^2P^0)$:	7319 and others	5.00	7
$2p^23s(^2P)-2p^23p(^2S^0)$	6641 6721	25.18	8
$2p^23s(^2P)-2p^23p(^2P^0)$	3973 and others	26.45	
$2p^23s(^2D)-2p^23p(^2D^0)$	4347 4351	28.39	

NOTES TO TABLE 2

1. These lines appear to be present but are superimposed on one line of the *O* II permitted multiplet $2p^23s(^4P)-2p^23p(^4S^0)$. This identification should be treated with reserve until the apparent absence of the forbidden *O* II lines at λ 7319, which have much larger *A* values, is explained.
2. The other lines of the multiplet are obscured by NG (1, 3) and (0, 2).
3. Other lines of the multiplet are obscured by $H\gamma$ and an *O* I line.
4. The other line of the multiplet which would be weak is missing.
5. The third line of the multiplet appears to be blended with the forbidden *O* II line $^4S^0-^2D^0$.
6. Other strong lines of the multiplet obscured by VK (2, 13).
7. Appears to be missing, although our spectra are weak in this region.
8. These lines obscured by 1 PG (6, 3) and 1 PG (5, 2) but appear to be absent.

DISCUSSION

As in the case of *O* I the majority of the low-level *O* II multiplets are present in the spectrum. Vegard[9] claims the presence of the lines λ 4185 and λ 4189 from the transition $2p^23p(^2F^0)-2p^23d(^2G)$, the excitation potential being 31.18 e.v. These lines are in the region of the bands VK (3, 14) and NG (2, 3) and are not in our spectra. Although the excitation of the *O* II lines appears to be normal, a proper discussion must await the measurement of the intensities.

[9] *C.R.*, **230**, 1884, 1950.

TABLE 3

N I LINES

MULTIPLET	WAVE LENGTH A	EXCITATION POTENTIAL (E.V.)	NOTES
$2p^3(^4S^0)-2p^3(^2D^0)$	5198 5201	2.37	
$2p^3(^4S^0)-2p^3(^2P^0)$	3466	3.56	
$2p^23s(^4P)-2p^23p(^4D^0)$	8680 8703 8712 8719	11.70	
$2p^23s(^4P)-2p^23p(^4P^0)$	8186 8216 8223 8242	11.79	
$2p^23s(^2P)-2p^24p(^2S^0)$	4915 4935	13.14	
	Absent or Obscured Low-Level Multiplets		
$2p^23s(^4P)-2p^23p(^4S^0)$	7468 and others	11.94	1
$2p^23s(^2P)-2p^23p(^2P^0)$	8629 and others	12.07	2
$2p^23s(^4P)-2p^24p(^4D^0)$	4253	13.19	3
$2s2p^4(^4P)-2p^24p(^4D^0)$	5329 and others	13.19	4
$2s2p^4(^4P)-2p^24p(^4P^0)$	5281	13.21	
$2p^23s(^4P)-2p^24p(^4P^0)$	4223 and others	13.21	5
$2p^23s(^4P)-2p^24p(^4S^0)$	4151 and others	13.26	

NOTES TO TABLE 3

1. These lines obscured by 1 PG (4, 2).
2. These lines partly obscured by O_2 (0, 1) but appear to be absent.
3. Obscured by NG (0, 1) but appears to be absent.
4. Vegard (*C.R.*, **230**, 1884, 1950) lists this line, but it is more likely to be the *O* I line at this same wave length.
5. Obscured by NG (1, 2) but appear to be absent.

DISCUSSION

It has been stated that the forbidden lines at λ 5198 and λ 5201 appear only in high-altitude displays, since the levels from which these lines originate have long lives and hence are partly depopulated by collisions of the second kind. However, these lines are present in all the spectra we have secured of the λ 5000 region, and the majority of the exposures were on normal arc and band structures. Part of the multiplet $2p^23s(^4P)-2p^24p(^4S^0)$, the strongest line of which is at λ 4151, has been listed by Barbier and Williams,[7] but it is not in our spectra. Similarly, both Barbier and Williams[8] and Vegard[9] include part of the multiplet $2p^23s(^2P)-2p^23p(^2D^0)$, the strongest line of which is at λ 4110, but the identifications are doubtful. The absence of the multiplet $2p^23s(^2P)-2p^23p(^2P^0)$ in the 8600 A region seems surprising, but one would need to compute the intensities for different excitation mechanisms to be sure. There is a strong line of wave length 6483 A which could be interpreted as due to the *N* I transition $2p^23p(^4D^0)-2p^24d(^4F)$ excitation potential, 13.62 e.v., but, in view of the greater intensity of *N* II lines in the aurora, it more likely belongs to the spectrum of this ion.

rate the hydrogen lines and the neighboring features. In no case with the instrument in the magnetic zenith have we found a wave-length shift for $H\alpha$ exceeding 10 A or an appreciable extension of the violet wing, and the spectra include several active displays. Meinel found the violet wing of $H\alpha$ was shifted 71 A in the spectrum of the intense auroral display of August 18–20, 1950.

d) Nitrogen bands. The N_2 bands of appreciable intensity in the auroral spectrum are listed in Tables 5–8. Hunten,[10] using a photomultiplier scanning spectrograph at the

TABLE 4

N II LINES

Multiplet	Wave Length A	Excitation Potential (e.v.)	Notes
$2p3s(^1P^0)-2p3p(^1P)$	6482	20.32	
$2s2p^3(^1D^0)-2p3p(^1P)$	4895	20.32	
$2p3s(^3P^0)-2p3p(^3D)$	5667, 5676, 5680, 5686, 5711, 5731	20.58	
$2p3s(^3P^0)-2p3p(^3S)$	5011, 5045	20.85	
$2p3s(^3P^0)-2p3p(^3P)$	4601, 4607, 4621, 4631	21.07	
$2p3s(^1P^0)-2p3d(^1D)$	3995	21.51	
$2p3p(^3D)-2p3d(^3F^0)$	5001, 5005, 5016, 5026	23.04	1
	Absent or Obscured Low-Level Multiplets		
$2p^2(^3P)-2p^2(^1D)$	6584 and others	1.89	2
$2p^2(^1D)-2p^2(^1S)$	5755	4.04	3
$2p3s(^1P^0)-2p3p(^1S)$	3437	22.01	4

NOTES TO TABLE 4

1. The intensity distribution within this multiplet is anomalous.
2. This line is in the region of 1 PG (6, 3).
3. This line is in the region of 1 PG (12, 8).
4. This line is in the region of VK (1, 10).

DISCUSSION

It can be seen that all the permitted low-level multiplets up to an excitation potential of 23.04 are satisfactorily accounted for. Vegard[9] includes parts of a number of higher-level multiplets, but these either do not appear or are very weak in our spectra. In most cases the lines in question are in the region of other diffuse features.

[10] Private communication.

TABLE 5

VEGARD-KAPLAN BANDS

v'	v''	Wave Length A	v'	v''	Wave Length A
0	10	3602	2	12	3767
1	9	3198*	2	13	4072
1	10	3425	2	15	4837
1	11	3683	3	14	4171
1	12	3979	3	15	4535
2	11	3503	5	17	4771

* In spectra secured with a quartz-prism instrument (*J. Geophys. Res.*, **57**, 51, 1952).

DISCUSSION

A few remarks follow about other VK bands which might be expected to appear.

(0, 11) 3889. This is in the region of NG (0, 0) but cannot be seen in the rotational structure.

(0, 12) 4218. There is a very weak feature at this wave length which is probably the band.

(1, 13) 4320. There is an *O* II line here, and the band appears to be absent.

(2, 10) 3268. Our spectra are weak in this region.

(2, 14) 4423. There are weak, fuzzy features in this region.

(3, 13) 3855. This is in the region of NG (2, 2) but appears to be absent.

(4, 14) 3948. A very weak feature here could be the band.

(4, 16) 4650. This is in the region of NG (1, 3).

(5, 15) 4043. There is a weak feature here, but it does not appear to be a VK band.

(6, 16) 3940. This is in the region of 2 PG (2, 5).

TABLE 6

FIRST POSITIVE BANDS

v'	v''	Wave Length A	v'	v''	Wave Length A
1	0	8912	6	4	7273*
2	0	7753	7	3	6014
2	1	8722†	7	4	6545
3	0	6875‡	7	5	7165
3	1	7626	8	4	5959
3	2	8542	8	5	6469
4	0	6185	8	6	7059§
12	9		9	5	5906
4	1	6789	9	6	6395
4	2	7504	9	7	6968
5	1	6127	10	6	5854
5	2	6705	10	7	6323
5	3	7387	11	7	5804
6	2	6070	11	8	6253
6	3	6624	12	8	5755

* This band can be separated from the (4, 2) Meinel N_2^+ band.

† This band is in the region of *N* I lines but is visible.

‡ This band can be separated from the (2, 0) Meinel N_2^+ band.

§ This band can be separated from the (3, 1) Meinel N_2^+ band.

TABLE 7

SECOND POSITIVE BANDS

v'	v''	Wave Length A	v'	v''	Wave Length A
0	0	3371	1	6	4574
0	1	3577	2	1	3136
0	2	3805	2	2	3309
0	3	4059	2	4	3710
1	0	3159	2	5	3943
1	1	3339	3	2	3117
1	2	3537	3	3	3285
1	3	3755	3	5	3672
1	4	3998	3	7	4142
			4	8	4095

DISCUSSION

A few remarks are made about bands which might be expected to appear.

(0, 4) 4344. This band is in the region of $H\gamma$, and the two features are not well resolved.

(1, 5) 4270. This band is in the region of NG (0, 1) and will distort the rotational profile of this latter band.

(2, 3) 3501. This band is in the region of VK (2, 11).

(2, 6) 4200. This band is in the region of NG (2, 3).

(3, 4) 3469. This is in the region of the forbidden *N* I line.

(3, 6) 3895. This is in the region of NG (0, 0) and will distort the rotational profile of this latter band.

(3, 8) 4417. This is in the region of an *O* II line.

(4, 7) 3858. This is in the region of NG (2, 2).

The bands of wave length less than λ 3373 appeared in spectra secured with a quartz-prism instrument.[11]

TABLE 8

NEGATIVE GROUP BANDS

v'	v''	Wave Length A	v'	v''	Wave Length A
0	0	3914	2	2	3858
0	1	4278	2	3	4199
0	2	4709	2	4	4600
0	3	5228	2	5	5077
1	0	3582	3	2	3549*
1	1	3884	3	5	4553
1	2	4236	4	6	4516
1	3	4652	4	7	4958
1	4	5149	5	7	4490
2	1	3564	6	8	4468

* This band is present in spectra of the sunlit aurora but not in the dark aurora. The spectra of the sunlit aurora were secured in northern Saskatchewan during May and June, 1951. The (3, 4) band at a wave length of λ 4167 is listed by Vegard (*C.R.*, **230**, 1884, 1950), but we cannot be sure of this in our spectra. The (3, 2) band has the greatest theoretical strength in the (3, v'') progression. A weak feature at λ 4882 could be the (6, 9) band. If this is so, then the (5, 8) band will add to the *N* I emission at λ 4915.

[11] *J. Geophys. Res.*, **57**, 51, 1952.

University of Saskatchewan, has found a few additional bands appearing for a short time in active displays.

e) Other bands. The six $A^2\pi - X^2\Sigma$ N_2^+ bands found by Meinel[5] are present in all our red and infrared spectra. The first negative group O_2^+ bands appearing in our spectra are (0, 0) 6026, (1, 0) 5632, and (2, 0) 5296. The (0, 0) band is in the region of 1 PG (7, 3), but it is apparent that both features are present. The (0, 1) and (0, 2) bands at λ 6419 and λ 6856 might also be expected to appear. They seem to be missing, but the spectral range λλ 6000–6900 is very complex and will require further examination with higher-dispersion spectra. The extensive band whose head is at λ 5632 very likely includes both the (1, 0) and (2, 1) bands. Similarly, the feature at λ 5296 likely includes the (2, 0) and (3, 1) bands.

CONCLUDING REMARKS

The identifications presented in the various tables form a basis for the discussion of the excitation of the aurora. This problem will be considered in a paper to follow, once the intensities of the spectral features have been determined. The writers have purposely omitted some fifty weak features of uncertain origin, a number of which appear in denser but lower dispersion spectra secured by Vegard[9] and Barbier and Williams.[8] These features, even if correctly identified, will not seriously affect arguments regarding excitation conditions. Furthermore, we have found that long exposures with a high light-gathering power spectrograph will record numerous airglow features, mostly *OH* bands, and the fainter lines in an auroral spectrum must be examined carefully.

NOTES

IDENTIFICATION OF CARBON MONOXIDE IN THE ATMOSPHERE ABOVE FLAGSTAFF, ARIZONA*

The existence of carbon monoxide in the atmosphere above Columbus, Ohio, was announced by Migeotte in 1948.[1] Apropos of this observation, Adel sought evidence of atmospheric carbon monoxide in solar-telluric spectra made with considerably less resolving power at the Lowell Observatory, Flagstaff, Arizona, in the autumn of 1940. However, it was not possible at that time to make an unambiguous identification, and it was consequently concluded that the Columbus carbon monoxide was of local origin.[2]

Recently the near infrared region of the solar spectrum was reobserved at Columbus by Shaw, Chapman, *et al.*,[3] whose published spectra, obtained with a grating having 7200 lines per inch have been employed by the author to isolate the *CO* lines in the Flagstaff observations.

The resolution offered by a grating with 2400 lines per inch, which the author em-

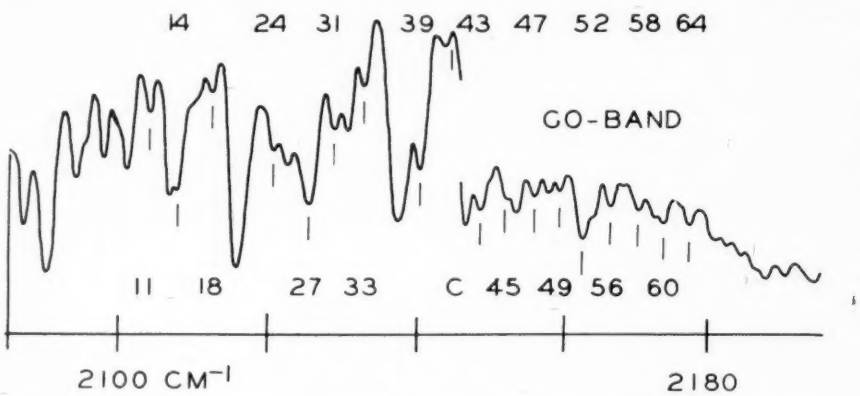

FIG. 2.—Solar-telluric spectrum, 4.6 μ, Flagstaff, Arizona, 1940. (Tracing made from original record)

ployed in his 1940 examination of the solar-telluric spectrum, does not make it easily possible, in the 4.6 μ region, independently to differentiate uniquely between the carbon monoxide absorption and the general solar-telluric background. However, with the 7200-line work of Shaw, Chapman, *et al.*, as a comparison standard, the task of *CO* identification in the 1940 Flagstaff spectra becomes a straightforward and simple one.

Figure 1 reproduces the original 1940 Flagstaff observation of the solar-telluric spec-

* This work was supported in part by Contract No. AF19(122)-198 between the United States Air Force and the Arizona State College at Flagstaff, Arizona, through sponsorship of the Geophysics Research Division, Air Force Cambridge Research Center, Air Research and Development Command.

[1] *Phys. Rev.*, **75**, 1108, 1949.

[2] Arthur Adel, *Phys. Rev.*, **75**, 1766, 1949.

[3] J. H. Shaw, R. M. Chapman, J. N. Howard, and M. L. Oxholm, *Ap. J.*, **113**, 268, 1951.

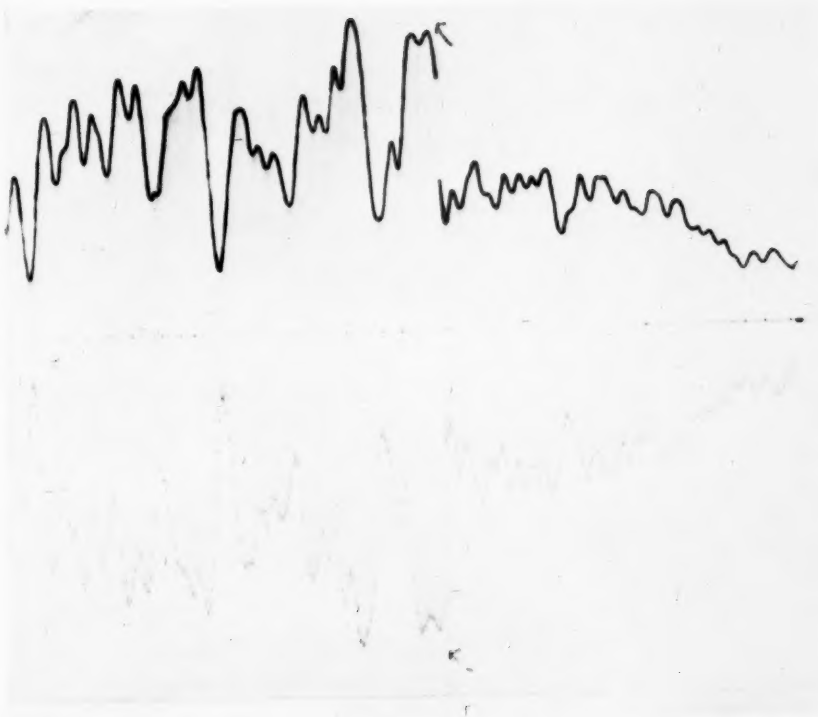

FIG. 1.—Solar-telluric spectrum, 4.6 μ, Flagstaff, Arizona, 1940. (Original record)

trum in the 4.6 μ region. Figure 2 is a trace made from Figure 1. Carbon monoxide structure is plainly visible in these figures. The absorption lines of *CO* are indicated in Figure 2 by short vertical dashes, and, in addition, the band center has been designated by the letter *C*. The numbering in the identified lines in Figure 2 is in each case 100 less than that of the corresponding line in the published spectra of Shaw, Chapman, *et al.* (The break in the curve is due to a change in coelostat aperture.) The line positions are given in Table 1.

TABLE 1

Frequency (Cm^{-1})	Number	Identification	Frequency (Cm^{-1})	Number	Identification
2087.3			2150.0		
2090.3			2151.8	45	*CO*
2094.1			2153.5		
2095.6			2155.7	47	*CO*
2098.0			2157.6		
2101.1			2159.2	49	*CO*
2104.0	11	*CO*	2162.5	52	*CO*
2106.8			2164.3		
2108.0	14	*CO*	2166.6	56	*CO*
2110.4			2168.2		
2112.1	18	*CO*	2170.3	58	*CO*
2115.7	21	*CO*	2172.5		
2120.7	24?	*CO*	2173.9	60	*CO*
2122.5			2175.8		
2125.6	27	*CO*	2177.4	64	*CO*
2128.9	31	*CO*	2180.8		
2130.5			2182.5		
2132.6	33	*CO*	2184.6		
2137.3			2186.2		
2140.1			2188.0		
2143.4			2190.8		
2146.5			2194.4		
2148.5	43	*CO*			

In 1950 Migeotte and Nevin announced the presence of carbon monoxide structure in solar spectra obtained at the International Research Station at the Jungfraujoch, Switzerland.[4] They found the absorption intensity in April, 1951, to be four times as great as that in August, 1950.

The Flagstaff work may be regarded as constituting one more link in the chain of evidence that atmospheric carbon monoxide is planet-wide, and it furthermore possesses historical importance in being the earliest record of atmospheric carbon monoxide absorption.

ARTHUR ADEL

ARIZONA STATE COLLEGE
FLAGSTAFF, ARIZONA
January 28, 1952

[4] *Physica*, 16, 423, 1950.

NOTE ON THE THEORY OF THE STARK EFFECT IN STELLAR SPECTRA

An interesting feature of the spectra of certain A-type stars is the simultaneous occurrence of narrow metallic lines with very broad hydrogen lines. As an example we show in Figure 1 an intensity record of the $H\gamma$ line of Castor A, which is seen to have a width of 200 A, although several narrow metallic lines exist in the same spectral region.[1]

Broadening of the hydrogen lines can be produced by the disturbing effects of the interaction of the absorbing atom with neighboring atoms, effects which interfere with the quantum states of the absorber so that they are not quite sharp. The great width of the hydrogen lines has been attributed[2] to the Stark effect of protons and electrons, these being counted as having identical effects much greater than those of the heavier ions. In a general way it can be seen at once that neutral atoms will not make a significant contribution to the line broadening. The pressure in an A-type main-sequence atmosphere is generally considered to be about 1/200 atm., and in a discharge tube at this pressure the Balmer lines are quite sharp. The current theory as given by Verweij divides the problem into three parts. First, the probability distribution of the electric field is calculated, assuming that it is described by the Holtsmark distribution.[3] Second, the Stark effect due to any field is calculated as if that field were homogeneous and steady, so that the well-known quantum-mechanical treatment of Schrödinger[4] can be used, and the line absorption coefficient is then derived by using the Holtsmark probability distribution. Third, the line profile is obtained by a process of integration of the relevant equation of transfer through the reversing layer. This procedure is rather complicated, and it is not easy to see how the final result is affected by the various approximations involved. However, it appears that in certain cases there are grounds for doubting the validity of the treatment of the first two parts of the problem.

The Holtsmark probability distribution $W(\beta)$ gives the probability that the field strength at a point in an assemblage of atoms and ions will lie between β, $\beta + d\beta$ times a certain average or normal field strength. Denoting this field by F_0, we have[5]

$$F_0 = 46.8 \left(\frac{2P_e}{T}\right)^{2/3} \text{e.s.u.}$$

and

$$W(\beta) = \frac{2}{\pi} \beta \int_0^\infty \exp(-v^{3/2})\, y \sin(\beta v)\, dv .$$

Taking $T = 10{,}000°$, $\log_{10} P_e = 3.7$ as the conditions which correspond roughly to an A0 dwarf atmosphere, one has

$$F_0 = 46.8 \text{ e.s.u.} = 14{,}040 \text{ volts cm}^{-1}.$$

An asymptotic expansion for $W(\beta)$ has been given by van der Corput,[6] the first term of which is given by

$$W(\beta) \sim \frac{\sqrt{2}}{\pi} \frac{(5/2)!}{\beta^{5/2}},$$

[1] Cf. *Pub. Dom. Ap. Obs. Victoria*, **8**, 257, Pl. VI, 1949.

[2] S. Verweij, *Pub. Astr. Inst. Amsterdam*, No. 5, 1936.

[3] J. Holtsmark, *Ann. d. phys.*, **58**, 576, 1919.

[4] *Ann. d. phys.*, **80**, 467, 1926.

[5] Holtsmark, *loc. cit.*

[6] Verweij, *op. cit.*, p. 10.

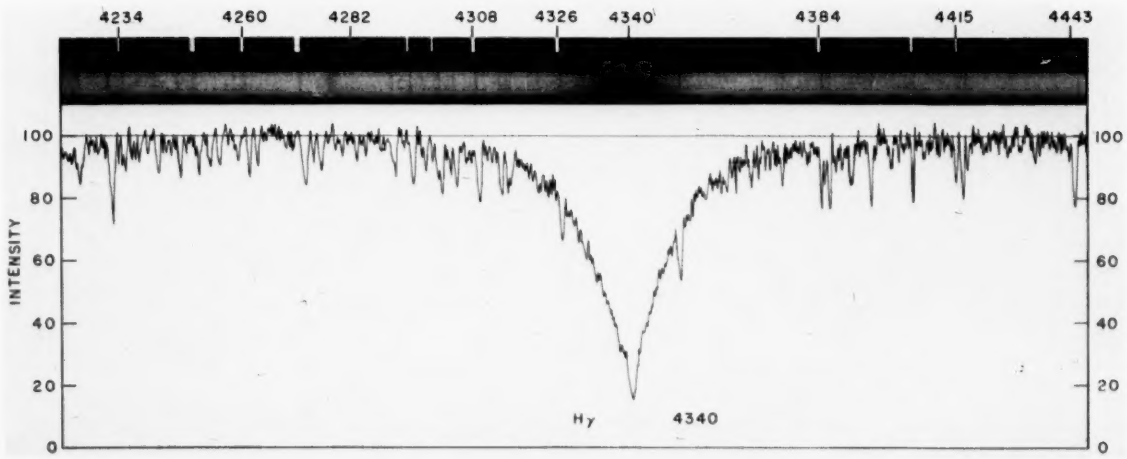

FIG. 1.—The spectrum and intensity record of $H\gamma$ line of Castor A

from which we have for example $W(25) = 5.0 \times 10^{-4}$, $W(50) = 9 \times 10^{-5}$, whereas the maximum value of $W(\beta)$ is 36.7×10^{-2}, occurring at $\beta = 1.6$. Following Schrödinger, it can be shown that a field of 46.8 e.s.u. will split the $H\gamma$ line into various components, the significant members being displaced as much as 3 A from the undisturbed line. The existence of appreciable absorption at 75 A from the line center must therefore involve values of $\beta = 25$ at least; it is important, therefore, that $W(\beta)$ be valid for large β. On the other hand, there is an effect due to the different depths of formation of the line profile, which will tend to give rise to a broad line, since the far wings of the line originate in the regions of greatest depth and density; but this effect will be marked only if the assumed electron pressure $\log_{10} P_e = 3.7$ does not correspond to the depth of formation of weak lines, which appears unlikely. On the contrary, this value of the electron pressure is probably greater than that obtaining in the reversing layer.

Furthermore, by considering the method of deriving the Holtsmark probability distribution, one can see that it seriously overestimates the effect of large fields. The value of $W(\beta)$ is deduced from the following assumptions: (1) the influence of the perturbing particles is described by the inverse-square law; (2) the perturbing particles are randomly distributed over all elements of volume. It can be shown that for values of $\beta \geq 2$ the distribution given by $W(\beta)$ is sensibly that due to the nearest particle,[7] while even for $\beta = 1$ the distributions are not widely different, although they become quite separate as $\beta \to 0$, of course. Now a field of 46.8 e.s.u. corresponds to a distance of the perturbing particles of 3.18×10^{-6} cm, which, at the average speed of electrons in a gas at 10,000°, is traversed in 5.13×10^{-14} sec, which is of the same order as the period in the Bohr orbit corresponding to $n = 5$, viz., 1.89×10^{-14} sec. The Maxwellian velocity distribution states that the number of electrons with velocities within v, $v + dv$ is proportional to

$$\left(\frac{v}{v_0}\right)^2 \exp -\left(\frac{v}{v_0}\right)^2,$$

where v_0 is the most probable velocity, in this case 5.5×10^7 cm/sec. Thus there is a significant number of electrons with velocities two or three times greater than the average velocity; in particular, there will be an appreciable number of electrons moving at such speeds that they traverse the "normal" distance 3.18×10^{-6} cm in times equal to, or shorter than, the relevant Bohr period.[8] For comparison it may also be noted that, whereas the distance of approach corresponding to the "normal" field is 3.18×10^{-6} cm, the radius of the fifth Bohr orbit for hydrogen is 13.4×10^{-8} cm, so that the "normal" distance is 24.1 Bohr radii (of the five-quantum orbit).

Under these circumstances it seems unlikely that the second condition contemplated in deriving the probability distribution will be applicable. Also, to determine the effect of a fast electron, the atomic system must be treated quantum-mechanically, the wave equation of the system being akin to that used in the investigation of the negative hydrogen ion. In the immediate neighborhood of the atom one cannot suppose that there is a random distribution of perturbers, since within this distance electrons tend to be "captured," whereas protons do not. One would expect the fluctuating Stark effect due to electrons to be the more powerful influence in distorting the energy levels of the hydrogen atom, since there will exist a quasi-resonance effect as distinct from the almost adiabatic conditions under which the proton field is established.[9]

Apart from the work of Eddington cited, it has been pointed out by Unsöld[10] that the Stark effect due to electrons in stellar atmospheres cannot be calculated as for steady

[7] Russell and Stewart, *Ap. J.*, **59**, 197, 1924.

[8] Cf. Eddington, *Internal Constitution of the Stars* (Cambridge: At the University Press, 1926), p. 353.

[9] Cf. Eddington, *loc. cit.*

[10] *Physik der Sternatmosphären* (Berlin: J. Springer, 1938), p. 181.

fields. The tendency recently[11] has been to suppose that the effects are negligible, but this supposition does not appear justified. It seems more reasonable to suppose that the great width of the hydrogen lines observed in A-type main-sequence spectra arises from the perturbing effect of the electrons.

An interesting exercise in the application of quantum mechanics would be the calculation of the effect of a closely approaching electron on the energy levels of the hydrogen atom, when the velocity of the electron is such that its field fluctuates rapidly in a time comparable with the Bohr period of the atomic electron; for such a case neither the "sudden" nor the "adiabatic" hypothesis would be valid. This problem corresponds to the intractable case mentioned by Spitzer[12] and is recommended to the attention of theorists.

One would expect the effect of electrons on $H\gamma$ to become noticeable at about 20 A from the line center; although the extensive wings appear due to this cause, there is not necessarily a large contribution to the equivalent width. In fact, reference to Figure 1 shows that this contribution is quite small, the great part of the equivalent width arising from that part of the line within 20 A of the line center.

G. J. Odgers

Dominion Astrophysical Observatory
Victoria, B.C.
March 18, 1952

NOTE ON THE STARK BROADENING OF $H\gamma$

The statistical theory of the Stark effect as originally employed by Verweij[1] to explain the shapes of the hydrogen lines in early-type stars has given a generally successful explanation of the observed phenomena. However, it is known that this theory is at best an approximation, so it is of interest to investigate how good a quantitative explanation of the observations is obtained. To do this, the strength and shape of $H\gamma$ in an early-type model atmosphere[2] have been computed, and the results obtained are compared with observation.

The method, outlined previously,[3] of computing the profiles of hydrogen lines in model atmospheres has been followed, it being assumed that the line-absorption coefficient is given by the statistical Stark effect due to protons only and that the line is formed by pure absorption. An electron carries the same charge as a proton and therefore might be expected to contribute equally to the Stark effect of the hydrogen lines. However, it may be shown[4] that the statistical theory cannot be used for the electrons because of their great speed relative to the absorbing neutral hydrogen atoms. What the effect of the electrons is and how it should be treated in an adequate physical theory are other questions. Unsöld[5] has stated that we may neglect the effect of the electrons. We may hope to test this conclusion by computing the strength and shape of $H\gamma$ under the assumption of broadening by protons only.

The computed profile for $H\gamma$, together with that observed in 10 Lacertae, O9 V, and in σ Orionis, O9.5 V, is given in Table 1. The spectral type of the model atmosphere has

[11] Cf. Unsöld, *Vierteljahrs. d. Astr. Gesellsch.*, **78**, 251, 1943.

[12] *Phys. Rev.*, **56**, 47, 1939.

[1] *Pub. Astr. Inst. U. Amsterdam*, No. 5, 1936.

[2] A. B. Underhill, *Ap. J.*, **111**, 203, 1950; *Pub. Copenhagen Obs.*, No. 151, 1950.

[3] A. B. Underhill, *Pub. Dom. Ap. Obs. Victoria*, **8**, 357, 1951.

[4] See, e.g., the review article by Unsöld, *Viertel. Astr. Ges.*, **78**, 213, 1943.

[5] *Ibid.*, p. 251.

been estimated[2] as halfway between that of 10 Lacertae and τ Scorpii, that is, about O9.5 V, and it has been shown[6] that it is probable that this model atmosphere gives a reliable representation of a late O-type main-sequence atmosphere. The observed profile of $H\gamma$ in 10 Lacertae, which includes the blended and unresolved *He* II line λ 4339, is the mean of both sides of the profile from two 2-prism plates, dispersion 10.5 A/mm, while that for σ Orionis is the mean of both sides of the profile from four single-prism plates, dispersion 30.3 A/mm. In no case were there significant differences between the red side of the profile and the violet side or variations from plate to plate.

The mean equivalent width of the blended feature at $H\gamma$ in 10 Lacertae from published work by Petrie,[7] Baker,[8] and Aller[9] and from eight plates of various dispersions taken recently at this observatory is 2.84 E.A., while that for σ Orionis from four single-prism plates is 2.97 E.A. The strength of *He* II λ 4339 may be estimated by taking $\frac{1}{2}\{W(\lambda\,4541) + W(\lambda\,4200)\}$; it is found to be 0.62 E.A. for 10 Lacertae and 0.25 E.A. for σ Orionis. Thus the equivalent width of $H\gamma$ alone is estimated to be 2.22 E.A. in 10 Lacertae and 2.72 E.A. in σ Orionis. The mean equivalent width of $H\gamma$ in τ Scorpii, B0 V, is, from measures by Unsöld[10] and Williams,[11] 3.19 E.A. Since the model is halfway in spectral type between 10 Lacertae and τ Scorpii, unblended $H\gamma$ should be expected to have an equivalent width close to 2.70 E.A., which is about the equivalent width observed for the O9.5 V star σ Orionis. The computed equivalent width of $H\gamma$ is 2.35 E.A., a value smaller than the expected value by about 13 per cent. This deficiency possibly is caused by the neglect of the Stark broadening due to the electrons.

TABLE 1

LINE PROFILE OF $H\gamma$: RESIDUAL INTENSITIES

$\Delta\lambda$ (A)	Model Atmosphere O9.5 V	σ Orionis O9.5 V	10 Lacertae O9 V	$\Delta\lambda$ (A)	Model Atmosphere O9.5 V	σ Orionis O9.5 V	10 Lacertae O9 V
0	0.617	0.609	0.520	4	0.894	0.854	0.892
1	.693	.648	.648	7	.967	.936	.961
2	0.787	0.732	0.770	10	0.988	0.982	0.988

The computed and observed profiles are drawn in Figure 1. It is clear that the computed profile fits the 10 Lacertae profile better than it fits the profile from σ Orionis, although σ Orionis matches the model best in spectral type. The discrepancies within an angstrom or so of the center are not significant, as the structure of the model atmosphere is not known sufficiently accurately in the extreme outermost layers where the central parts of this strong line are formed, nor is it certain that the assumption of pure absorption is valid for the center of the line. However, one would expect a better fit in the wings than is found. These results indicate that the simple statistical theory of the Stark effect due to protons only does not give a sufficient broadening of the hydrogen lines.

An estimate of how much the electrons might add to the Stark broadening may be obtained by considering the electrons in the way Verweij[1] did—that is, by increasing the mean field strength at each point in the atmosphere by an amount $(2)^{2/3} = 1.585$. Such a procedure would decrease the residual intensity at $\Delta\lambda = 2$ A from about 0.79 to about 0.72; at $\Delta\lambda = 4$ A from about 0.89 to about 0.81; and at $\Delta\lambda = 7$ A from about 0.97

[6] A. B. Underhill, *Canadian J. Phys.*, **29**, 447, 1951; *Contr. Dom. Ap. Obs. Victoria*, No. 23, 1951.

[7] *Pub. Dom. Ap. Obs. Victoria*, **7**, 321, 1947.

[8] *Pub. R. Obs. Edinburgh*, **1**, 15, 1949.

[9] *Ap. J.*, **104**, 347, 1946.

[10] *Zs. f. Ap.*, **21**, 1, 1941.

[11] *Ap. J.*, **83**, 279, 1936.

to about 0.92. This treatment for the electrons leads to a line profile, compared with that in the spectrum of σ Orionis, too deep in the wings by about as much as it is too shallow when the Stark effect of the protons only is considered. It seems that although the broadening effects of the electrons are not negligible, they cannot be roughly evaluated by merely doubling the effect of the protons.

In conclusion it may be noted that the Holtsmark distribution function tends to overestimate the effects of large fields;[12] hence discrepancies in the wings of the line, such as

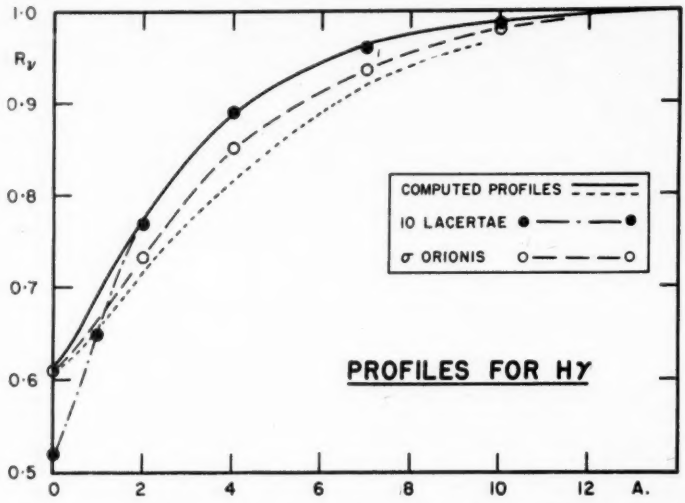

FIG. 1.—The computed and observed profiles for $H\gamma$. The solid line gives the computed profile when the broadening is due to the statistical Stark effect of protons only, and the broken line gives the estimated profile when the effect of the protons is doubled.

those found here, might be even greater than indicated, if a more accurate theory of the interaction of protons with neutral hydrogen atoms were used. M. Krogdahl[13] has shown that consideration of the time dependence of the collisions between protons and neutral atoms can cause little change in the simple statistical theory of the Stark effect of $H\gamma$ in stellar atmospheres used here.

ANNE B. UNDERHILL

DOMINION ASTROPHYSICAL OBSERVATORY
VICTORIA, B.C.
March 18, 1952

[12] S. Chandrasekhar, *Rev. Mod. Phys.*, **15**, 73, 1943.

[13] *Ap. J.*, **110**, 355, 1949.

ON THE ACCURACY OF JOHNSON'S COLORS AND MAGNITUDES OF THE PLEIADES

In order at least partially to resolve the differences among the various color and magnitude observations of the brighter members of the Pleiades,[1,2] H. L. Johnson, in the summer of 1951, asked whether or not a new and independent series of colors and magnitudes could be obtained by the author. This new series of observations was secured in January, 1952. The equipment employed consisted of the 82-inch reflector of the McDonald Observatory and the photometer generally used by the author. This equipment is entirely independent of that employed by Johnson[2] except for the telescope. However, the same

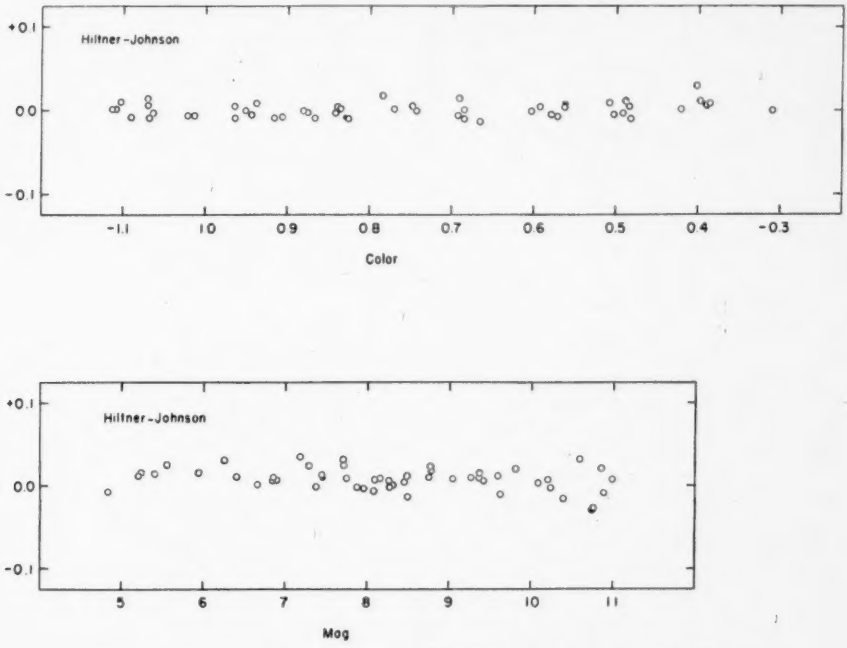

FIG. 1.—Comparison between the colors and magnitudes of Johnson and Hiltner

type of filters was used; a Corning 5030 plus a Schott GG-13 for the blue and a Corning 3384 for the yellow. The amplifier was calibrated in the laboratory against a precision potentiometer.

The observations were made in the following manner: Five deflections on the star were made in the order yellow, blue, ultraviolet (not reported in the present paper), blue, and yellow. These deflections were then followed by three deflections of the sky—one in each color. A diaphragm with a diameter of 15 seconds of arc was normally used.

Three stars in the cluster were selected as reference stars and hence were observed approximately every hour. In the reductions a mean color extinction was assumed. The reference stars then served as a check on the validity of this assumption. The night of Janu-

[1] O. J. Eggen, *Ap. J.*, **111**, 81, 1950.

[2] H. L. Johnson and W. W. Morgan, *Ap. J.*, **114**, 522, 1951.

TABLE 1

COLORS AND MAGNITUDES OF THE PLEIADES

EGGEN NO.	COLORS					MAGNITUDES			
	C'_y				C_y MEAN				
	JAN. 4	JAN. 5	JAN. 7	MEAN		JAN. 4	JAN. 5	JAN. 7	MEAN
2	−0.495			−0.495		8.089			8.089
3	− .576	−0.573		− .574	−0.784	8.309	8.311		8.310
4	− .426			− .426		9.800			9.800
5	− .630	− .619	−0.624	− .624	−0.842	8.093	8.092	8.106	8.097
		− .621					8.097		
6	− .330			− .330		10.019			10.019
7	− .394			− .394	−0.579	9.369			9.369
8	− .570	− .552		− .561	−0.770	8.264	8.267		8.266
9		− .314		− .314	−0.488		10.207		10.207
10		− .824		− .824	−1.070		5.256		5.256
12	− .456			− .456		9.179			9.179
13		− .236		− .236	−0.398		10.861		10.861
14	− .458			− .458		9.175			9.175
15		− .492		− .492	−0.691		8.751		8.751
16		− .853		− .853	−1.103		5.414		5.414
18	− .411	− .401		− .406	−0.593	9.271	9.270		9.270
19	− .610			− .610	−0.826	8.084			8.084
20		− .487		− .487	−0.685		8.788		8.788
21		− .240		− .240	−0.403		10.592		10.592
22		− .652	− .660	− .653	−0.875		7.191	7.202	7.195
		− .646					7.193		
23		− .311		− .311	−0.484		10.083		10.083
24		− .332		− .332	−0.508		9.810		9.810
26	− .629	− .619	− .628	− .622	−0.839	7.882	7.891	7.888	7.888
		− .613					7.892		
27		− .824		− .824	−1.070		5.565		5.565
28	− .822			− .822	−1.068	6.251			6.251
30	− .251			− .251		10.564			10.564
32		− .229		− .229	−0.390		10.892		10.892
33	− .712	− .706	− .712	− .708	−0.938	7.290	7.293		7.294
		− .703					7.300		
34	− .495	− .492	− .490	− .494	−0.693	8.281	8.277	8.280	8.278
	− .504	− .494	− .495			8.277	8.276	8.279	
	− .499	− .485				8.277	8.280		
	− .502	− .483				8.275	8.278		
35		− .159		− .159	−0.310		10.741		10.741
36	− .388			− .388	−0.572	9.592			9.592
39		− .225		− .225	−0.386		10.998		10.998
40	− .773	− .780	− .779	− .781	−1.021	6.669	6.674	6.669	6.672
	− .785	− .778	− .787			6.674	6.675	6.667	
	− .779	− .780	− .783			6.674	6.672	6.670	
	− .783	− .780				6.675	6.673		
41	− .538	− .537		− .538	−0.743	8.493	8.501		8.497
42	− .379			− .379	−0.562	9.773			9.773
43		− .774		− .774	−1.013		6.856		6.856
		− .773					6.857		
44	− .624	− .608	− .622	− .618	−0.835	7.709	7.728	7.699	7.712
46		− .654	− .662	− .658	−0.880		7.759	7.757	7.758
47	− .744	− .736	− .741	− .740	−0.964	6.730	6.725	6.720	6.725
49		− .328		− .328	−0.503		10.247		10.247
50	− .318			− .318	−0.492	9.620			9.620
51	− .487			− .487	−0.685	8.454			8.454
52		− .380		− .380	−0.563		9.426		9.426
54		− .857		− .857	−1.108		5.212		5.212
55		−0.309		− .309	−0.482		10.395		10.395
56	−0.689		−0.689	−0.689	−0.916	6.906		6.908	6.907

TABLE 1—*Continued*

Eggen No.	Colors					Magnitudes			
	C'_y				$\bar{C}_y$ Mean				
	Jan. 4	Jan. 5	Jan. 7	Mean		Jan. 4	Jan. 5	Jan. 7	Mean
57	.....	−0.256	.....	−0.256	−0.421	.....	10.763	.....	10.763
58	−0.542	.....	.....	− .542	−0.748	8.492	.....	.....	8.492
60	.....	− .862	.....	− .862	−1.113	.....	4.843	.....	4.843
61	− .612	.....	.....	− .612	−0.828	8.179	.....	.....	8.179
62	− .713	.....	−0.716	− .714	−0.944	7.460	.....	7.461	7.460
63	− .818	.....	.....	− .818	−1.063	6.411	.....	.....	6.411
64	− .645	.....	.....	− .645	−0.866	7.977	.....	.....	7.977
65	− .415	.....	.....	− .415	−0.603	9.376	.....	.....	9.376
66	− .617	.....	.....	− .617	.....	8.156	.....	.....	8.156
67	− .842	.....	.....	− .842	−1.090	5.956	.....	.....	5.956
68	− .728	.....	− .734	− .731	−0.964	7.454	.....	7.452	7.453
69	− .677	.....	− .682	− .680	−0.906	7.389	.....	.....	7.389
70	− .717	.....	− .724	− .720	−0.951	6.860	.....	6.861	6.860
71	− .470	.....	.....	− .470	−0.666	9.048	.....	.....	9.048
75	.....	− .649	− .648	− .648	.....	.....	7.719	7.723	7.721
77	.....	− .664	− .662	− .663	.....	.....	7.633	7.659	7.646
H669	+ .694	+ .699	+ .703	+0.696	+0.666	.....	.....	.....	.....
	+ .696	+ .699	+0.694						
	+ .686	+ .702							
	+0.687	+0.705							

ary 7 (U.T.) required a correction of 0.017 mag. in color, in order to place the observations for this night in agreement with the two previous nights. This correction of 0.017 mag. was evaluated from the observations of the three comparison stars on the assumption that their colors were nonvariable. A total observing time of $8\frac{1}{4}$ hours was involved, during which 118 observations, as described above, were obtained.

The observations are recorded in Table 1. The first column is the number of the star assigned by Eggen.[1] The next three columns give the individual observations of natural colors for the three nights. The fifth column is the mean of the previous three. The sixth column gives the colors on the natural system of Johnson.[2] The conversion equation from the author's natural colors to that of Johnson's is:

$$C_y = 1.142C'_y - 0.129 .$$

The next three columns give the natural yellow magnitudes as observed on the individual nights, while the last column is the mean of the previous three.

A comparison of the present series with that of Johnson's can best be done with a plot of the differences. It is seen in Figure 1 that the two series of colors and magnitudes are in excellent agreement. The probable error of the difference in color is ± 0.0049 mag.; and that of a magnitude, ± 0.0078 mag. This probable error contains, of course, errors in *both* series. In comparing the magnitudes in the two series, one must recall that the color term between the two systems was neglected.

The two series are in such excellent agreement that the color-magnitude diagram as published by Johnson and Morgan[2] for the Pleiades is almost identical with that for the present series. No star can be moved more than the diameter of the dot representing that star.

W. A. Hiltner

Yerkes and MacDonald Observatories
April 29, 1952

THE RELATIVE POPULATIONS OF THE *He* I 2^1S AND 2^3S STATES IN THE ORION NEBULA

O. C. Wilson[1] discussed intensities of *He* I absorption lines produced by the nebulae surrounding the Trapezium stars in the spectrum of θ_1 Orionis C. Assuming the lines on the linear part of the curve of growth, he derived

$$\frac{N_3}{N_1} = \frac{N\,(2^3S)}{N\,(2^1S)} \geqq 2.5$$

from measured equivalent width. The theoretical calculation of N_3/N_1 by O. Struve and K. Wurm[2] for *He* I, excited by strongly diluted radiation with a temperature of 2.5×10^4 and $10^{4\circ}$ K, provides values between 6 and 12. Wilson is inclined to explain this divergence by the hypothesis that the states 2^1S and 2^3S are not metastable in a strict sense.

But new calculations of the population of *He* I levels[3] which allow for a larger number of states show that the former values should be enlarged by a factor of from 3 to 10. For an electron temperature of $10^{4\circ}$ K, different temperatures of radiation, and different dilutions the values of N_3/N_1 shown in the accompanying tabulation were found.

T_r (° K)	N_3/N_1			T_r (° K)	N_3/N_1		
	$W=10^{-1}$	$W=10^{-2}$	$W\sim 0$		$W=10^{-1}$	$W=10^{-2}$	$W\sim 0$
1×10^4	63	127	147	2.5×10^4	28	72	84

It is obvious that there are no discrepancies between the theory developed by Struve and the observations quoted by Wilson.

P. WELLMANN

HAMBURG-BERGEDORF
May 10, 1952

INTERNAL MOTIONS WITHIN INTERSTELLAR CLOUDS

In a recent intercomparison[1] of *Na* and *Ca* interstellar lines by Routly and Spitzer, the doublet ratios and equivalent widths were used to determine N, the number of absorbing atoms in the line of sight per square centimeter, and also the parameter b, which measures the width of the absorption-coefficient profile. In this work it was assumed that the width of the absorption coefficient is due entirely to Doppler broadening and that the number of atoms with a velocity between v and $v + dv$ is proportional to $\exp(-v^2/b^2)$, where v is the velocity relative to the center of gravity of the cloud. The root-mean-square dispersion of radial velocities of atoms within the cloud equals $b/2^{1/2}$.

Numerical values of b found in this work[1] ranged from 0.7 to 18 km/sec, averaging 6.4 km/sec; half the values lay between about 4 and 8 km/sec. Some tendency was apparent for $b(Ca\ \text{II})$ to exceed $b(Na\ \text{I})$ for the stronger lines, an effect to be expected from the increased value of the ratio $n(Ca\ \text{II})/n(Na\ \text{I})$ in the clouds of greater velocity.

To obtain a general check on the values of b obtained indirectly from equivalent widths, a few values of b have now been determined directly from line profiles. The mate-

[1] *Ap. J.*, **91**, 360, 1940.
[2] *Ap. J.*, **88**, 84, 1938.
[3] P. Wellmann, *Zs. f. Ap.*, **30**, 71, 1952.
[1] *Ap. J.*, **115**, 227, 1952.

rial available consisted of the microphotometer tracings already used for the investigation of equivalent widths. Measurements were made only on well-resolved components of moderately high velocity, since each such component may reasonably be attributed to a single cloud. For the D lines the enhanced grain on the 103*a*-D plates made such measurements particularly difficult, and results are given here for K and H only, based on plates taken by W. S. Adams[2] with the 114-inch camera at the 100-inch telescope (dispersion 2.9 A mm).

To carry out the measurements the log of the relative depth for each line was plotted against the square of the distance x from the line center. From the best straight line drawn through the plotted points the value of x was determined for a line depth corresponding to half the central depth; this quantity, the half-half depth, is designated by Δ_{app}. The same procedure was followed for the emission lines in the comparison spectrum, and a corresponding Δ_{inst}, the half-half width of the instrumental profile, was found. Values of Δ_{inst} average 4.0 km/sec at about 3950 A. The true value of Δ was then found from the usual equation,

$$\Delta = (\Delta_{app}^2 - \Delta_{inst}^2)^{1/2} .$$

Values of the ratio Δ/Δ_{app} ranged from 0.46 to 0.87, averaging 0.73 for the six lines measured.

Finally, values of b were determined. For unsaturated lines, $b = \Delta/(\log_e 2)^{1/2} = 1.2\Delta$. For saturated lines, however, one must use the formula

$$b = \Delta \left[\log_e \left(\frac{C}{\log_e \{ 2/(1 + e^{-C}) \}} \right) \right]^{-1/2} ,$$

where C is the optical depth at the line center. Values of C may be found from the observed doublet ratio and the theoretical curve of growth. Since most of the lines were relatively unsaturated, the values of $b/1.2\Delta$ were near unity, averaging 0.93.

TABLE 1

DOPPLER WIDTHS OF INTERSTELLAR COMPONENTS

HD	V (Km/Sec)	Line	Doublet Ratio	Δ_{app}	b (Km/Sec)
42087	−35.7	K	1.89	5.6	4.5
		H		7.1	6.7
167264	+40.6	K	1.69	5.2	3.4
		H		4.4	2.2
199478	+54.6	K	1.96	7.7	7.8
		H		6.2	5.6

Resultant values of b are given in Table 1. For each component the radial velocity, corrected[1] for solar motion, is given in the second column. Values of the doublet ratio, taken from Spitzer, Epstein, and Li Hen,[3] are given in the fourth column.

Since for each line only one plate of sufficiently high quality was available, the present material is entirely provisional. Differences between the values of b found between K and H in the same star indicate a probable error in the neighborhood of 1 km/sec. When account is taken of possible additional errors arising from the calibration or from the

[2] *Ap. J.*, **109**, 354, 1949.

[3] *Ann. d'Ap.*, **13**, 147, 1950.

instrumental contour used, the differences between the values of b found for different stars lose all significance.

The average value of b for the six lines in Table 1 is 5.0 km/sec. The probable error in this average value should be less than 1 km/sec. This mean value of b, in good agreement with the general run of values found[1] indirectly for the stronger lines, would imply a kinetic temperature of 40,000° for the *Ca* II ions, if the motions were entirely thermal. According to the computations by Spitzer and Savedoff,[4] the temperature of an interstellar cloud is not likely to exceed 10,000° K and in an *H* I region is probably more nearly 60° K. In a cloud moving at high velocity, somewhat greater temperatures might be expected, but probably not so great as 40,000°. Tentatively, the observed values of b may be attributed to macroscopic motions in the line of sight. More complete measurements of this type, extended to the D lines as well, would indicate possible differences in distribution between *Na* I and *Ca* II within a single cloud and would also yield information on the variation of the dispersion of atomic velocities from cloud to cloud.

LYMAN SPITZER, JR.
ANDREW SKUMANICH

PRINCETON UNIVERSITY OBSERVATORY
April 7, 1952

[4] *Ap. J.*, 111, 593, 1950.

REVIEWS

Problems of Cosmical Aerodynamics. Edited by J. M. BURGERS and H. C. VAN DE HULST. Dayton, Ohio: Central Air Documents Office, 1951. Pp. 237+v.

A Symposium on the Motion of Gaseous Masses of Cosmical Dimensions was held at Paris during the period August 16–19, 1949, under the joint auspices of the International Union of Theoretical and Applied Mechanics and the International Astronomical Union. The symposium was made possible by a grant-in-aid from UNESCO, and publication of the proceedings, reviewed here, was supported by the United States Air Force.

Among the stated aims of the symposium were "to give opportunity to astronomers to present their problems and points of view, and to make aerodynamicists acquainted with the observational facts; . . . to obtain from aerodynamicists an exposition of the present status of fluid mechanics which might be applicable to astronomical problems and to formulate problems in such a way that mathematicians and fluid mechanics people can start to work on them . . . [and that] the character of the Symposium should be that of a round-table conference. . . ." Most of the papers were completely rewritten by the authors after the symposium. Records of eleven general discussions are also included. These have been edited to eliminate irrelevant material, but the account is nevertheless as lively as a report in the *Observatory* of a meeting of the Royal Astronomical Society.

Three introductory papers, concerned largely with presenting a summary of the known physical properties of interstellar material, were given by Oort, Strömgren, and Spitzer. Anyone who is interested in finding a readable and authoritative account of these matters will find these articles very rewarding.

Magneto-hydrodynamic phenomena are considered in the next two papers. Alfvén describes some remarkable experiments that one of his co-workers, Mr. S. Lundquist, performed in the laboratory. An elegant generalized linear theory of electromagnetic, magneto-hydrodynamic, and acoustic waves is described by van de Hulst in a succeeding article.

Supersonic flow and shock waves are treated in the next nine papers. An astronomer might wish that the first two, by Burgers and McVittie, were of a more introductory (and less mathematical) nature. Seeger has included some excellent photographs of laboratory projectiles traveling with Mach numbers of the order of 20. Even though the scale of those experiments is small compared to that of interstellar phenomena, it is illuminating to see shock-wave phenomena represented so graphically. In order to present the observational side, Mrs. Payne-Gaposchkin and van de Hulst have described various aspects of the nova phenomenon. Oort and Miss Kluyver present two papers in which the effect of collision of the expanding nova shells with interstellar matter is considered as a means of accounting for the fineness of detail in the expanding shell and other peculiarities in its behavior. Burgers has studied the behavior of a shock wave traveling through a gas of decreasing density, and Schatzman reviews his studies of the heating of the solar atmosphere by shock waves.

The turbulent motions of gaseous masses of large dimensions are considered in the last nine papers. The first, by von Karman, should be valuable, even though it is brief, since so far as the reviewer knows there does not now exist any primer on turbulence theory for astronomers. It is to be regretted that the distinguished author did not have space and time to correct some typographical errors in the formulae and generally to render his account more lucid. In the next article Batchelor gives an excellent outline of the application of methods of dimensional analysis to turbulence phenomena, including cases in which an appreciable amount of energy is stored in magnetic fields. Von Weizsäcker describes an interesting attempt of one of his students, von Hoerner, to compare the turbulent radial-velocity distribution in the Orion Nebula with the Kolmogoroff law. A study of the rotation of a number of spiral galaxies is described by Baade and Mayall, in which their data are considerably strengthened by new measurements of the radial velocities of emission objects. Lindblad summarizes his ideas concerning the formation of spiral galaxies, and in another paper von Weizsäcker is a proponent of the "milk in a cup of

coffee" theory. He also reports on further work by von Hoerner which attempts to account for the existence and persistence of separate clouds in interstellar matter. Hoyle has suggested a theory of the origin of angular momentum in galaxies which implies that the momentum was acquired after the galaxy first came into existence. In the subsequent discussion Heisenberg has objected to this assumption on grounds that if a galaxy were initially an irregular fragment formed during the initial expansion of the universe it would be likely to have an appreciable initial angular momentum. Zwicky has discussed the morphology of the universe in very broad terms. At one point he makes the statement that recent pictures taken with the 48-inch Schmidt camera of the Coma cluster reveal the existence of luminous interstellar matter for the first time. It is too bad that he does not give us further particulars on this point. In the final article Minnaert describes some of the hydrodynamical problems which must be solved if we are to understand the behavior of the sun. He emphasizes that the wealth of detail which can be observed is a joy to the observer but places difficult obstacles in the way of a theoretician.

The authors and the editors are to be congratulated on their labors. Though their hypotheses may occasionally strike one as being speculative, they rarely fail to be interesting.

G. KELLER

Perkins Observatory

The FACE of the MOON

BY RALPH B. BALDWIN

An answer, in terms of the meteorite theory, to the question of how the moon came to exist in its present form.

The study of the moon—a mirror for the study of the earth.

256 pages. 6¼"×9¼". Illustrated. $5.00.

THE UNIVERSITY OF CHICAGO PRESS

New 1952 Model

35-mm. EXAKTA "VX"

Single Lens Reflex Camera

One lens both for viewing and picture taking assures perfect sharpness, accurate exposure, maximum depth of field, and correct composition for color. You always see the exact image before you take the picture —whether the subject is an inch or a mile away, whether it is microscopic or gigantic, whether it is moving or stationary. Instantly interchangeable lenses permit telephoto, wide angle, close-up, copy and microscope photography. With f2.8 Zeiss Tessar "T" Coated Lens with Pre-Set Diaphragm Control.....$269.50 tax included

Write Dept. 1100 For Free Booklet "K"

NATURE PHOTOGRAPHY WITH MINIATURE CAMERAS by Alfred M. Bailey (Denver Museum of Natural History). This eminent explorer and scientist displays his finest Exakta photographs and others along with explanatory material. 35 full page photographs. 64 pages.....50c

EXAKTA CAMERA COMPANY
46 W. 29th St. New York 1, N.Y.

A Completely Revised Edition

THE ATMOSPHERES OF THE EARTH AND PLANETS

By GERARD P. KUIPER

Important new material has been added to make this edition the most modern and complete monograph on planetary atmospheres.

Additions Include:

—Information recently obtained in V-2 flights about our upper air and the x-ray spectrum of the sun.

—Identification of the strong red and infrared emissions of the night sky.

—A new determination of the cosmic abundances of the chemical elements.

—A derivation of the ozone temperature in the upper stratosphere.

—A determination of the age of meteorites.

—A discussion of the presence of nitrous oxide in the lower atmosphere and its connection with the life cycle.

—A reconstruction of the conditions leading to the escape of the "proto-atmosphere."

—A new section on Jovian planets.

—A development of the atmospheric conditions on Mars.

Paperbound $5.50 *Clothbound $8.50*

THE UNIVERSITY OF CHICAGO PRESS

5750 ELLIS AVENUE CHICAGO 37, ILLINOIS

Latest Volume in the
International Astrophysics Series

COMETS AND METEOR STREAMS

By J. G. Porter, *H.M. Nautical Almanac Office*. This book surveys the advances made in our knowledge of comets and cometary statistics from the time of Halley to the present day. A valuable feature is the extensive treatment of the computation of comet orbits; later sections deal with meteor information gained by radar technique. J. G. Porter has acquired an international reputation for his work on comets and meteors. This book forms a link between the descriptive textbook and the more specialized treatises on orbits. *1952. 123 pages. $5.25.*

And another in this series
already published... and applauded

THE AURORAE

By Leiv Harang, *Norwegian Defense Research Establishment*. "An interesting collection of experimental facts concerning the aurora and experimental methods for the safety of aurorae. . . . Contains an excellent description of the photographic and other techniques used for studying the appearance, spatial location, and spectra of the aurora. The results of numerous investigations are referred to and briefly summarized. . . . Students of the upper atmosphere and of terrestial electric and magnetic phenomena will find this volume a useful addition to their bookshelves."—*Journal of the American Rocket Society. 1951. 166 pages. $4.50.*

Another fascinating title...
the first book on the subject

RADIO ASTRONOMY

By Bernard Lovell *and* J. A. Clegg. The authors point out the most important aspects of the new science of radio astronomy which has emerged since World War II—out of the application of radio and radar techniques to problems of the upper atmosphere. The book has been designed to have the widest possible interest; it embraces meteor observations, solar observations, galactic noise, and the electronic methods and formulae involved. *1952. 227 pages. $4.00.*

Write today for approval copies.

JOHN WILEY & SONS, Inc. 440 Fourth Ave. New York 16, N.Y.